Organic Monolayers on Oxide-Free Silicon

Self-Assembly, Functionalization, Patterning and Electronic Characterization

Thesis committee:

Thesis supervisor
Prof. dr. H. Zuilhof
Professor of Organic Chemistry
Wageningen University

Other members

Prof. dr. B. Fabre	University of Rennes 1, France
Prof. dr. B. J. Ravoo	University of Münster, Germany
Prof. dr. D. J. Broer	Eindhoven University of Technology
Prof. dr. M. A. Cohen Stuart	Wageningen University

This research was conducted under the auspices of the graduate school VLAG.

Organic Monolayers on Oxide-Free Silicon

Self-Assembly, Functionalization, Patterning and Electronic Characterization

Luc Scheres

Thesis

Submitted in fulfillment of the requirements for the degree of doctor
at Wageningen University
by the authority of the Rector Magnificus
Prof. dr. M. J. Kropff
in the presence of the
Thesis Committee appointed by the Academic Board
to be defended in public
on Monday 28 June 2010
at 1.30 p.m. in the Aula.

Luc Scheres
Organic Monolayers on Oxide-Free Silicon; Self-Assembly, Functionalization, Patterning and Electronic Characterization
PhD thesis, Wageningen University, Wageningen, The Netherlands, 2010
ISBN: 978-90-8585-664-1

Table of Contents

Chapter 1

General Introduction

1.1 Organic Monolayers on Solid Substrates

Organic monolayers are layers that are precisely one organic molecule thick, and which are attached in a dense packing onto a solid substrate. The attachment can be weak or strong, and can rely on either physisorption (e.g. electrostatic interactions) or chemisorption (formation of chemical bonds). Since the pioneering work on organic monolayers on gold,[1] glass[2] and oxidized aluminum[3] in the early 1980s, the field of organic monolayers has grown exponentially, and nowadays organic monolayers on innumerable metals, oxides and semiconductors have been reported in literature. With these extremely thin organic films (typical thickness ca. 2 - 5 nm) the surface properties of the underlying substrate can be precisely controlled, and therefore organic monolayers find rapidly increasing application in many fields of interest, including surface wettability and lubrication, surface passivation, chemical and biological sensing, and molecular electronics.[4,5]

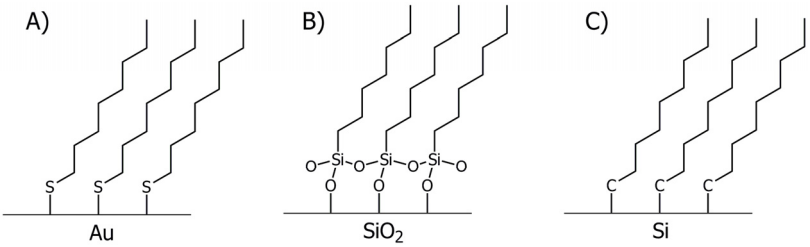

Figure 1. Schematic representation of some key examples of organic monolayers: (A) alkylthiols on gold, (B) alkylsilanes onto glass, and (C) 1-alkenes on oxide-free silicon.

Organic monolayers of alkylthiols on gold and alkylsilanes on oxidized surfaces are obviously the most extensively studied systems (Figure 1A and B).[4-6] Due to the high affinity of the thiol group for the gold surface, the self-assembly of alkylthiol monolayers on gold is a highly flexible process, which is clearly displayed by the wide variety of functional and rather complex monolayers that have been prepared.[4] In addition, the semi-covalent nature of the Au-S bond allows diffusion of already absorbed chains along the surface, and as a result well-ordered and nearly defect-free monolayers can be obtained in a simple and reproducible manner.[4,6] However, the semi-covalent Au-S bond is also the shortcoming of these monolayers, because its limited strength provides alkylthiol monolayers with only moderate thermal and chemical stability. This stability, both thermally and chemically, is significantly increased by the use of a covalent C-Si-O linkage to an oxide, as results from the attachment of alkylsilanes onto oxidic surfaces.[5] The

increased stability comes at a price, however, as the preparation of alkylsilane monolayers on oxidized surfaces is highly dependent on the reaction conditions, and therefore considerably less simple and reproducible than achievable for alkylthiols on gold. In addition, while organosilane-derived monolayers can be prepared with a wide variety of functional moieties, their long-term applicability remains less than ideal since the interfacial Si–O bonds are susceptible to hydrolysis.

1.2 Monolayers on Oxide-Free, Hydrogen-Terminated Silicon

Due to the ongoing miniaturization of semiconductor devices, there is a significant interest in the surface modification of silicon. In this perspective, organic monolayers directly bound to oxide-free, hydrogen-terminated silicon are interesting candidates as they can easily be implemented in existing technology for the fabrication of silicon-based micro- and nanostructured devices (Figure 1C). The direct covalent linkage (Si–C bond) to the silicon surface provides a well-defined organic monolayer-silicon interface, and the non-polar character of this strong bond makes these monolayers thermally and chemically very robust.[7,8] Moreover, because an intervening SiO_2 layer is essentially absent, direct electronic coupling between any organic functionality and the silicon substrate is possible, which provides an opportunity to enhance the device performance compared to SiO_2-covered electronic devices.[9-13] Furthermore, using a semiconductor instead of a metal as a substrate/electrode has the advantage that – depending on the desired electronic properties of the final device – semiconductors with different doping levels and doping types can be used.[12-15] As a result organic monolayers on oxide-free silicon have great potential in the field of biosensors, molecular electronics and photovoltaic devices.[10,11,13,16-23]

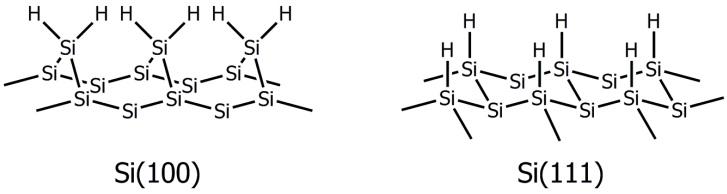

Figure 2. Schematic representation of hydrogen-terminated Si(100) (left) and Si(111) (right).

1.3 Surface Orientations of Silicon

The most common surface orientations of commercially available silicon are Si(100) and Si(111). Upon exposure to air both become rapidly coated with a self-limiting, thin native oxide that can be removed thermally under UHV conditions or wet-chemically by immersion in aqueous fluoride-containing solutions.[17,19,24,25] Typically, Si(100) wafers are treated with 2.5% HF to yield dihydride-terminated Si(100) surfaces that are on the nanometer scale still rough. In contrast, Si(111) yields atomically flat terraces with monohydride-termination, because during etching in argon-saturated 40% NH_4F solution the initially rough Si(111) surface will spontaneously smoothen as a result of the differences in reactivities of different crystal faces.[26] Both hydrogen-terminated Si surfaces are sufficiently stable that they can be handled in air for short periods of time (tens of seconds), allowing wet-chemical modification routes like the formation of organic monolayers as described in this thesis. Because the lattice constant of thermally grown silicon dioxide (SiO_2) matches best with the crystal plane of Si(100), for electronic devices that use the oxide as an electrical insulator Si(100) is the most used crystal orientation, since this results in the lowest concentration of defects at the SiO_2-Si interface. However, due to its atomic flatness and nearly defect-free hydrogen-termination, Si(111) is the best substrate for new hybrid organic monolayer-silicon devices.[18]

1.4 Monolayer Formation on Hydrogen-Terminated Silicon

Since the first reports of Chidsey and Linford,[8,27] numerous new methods have been reported, and nowadays organic monolayers on oxide-free, hydrogen-terminated silicon can be prepared under a variety of conditions with both 1-alkenes and 1-alkynes. Over the last ten years several reviews about this topic have appeared in literature.[9,16,17,19,24,25,28,29] Although initially harsh conditions (neat 1-alkenes or 1-alkynes with radical initiators and heat)[8,27,30] were required for the modification of planar silicon surfaces, the last decade displays a trend towards milder reaction conditions. In 1999 Sieval et al.[31] already showed that instead of neat 1-alkenes also dilute solutions of 1-alkenes can be used for monolayer formation on H-Si(100) under thermal conditions. Subsequently, Cicero et al.[32] demonstrated monolayer assembly on H-Si(111) by UV illumination at room temperature, and Stewart and Buriak reported visible light-promoted modification of porous silicon with 1-alkenes and 1-alkynes.[33,34] Not much later, it was shown by Sun et al.[35,36] that also on

planar silicon surfaces visible light can initiate monolayer formation, even in dilute solutions.

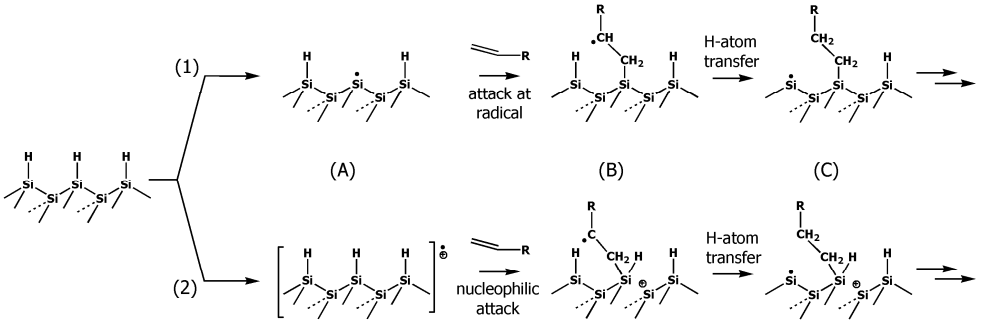

Figure 3. Representation of the proposed radical chain mechanisms for 1-alkenes (1) with radical initiators or UV irradiation and (2) with thermal activation or visible-light irradiation.

Currently it is widely accepted that monolayer formation occurs via a radical-chain mechanism on the surface (Figure 3), even during mild visible light-induced monolayer assembly at room temperature.[8,32,37] However, the exact initiation mechanism of the radical-chain reaction, especially under these mild reaction conditions, is not completely understood yet. Radical initiators[8] and UV light[32,38] are capable of breaking the H-Si bond homolytically, which yields silicon radicals (silicon dangling bonds) that can act as a starting point for the radical chain propagation (Figure 3, route 1). In contrast, when using thermal conditions[8,30,39,40] or visible light at room temperature,[35-37] insufficient energy for homolytic cleavage of the strong H-Si bond is available. Nevertheless, as evidenced by scanning tunnelling microscopy (STM), monolayer formation still occurs via island growth.[37,41,42] This implies that propagation of the radical chain reaction still proceeds, but a different initiation mechanism must be active under mild reaction conditions. Inspired by the visible light-induced monolayer formation at room temperature, Sun et al.[36] proposed a initiation mechanism based on photoexcited electron-hole pairs (excitons) near the silicon surface. These electron-hole pairs are susceptible to nucleophilic attack by a 1-alkene or 1-alkyne resulting in the formation of a Si–C bond and a carbon radical at the β-position (Figure 3, route 2). This radical can then abstract a hydrogen atom from an adjacent H-Si site and leave a highly reactive silicon radical at the surface. A new incoming alkene or alkyne molecule can react with this silyl radical and in this way propagate the radical chain reaction at the H-Si surface. However, we note that although the increasingly milder reaction conditions that were shown to work with 1-alkenes will extend the range of functional groups that can be attached directly onto Si,[43] at the same time the quality and

thus the stability of these organic monolayers is decreased with respect to those obtained under harsher attachment conditions.[35,36,42,44]

1.5 Outstanding Issues

For all potential applications the stability of the monolayer and its oxide-free monolayer-silicon interface are the crucial issues. Both depend, in principle, on the exclusion of water and oxygen from the monolayer-silicon interface. If water and oxygen can get to the interface via some defects in the monolayer, they will react with the many remaining H-Si sites (45-50% of the H-Si sites remain after completion of an alkyl monolayer)[8,32,40,45-47] and some small oxide patches will be formed. These trace amounts of oxide facilitate hydrolysis-based degradation of the monolayer via an excavation mechanism, and introduce electrically active interface states that change the electronic properties of the underlying Si drastically. Thus, the primary role of the organic monolayer is to provide a hydrophobic environment that is not readily penetrated by water and oxygen molecules, and therefore the densest possible packing of the monolayer is desirable. As monolayer formation occurs via a meandering radical chain reaction on the silicon surface, and because diffusion of already absorbed chains to improve the ordering – as observed for alkylthiol monolayers on gold[4,6] – cannot take place due to the strong covalent Si–C bond, steric hindrance of the covalently bound chains prevents insertion of new chains. Consequently, filling the last pinholes in the monolayer is hard and thus organic monolayers on oxide-free silicon are in general less ordered and almost never completely defect free. As a result the oxide-free monolayer-silicon interface, generally, has a limited long-term stability.[44,48]

Furthermore, because many functional groups (including -OH, -CHO, -NH_2, -Br, -SH) are reactive towards a H-Si surface,[49-51] preparation of ω-functionalized monolayers on H-Si is considerably more difficult than, for instance, with alkylthiols on gold. Here, the use of protected precursors, which do not react with the H-Si surface and after completion can be deprotected to yield the desired functional monolayer, could offer an outcome.[30,52-55] However, often quite harsh deprotection conditions are required that consequently affect the quality of the monolayer-substrate interface. As mentioned above, also the use of milder reaction conditions could be helpful. An nice example is the carboxylic acid (-COOH) functionality, which binds to the H-Si surface at elevated temperatures,[27] whereas under mild photochemical reaction conditions carboxylic acid-terminated monolayers with only small to negligible indications of upside-down attachment were reported.[51,56] Nevertheless, hydrogen bonding causes acid bilayer formation, which makes these monolayers hard to

clean,[16,50] while for further functionalization an additional activation step via carboxylic anhydrides or *N*-hydroxysuccinimide (NHS) chemistry is still needed.[53,55,57,58] In addition, we note that the last years some interesting ω-functionalized monolayers are prepared, which showed no signs of upside-down attachment, are easy to clean, and allow further functionalization in a single step.[59-64]

Finally, in view of the broad range of available patterning techniques,[4,5,65-67] it is somewhat remarkable that thus far, only a limited number of patterning routes for organic monolayers on oxide-free silicon has been reported. In particular, because monolayer formation on H-Si can be initiated with UV or visible light, mainly photolithographic procedures were applied.[34,38,57,68-70] In addition, microcontact printing (μCP) – a fast and simple patterning technique, which is frequently used for alkylthiols on gold and alkylsilanes on oxide surfaces[4,5,71] – is currently not feasible with 1-alkenes and 1-alkynes directly on H-Si, due to the extended reaction times required for monolayer formation and related difficulties to remain a oxide-free monolayer-silicon interface. Only recently a number of elegant soft lithographic[56,60,72-76] and scanning probe[77-85] methods for patterning of organic monolayer on oxide-free silicon were published.

1.6 Outline of this Thesis

Since the abovementioned issues hamper the development and fabrication of functional hybrid organic monolayer-silicon devices the fundamental work presented in this thesis focused on solving these problems. To this aim detailed studies were performed to improve the quality of organic monolayers on oxide-free silicon and to deepen the understanding of both the process of formation and the resulting structure of these monolayers.

In Chapter 2 a new and very mild method to produce covalently bound organic monolayers on hydrogen-terminated Si with 1-alkynes is described. Apart from being the mildest method reported thus far, the resulting monolayers approach the highest quality yet reported for organic monolayers on Si. Subsequently, to pinpoint the precise origin of this self-assembly process, we compared the reactivity of 1-alkenes and 1-alkynes towards H-Si(111) in Chapter 3.

In Chapter 4 the structural properties of completed alkyl and alkenyl monolayers on oxide-free silicon are studied in detail, and although there is only a minor difference in the linkage to the silicon surface (Si–C–C versus Si–C=C), the final monolayer structures are considerably different in quality and packing density. In Chapter 5 molecular mechanics

studies are combined with composite high-quality ab initio G3 calculations to clarify the experimentally observed structural differences.

Chapter 6 describes the preparation of well-defined acid fluoride-terminated monolayers, and their subsequent use as a platform for reactive microcontact printing (μCP) with primary amine inks. The efficiency of this indirect printing approach was investigated by printing with a flat stamp, and because of the high selectivity of the amide formation, functionalized oligo-DNA could be printed, which was still accessible for hybridization.

In Chapter 7 a new and alternative patterning strategy, called photothermal laser patterning is described. In this approach a focused laser beam is used to locally heat the silicon substrate and decompose the organic monolayer. By backfilling the laser-written lines with a second organic monolayer that differs in its terminal functionality, chemically patterned monolayers with ~100 nm-feature sizes on oxide-free silicon were obtained.

The electronic characterization of alkyl and alkenyl monolayers on moderately and highly doped n-Si(111) substrates is presented in Chapter 8. By means of Hg/organic monolayer/Si junctions the current density-voltage and capacitance-voltage behavior is analyzed, and the influence of the doping density and the monolayer type on the charge transport properties of the junctions is studied.

Chapter 9 describes the preparation and thorough characterization of two bent-core liquid crystalline monolayers on Si.

Finally, in Chapter 10 the most important achievements, as well as some remaining questions, additional ideas and recommendations for further research are discussed that place this work into context.

References

(1) Nuzzo, R. G.; Allara, D. L. *J. Am. Chem. Soc.* **1983**, *105*, 4481-4483.

(2) Maoz, R.; Sagiv, J. *J. Coll. Inter. Sci.* **1984**, *100*, 465-496.

(3) Allara, D. L.; Nuzzo, R. G. *Langmuir* **1985**, *1*, 45-52.

(4) Love, J. C.; Estroff, L. A.; Kriebel, J. K.; Nuzzo, R. G.; Whitesides, G. M. *Chem. Rev.* **2005**, *105*, 1103-1169.

(5) Onclin, S.; Ravoo, B. J.; Reinhoudt, D. N. *Angew. Chem. Int. Ed.* **2005**, *44*, 6282-6304.

(6) Ulman, A. *Chem. Rev.* **1996**, *96*, 1533-1554.

(7) Sung, M. M.; Kluth, G. J.; Yauw, O. W.; Maboudian, R. *Langmuir* **1997**, *13*, 6164-6168.

(8) Linford, M. R.; Fenter, P.; Eisenberger, P. M.; Chidsey, C. E. D. *J. Am. Chem. Soc.* **1995**, *117*, 3145-3155.

(9) Aswal, D. K.; Lenfant, S.; Guerin, D.; Yakhmi, J. V.; Vuillaume, D. *Anal. Chim. Acta* **2006**, *568*, 84-108.

(10) Vilan, A.; Yaffe, O.; Biller, A.; Salomon, A.; Kahn, A.; Cahen, D. *Adv. Mater.* **2009**, *22*, 140-159.

(11) Hiremath, R. K.; Rabinal, M. K.; Mulimani, B. G.; Khazi, I. M. *Langmuir* **2008**, *24*, 11300-11306.

(12) Salomon, A.; Böcking, T.; Gooding, J.; Cahen, D. *Nano Lett.* **2006**, *6*, 2873-2876.

(13) Cahen, D.; Kahn, A.; Umbach, E. *Materials Today* **2005**, *8*, 32-41.

(14) Salomon, A.; Böcking, T.; Seitz, O.; Markus, T.; Amy, F.; Chan, C.; Zhao, W.; Cahen, D.; Kahn, A. *Adv. Mater.* **2007**, *19*, 445-450.

(15) Miramond, C.; Vuillaume, D. *J. Appl. Phys.* **2004**, *96*, 1529-1536.

(16) Boukherroub, R. *Curr. Opin. Solid State Mater. Sci.* **2005**, *9*, 66-72.

(17) Buriak, J. M. *Chem. Rev.* **2002**, *102*, 1271-1308.

(18) Hamers, R. J. *Ann. Rev. Anal. Chem.* **2008**, *1*, 707-736.

(19) Wayner, D. D. M.; Wolkow, R. A. *J. Chem. Soc., Perkin Trans. 2* **2002**, 23-34.

(20) Har-Lavan, R.; Ron, I.; Thieblemont, F.; Cahen, D. *Appl. Phys. Lett.* **2009**, *94*.

(21) Yaffe, O.; Scheres, L.; Puniredd, S. R.; Stein, N.; Biller, A.; Lavan, R. H.; Shpaisman, H.; Zuilhof, H.; Haick, H.; Cahen, D.; Vilan, A. *Nano Lett.* **2009**, *9*, 2390-2394.

(22) Hamers, R. J. In *Bioelectronics: From Theory to Applications* Willner, I., Katz, E., Eds. 2005; Vol. Chapter 7, p 209-230.

(23) Maldonado, S.; Knapp, D.; Lewis, N. S. *J. Am. Chem. Soc.* **2008**, *130*, 3300-3301.

(24) Sieval, A. B.; Linke, R.; Zuilhof, H.; Sudhölter, E. J. R. *Adv. Mater.* **2000**, *12*, 1457-1460.

(25) Leftwich, T. R.; Teplyakov, A. V. *Surf. Sci. Rep.* **2008**, *63*, 1-71.

(26) Allongue, P.; de Villeneuve, C. H.; Morin, S.; Boukherroub, R.; Wayner, D. D. M. *Electrochim. Acta* **2000**, *45*, 4591-4598.

(27) Linford, M. R.; Chidsey, C. E. D. *J. Am. Chem. Soc.* **1993**, *115*, 12631-12632.

(28) Bent, S. F. *Surf. Sci.* **2002**, *500*, 879-903.

(29) Shirahata, N.; Hozumi, A.; Yonezawa, T. *Chem. Rec.* **2005**, *5*, 145-159.

(30) Sieval, A. B.; Demirel, A. L.; Nissink, J. W. M.; Linford, M. R.; van der Maas, J. H.; de Jeu, W. H.; Zuilhof, H.; Sudhölter, E. J. R. *Langmuir* **1998**, *14*, 1759-1768.

(31) Sieval, A. B.; Vleeming, V.; Zuilhof, H.; Sudhölter, E. J. R. *Langmuir* **1999**, *15*, 8288-8291.

(32) Cicero, R. L.; Linford, M. R.; Chidsey, C. E. D. *Langmuir* **2000**, *16*, 5688-5695.

(33) Stewart, M. P.; Buriak, J. M. *J. Am. Chem. Soc.* **2001**, *123*, 7821-7830.

(34) Stewart, M. P.; Buriak, J. M. *Angew. Chem. Int. Ed.* **1998**, *37*, 3257-3260.

(35) Sun, Q. Y.; de Smet, L. C. P. M.; van Lagen, B.; Wright, A.; Zuilhof, H.; Sudhölter, E. J. R. *Angew. Chem., Int. Ed.* **2004**, *43*, 1352-1355.

(36) Sun, Q. Y.; de Smet, L. C. P. M.; van Lagen, B.; Giesbers, M.; Thune, P. C.; van Engelenburg, J.; de Wolf, F. A.; Zuilhof, H.; Sudhölter, E. J. R. *J. Am. Chem. Soc.* **2005**, *127*, 2514-2523.

(37) Eves, B. J.; Sun, Q. Y.; Lopinski, G. P.; Zuilhof, H. *J. Am. Chem. Soc.* **2004**, *126*, 14318-14319.

(38) Effenberger, F.; Gotz, G.; Bidlingmaier, B.; Wezstein, M. *Angew. Chem., Int. Ed.* **1998**, *37*, 2462-2464.

(39) Sieval, A. B.; Opitz, R.; Maas, H. P. A.; Schoeman, M. G.; Meijer, G.; Vergeldt, F. J.; Zuilhof, H.; Sudhölter, E. J. R. *Langmuir* **2000**, *16*, 10359-10368.

(40) Sieval, A. B.; van den Hout, B.; Zuilhof, H.; Sudhölter, E. J. R. *Langmuir* **2001**, *17*, 2172-2181.

(41) Mischki, T. K.; Lopinski, G. P.; Wayner, D. D. M. *Langmuir* **2009**, *25*, 5626-5630.

(42) de Smet, L. C. P. M.; Pukin, A. V.; Sun, Q. Y.; Eves, B. J.; Lopinski, G. P.; Visser, G. M.; Zuilhof, H.; Sudhölter, E. J. R. *Appl. Surf. Sci.* **2005**, *252*, 24-30.

(43) de Smet, L. C. P. M.; Stork, G. A.; Hurenkamp, G. H. F.; Sun, Q. Y.; Topal, H.; Vronen, P. J. E.; Sieval, A. B.; Wright, A.; Visser, G. M.; Zuilhof, H.; Sudhölter, E. J. R. *J. Am. Chem. Soc.* **2003**, *125*, 13916-13917.

(44) Faber, E. J.; de Smet, L. C. P. M.; Olthuis, W.; Zuilhof, H.; Sudhölter, E. J. R.; Bergveld, P.; van den Berg, A. *ChemPhysChem* **2005**, *6*, 2153-2166.

(45) Wallart, X.; de Villeneuve, C. H.; Allongue, P. *J. Am. Chem. Soc.* **2005**, *127*, 7871-7878.

(46) Yuan, S. L.; Cai, Z. T.; Jiang, Y. S. *New J. Chem.* **2003**, *27*, 626-633.

(47) Sieval, A. B.; van den Hout, B.; Zuilhof, H.; Sudhölter, E. J. R. *Langmuir* **2000**, *16*, 2987-2990.

(48) Seitz, O.; Böcking, T.; Salomon, A.; Gooding, J. J.; Cahen, D. *Langmuir* **2006**, *22*, 6915-6922.

(49) Boukherroub, R.; Morin, S.; Sharpe, P.; Wayner, D. D. M.; Allongue, P. *Langmuir* **2000**, *16*, 7429-7434.

(50) Faucheux, A.; Gouget-Laemmel, A. C.; de Villeneuve, C. H.; Boukherroub, R.; Ozanam, F.; Allongue, P.; Chazalviel, J. N. *Langmuir* **2006**, *22*, 153-162.

(51) Asanuma, H.; Lopinski, G. P.; Yu, H. Z. *Langmuir* **2005**, *21*, 5013-5018.

(52) Sieval, A. B.; Linke, R.; Heij, G.; Meijer, G.; Zuilhof, H.; Sudhölter, E. J. R. *Langmuir* **2001**, *17*, 7554-7559.

(53) Strother, T.; Cai, W.; Zhao, X. S.; Hamers, R. J.; Smith, L. M. *J. Am. Chem. Soc.* **2000**, *122*, 1205-1209.

(54) Böcking, T.; Salomon, A.; Cahen, D.; Gooding, J. J. *Langmuir* **2007**, *23*, 3236-3241.

(55) Fabre, B.; Hauquier, F. *J. Phys. Chem. B* **2006**, *110*, 6848-6855.

(56) Perring, M.; Dutta, S.; Arafat, S.; Mitchell, M.; Kenis, P. J. A.; Bowden, N. B. *Langmuir* **2005**, *21*, 10537-10544.

(57) Fabre, B.; Hauquier, F.; Herrier, C.; Pastorin, G.; Wu, W.; Bianco, A.; Prato, M.; Hapiot, P.; Zigah, D.; Prasciolu, M.; Vaccari, L. *Langmuir* **2008**, *24*, 6595-6602.

(58) Hauquier, F.; Ghilane, J.; Fabre, B.; Hapiot, P. *J. Am. Chem. Soc.* **2008**, *130*, 2748-2749.

(59) Yang, M.; Teeuwen, R. L. M.; Giesbers, M.; Baggerman, J.; Arafat, A.; de Wolf, F. A.; van Hest, J. C. M.; Zuilhof, H. *Langmuir* **2008**, *24*, 7931-7938.
(60) Scheres, L.; ter Maat, J.; Giesbers, M.; Zuilhof, H. *Small* **2010**, *6*, 642-650.
(61) Ciampi, S.; Böcking, T.; Kilian, K. A.; James, M.; Harper, J. B.; Gooding, J. J. *Langmuir* **2007**, *23*, 9320-9329.
(62) Li, Y.; Wang, D.; Buriak, J. M. *Langmuir* **2009**, *26*, 1232-1238.
(63) Böcking, T.; Killan, K. A.; Gaus, K.; Gooding, J. J. *Langmuir* **2006**, *22*, 3494-3496.
(64) Ng, A.; Ciampi, S.; James, M.; Harper, J. B.; Gooding, J. J. *Langmuir* **2009**, *25*, 13934-13941.
(65) Garcia, R.; Martinez, R. V.; Martinez, J. *Chem. Soc. Rev.* **2006**, *35*, 29-38.
(66) Smith, R. K.; Lewis, P. A.; Weiss, P. S. *Prog. Surf. Sci.* **2004**, *75*, 1-68.
(67) Woodson, M.; Liu, J. *Phys. Chem. Chem. Phys.* **2007**, *9*, 207-225.
(68) Wojtyk, J. T. C.; Tomietto, M.; Boukherroub, R.; Wayner, D. D. M. *J. Am. Chem. Soc.* **2001**, *123*, 1535-1536.
(69) Voicu, R.; Boukherroub, R.; Bartzoka, V.; Ward, T.; Wojtyk, J. T. C.; Wayner, D. D. M. *Langmuir* **2004**, *20*, 11713-11720.
(70) Yin, H. B.; Brown, T.; Wilkinson, J. S.; Eason, R. W.; Melvin, T. *Nucl. Acids Res.* **2004**, *32*, e118.
(71) Xia, Y. N.; Whitesides, G. M. *Angew. Chem., Int. Ed.* **1998**, *37*, 551-575.
(72) Jun, Y.; Le, D.; Zhu, X. Y. *Langmuir* **2002**, *18*, 3415-3417.
(73) Mizuno, H.; Buriak, J. M. *J. Am. Chem. Soc.* **2008**, *130*, 17656-17657.
(74) Rosso, M.; Giesbers, M.; Schroën, K.; Zuilhof, H. *Langmuir* **2009**, *26*, 866-872.
(75) Perring, M.; Mitchell, M.; Kenis, P. J. A.; Bowden, N. B. *Chem. Mater.* **2007**, *19*, 2903-2909.
(76) Mizuno, H.; Buriak, J. M. *ACS Appl. Mater. & Interfaces* **2009**, *1*, 2711-2720.
(77) Yang, M. L.; Zheng, Z. K.; Liu, Y. Q.; Zhang, B. L. *Nanotechnology* **2006**, *17*, 330-337.
(78) Yang, M. L.; Zheng, Z. K.; Liu, Y. Q.; Zhang, B. L. *J. Phys. Chem. B* **2006**, *110*, 10365-10373.
(79) Yang, M.; Wouters, D.; Giesbers, M.; Schubert, U. S.; Zuilhof, H. *ACS Nano* **2009**, *3*, 2887-2900.
(80) Yang, L.; Lua, Y. Y.; Lee, M. V.; Linford, M. R. *Acc. Chem. Res.* **2005**, *38*, 933-942.
(81) Niederhauser, T. L.; Lua, Y. Y.; Jiang, G. L.; Davis, S. D.; Matheson, R.; Hess, D. A.; Mowat, I. A.; Linford, M. R. *Angew. Chem., Int. Ed.* **2002**, *41*, 2353-2356.
(82) Niederhauser, T. L.; Jiang, G. L.; Lua, Y. Y.; Dorff, M. J.; Woolley, A. T.; Asplund, M. C.; Berges, D. A.; Linford, M. R. *Langmuir* **2001**, *17*, 5889-5900.
(83) Lua, Y. Y.; Fillmore, W. J. J.; Yang, L.; Lee, M. V.; Savage, P. B.; Asplund, M. C.; Linford, M. R. *Langmuir* **2005**, *21*, 2093-2097.
(84) Hurley, P. T.; Ribbe, A. E.; Buriak, J. M. *J. Am. Chem. Soc.* **2003**, *125*, 11334-11339.

(85) Khatri, O. P.; Han, J.; Ichii, T.; Murase, K.; Sugimura, H. *J. Phys. Chem. C* **2008**, *112*, 16182-16185.

Chapter 2

Self-Assembly of High-Quality Covalently Bound Organic Monolayers onto Silicon

Abstract. A very mild method has been developed to obtain covalently attached alkenyl monolayers on hydrogen-terminated silicon surfaces at room temperature in the dark. Apart from being the mildest method reported so far for the preparation of such monolayers, their quality – as indicated by water contact angles, XPS and infrared spectroscopy – equals within experimental error that of the best reported monolayers on silicon.

This chapter is published as:
'*Self-Assembly of High-Quality Covalently Bound Organic Monolayers onto Silicon*' Scheres, L.; Arafat, A.; Zuilhof, H. *Langmuir*, **2007**, *23*, 8343-8346.

2.1 Introduction

Over the last decade, the formation of organic monolayers onto hydrogen-terminated silicon (H-Si) has attracted a lot attention due to their potential application in future electronics.[1-5] The direct covalent linkage to the Si surface via a Si–C bond makes these monolayers chemically and thermally very stable compared to e.g. organosilane monolayers on silicon dioxide and thiols on gold.[6] Currently, several methods are available to produce these monolayers, all of which require a certain type of activation, such as heating,[7,8] UV light,[9,10] hydrosilylation catalysts,[11,12] Lewis acid catalysts,[13-15] Grignard and lithium reagents,[16-18] electrochemistry,[19] and chemo-mechanical scribing.[20-22] Covalent attachment without external activation (room temperature in the dark) has recently also been reported.[23] However, this reaction required chemically activated alkynes and very long reaction times (up to 40 h), while the activating ester moiety itself disturbs the packing of the monolayer, resulting in moderate-quality monolayers. This would limit the applicability thereof, as only high-quality organic monolayers proved to possess excellent electrical and passivating properties.[24-28] In the search for mild and generally applicable attachment methods, our group recently reported a visible-light initiated modification of H-Si at room temperature.[29-31] In this chapter, we report the first method to obtain high-quality covalently bound organic monolayers on H-Si with unactivated 1-alkynes at room temperature in the dark. Apart from further extending the range of compounds that can be attached in one step onto a Si surface, the quality of the organic monolayers onto Si prepared in this manner is at least as good as obtained via any other methods we know of.

2.2 Experimental

2.2.1 Materials

PE40/60, EtOH and CH_2Cl_2 were distilled prior to use. For rinsing and contact angle measurements, deionized water (18.3 MΩ cm resistivity) was used. Acetone (Sigma/Honeywell, semiconductor grade) and 40% ammonium fluoride solution (40% NH_4F) (Sigma/Honeywell, semiconductor grade) were used as received. 1-Hexadecyne (ABCR, Germany, 90%) was purified by column chromatography (eluent hexane) to remove trace amounts of 1-bromotetradecane, and subsequently distilled twice before use. Silicon wafers were (111)-oriented single-side and double polished, 475-550 μm thick, n-type, phosphorus doped samples, with a resistivity of 1.0 - 5.0 Ω cm (Siltronix, France).

2.2.2 Monolayer Preparation

Pieces of n-Si(111) were first rinsed several times with acetone followed by sonication for 10 min in acetone. Then the samples were cleaned using an oxygen plasma (set-up used: Harrick PDC-002) for 3 min. Subsequently, the Si(111) substrates were etched in an argon-saturated 40% aqueous NH_4F solution for 15 min under an argon atmosphere. After etching the samples were thoroughly rinsed with deionized water and finally blown dry with a stream of dry nitrogen.

A small three-necked flask equipped with a capillary as argon inlet, a reflux-condenser that was connected to a vacuum pump, and a stopper was charged with 1 gram of neat 1-hexadecyne (GC purity >99.9%) followed by positioning the tip of the capillary in the hexadecyne and turning on the argon flow through the capillary. The pressure in the flask was reduced until approximately 10 mbar and the flask was immersed in an oil bath with the appropriate temperature. The set-up was deoxygenated with argon for at least 30 min. Subsequently, the pressure was raised by filling the set-up with argon until atmospheric pressure was achieved. The freshly etched Si(111) substrate was transferred into hexadecyne, while an argon flow was maintained. The set-up was closed again, the pressure reduced and the capillary was moved away as far as possible from the surface of the liquid to prevent disturbance of the monolayer formation by the strong argon flow. If necessary the reaction flask was heated with an oil bath and kept in ambient light (meaning: standard fluorescent lamps in fume hood were on) or in dark (meaning: dark glassware and wrapped in aluminum foil). To stop the reaction the reaction flask was backfilled with argon until atmospheric pressure and the sample was removed from the hexadecyne. After excessively rinsing with respectively PE40/60, EtOH and CH_2Cl_2, and sonication for 15 min in CH_2Cl_2 to remove physisorbed molecules the samples were blown dry with a stream of dry nitrogen.

2.2.3 Monolayer Characterization

Static water contact angles were measured with a Krüss Erma G-1 goniometer under ambient conditions. Small droplets of 3.0 µl deionized water were dispensed with an Eppendorf micropipette. At least six drops on different locations on the surface were measured. The error of the contact angles is ± 1°.

Infrared reflection-absorption spectra (IRRAS) were collected with a Bruker spectrometer (model Tensor 27) equipped with a variable-angle reflection AutoSeagull

accessory. A Harrick grid polarizer was placed in front of the sample for measuring spectra with p-polarized (parallel) light. The variable-angle reflection accessory was set on 68°, consequently the angle of the incoming light makes an angle of 68° with respect to the surface normal. Further the spectra were taken at a resolution of 4 cm^{-1} by adding 16384 scans and referenced to a clean native oxide-covered silicon sample without further data manipulation.

XPS measurements were performed on a Jeol JPS-9200 system using a standard Al Kα source with an X-ray power of 300 W, an analyzer pass energy of 10 eV and energy resolution < 0.65 eV. All C_{1s} (C–C) peaks were calibrated to a binding energy of 285.0.

2.3 Results and Discussion

Freshly etched Si(111) surfaces were modified at 20-80 °C under an argon atmosphere of ~10 mbar with neat 1-alkyne in ambient light and in the dark. The argon atmosphere was created through a capillary, which allowed us to maintain the low pressure. The resulting monolayers were rinsed with petroleum ether, ethanol, and CH_2Cl_2 and sonicated for 5 min in CH_2Cl_2 before characterization (see Experimental for details).

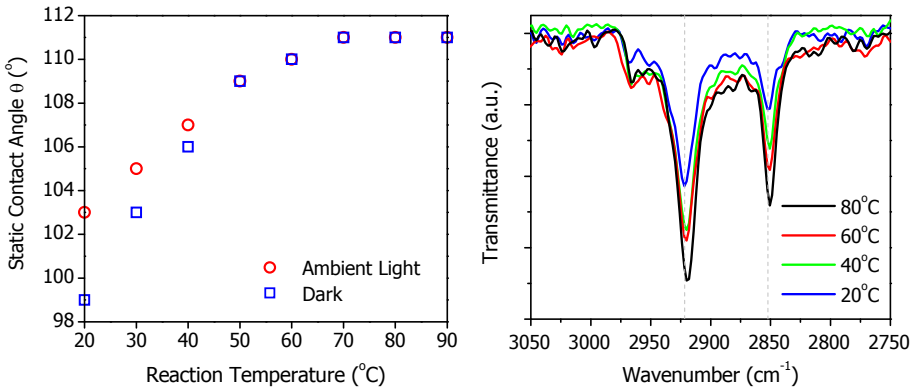

Figure 1. Static water contact angle data (left) and IRRA spectra (right) of 1-hexadecyne-derived monolayers on H-Si(111) after 2 h in ambient light (○) and in the dark (□) as a function of reaction temperature.

The effect of reaction temperature, in ambient light and in the dark, was studied by measuring the static water contact angles (θ) after 2 h, as shown in Figure 1. The static contact angles increase gradually with reaction temperature and already after 2 h at 70 °C

the maximum contact angle of ~111° is obtained, indicative of high-quality densely packed organic monolayers that are at least as good as prepared by other methods.[7-12,16-18,29-31] While absolute values of contact angle data seem to vary slightly in the literature, these values of 111° are in our labs consistently ~1° higher than for monolayers obtained thermally under reflux in mesitylene, which until now yielded the highest-quality alkyl monolayers on Si.[32] Therefore the currently reported method, apart from being the mildest, also yields high-quality monolayers onto Si. Although both reaction conditions, ambient light and in the dark, yield the plateau value of ~111° at the same temperature, below 50 °C considerably lower contact angles are obtained for the reactions in the dark. This demonstrates the catalytic role of light in the formation of monolayers at these temperatures.

Above 50 °C, thermal initiation overwhelms light initiation and the influence of the light becomes negligible. Nevertheless, since the contact angle of a freshly etched Si(111) surface is ~87°, the contact angle data demonstrate that even at 20 °C monolayer formation still occurs under ambient light and even in the dark (after 2 h 103° and 99°, respectively).

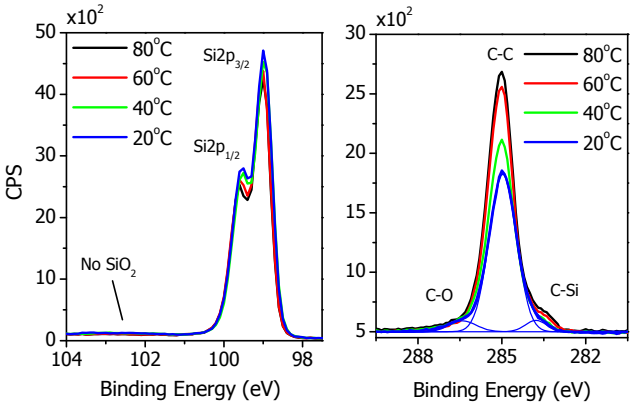

Figure 2. XPS spectra of hexadecenyl monolayers on H-Si(111) prepared for 2 h at 20, 40, 60 and 80 °C, respectively. Si_{2p} narrow scan (left) and C_{1s} narrow scan and deconvolution (right) of the monolayer obtained at 20 °C.

Infrared reflection-absorption spectroscopy (IRRAS)[29,33] displays an increasing intensity of the C–H stretching vibrations with reaction temperature, which supports the gradual growth of the covalently bound organic monolayer. Furthermore, a frequency shift of the antisymmetric (ν_a) and symmetric (ν_s) methylene stretching vibrations was observed from 2922 and 2852 cm^{-1} for an uncompleted monolayer (2 h at 20 °C) to 2919 and 2850 cm^{-1}

for a completed monolayer (2 h at 80 °C). The latter frequencies are indicative of highly ordered covalently bound monolayers with (*E*)-1-hexadecenyl chains.[9,10,34]

In addition, the obtained monolayers were analyzed by X-ray photoelectron spectroscopy (XPS). A narrow scan of the Si_{2p} region (Figure 2, left) shows a decreasing Si_{2p} signal (~99 eV) with increased reaction temperature, which is attributed to the increased coverage of the Si substrate by the hexadecenyl monolayer. In line with this, the C_{1s} emission at ~285 eV (Figure 2, right) increases with reaction temperature with a maximum intensity for the completed monolayer obtained at 80 °C. No significant surface oxidation took place during the reaction as revealed by the absence of a peak at ~103 eV (SiO_2) in the Si_{2p} scan.

Deconvolution of the C_{1s} peak of the 20 °C experiment results in three contributions, as shown in Figure 2. The components at 283.8, 285.0 and 286.4 eV have been assigned to carbon bound to the less electronegative Si (C–Si), aliphatic carbon atoms, and to adventitious contaminations, respectively.[35] The relative intensity of the C–Si contribution is roughly ~1/16 of the total C signal, which is as expected for a covalently bound monolayer with 16 carbon atoms. This XPS spectrum also provides evidence that even at 20 °C covalent Si–C bonds with the Si surface are formed.

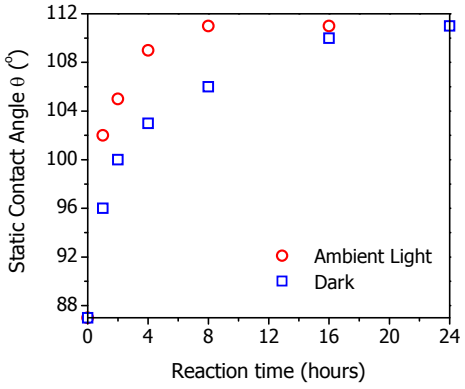

Figure 3. Static contact angle θ of 1-hexadecyne-derived monolayers on H-Si(111) at 20 °C in ambient ligth (○) and in the dark (□) as a function of reaction time.

All data show that the formation of covalently bound monolayers on H-Si(111) even occurs at room temperature. For this reason the study was extended by experiments for elongated reaction times at 20 °C in ambient light and in the dark. The contact angles of the resulting monolayers are plotted as a function of reaction time in Figure 3. In ambient light the maximum contact angle of ~111° is reached within 8 h; in the dark the reaction is

slightly slower, but still within 24 h densely packed organic monolayers are prepared at room temperature!

The effect of the reaction time was also investigated with IRRAS. As can be seen in Figure 4 (left), the intensity of the methylene stretching vibrations grows in time and reaches the highest intensity within 8 h. As for the temperature series, the CH_2 stretching frequencies decrease to 2919 and 2850 cm^{-1} upon completing the monolayer, corresponding to highly ordered organic monolayers.

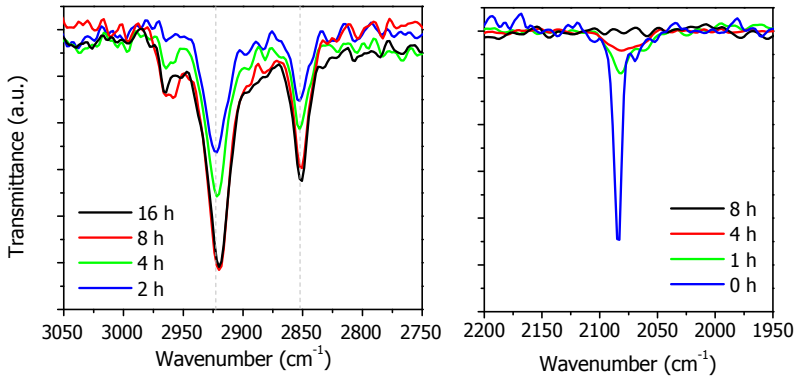

Figure 4. IR data of 1-hexadecyne-derived monolayers on H-Si(111) at 20 °C as a function of reaction time. C–H region (left), Si–H region (right).

Three more experiments confirm the covalent attachment of 1-alkynes to the surface:

(1) IRRAS (Figure 4, right) shows the Si–H stretching vibration (2083 cm^{-1}) of a freshly etched Si(111) surface, which disappears in time upon reaction with 1-hexadecyne at room temperature, in line with the conversion of these sites to Si–C bonds. While it is known that complete disappearance of this Si–H signal does not correspond to complete disappearance of the Si–H sites, but rather to a combination of the reduction of the number of Si–H sites and line broadening of the remaining Si–H signal due to surface heterogeneity, the observed disappearance is at least in line with expectations for this surface reaction.

(2) Attenuated total reflectance infrared (ATR-IR) spectroscopy reveals a clear additional absorbance at 1601 cm^{-1}, assigned to the C=C stretching mode of the hexadecenyl chains (see Figure 5). The peak is rather small, in fact near-impossible to detect by IRRAS (multiple-reflection versus single-reflection sensitivity), which may indicate either that part of the triple C≡C bonds have reacted twice,[36] or simply that the relatively polarity of the C=C is small. Our data do not reveal the relative weight of these two explanations.

(3) Extensive Soxlet extraction with 1,2-dichloroethane (b.p. 84 °C) leaves the monolayer unaffected (no change in e.g. contact angle or AFM-detected topography). All these data exclude the possibility that the detected monolayers result from physical adsorption rather than chemical formation of Si–C bonds.

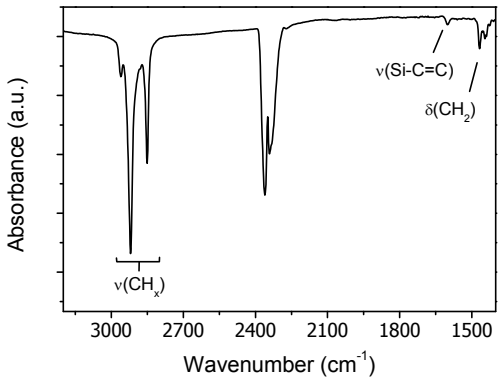

Figure 5. ATR-IR spectrum of a 1-hexadecyne-derived monolayer on H-Si(111) after 16 h at 20 ºC revealing the C=C moiety at 1601 cm^{-1}.

2.4 Conclusions

In summary, we developed a new method to produce covalently bound organic alkenyl monolayers on hydrogen-terminated Si(111) with 1-alkynes at room temperature. The reaction conditions are milder than any previously reported method, while the resulting monolayers approach in fact the highest quality yet reported for organic monolayers on Si. This will further extend the range of functional groups that can be attached directly (i.e. without need of surface-bound conversions) onto Si, whereas it also provides better control over the properties of the modified surface. While we ascribe this improvement partially to the low, yet easily controllable concentration of oxygen under the reaction conditions used, the precise contributions to this improvement are investigated in Chapter 3.

References

(1) Sieval, A. B.; Linke, R.; Zuilhof, H.; Sudhölter, E. J. R. *Adv. Mater.* **2000**, *12*, 1457-1460.

(2) Wayner, D. D. M.; Wolkow, R. A. *J. Chem. Soc., Perkin Trans. 2* **2002**, 23-34.

(3) Buriak, J. M. *Chem. Rev.* **2002**, *102*, 1271-1308.

(4) Boukherroub, R. *Curr. Opin. Solid State Mater. Sci.* **2005**, *9*, 66-72.

(5) Shirahata, N.; Hozumi, A.; Yonezawa, T. *Chem. Rec.* **2005**, *5*, 145-159.

(6) Sung, M. M.; Kluth, G. J.; Yauw, O. W.; Maboudian, R. *Langmuir* **1997**, *13*, 6164-6168.

(7) Linford, M. R.; Fenter, P.; Eisenberger, P. M.; Chidsey, C. E. D. *J. Am. Chem. Soc.* **1995**, *117*, 3145-3155.

(8) Sieval, A. B.; Demirel, A. L.; Nissink, J. W. M.; Linford, M. R.; van der Maas, J. H.; de Jeu, W. H.; Zuilhof, H.; Sudhölter, E. J. R. *Langmuir* **1998**, *14*, 1759-1768.

(9) Cicero, R. L.; Linford, M. R.; Chidsey, C. E. D. *Langmuir* **2000**, *16*, 5688-5695.

(10) Terry, J.; Linford, M. R.; Wigren, C.; Cao, R. Y.; Pianetta, P.; Chidsey, C. E. D. *Appl. Phys. Lett.* **1997**, *71*, 1056-1058.

(11) Boukherroub, R.; Morin, S.; Bensebaa, F.; Wayner, D. D. M. *Langmuir* **1999**, *15*, 3831-3835.

(12) Buriak, J. M.; Stewart, M. P.; Geders, T. W.; Allen, M. J.; Choi, H. C.; Smith, J.; Raftery, D.; Canham, L. T. *J. Am. Chem. Soc.* **1999**, *121*, 11491-11502.

(13) Buriak, J. M.; Allen, M. J. *J. Lumin.* **1998**, *80*, 29-35.

(14) Buriak, J. M.; Allen, M. J. *J. Am. Chem. Soc.* **1998**, *120*, 1339-1340.

(15) Holland, J. M.; Stewart, M. P.; Allen, M. J.; Buriak, J. M. *J. Solid State Chem.* **1999**, *147*, 251-258.

(16) Hurley, P. T.; Nemanick, E. J.; Brunschwig, B. S.; Lewis, N. S. *J. Am. Chem. Soc.* **2006**, *128*, 9990-9991.

(17) Juang, A.; Scherman, O. A.; Grubbs, R. H.; Lewis, N. S. *Langmuir* **2001**, *17*, 1321-1323.

(18) Royea, W. J.; Juang, A.; Lewis, N. S. *Appl. Phys. Lett.* **2000**, *77*, 1988-1990.

(19) Ozanam, F.; Vieillard, C.; Warntjes, M.; Dubois, T.; Pauly, M.; Chazalviel, J. N. *Can. J. Chem. Eng.* **1998**, *76*, 1020-1026.

(20) Niederhauser, T. L.; Jiang, G. L.; Lua, Y. Y.; Dorff, M. J.; Woolley, A. T.; Asplund, M. C.; Berges, D. A.; Linford, M. R. *Langmuir* **2001**, *17*, 5889-5900.

(21) Niederhauser, T. L.; Lua, Y. Y.; Jiang, G. L.; Davis, S. D.; Matheson, R.; Hess, D. A.; Mowat, I. A.; Linford, M. R. *Angew. Chem., Int. Ed.* **2002**, *41*, 2353-2356.

(22) Yang, L.; Lua, Y. Y.; Lee, M. V.; Linford, M. R. *Acc. Chem. Res.* **2005**, *38*, 933-942.

(23) Liu, Y.; Yamazaki, S.; Yamabe, S.; Nakato, Y. *J. Mater. Chem.* **2005**, *15*, 4906-4913.

(24) Liu, Y. J.; Yu, H. Z. *ChemPhysChem* **2002**, *3*, 799-802.

(25) Webb, L. J.; Lewis, N. S. *J. Phys. Chem. B* **2003**, *107*, 5404-5412.

(26) Faber, E. J.; de Smet, L. C. P. M.; Olthuis, W.; Zuilhof, H.; Sudhölter, E. J. R.; Bergveld, P.; van den Berg, A. *ChemPhysChem* **2005**, *6*, 2153-2166.

(27) Seitz, O.; Böcking, T.; Salomon, A.; Gooding, J. J.; Cahen, D. *Langmuir* **2006**, *22*, 6915-6922.

(28) Faber, E. J.; Sparreboom, W.; Groeneveld, W.; de Smet, L. C. P. M.; Bomer, J.; Olthuis, W.; Zuilhof, H.; Sudhölter, E. J. R.; Bergveld, P.; van den Berg, A. *ChemPhysChem* **2007**, *8*, 101-112.

(29) Sun, Q. Y.; de Smet, L. C. P. M.; van Lagen, B.; Giesbers, M.; Thune, P. C.; van Engelenburg, J.; de Wolf, F. A.; Zuilhof, H.; Sudhölter, E. J. R. *J. Am. Chem. Soc.* **2005**, *127*, 2514-2523.

(30) Sun, Q. Y.; de Smet, L. C. P. M.; van Lagen, B.; Wright, A.; Zuilhof, H.; Sudhölter, E. J. R. *Angew. Chem., Int. Ed.* **2004**, *43*, 1352-1355.

(31) de Smet, L. C. P. M.; Stork, G. A.; Hurenkamp, G. H. F.; Sun, Q. Y.; Topal, H.; Vronen, P. J. E.; Sieval, A. B.; Wright, A.; Visser, G. M.; Zuilhof, H.; Sudhölter, E. J. R. *J. Am. Chem. Soc.* **2003**, *125*, 13916-13917.

(32) Sieval, A. B.; Vleeming, V.; Zuilhof, H.; Sudhölter, E. J. R. *Langmuir* **1999**, *15*, 8288-8291.

(33) Brunner, H.; Mayer, U.; Hoffmann, H. *Appl. Spectrosc.* **1997**, *51*, 209-217.

(34) Ulman, A. *Chem. Rev.* **1996**, *96*, 1533-1554.

(35) Wallart, X.; de Villeneuve, C. H.; Allongue, P. *J. Am. Chem. Soc.* **2005**, *127*, 7871-7878.

(36) Sieval, A. B.; Opitz, R.; Maas, H. P. A.; Schoeman, M. G.; Meijer, G.; Vergeldt, F. J.; Zuilhof, H.; Sudhölter, E. J. R. *Langmuir* **2000**, *16*, 10359-10368.

Chapter 3

Self-Assembly of Organic Monolayers onto Hydrogen-Terminated Silicon: 1-Alkynes are Better than 1-Alkenes

Abstract. In Chapter 2 a new method for preparation of high-quality organic monolayers with 1-alkynes at room temperature in the dark, i.e. without any external activation, is described. To pinpoint the precise origin of this self-assembly process, and to compare the reactivity of 1-alkenes and 1-alkynes towards hydrogen-terminated Si(111), we followed the gradual formation of both monolayers at room temperature by static water contact angles measurements. Subsequently, attenuated total reflection infrared spectroscopy (ATR-IR) and X-ray photoelectron spectroscopy (XPS) were used to obtain detailed information about the structure and quality of the resulting monolayers. Our data clearly demonstrate that 1-alkynes are considerably more reactive towards H–Si(111) than 1-alkenes. 1-Alkynes are able to self-assemble into densely packed hydrophobic monolayers without any external activation, i.e. at room temperature under ambient light and even in the dark, while for 1-alkenes under the same conditions hardly any reactivity towards H–Si(111) was observed. The self-assembly of 1-alkynes on H–Si(111) at room temperature is explained by 3 factors: the higher nucleophilicity of 1-alkynes, which results in a facile attack at the electron-hole pairs at the H–Si surface and an easy Si–C bond formation, the stabilization of the β-radical by delocalization over the double bond, and the lower energy barrier encountered for H-abstractions.

This chapter is published as:
'*Self-Assembly of Organic Monolayers onto Hydrogen-Terminated Silicon: 1-Alkynes are Better than 1-Alkenes*' Scheres, L.; Giesbers, M.; Zuilhof, H. *Langmuir*, **2010**, ASAP, doi: la100858q.

3.1 Introduction

Organic monolayers on oxide-free silicon are directly bound to silicon via a strong covalent Si–C bond and therefore these monolayers are thermally stable,[1] and chemically more stable than corresponding alkoxyl monolayers[2] and organosilane monolayers on oxide surfaces.[3] Furthermore, the absence of an intermediate SiO_2 layer results in a well-defined monolayer-silicon interface that allows direct electronic coupling between the organic functionality and the silicon substrate. As a consequence these monolayers possess great potential in the fields of biosensing,[4-9] molecular electronics[9-19] and solar cells.[6,7,16,17]

Since the seminal work of Chidsey et al.,[3] numerous new methods have been reported, and now organic monolayers on oxide-free silicon can be prepared under a wide variety of conditions with both 1-alkenes and 1-alkynes. Although initially harsh conditions (heat,[3,20-22] radical initiators[3] and UV irradiation[23,24]) were required for planar silicon surfaces, over the last decade our group has developed methods that allowed significantly milder reaction conditions, and we recently reported mild visible light-induced monolayer formation in dilute solutions,[25,26] and even monolayer formation at room temperature in the dark (Chapter 2).[27] We note that, except for the last mentioned method, in all cases a certain type of external activation is required to attach the 1-alkenes or 1-alkynes to the H–Si surface.

Currently it is widely accepted that monolayer formation occurs via a radical-chain mechanism on the surface (Figure 1), even during mild visible light-induced monolayer assembly at room temperature.[3,23,28] However, the exact initiation mechanism of the radical chain reaction, especially under these mild reaction conditions, is not completely understood yet. Radical initiators[3] and UV light[23,24] are capable of breaking the H–Si bond homolytically, which yields silicon radicals (silicon dangling bonds) that can act as starting point for the radical chain propagation (Figure 1, route 1). In contrast, when using thermal conditions[3,21,29,30] or visible light at room temperature,[25,26,28] insufficient energy for homolytic cleavage of the strong H–Si bond is added. Nevertheless, as evidenced by scanning tunnelling microscopy (STM), monolayer formation still occurs via island growth.[28,31,32] This implies that propagation of the radical chain reaction still proceeds, but a different initiation mechanism must be active under mild reaction conditions. Up to now four initiation mechanisms have been proposed:

(1) For thermally induced monolayer formation (150 - 200 °C), a non-radical mechanism via a four-atom transition state between the terminal double bond of an alkene and H–Si surface bond has been proposed by Coletti et al.[33] Their results clearly indicate that this concerted route is energetically possible at elevated temperatures, but probably not at room

temperature. In addition, it is unlikely that this four-atom transition state can act as starting point for a radical chain reaction, because the attachment of the first molecule lacks the formation of silicon dangling bond (silicon radical) that can start the chain reaction.

(2) Recently, Mischki et al.[31] demonstrated the key role of degraded hydrocarbons on the initiation of the radical chain mechanism under thermal conditions (150 °C). The silanol groups on the glass surface of the reaction vessel catalyze the degradation of hydrocarbons, which subsequently initiate the radical chain mechanism. However, for visible-light irradiation at room temperature negligible degradation of hydrocarbons by silanol groups is expected.

(3) Inspired by the dopant dependence as observed for visible light-induced monolayer formation at room temperature, Sun et al.[25] proposed a initiation mechanism based on photoexcited electron-hole pairs (excitons) near the silicon surface. These electron-hole pairs are susceptible to nucleophilic attack by 1-alkene or 1-alkyne resulting in the formation of a Si–C bond and a carbon radical at the β-position (Figure 1, route 2). Not much later, DFT calculations by Kanai and Selloni,[34] demonstrated the necessity of photo-excitation for the initiation of the radical chain reaction on H–Si(111) at room temperature.

(4) In agreement with Mischki et al.,[31] we note that independent of the reaction conditions used, it is difficult to completely exclude the role of trace amounts of molecular oxygen as a source of silyl radicals that can start the chain reaction.

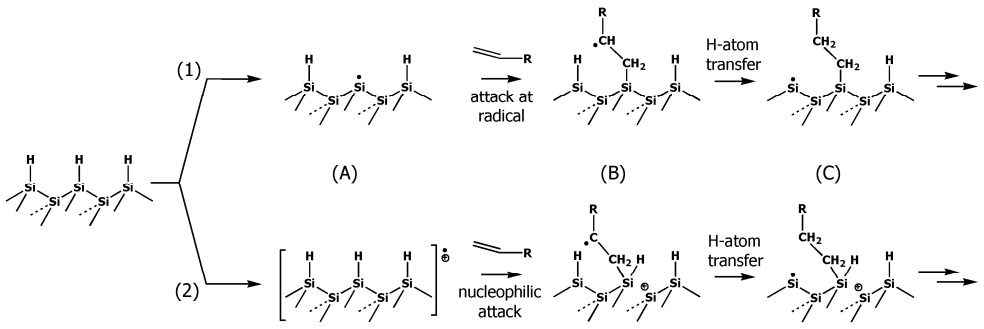

Figure 1: Proposed radical chain mechanisms for 1-alkenes (1) with radical initiators or UV irradiation and (2) with thermal activation or visible-light irradiation.

As mentioned before, both 1-alkenes and 1-alkynes can be used for monolayer assembly on H–Si surfaces. On H–Si(111), 1-alkenes result in alkyl monolayers with a Si–C–C linkage to the silicon surface, while 1-alkynes yield alkenyl monolayers with a Si–C=C

linkage (Figure 2).[3,23,27] Although the structural difference between both linkages is rather small, it significantly affects the final monolayer structure, that is, for alkyl monolayers the maximum surface coverages was determined to be approximately 50%,[3,23,30,35-38] whereas for alkenyl monolayers a surface coverage close to 65% was found (see Chapter 4).[38] Concerning the reactivity – in contrast to hydrosilylation reactions conducted in solution,[39] for which clear differences were observed – no detailed reactivity difference of 1-alkenes and 1-alkynes towards H–Si(111) surfaces have been reported yet. Most probably, because all reported monolayer preparation methods use a large excess of activation energy (thermal, UV, or visible light) in combination with the appropriate reaction times to obtain completed monolayers, a possible reactivity difference of 1-alkenes and 1-alkynes was imperceptible. However, we note that during the preparation of this chapter an elegant approach, using mixtures of bifunctional 1-alkenes and 1-alkynes, to compare monolayer assembly with 1-alkenes and 1-alkynes on H–Si(100) under thermal conditions (120 °C) was published that showed 1-alkynes to be more reactive than 1-alkenes.[40] In addition, as evidenced by recent work of Lee et al.,[41] who observed some unanticipated C=C bonds in alkyl monolayers prepared onto H–Si(100), the precise mechanism of the surface-bound hydrosilylation continues to have some unresolved issues. Clarification of this mechanism leading to a better fundamental understanding of passivation and functionalization of hydrogen-terminated silicon by organic monolayers is valuable, as this will enhance the development of new and stable molecular electronic and biosensor devices on oxide-free Si substrates.

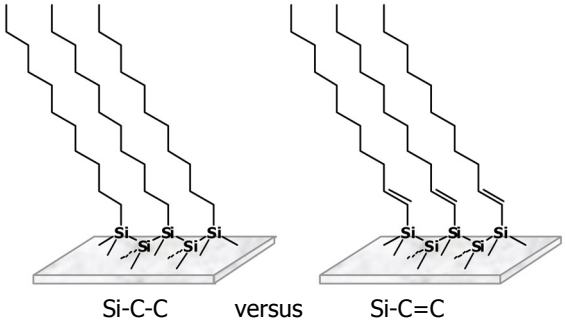

Figure 2: Different linkage of organic monolayers on H–Si(111); alkyl monolayer (left) and alkenyl monolayer (right).

Therefore, to pinpoint the precise origin of the observed self-assembly process (i.e. monolayer formation at room temperature in the dark),[27] and to achieve a more

comprehensive understanding of monolayer formation on H–Si(111), we compared the reactivity of 1-alkenes and 1-alkynes towards H–Si(111) by following the gradual formation of both monolayers at room temperature by static water contact angles measurements. Subsequently, attenuated total reflection infrared spectroscopy (ATR-IR) and X-ray photoelectron spectroscopy (XPS) were used to obtain detailed information about the structure, completeness and quality of the resulting monolayers.

3.2 Experimental Section

3.2.1 Materials

PE40/60, EtOH and CH_2Cl_2 were distilled prior to use. For rinsing and contact angle measurements, deionized water (18.3 MΩ cm resistivity) was used. Acetone (Sigma/Honeywell, semiconductor grade) and 40% ammonium fluoride solution (40% NH_4F) (Sigma/Honeywell, semiconductor grade) were used as received. 1-Hexadecene (Fluka, +99%) was distilled twice before use and 1-hexadecyne (ABCR, Germany, 90%) was purified by column chromatography (eluent hexane) to remove trace amounts of 1-bromotetradecane, and subsequently distilled twice before use. Silicon wafers were (111)-oriented single-side and double polished, 475-550 μm thick, n-type, phosphorus doped samples, with a resistivity of 1.0 - 5.0 Ω cm (Siltronix, France).

3.2.2 Monolayer Preparation

Pieces of n-Si(111) wafer were first rinsed several times with acetone, followed by sonication for 10 min in acetone. Then the samples were cleaned using oxygen plasma (Harrick PDC-002 setup) for 3 min Subsequently, the Si(111) substrates were etched in an argon-saturated 40% aqueous NH_4F solution for 15 min under an argon atmosphere. After being etched, the samples were rinsed with water and finally blown dry with a stream of nitrogen. A small three-necked flask, equipped with a thin capillary as the argon inlet and a reflux-condenser connected to a vacuum pump, was charged with neat 1-hexadecyne or 1-hexadecene (GC purity >99.9%). The tip of the capillary was positioned in the reactive compound and the argon flow through the capillary was turned on. Subsequently, the pressure in the flask was reduced to approximately 10 mbar and the setup was deoxygenated with argon for at least 30 min. Subsequently, the pressure was raised by filling the setup with argon until atmospheric pressure was achieved. The freshly etched

Si(111) substrate was transferred into the reactive compound while an argon flow was maintained. The setup was closed again, the pressure was reduced, and the capillary was moved away as far as possible from the surface of the liquid to prevent the disturbance of monolayer formation by the strong argon flow. The reactions were performed at room temperature under ambient light (i.e., standard fluorescent lamps in the fume hood were on) or in the dark (i.e., in dark glassware and wrapped in aluminium foil). To stop the reaction, the reaction flask was backfilled with argon until atmospheric pressure was attained, and the sample was taken out. After rinsing extensively with PE40/60, EtOH, and CH_2Cl_2 and sonicating for 5 min in CH_2Cl_2 to remove physisorbed molecules, the samples were blown dry with a stream of dry nitrogen.

3.2.3 Monolayer Characterization

Static water contact angles were measured with an automated Krüss DSA 100 goniometer. At least six small droplets of 2.0 μl deionized water were dispensed and the contact angles were determined using a Tangent 2 fitting model. The error in the contact angles is less than 1°.

Attenuated total reflectance infrared (ATR-IR) spectra were collected with a Bruker spectrometer (model Tensor 27) equipped with a Harrick ATR accessory and MCT-detector. A Harrick grid polarizer was placed in front of the sample for measuring spectra with p-polarized (parallel) light. Double polished n-Si(111) wafers were cut into pieces of 5 × 1 cm and polished to obtain ATR-crystals with 45º bevels (± 100 internal reflections). The spectra were taken at a resolution of 4 cm^{-1} by adding 2048 scans while flushing with dry N_2, and were referenced to a clean native oxide-covered ATR-crystal. A slight linear baseline correction was applied.

X-ray photoelectron spectroscopy (XPS) analysis was performed using a JPS-9200 photoelectron spectrometer (JEOL, Japan). The high-resolution spectra were obtained under UHV conditions using monochromatic Al Kα X-ray radiation at 12 kV and 25 mA, using an analyzer pass energy of 10 eV. All high-resolution spectra were corrected with a linear background before fitting.

3.3 Results and Discussion

To examine the influence of the terminal functionality on the kinetics of monolayer formation, pieces of freshly etched H–Si(111) were modified with neat 1-hexadecyne or 1-hexadecene at 20 ºC, with reaction times of up to 16 h. The static contact angles (θ) of the resulting monolayers are plotted in Figure 3. Although for both 1-hexadecene and 1-hexadecyne the contact angles increased gradually in time, monolayer formation with 1-hexadecyne resulted in all cases in higher contact angles compared to the corresponding 1-hexadecene experiments. With 1-hexadecyne, the plateau value of 110 - 111º, indicative of densely packed hydrophobic monolayers, was reached within 8 h. However, with 1-hexadecene even after doubling the reaction time to 16 h, the contact angles did not exceed ~100º, a value indicative of incomplete and disordered monolayers.

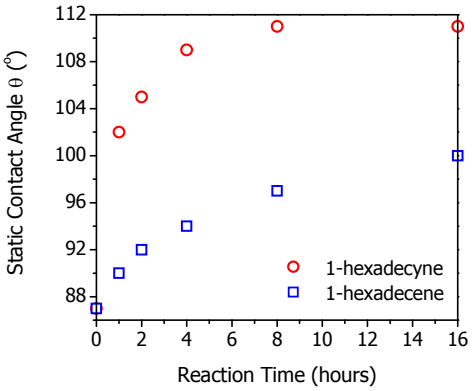

Figure 3. Static contact angle θ of 1-hexadecyne (○) and 1-hexadecene-derived (□) monolayers on H–Si(111) at 20 °C under ambient light as a function of reaction time.

To further investigate the reactivity difference, ATR-IR spectra of 1-hexadecyne and 1-hexadecene-derived monolayers were recorded after 16 h reaction at 20 °C. With ATR-IR, detailed information about the molecular order in the monolayers can be obtained. For highly ordered (i.e. crystalline) monolayers, the peak positions of the antisymmetric (ν_a) and symmetric (ν_s) C–H stretching vibrations can be found at 2918 ± 1 and 2851 ± 1 cm^{-1}, respectively; whereas for disordered (i.e., liquid) monolayers, these frequencies shift to 2924 ± 1 and 2854 ± 1 cm^{-1}, respectively.[19,42] As shown in Figure 4, the completed 1-hexadecyne monolayer results in a significantly higher intensity of the C–H stretching vibrations than the uncompleted 1-hexadecene monolayer. The frequencies of the

antisymmetric and symmetric C-H stretching vibrations shift from 2919 and 2851 cm^{-1} for the completed and highly ordered 1-hexadecyne-derived monolayer to 2924 and 2854 cm^{-1} for the incomplete and disordered 1-hexadecene-derived monolayer. Furthermore, a considerable peak at 2083 cm^{-1}, attributed to the H–Si stretching vibration, is still present in the 1-hexadecene-derived spectrum and corresponds to a large number of unreacted H–Si sites at the silicon surface. The presence of this substantial H–Si peak does not only demonstrate that the 1-hexadecene monolayer is far from complete, but also underlines that the extra efforts made to exclude molecular oxygen during reaction, i.e. argon atmosphere at 10 mbar,[27] prevent oxidation of the H–Si surface over a prolonged period of time. In addition, in line with the observation that the maximum coverage of an alkenyl monolayer on H–Si(111) is close to 65% (see Chapter 4),[38] no H–Si peak could be detected at the 1-hexadecyne-modified Si surface. Due to surface heterogeneity upon monolayer formation, the H–Si signal broadens and the remaining H–Si bonds become hard to detect.[43,44] As shown in Figure 2, monolayers prepared with 1-alkenes and 1-alkynes are differently linked to the H–Si(111) surface. This difference in bonding is clearly visualized by the presence of a small peak in the 1-hexadecyne-derived spectrum at 1601 cm^{-1}, which is assigned to the C=C stretching mode of the Si–C=C moiety, and is therefore absent in the 1-hexadecene spectrum.[3,23,27] Furthermore, we note that the side reaction that is responsible for the unanticipated C=C bonds in alkyl monolayer prepared by thermal reaction on Si(100), as described by Lee et al.,[41] seems to be negligible under the mild reaction conditions under current investigation.

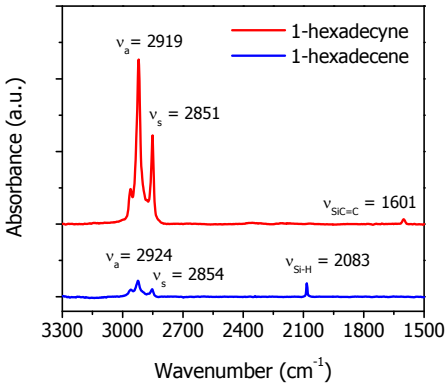

Figure 4. ATR-IR spectra of 1-hexadecyne-derived (upper, red) and 1-hexadecene-derived (lower, blue) monolayers on H–Si(111) after 16 h at 20 °C under ambient light.

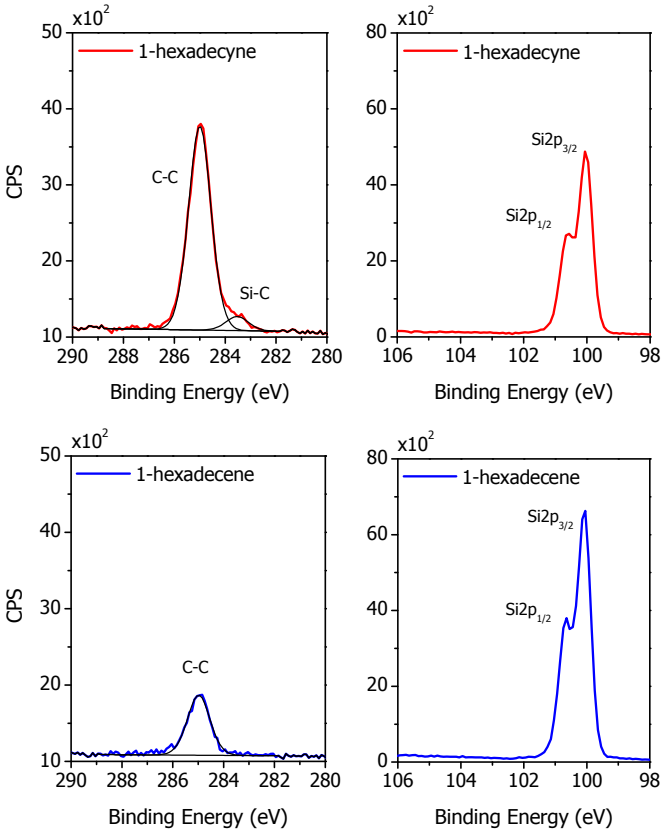

Figure 5. XPS narrow scans of C_{1s} and Si_{2p} regions of 1-hexadecene (bottom, blue) and 1-hexadecyne-derived (top, red) monolayers on H–Si(111) after 16 h at 20 °C under ambient light.

The obtained monolayers were also analyzed by XPS and the resulting C_{1s} and Si_{2p} narrow scans are depicted in Figure 5. In line with the ATR-IR data, a large difference in the intensity of C_{1s} emission has been observed, clearly displaying the minimal reactivity of the 1-hexadecene and the relatively high reactivity of 1-hexadecyne at room temperature. Consequently, the 1-hexadecene-modified Si surface yields a large Si_{2p} peak, and the more reactive 1-hexadecyne results in a modified Si surface with a relatively small Si_{2p} emission due to the increased coverage of the Si substrate by the hexadecenyl monolayer. We note that for both monolayers, and in particular the 1-hexadecene-treated Si surface, the Si_{2p} narrow scan has a completely flat baseline around 103 - 104 eV, in line with the absence of even trace amounts of silicon oxide (SiO_2). For the incomplete 1-hexadecyl monolayer this

is in excellent agreement with the presence of the H–Si peak in the ATR-IR spectrum, even after 16 h of reaction.

To explore the influence of ambient light on the monolayer formation under these mild conditions, we followed monolayer formation in the dark (at room temperature) by static contact angle (θ) measurements. The resulting plot is shown in Figure 6, and a comparison with the ambient light data in Figure 3 clearly displays the catalytic role of light on the monolayer formation at room temperature. With 1-hexadecyne under ambient light, the maximum contact angle of 110 - 111° is reached within 8 h, while in the dark it takes at least 24 h. Similarly, also monolayer formation with 1-hexadecene is slower in the dark and after 24 h of reaction a contact angle of only 97° has been measured.

The above data clearly show that there is a significant difference in the reactivity of 1-alkenes and 1-alkynes towards H–Si(111). 1-Alkynes are reactive enough to form densely packed monolayers at room temperature within 8 (ambient light) to 24 h (dark), whereas with 1-alkenes only incomplete monolayers were obtained. The low reactivity of even pure 1-alkenes towards H–Si surfaces at room temperature in the dark is in good agreement with earlier work of Sun et al.,[25] who observed negligible monolayer formation in dilute solutions of 1-alkenes at room temperature in the dark.

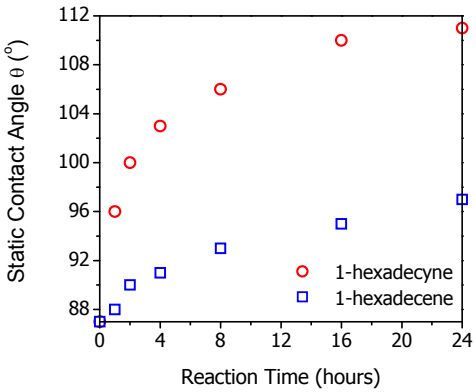

Figure 6. Static contact angle θ of 1-hexadecyne (○) and 1-hexadecene-derived (□) monolayers on H–Si(111) at 20 °C in the dark as a function of reaction time.

In all our experiments freshly etched, fully hydrogen-terminated Si(111) surfaces were used. Hence, it is unlikely that silicon dangling bonds, which can act as an initiation point for the radical chain reaction, are present on a sufficiently large scale at these nearly defect-free H–Si(111) surfaces to account for the formation of densely packed monolayers.[45] Since

under the mild reaction conditions used, homolytic cleavage of the H–Si bonds is also not expected to occur, a mild initiation mechanism must be active during our experiments. Of the four initiation mechanisms discussed in the Introduction, the first two (the concerted non-radical route and the initiation by degraded 1-alkenes) are only feasible at elevated temperatures and not at room temperature. Also the third mechanism, initiation by trace amounts of molecular oxygen, seems unlikely, because the extra efforts made to exclude molecular oxygen from the reaction flask (argon atmosphere at 10 mbar) turned out to be very efficient. In fact, even after 16 h in almost unreactive 1-hexadecene a sharp peak corresponding to the H–Si stretching vibration was present in the ATR spectrum (Figure 4), while in the XPS Si_{2p} narrow scans not even trace amounts of SiO_2 were detected (see Figure 5). Consequently, the exciton-based mechanism,[25,26,32] which has subsequently been supported by the DFT calculations of Kanai and Selloni,[34] is the only remaining and viable initiation route. In this mechanism an electron-hole pair is formed by excitation of an electron from the valence band into the conduction band, yielding a surface that is susceptible to nucleophilic attack by the reactive compound. This means that – due to the higher nucleophilicity of 1-alkynes[46] – the reaction with the H–Si surface (i.e. Si–C bond formation. Figure 1, from A to B) will be easier for 1-alkynes than for 1-alkenes, in line with the observed 1-alkene/1-alkyne reactivity difference.

The excitation of a valence band electron into the conduction band can be achieved either by thermal excitation or by photo-excitation, and the latter is also for non-UV light expected to be wavelength dependent. Photo-excitation occurs at all wavelengths short enough to overcome the silicon bandgap of 1.1 eV.[47] However, the longer the wavelengths used, the deeper in the Si substrate the light is absorbed: i.e., 400 nm light has an absorption depth of ~100 nm and Si has an absorption coefficient α of $\sim 1 \times 10^5$ cm^{-1} at this wavelength, whereas for 1000 nm light this is ~100 μm and 1×10^2 cm^{-1}, respectively.[47] This implies that electron-hole pairs created using shorter wavelengths are formed closer to the surface. Of course, the carrier diffusion length L of n-Si is also in the order of microns and therefore the charges created deep in the Si are still able to reach the surface.[47,48] But, since the latter (transport) does not fully dominate the first phenomenon (formation), likely the longer wavelengths will be less efficient in exciton generation near the Si surface. Therefore, as observed by Sun et al.,[25] the wavelength has an substantial influence on the rate of monolayer formation. Our experiments were performed under ambient light, i.e. using long wavelengths (400 - 850 nm; maximum intensity peaks of the lamps used to illuminate our labs were found at 440, 560 and 630 nm) with relatively low intensity. As a result the efficiency of electron-hole pair formation near the Si surface will be low,

however, due to the reactivity of 1-alkynes this is still enough to form well-ordered monolayers within 8 h at room temperature. In the dark photo-excitation cannot occur, and the – still occurring, albeit slower – monolayer formation in the dark is thus attributed to thermal excitation, as at room temperature sufficient thermal energy is available to form electron-hole pairs in doped silicon that can induce the radical chain reaction.[47] Of course, the number of excitons generated by thermal excitation in the dark is considerably smaller than the number of excitons formed by photo-excitation by ambient light,[47] and this is in line with our contact angle data (Figure 3 and 6), which clearly demonstrate slower monolayer formation in the dark.

In addition, the terminal alkyne functionality does not only affect the initiation step of the monolayer formation, but also the intermediate β-radical state and the corresponding propagation step (Figure 7). As shown by DFT studies of Takeuchi et al.[49] alkenes will encounter both less stabilization of the radical intermediates than alkynes (relative ease of formation of alkyl vs. vinyl radicals) and a higher activation barrier for H-atom abstraction from the H–Si surface than the alkynes. As a result, propagation is expected to be more facile for alkynes, thus further favoring alkyne reactivity. The observation that alkenes react at all, if only very slowly, at room temperature, may seem unlikely based on Takeuchi's studies of the reactivity of ethene,[49] but as shown by Wolkow,[50] longer alkyl chains display favorable dispersion interactions, which may actually just tilt the balance towards noticeable reactivity. Finally, the larger overall reaction exothermicity as calculated for alkynes suggests not only faster monolayer formation with 1-alkynes but indicates also a more stable and a more densely packed organic monolayer, which might support the superior oxidation-inhibiting nature of the Si–C=C linkage (see Chapter 4 and 5).[51]

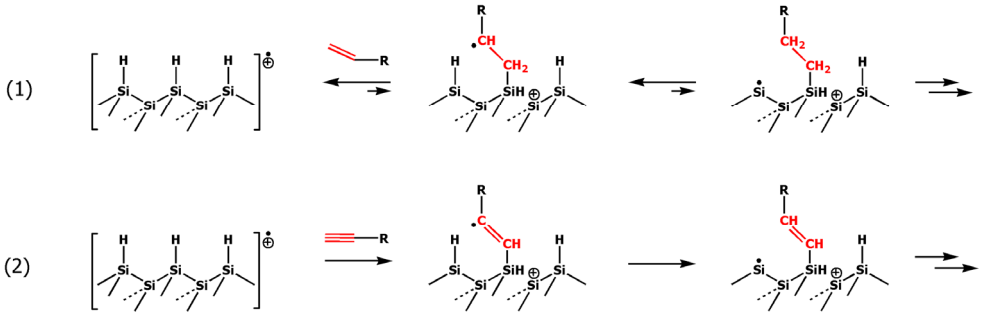

Figure 7. Representation of the proposed radical chain mechanism and the corresponding reactivity difference of (1) 1-alkenes and (2) 1-alkynes.

3.4 Conclusions

1-Alkynes are considerably more reactive towards H–Si(111) than 1-alkenes, as follows from the development of the static water contact angle during the reaction. The combination of higher intrinsic reactivity, better stabilized intermediates and an overall more exothermic reaction allows 1-alkynes to self-assemble into high-quality, densely packed hydrophobic monolayers without any external activation, i.e. at room temperature under ambient light and even in the dark. Under the same conditions hardly any reactivity towards H–Si(111) was observed for 1-alkenes. The self-assembly process of 1-alkynes on H–Si(111) at room temperature is initiated by the nucleophilic attack of 1-alkynes on positive charges near the surface, resulting from photochemically or thermally induced excitons near the H–Si surface. 1-Alkynes thus form more densely packed monolayers that are less prone to oxidation than feasible with 1-alkenes and these monolayers are also conveniently produced at a higher rate – in short: monolayers derived from 1-alkynes are better. This very mild procedure provides an easier access to densely packed monolayers, which is expected to contribute to the development of new and stable molecular electronic and biosensor devices on oxide-free Si substrates.[10]

References:

(1) Sung, M. M.; Kluth, G. J.; Yauw, O. W.; Maboudian, R. *Langmuir* **1997**, *13*, 6164-6168.

(2) Sano, H.; Maeda, H.; Ichii, T.; Murase, K.; Noda, K.; Matsushige, K.; Sugimura, H. *Langmuir* **2009**, *25*, 5516-5525.

(3) Linford, M. R.; Fenter, P.; Eisenberger, P. M.; Chidsey, C. E. D. *J. Am. Chem. Soc.* **1995**, *117*, 3145-3155.

(4) Boukherroub, R. *Curr. Opin. Solid State Mater. Sci.* **2005**, *9*, 66-72.

(5) Buriak, J. M. *Chem. Rev.* **2002**, *102*, 1271-1308.

(6) Hamers, R. J. *Ann. Rev. Anal. Chem.* **2008**, *1*, 707-736.

(7) Hamers, R. J. In *Bioelectronics: From Theory to Applications* Willner, I., Katz, E., Eds. 2005; Vol. Chapter 7, p 209-230.

(8) Wayner, D. D. M.; Wolkow, R. A. *J. Chem. Soc., Perkin Trans. 2* **2002**, 23-34.

(9) Vilan, A.; Yaffe, O.; Biller, A.; Salomon, A.; Kahn, A.; Cahen, D. *Adv. Mater.* **2009**, *22*, 140-159.

(10) Yaffe, O.; Scheres, L.; Puniredd, S. R.; Stein, N.; Biller, A.; Lavan, R. H.; Shpaisman, H.; Zuilhof, H.; Haick, H.; Cahen, D.; Vilan, A. *Nano Lett.* **2009**, *9*, 2390-2394.

(11) Hiremath, R. K.; Rabinal, M. K.; Mulimani, B. G.; Khazi, I. M. *Langmuir* **2008**, *24*, 11300-11306.

(12) Faber, E. J.; de Smet, L. C. P. M.; Olthuis, W.; Zuilhof, H.; Sudhölter, E. J. R.; Bergveld, P.; van den Berg, A. *ChemPhysChem* **2005**, *6*, 2153-2166.

(13) Faber, E. J.; Sparreboom, W.; Groeneveld, W.; de Smet, L. C. P. M.; Bomer, J.; Olthuis, W.; Zuilhof, H.; Sudhölter, E. J. R.; Bergveld, P.; van den Berg, A. *ChemPhysChem* **2007**, *8*, 101-112.

(14) Liu, Y. J.; Yu, H. Z. *ChemPhysChem* **2002**, *3*, 799-802.

(15) Liu, Y. J.; Yu, H. Z. *ChemPhysChem* **2003**, *4*, 335-342.

(16) Salomon, A.; Böcking, T.; Chan, C. K.; Amy, F.; Girshevitz, O.; Cahen, D.; Kahn, A. *Phys. Rev. Lett.* **2005**, *95*.

(17) Salomon, A.; Böcking, T.; Seitz, O.; Markus, T.; Amy, F.; Chan, C.; Zhao, W.; Cahen, D.; Kahn, A. *Adv. Mater.* **2007**, *19*, 445-450.

(18) Seitz, O.; Böcking, T.; Salomon, A.; Gooding, J. J.; Cahen, D. *Langmuir* **2006**, *22*, 6915-6922.

(19) Aswal, D. K.; Lenfant, S.; Guerin, D.; Yakhmi, J. V.; Vuillaume, D. *Anal. Chim. Acta* **2006**, *568*, 84-108.

(20) Sieval, A. B.; Linke, R.; Zuilhof, H.; Sudhölter, E. J. R. *Adv. Mater.* **2000**, *12*, 1457-1460.

(21) Sieval, A. B.; Opitz, R.; Maas, H. P. A.; Schoeman, M. G.; Meijer, G.; Vergeldt, F. J.; Zuilhof, H.; Sudhölter, E. J. R. *Langmuir* **2000**, *16*, 10359-10368.

(22) Sieval, A. B.; Vleeming, V.; Zuilhof, H.; Sudhölter, E. J. R. *Langmuir* **1999**, *15*, 8288-8291.

(23) Cicero, R. L.; Linford, M. R.; Chidsey, C. E. D. *Langmuir* **2000**, *16*, 5688-5695.

(24) Effenberger, F.; Gotz, G.; Bidlingmaier, B.; Wezstein, M. *Angew. Chem., Int. Ed.* **1998**, *37*, 2462-2464.

(25) Sun, Q. Y.; de Smet, L. C. P. M.; van Lagen, B.; Giesbers, M.; Thune, P. C.; van Engelenburg, J.; de Wolf, F. A.; Zuilhof, H.; Sudhölter, E. J. R. *J. Am. Chem. Soc.* **2005**, *127*, 2514-2523.

(26) Sun, Q. Y.; de Smet, L. C. P. M.; van Lagen, B.; Wright, A.; Zuilhof, H.; Sudhölter, E. J. R. *Angew. Chem., Int. Ed.* **2004**, *43*, 1352-1355.

(27) Scheres, L.; Arafat, A.; Zuilhof, H. *Langmuir* **2007**, *23*, 8343-8346.

(28) Eves, B. J.; Sun, Q. Y.; Lopinski, G. P.; Zuilhof, H. *J. Am. Chem. Soc.* **2004**, *126*, 14318-14319.

(29) Sieval, A. B.; Demirel, A. L.; Nissink, J. W. M.; Linford, M. R.; van der Maas, J. H.; de Jeu, W. H.; Zuilhof, H.; Sudhölter, E. J. R. *Langmuir* **1998**, *14*, 1759-1768.

(30) Sieval, A. B.; van den Hout, B.; Zuilhof, H.; Sudhölter, E. J. R. *Langmuir* **2001**, *17*, 2172-2181.

(31) Mischki, T. K.; Lopinski, G. P.; Wayner, D. D. M. *Langmuir* **2009**, *25*, 5626-5630.

(32) de Smet, L. C. P. M.; Pukin, A. V.; Sun, Q. Y.; Eves, B. J.; Lopinski, G. P.; Visser, G. M.; Zuilhof, H.; Sudhölter, E. J. R. *Appl. Surf. Sci.* **2005**, *252*, 24-30.

(33) Coletti, C.; Marrone, A.; Giorgi, G.; Sgamellotti, A.; Cerofolini, G.; Re, N. *Langmuir* **2006**, *22*, 9949-9956.
(34) Kanai, Y.; Selloni, A. *J. Am. Chem. Soc.* **2006**, *128*, 3892-3893.
(35) Yuan, S. L.; Cai, Z. T.; Jiang, Y. S. *New J. Chem.* **2003**, *27*, 626-633.
(36) Wallart, X.; de Villeneuve, C. H.; Allongue, P. *J. Am. Chem. Soc.* **2005**, *127*, 7871-7878.
(37) Sieval, A. B.; van den Hout, B.; Zuilhof, H.; Sudhölter, E. J. R. *Langmuir* **2000**, *16*, 2987-2990.
(38) Scheres, L.; Giesbers, M.; Zuilhof, H. *Langmuir* **2010**, *26*, 4790-4795.
(39) Ojima, I. In *The Chemistry of Organic Silicon Compounds*; Patai, S., Rappoport, Z., Eds.; John Wiley & Sons: New York, 1989; Vol. 2, p 1484.
(40) Ng, A.; Ciampi, S.; James, M.; Harper, J. B.; Gooding, J. J. *Langmuir* **2009**, *25*, 13934-13941.
(41) Lee, M. V.; Lee, J. R. I.; Brehmer, D. E.; Linford, M. R.; Willey, T. M. *Langmuir* **2010**, *26*, 1512-1515.
(42) Porter, M. D.; Bright, T. B.; Allara, D. L.; Chidsey, C. E. D. *J. Am. Chem. Soc.* **1987**, *109*, 3559-3568.
(43) Hacker, C. A.; Anderson, K. A.; Richter, L. J.; Richter, C. A. *Langmuir* **2005**, *21*, 882-889.
(44) Boukherroub, R.; Morin, S.; Sharpe, P.; Wayner, D. D. M.; Allongue, P. *Langmuir* **2000**, *16*, 7429-7434.
(45) Allongue, P.; de Villeneuve, C. H.; Morin, S.; Boukherroub, R.; Wayner, D. D. M. *Electrochim. Acta* **2000**, *45*, 4591-4598.
(46) Dichiarante, V.; Fagnoni, M.; Albini, A. *J. Org. Chem.* **2008**, *73*, 1282-1289.
(47) Sze, S. M.; Kwok, K. N. *Physics of Semiconductor Devices, 3rd Edition*; Wiley: New Jersey, 2007.
(48) Cai, W.; Lin, Z.; Strother, T.; Smith, L. M.; Hamers, R. J. *J. Phys. Chem. B* **2002**, *106*, 2656-2664.
(49) Takeuchi, N.; Kanai, Y.; Selloni, A. *J. Am. Chem. Soc.* **2004**, *126*, 15890-15896.
(50) DiLabio, G. A.; Piva, P. G.; Kruse, P.; Wolkow, R. A. *J. Am. Chem. Soc.* **2004**, *126*, 16048-16050.
(51) Puniredd, S. R.; Assad, O.; Haick, H. *J. Am. Chem. Soc.* **2008**, *130*, 13727-13734.

Chapter 4

Organic Monolayers onto Oxide-Free Silicon with Improved Surface Coverage: Alkynes versus Alkenes

Abstract. On H-Si(111) monolayer assembly with 1-alkenes results in alkyl monolayers with a Si–C–C linkage to the silicon, while 1-alkynes yield alkenyl monolayers with a Si–C=C linkage to the silicon. To investigate the influence of the different linkage groups on the final monolayer structure organic monolayers were prepared from 1-alkenes and 1-alkynes with chain lengths from C_{12} to C_{18}, and the final monolayer structures were studied in detail by static water contact angles measurements, ellipsometry, attenuated total reflectance infrared spectroscopy (ATR-IR) and X-ray photoelectron spectroscopy (XPS). The thicknesses, tilt angles and packing densities of the alkyl monolayers are in good agreement with literature, whereas increased thicknesses, reduced tilt angles and improved packing densities were observed for the alkenyl monolayers. Finally, the surface coverages for alkyl monolayers was determined to be 50-55% (in line with literature values), while that for the alkenyl monolayers increased with the chain length from 55% for C_{12} to as high as 65% for C_{18}! The latter value is very close to the theoretical maximum of 69% obtainable on H-Si(111). Such enhanced monolayer quality and increased surface coverage of the alkenyl monolayers – in combination with the oxidation-inhibiting nature of the Si–C=C linkage – significantly increases the chance of successful implementation of organic monolayers on oxide-free silicon in molecular electronic and biosensor devices, especially in view of the importance of a defect-free monolayer structure and the corresponding stability of the monolayer-silicon interface.

This chapter is published as:
'Organic Monolayers onto Oxide-Free Silicon with Improved Surface Coverage: Alkynes versus Alkenes' Scheres, L.; Giesbers, M.; Zuilhof, H. *Langmuir*, **2010**, *26*, 4790-4795

4.1 Introduction

The ongoing miniaturization of microelectronic devices results in an increasing interest in surface modification of silicon. Under a wide variety of conditions, organic monolayers of 1-alkenes or 1-alkynes can be prepared on hydrogen-terminated silicon (H-Si).[1-17] These organic monolayers are directly bound to the silicon surface via a chemically stable Si–C bond and as a consequence a well-defined monolayer-silicon interface is formed. Because an intervening SiO_2 layer is essentially absent, direct electronic coupling between the organic functionality and the silicon substrate is possible.[18-25] This makes these monolayers highly interesting for biosensor, molecular electronics and solar cell applications.[22,26-31]

For all these potential applications the stability of the monolayer and the monolayer-silicon interface are the most important issues, as trace amounts of oxide result in interface states that degrade the electronic properties of the underlying Si. In addition, it has been shown that upon monolayer formation with 1-alkenes on Si(111) only 50-55% of the reactive H-Si sites can be substituted by alkyl chains, leaving 45-50% of the H-Si sites unreacted after completion of the monolayer.[2,6,32-35] As monolayer formation occurs via a meandering radical chain reaction on the silicon surface[36,37] and steric hindrance of the covalently bound chains prevents insertion of new chains, filling the last pinholes in the monolayer is hard.[25] Nevertheless, a nearly defect-free monolayer is crucial for the long-term stability in ambient and aqueous environment, because water and oxygen can easily penetrate via such defects through the monolayer and thus react with the large number of unreacted H-Si sites at the monolayer-silicon interface. The resulting oxide patches create electrically active surface states that will change the electrical properties of the underlying silicon drastically.[25]

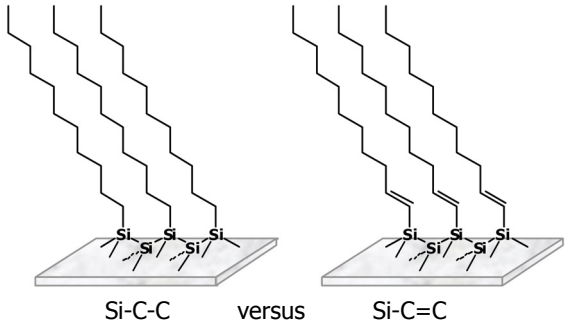

Figure 1. Different linkage of organic monolayers on H-Si(111); alkyl monolayer (left) and alkenyl monolayer (right).

In Chapter 3 it was demonstrated that 1-alkynes are far more reactive towards H-Si(111) than 1-alkenes.[38] Besides this reactivity difference during monolayer formation, the final monolayers on Si(111) are also structurally different. On H-Si(111) monolayer assembly with 1-alkenes results in alkyl monolayers with a Si–C–C linkage, while 1-alkynes yield alkenyl monolayers with a Si–C=C linkage (Figure 1).[2,6,15,34] In contrast to Si–C–C, the Si–C=C linkage is known to inhibit oxidation of the underlying silicon and therefore can enhance the monolayer stability.[39] In addition, structural differences like the hybridization change (sp^3 versus sp^2), the difference in Van der Waals radii and the differing number of methylene groups, will all influence the overall monolayer packing density, the number of unfavorable conformations and monolayer coverage. In other words: the sum of all these small contributions might affect the overall monolayer structure significantly. This stimulated us to investigate in detail the structure of 1-alkene and 1-alkyne-derived monolayers on H-Si(111) with chain lengths from C_{12} to C_{18}. All monolayers were characterized by water contact angle measurements, ellipsometry, attenuated total reflectance infrared (ATR-IR) spectroscopy and X-ray photoelectron spectroscopy (XPS).

4.2 Experimental

4.2.1 Materials

PE40/60, EtOH and CH_2Cl_2 were distilled prior to use. For rinsing and contact angle measurements, deionized water (18.3 MΩ cm resistivity) was used. Acetone (Sigma/Honeywell, semiconductor grade) and 40% ammonium fluoride solution (40% NH_4F) (Sigma/Honeywell, semiconductor grade) were used as received. 1-Dodecene (Sigma, +99%), 1-tetradecene (Fluka, +99%), 1-hexadecene (Sigma, +99%) and 1-octadecene (Fluka, +99%) were distilled twice before use and 1-dodecyne (Sigma, +98%), 1-tetradecyne (Sigma, +97%), 1-hexadecyne (ABCR, Germany, 90%) and 1-octadecyne (ABCR, Germany, 90%) were purified by column chromatography (eluent hexane) to remove trace amounts of 1-bromoalkanes, and subsequently distilled twice before use. Silicon wafers were (111)-oriented single-side and double polished, 475 - 550 μm thick, n-type, phosphorus-doped samples, with a resistivity of 1.0-5.0 Ω cm (Siltronix, France).

4.2.2 Monolayer Preparation

Pieces of n-Si(111) wafer were first rinsed several times with acetone, followed by sonication in acetone for 10 min. Then the samples were cleaned using oxygen plasma (Harrick PDC-002 setup) for 3 min. Subsequently, the Si(111) substrates were etched in an argon-saturated 40% NH_4F solution for 15 min. under an argon atmosphere. After being etched, the samples were thoroughly rinsed with water and finally blown dry with a stream of nitrogen. A small three-necked flask, equipped with a capillary as the argon inlet and a reflux-condenser connected to a vacuum pump, was charged with neat 1-alkyne or 1-alkene (GC purity >99.9%). The tip of the capillary was positioned in the reactive compound and the argon flow through the capillary was turned on. Subsequently, the pressure in the flask was reduced to approximately 10 mbar and the setup was deoxygenated with argon for at least 30 min at 100 °C. Subsequently, the pressure was raised by filling the setup with argon until atmospheric pressure was achieved. The freshly etched Si(111) substrate was transferred into 1-alkyne or 1-alkene while an argon flow was maintained. The setup was closed again, the pressure was reduced, and the capillary was moved away as far as possible from the surface of the liquid to prevent the disturbance of monolayer formation by the strong argon flow. After 6 h at 100 °C the reaction was stopped, the reaction flask was backfilled with argon until atmospheric pressure was attained, and the sample was taken out. After rinsing extensively with light petroleum ether (b.p. 40-60 °C, PE 40/60), EtOH, and CH_2Cl_2 and sonicating for 5 min in CH_2Cl_2 to remove physisorbed molecules, the samples were blown dry with a stream of dry nitrogen.

4.2.3 Monolayer Characterization

Static water contact angles were measured with an automated Krüss DSA 100 goniometer. At least six small droplets of 2.0 µl deionized water were dispensed and the contact angles were determined using a Tangent 2 fitting model. The error in the contact angles is less than 1°.

The ellipsometric thicknesses were measured with a Sentech Instruments (Type SE-400) ellipsometer, operating at 632.8 nm (He-Ne-laser) and an angle of incidence of 70°. First the optical constants of the substrate were determined with a piece of freshly etched H-Si(111) (n = 3.821 and k = 0.051). The thicknesses of the monolayers were determined with a planar three-layer (ambient, organic monolayer, substrate) isotropic model with assumed refractive indices of 1.00 and 1.46 for ambient and the organic monolayer, respectively.

The reported values are the average of at least eight measurements taken at different locations on several samples and the error is less than 1 Å.

Attenuated total reflectance infrared spectroscopy (ATR-IR) spectra were collected with a Bruker spectrometer (model Tensor 27) equipped with a Harrick ATR accessory and MCT-detector. A Harrick grid polarizer was placed in front of the sample for measuring spectra with s- and p-polarized light. Double polished n-Si(111) wafers were cut into pieces of 5 × 1 cm and polished to obtain ATR crystals with 45º bevels (± 100 internal reflections). All spectra were taken at a resolution of 1 cm^{-1} by adding 2048 scans while flushing with dry N_2, and were referenced to a clean native oxide-covered ATR-crystal. If necessary a slight baseline correction was applied. For the dichroism experiments we followed a procedure described in literature before.[2,3] In brief, the intensities of the methylene stretching vibrations in the s- and p-polarized spectra (A_s and A_p, respectively) result in the dichroic ratios:

$$D = A_S / A_p \qquad (1)$$

These dichroic ratios are converted into the angles between the transition dipole moments (α) and the surface normal for the symmetric and asymmetric methylene stretching vibrations (α_s and α_a) with the following equation:

$$\alpha = \tan^{-1}\left(\frac{2DE_z^2}{E_y^2 - DE_x^2}\right)^{1/2} \qquad (2)$$

where E_x, E_y and E_z are the electric fields of the polarized light for the x, y and z-directions, respectively. Using refractive indices of $n_{si} = 3.5$ and $n_{monolayer} = 1.5$ results in the values: $E_x = 1.409$, Ey = 1.476 and $E_z = 0.684$. Finally, by assuming that the chains in the monolayers have an all-trans conformation, the tilt angle (θ) of the chains can be calculated with:

$$\theta = \cos^{-1}\sqrt{1 - \cos^2\alpha_S - \cos^2\alpha_a} \qquad (3)$$

X-ray photoelectron spectroscopy (XPS) analysis was performed using a JPS-9200 photoelectron spectrometer (JEOL, Japan). The XPS narrows scans were recorded under UHV conditions using monochromatic Al Kα X-ray radiation at 12 kV and 25 mA using an

analyzer pass energy of 10 eV at a takeoff angle φ (angle between sample and detector) of 80°. For a precise determination of the atomic C/Si ratio of organic monolayers on Si(111) the influence of x-ray photodiffraction (XPD) on the XPS signal had to be accounted for.[33] Therefore the samples were rotated 360° around the surface normal, yielding rotationally averaged C_{1s} and Si_{2p} emissions to obtain a truly quantitative C/Si ratio, which is now independent of the orientation of the sample. As our sample holder only allows rotation of the samples at a takeoff angle of 90° we used a non-monochromatic Al Kα X-ray radiation (twin source) at 10 kV and 15 mA with an analyzer pass energy of 50 eV and a takeoff angle of 90° for these measurements. All spectra were corrected with a slight linear background before fitting.

4.3 Results and Discussion

To investigate the influence of the structurally different linkage to the Si(111) substrate (Si–C–C and Si–C=C, respectively) on the quality and structure of the final monolayer, monolayers were prepared using 1-alkenes and 1-alkynes with chain lengths from C_{12} to C_{18}. To be fully sure that the monolayer formation was complete, the reaction conditions were 6 h at 100 °C, instead of the standard conditions of 2 h at 80 °C, which were found to be sufficient for preparation of high-quality monolayers with 1-alkynes on H-Si(111).[15] After monolayer preparation all Si substrates were hydrophobic with static water contact angles of 110 - 111°, indicative of well-ordered nonfunctionalized monolayers. These values are comparable with literature values,[2,6,15-17,38] and as expected not affected by the chain length and type of linkage to the silicon substrate.

The ellipsometric thicknesses of all alkyl (Si–C–C) and alkenyl (Si–C=C) monolayers are depicted in Figure 2. The dashed lines in Figure 2 represent the theoretical monolayer thickness d_{TH}, as calculated with (see Appendix 1):[2,33]

$$d_{TH}(\text{Å}) = 1.89 + \left(\frac{n}{2} - 1\right) \times 2.54 \times \cos(\theta) + 1.56 \times \sin(35.5° + \theta) \qquad (4)$$

where *n* is the number of carbons in the chain, and θ is the tilt angle of the chains with respect to the surface normal; d_{TH} was calculated for the range of θ from 0° to 50°.[2,33] As expected, a gradual increase in monolayer thickness with the chain length is found for both types of monolayers. For 1-alkene-derived monolayers the thicknesses and tilt angles are in

good agreement with experimental[2] and molecular modeling-derived[2,32] literature values (e.g. 1-octadecene monolayer: thickness 19 Å, tilt angle ~36°). However to our initial surprise, all 1-alkyne monolayers are thicker than the corresponding 1-alkene monolayers, with estimated tilt angles of ~20°.

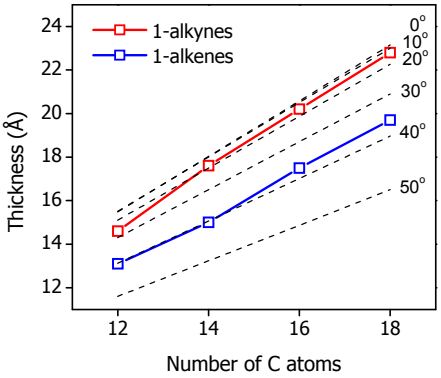

Figure 2. Ellipsometric thickness of 1-alkene (lower blue curve) and 1-alkyne (upper red curve) monolayers on H-Si(111) and the theoretical monolayer thicknesses d_{TH} for tilt angles θ from 0 - 50° (dashed lines).

Surprised by the ellipsometry data, double-polished ATR crystals were modified with 1-alkenes and 1-alkynes to obtain detailed information about the structure and order in both types of monolayers. As an example the ATR-IR spectra of 1-octadecene and 1-octadecyne-derived monolayers on H-Si(111) are shown in Figure 3. The difference in bonding to the silicon substrate is clearly visible by the presence of a small peak at 1602.8 cm^{-1} in the 1-octadecyne spectrum, which is assigned to C=C stretching mode of the Si–C=C moiety, and which is absent in the 1-octadecene spectrum.[2,6,15,34] In addition, there is a clear difference in the positions of the antisymmetric (ν_a) and symmetric (ν_s) methylene stretching vibrations. For the 1-octadecyne monolayer these vibrations are detected at 2917.7 and 2850.2 cm^{-1}, indicative of a highly-ordered monolayer in which the chains adopt an all-trans conformation, i.e. a near-crystalline packing. In contrast, for the 1-octadecene monolayer the methylene vibrations are found at higher frequencies, 2919.6 and 2851.1 cm^{-1}, corresponding to a less ordered structure and a significant number of gauche defects present in the monolayer. Apparently, having two methylene groups less available for favorable Van der Waals interactions than the corresponding octadecyl chains is compensated for by other factors; an in-depth molecular modeling study of these differences can be found in Chapter 5.[40] As can been seen in Table 1, this phenomenon is

observed for all chain lengths. For both alkyl and alkenyl monolayers, the frequencies of the methylene stretching vibrations shift to lower values with increasing chain length, and although the frequency difference becomes smaller for the shorter chain lengths, in all cases the alkenyl monolayers are more ordered than the corresponding alkyl monolayers.

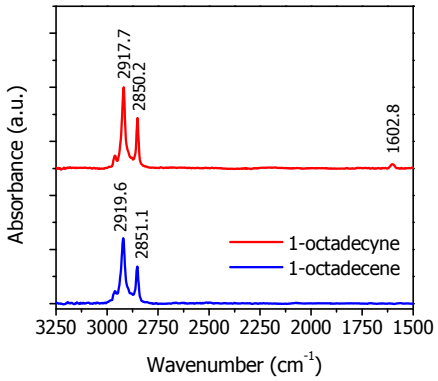

Figure 3. ATR spectra (p-polarization) of 1-octadecene (lower blue curve) and 1-octadecyne (upper red curve) monolayers on H-Si(111).

To check the ellipsometric thicknesses and the related tilt angles, we carried out ATR-dichroism experiments, i.e. we measured ATR-IR of all alkyl and alkenyl monolayers with s- and p-polarized light and by assuming that the chains adopt an all-trans conformation we obtained the tilt angles of the chains with respect to the surface normal. As shown in Table 1, all 1-alkene monolayers have tilt angles θ_{IR} in the range of 37-40° (experimental error: ± 3°), so there is no influence of the chain length. These values are in good agreement with tilt angles deduced from the ellipsometry data (Figure 2) and literature values for 1-alkene monolayers on Si(111) (30-45°).[2,3,32-34] In contrast, for the 1-alkyne-derived monolayers the chain length does affect the orientation of the chains. For example, the tilt angle decreases from 35° for 1-dodecyne to 22° for 1-octadecyne. By insertion in equation 4, these tilt angles θ_{IR} are converted into the corresponding monolayer thicknesses d_{ML} and the results are depicted in the last column of Table 1. As expected by the smaller tilt angles, higher monolayer thicknesses have been obtained for the 1-alkyne-derived monolayers. It should be noted that there is a length-dependent difference between $\theta_{ellipsometry}$ and θ_{IR}; this difference decreases from ~15° for 1-dodecyne to zero within experimental error for the 1-octadecyne monolayer (vide infra).

Table 1. ATR-IR positions (ν_a and ν_s), IR dichroism tilt angles θ_{IR} and the corresponding monolayer thicknesses d_{ML} of the 1-alkene and 1-alkyne monolayers on H-Si(111).

Reactant	$\nu_a^{s\text{-}pol}$ (cm^{-1}) $\nu_a^{p\text{-}pol}$ (cm^{-1})	$\nu_s^{s\text{-}pol}$ (cm^{-1}) $\nu_s^{p\text{-}pol}$ (cm-1)	Tilt angle (°) θ_{IR}	Monolayer thickness (Å) d_{ML}
1-dodecene	2921.6 2921.8	2852.3 2852.2	37	13
1-tetradecene	2920.9 2921.0	2852.2 2851.9	40	15
1-hexadecene	2921.1 2920.7	2851.9 2851.6	37	17
1-octadecene	2920.0 2919.6	2851.5 2851.1	40	19
1-dodecyne	2921.3 2921.3	2851.6 2851.8	35	14
1-tetradecyne	2920.9 2920.9	2851.4 2851.7	34	16
1-hexadecyne	2919.1 2918.5	2851.1 2851.0	27	19
1-octadecyne	2917.3 2917.7	2850.3 2850.2	22	22

Finally, XPS was used to analyze both types of monolayers. Also in the XPS C_{1s} narrow scans (Figure 4) the structurally different linkage of the alkyl and alkenyl monolayers to the silicon surface is evident. For the 1-octadecene monolayer the emission of the carbon bound to the silicon (Si–C) lays very close to the binding energy of the aliphatic carbons, and therefore the narrow scan consists of only one main peak at 285.0 eV. Conversely, the C_{1s} narrow scan of the 1-octadecyne monolayer can easily be deconvoluted into two contributions. The higher electron density of the double bond shifts the emission of the silicon-linked carbon to a binding energy of 283.8 eV – a result supported by B3LYP/6-311G(d,p) density functional theory (DFT) calculations (see Appendix 1 for details) – and therefore the silicon-linked carbon is easily discerned from the peak attributed to the aliphatic carbons at 285.0 eV.[33] In addition, the Si_{2p} narrow scans show the expected $Si_{2p3/2}$ and $Si_{2p1/2}$ emissions and no sign of silicon oxide (SiO_2) around 103 - 104 eV.

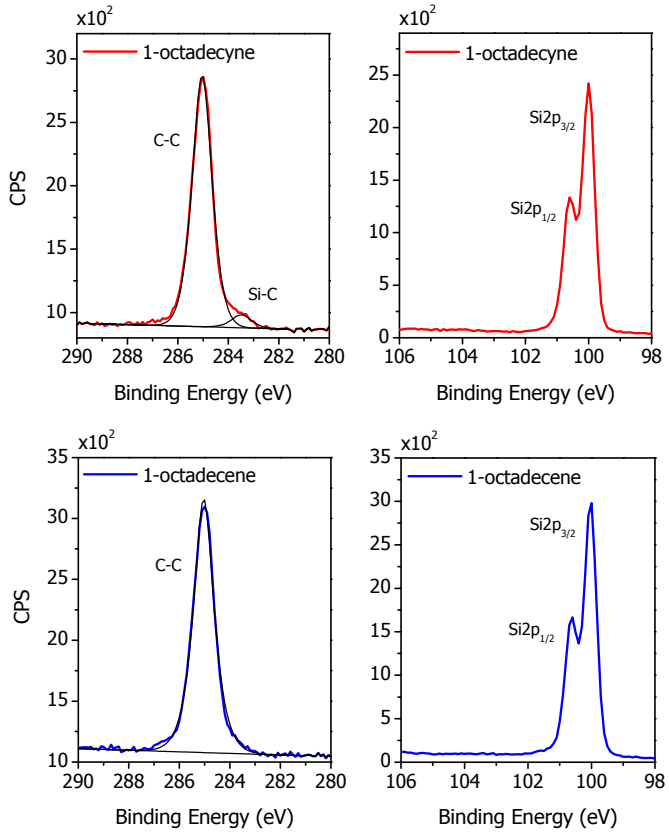

Figure 4. XPS C_{1s} and Si_{2p} narrow scans of 1-octadecene (bottom, blue) and 1-octadecyne-derived (top, red) monolayers on H-Si(111).

Besides the chemical composition, one can also extract the quantitative composition of the monolayer from the XPS data, i.e. the atomic C/Si ratio. However, for a precise determination of the C/Si ratio of organic monolayers on Si(111), one has to account for the influence of X-ray photodiffraction on the intensities of the XPS signal. Therefore, following the work of Wallart et al.,[33] the XPS samples were rotated 360° (in steps of 10°) around its surface normal, to obtain angle-averaged C_{1s} and Si_{2p} signals, so as to make our XPS measurements truly quantitative. Subsequently, the atomic C/Si ratios were converted into monolayer thicknesses (d_{ML}) using the following relationship:

$$d_{ML}(\text{Å}) = \lambda_{ML}^{Si} \times \sin(\varphi) \times \ln(1 + C/Si) \qquad (5)$$

where λ_{ML}^{Si} is the attenuation length of Si_{2p} photoelectrons in the organic monolayer (λ_{ML}^{Si} = 39.5 Å),[33] and φ is the angle between the surface plane and the detector (takeoff or polar angle; φ = 90°). An overview of the atomic C/Si ratios and the corresponding monolayer thicknesses is given in Table 2. As expected, the carbon amount is increasing with the chain length for both, but for 1-alkyne monolayers the rise in the C/Si ratio from C_{12} to C_{18} is larger. As a result the 1-octadecyne monolayer contains approximately 18% more carbon than the 1-octadecene monolayer and is approximately 3 to 4 Å thicker.

Table 2. Quantitative XPS data; atomic C/Si ratios and resulting monolayer thicknesses d_{ML} of 1-alkene and 1-alkyne monolayers on H-Si(111).

Reactant	Atomic ratio C/Si	Monolayer thickness (Å) d_{ML}
1-dodecene	27.5 / 72.5	13
1-tetradecene	29.7 / 70.3	14
1-hexadecene	32.8 / 67.2	16
1-octadecene	36.2 / 63.8	18
1-dodecyne	27.8 / 72.2	13
1-tetradecyne	32.2 / 67.8	15
1-hexadecyne	37.7 / 62.3	19
1-octadecyne	42.8 / 57.2	22

In principle, the thicknesses calculated from the observed atomic C/Si ratio can be internally checked by another XPS method,[33] which makes use of the relative carbon intensity of the distinct peak attributed to the carbon linked to the silicon ($R_{C\text{-}Si}$) in the C_{1s} narrow scans (Figure 4). The monolayer thickness d_{ML} can be calculated with the following equation:

$$R_{C-Si} = \frac{d_{ML}}{n \times \lambda_{ML}^{C} \times \sin(\varphi)} \times \frac{e^{-d_{TH\text{-}1.89} / \lambda_{ML}^{C} \times \sin(\varphi)}}{1 - e^{-d_{ML} / \lambda_{ML}^{C} \times \sin(\varphi)}} \qquad (6)$$

where λ_{ML}^{C} is the attenuation length of C_{1s} photoelectrons in the organic monolayer (λ_{ML}^{C} = 35.4 Å), *n* is the number of carbons in the chain (in this case 18 for a 1-octadecyne

monolayer), φ is the take-off angle (φ = 80° for the high-resolution spectra), and $d_{TH-1.89}$ is the theoretical monolayer thickness d_{TH} minus the Si-C bond length of 1.89 Å (d_{TH} was calculated with equation 4, by inserting a tilt angle of 20° for a 1-octadecyne monolayer, as determined in this work by three different techniques). For the 1-octadecyne monolayer, the relative carbon intensity of the carbon bound to the silicon is 4.3% (R_{C-Si} = 0.043) and this results in a monolayer thickness of 23 Å. This value corresponds well with the 22-23 Å found by ellipsometry, ATR-dichroism and XPS, and this also applies for values obtained with the other chain lengths. It should, however, be kept in mind that this method has for these long chains a significantly larger experimental error, due to the relatively large uncertainty in the relative carbon intensity of the carbon bound to the silicon (in C_{18} 1/17) and since a small change of R_{C-Si} already leads to a large change in the derived monolayer thickness (e.g. R_{C-Si} = 0.04 and 0.05 correspond to 17 Å and 35 Å, respectively). Although this approach is accurate for short chain (C_1-C_6) monolayers, it is thus rather imprecise for long chain (C_{12}-C_{18}) monolayers.

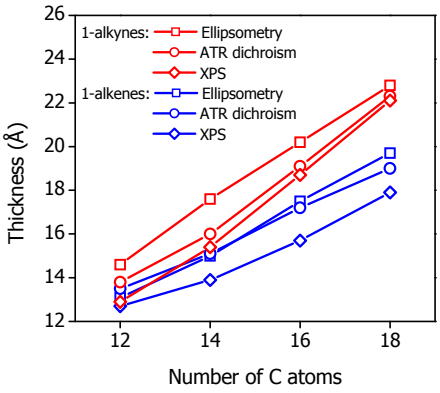

Figure 5. Overview of monolayer thicknesses obtained by ellipsometry (□), ATR dichroism (◇) and XPS (○) of 1-alkene (lower blue curves) and 1-alkyne (upper red curves) monolayers on H-Si(111).

To summarize we depicted the monolayer thicknesses obtained by the three different techniques in Figure 5. It seems that, as stated before in literature,[2] ellipsometry is slightly overestimating the monolayer thicknesses, approximately 1-2 Å compared to the reasonably equal ATR-dichroism and XPS data. Therefore we only used the more reliable monolayer thicknesses from the latter two techniques to estimate the surface coverage (θ_{ML}). By comparison with a high-quality alkanethiol monolayer on gold, the following equation converts the monolayer thickness into surface coverage:[33]

$$\theta_{ML} = \frac{d_{ML} \times D_{Au}}{d_{TH(30°)} \times D_{Si}} \qquad (7)$$

where D_{Au} is the surface density of chains in a perfect (tilt angle of 30°) alkanethiol monolayer on gold ($D_{Au} = 4.65 \times 10^{14}$ cm^{-2}); D_{Si} is the surface atom density on Si(111) ($D_{Si} = 7.8 \times 10^{14}$ cm^{-2}); and $d_{TH(30°)}$ is the theoretical thickness of an organic monolayer on Si with a tilt angle of 30°, as calculated with equation 4. As shown in Figure 6, all 1-alkene monolayers have a surface coverage in the range of 50-55%. Like the thicknesses and tilt angles, this is in excellent agreement with literature[2,6,32-34] and validates our approach. Because we showed already improved packing densities, higher monolayer thicknesses and increasing amounts of carbon for the 1-alkyne monolayers, it is not surprising that the surface coverage of the 1-alkyne monolayers increases from approximately 55% for C_{12} to 65% for C_{18}. We emphasize that this is a remarkably high coverage for the 1-octadecyne monolayer, in particular, if one considers that the theoretical maximum substitution percentage of H-Si(111) with alkyl monolayers (and alkenyl monolayers) is most likely close to 69%.[32]

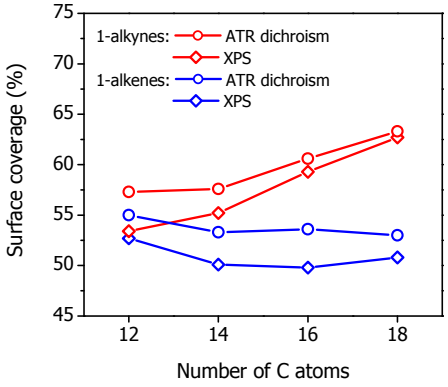

Figure 6. Surface coverage obtained by ATR dichroism (◇) and XPS (○) of 1-alkene (lower blue curves) and 1-alkyne (upper red curves) monolayer on H-Si(111).

The origin of the chain length dependence and higher surface coverages obtained with 1-alkynes on H-Si(111) is not completely clear yet, but the following aspects will certainly have an influence on the surface coverage and final structure of the alkenyl monolayers:

(1) The smaller Van der Waals radius of the Si–C=C group compared to the Si–C–C group. Molecular modeling has shown that when surface coverage with alkyl chains (Si–C–

C) exceeds 50-55% this results in more favorable interchain Van der Waals interactions in the top part of the monolayer, while close to the monolayer-silicon interface interpenetration of the methylene groups leads to significant number of unfavorable conformations. However, at surface coverages above 50-55% a smaller linker group, like Si–C=C, will result in less interpenetration and less unfavorable conformations close to the monolayer-silicon interface, whereas the short interchain distances still yield more and stronger Van der Waals interactions making higher surface coverages energetically favorable.[32,35]

(2) 1-Alkynes are significantly more reactive toward H-Si(111) than 1-alkenes.[15,38,41] Because of this higher reactivity the radical chain mechanism will proceed more easily with 1-alkynes, which can result in larger but also more densely packed islands. Also filling of the pinholes and defects between the islands will be easier with the smaller and more reactive 1-alkynes.

In addition to the reactivity difference, Takeuchi et al.[41] reported a larger stabilization energy for the Si–C=C linkage compared to the Si–C–C linkage. We note that the stabilization energy (or energy gain) upon covalent binding to the H-Si surface is the main driving force for monolayer formation, and consequently, monolayer structures with higher surface coverages, but also with little strain or few unfavorable conformations close to the monolayer-silicon interface, become thermodynamically possible due to the larger energy gain upon covalent binding of 1-alkynes to H-Si(111).

(3) The carbon atoms in the Si–C–C group adopt a sp^3-hybridization with bond angles of 109.5° and the carbons in the Si–C=C group have sp^2-hybridization with corresponding bond angles of 120°. Furthermore, the double bond in the Si–C=C linkage is more rigid and cannot rotate like the C–C bonds in the Si–C–C group. Consequently, the larger bond angles and rigidity of the C=C bond might enhance or even direct the whole chain to stand more upright.

(4) As mentioned before, for alkyl monolayers the optimal surface coverage of 50-55% is restricted by steric constrains near the Si surface and consequently no chain length depending surface coverage has been observed. Due to the smaller Van der Waals radius of the C=C bond, the optimal surface coverage of alkenyl monolayers is not restricted by steric constrains near the surface, and thus higher surface coverages are sterically possible. In this respect, adding extra chains to an alkenyl monolayer which is close to completion (for instance 50-55%) will be easier with the long octadecenyl chains than with short dodecenyl chains, as insertion of a long octadecenyl chain with 16 methylene groups will be accompanied by more favorable interchain Van der Waals interactions than insertion of

a relative short dodecenyl chain with only 10 methylene groups. This might also explain the chain length depending surface coverage observed for the alkenyl monolayer.

4.4 Conclusions

The structural differences of alkyl and alkenyl monolayers on oxide-free Si(111) with chain lengths from C_{12} to C_{18} unequivocally show that alkyne-derived monolayers are better than alkene-derived monolayers. This is revealed by a higher packing density, higher ordering of the alkyl chains, and smaller tilt angles with respect to the surface normal. Although the static contact angles were similar for all monolayers, ellipsometry, ATR-IR and quantitative XPS clearly showed a large effect of the different linkages to the silicon surface (Si–C–C versus Si–C=C) on the structure of the final monolayer. Finally, the surface coverages were determined for the alkenyl monolayers to increase with the chain length from 55% for C_{12} to 65% for C_{18}. These values are significantly higher than observed for the alkene-derived monolayers (50 – 55%), and even start to approach the theoretical maximum of 69% for long alkyl (and alkenyl) monolayers on H-Si(111). This enhanced monolayer quality and surface coverage of the alkenyl monolayers – in combination with the oxidation-inhibiting nature of the Si–C=C linkage – significantly increases the chance of a successful implementation of organic monolayers on oxide-free silicon in new and stable molecular electronic and biosensor devices, especially in view of the importance of a defect-free monolayer structure and the corresponding stability of the monolayer-silicon interface.

References

(1) Linford, M. R.; Chidsey, C. E. D. *J. Am. Chem. Soc.* **1993**, *115*, 12631-12632.

(2) Linford, M. R.; Fenter, P.; Eisenberger, P. M.; Chidsey, C. E. D. *J. Am. Chem. Soc.* **1995**, *117*, 3145-3155.

(3) Sieval, A. B.; Demirel, A. L.; Nissink, J. W. M.; Linford, M. R.; van der Maas, J. H.; de Jeu, W. H.; Zuilhof, H.; Sudhölter, E. J. R. *Langmuir* **1998**, *14*, 1759-1768.

(4) Buriak, J. M.; Allen, M. J. *J. Am. Chem. Soc.* **1998**, *120*, 1339-1340.

(5) Buriak, J. M.; Stewart, M. P.; Geders, T. W.; Allen, M. J.; Choi, H. C.; Smith, J.; Raftery, D.; Canham, L. T. *J. Am. Chem. Soc.* **1999**, *121*, 11491-11502.

(6) Cicero, R. L.; Linford, M. R.; Chidsey, C. E. D. *Langmuir* **2000**, *16*, 5688-5695.

(7) deVilleneuve, C. H.; Pinson, J.; Bernard, M. C.; Allongue, P. *J. Phys. Chem. B* **1997**, *101*, 2415-2420.
(8) Terry, J.; Linford, M. R.; Wigren, C.; Cao, R. Y.; Pianetta, P.; Chidsey, C. E. D. *Appl. Phys. Lett.* **1997**, *71*, 1056-1058.
(9) Hurley, P. T.; Nemanick, E. J.; Brunschwig, B. S.; Lewis, N. S. *J. Am. Chem. Soc.* **2006**, *128*, 9990-9991.
(10) Juang, A.; Scherman, O. A.; Grubbs, R. H.; Lewis, N. S. *Langmuir* **2001**, *17*, 1321-1323.
(11) Niederhauser, T. L.; Jiang, G. L.; Lua, Y. Y.; Dorff, M. J.; Woolley, A. T.; Asplund, M. C.; Berges, D. A.; Linford, M. R. *Langmuir* **2001**, *17*, 5889-5900.
(12) Niederhauser, T. L.; Lua, Y. Y.; Jiang, G. L.; Davis, S. D.; Matheson, R.; Hess, D. A.; Mowat, I. A.; Linford, M. R. *Angew. Chem., Int. Ed.* **2002**, *41*, 2353-2356.
(13) Royea, W. J.; Juang, A.; Lewis, N. S. *Appl. Phys. Lett.* **2000**, *77*, 1988-1990.
(14) Buriak, J. M.; Allen, M. J. *J. Lumin.* **1998**, *80*, 29-35.
(15) Scheres, L.; Arafat, A.; Zuilhof, H. *Langmuir* **2007**, *23*, 8343-8346.
(16) Sun, Q. Y.; de Smet, L. C. P. M.; van Lagen, B.; Wright, A.; Zuilhof, H.; Sudhölter, E. J. R. *Angew. Chem., Int. Ed.* **2004**, *43*, 1352-1355.
(17) Sun, Q. Y.; de Smet, L. C. P. M.; van Lagen, B.; Giesbers, M.; Thune, P. C.; van Engelenburg, J.; de Wolf, F. A.; Zuilhof, H.; Sudhölter, E. J. R. *J. Am. Chem. Soc.* **2005**, *127*, 2514-2523.
(18) Liu, Y. J.; Yu, H. Z. *ChemPhysChem* **2002**, *3*, 799-802.
(19) Liu, Y. J.; Yu, H. Z. *ChemPhysChem* **2003**, *4*, 335-342.
(20) Faber, E. J.; de Smet, L. C. P. M.; Olthuis, W.; Zuilhof, H.; Sudhölter, E. J. R.; Bergveld, P.; van den Berg, A. *ChemPhysChem* **2005**, *6*, 2153-2166.
(21) Faber, E. J.; Sparreboom, W.; Groeneveld, W.; de Smet, L. C. P. M.; Bomer, J.; Olthuis, W.; Zuilhof, H.; Sudhölter, E. J. R.; Bergveld, P.; van den Berg, A. *ChemPhysChem* **2007**, *8*, 101-112.
(22) Hiremath, R. K.; Rabinal, M. K.; Mulimani, B. G.; Khazi, I. M. *Langmuir* **2008**, *24*, 11300-11306.
(23) Salomon, A.; Böcking, T.; Chan, C. K.; Amy, F.; Girshevitz, O.; Cahen, D.; Kahn, A. *Phys. Rev. Lett.* **2005**, *95*.
(24) Salomon, A.; Böcking, T.; Seitz, O.; Markus, T.; Amy, F.; Chan, C.; Zhao, W.; Cahen, D.; Kahn, A. *Adv. Mater.* **2007**, *19*, 445-450.
(25) Seitz, O.; Böcking, T.; Salomon, A.; Gooding, J. J.; Cahen, D. *Langmuir* **2006**, *22*, 6915-6922.
(26) Boukherroub, R. *Curr. Opin. Solid State Mater. Sci.* **2005**, *9*, 66-72.
(27) Buriak, J. M. *Chem. Rev.* **2002**, *102*, 1271-1308.
(28) Hamers, R. J.; In *Bioelectronics: From Theory to Applications, Willner, I., Katz, E., Eds.;* **2005**, *Chapter 7*, pages 209-230.
(29) Wayner, D. D. M.; Wolkow, R. A. *J. Chem. Soc., Perkin Trans. 2* **2002**, 23-34.

(30) Har-Lavan, R.; Ron, I.; Thieblemont, F.; Cahen, D. *Appl. Phys. Lett.* **2009**, *94*.
(31) Yaffe, O.; Scheres, L.; Puniredd, S. R.; Stein, N.; Biller, A.; Lavan, R. H.; Shpaisman, H.; Zuilhof, H.; Haick, H.; Cahen, D.; Vilan, A. *Nano Lett.* **2009**, *9*, 2390-2394.
(32) Sieval, A. B.; van den Hout, B.; Zuilhof, H.; Sudhölter, E. J. R. *Langmuir* **2001**, *17*, 2172-2181.
(33) Wallart, X.; de Villeneuve, C. H.; Allongue, P. *J. Am. Chem. Soc.* **2005**, *127*, 7871-7878.
(34) Yuan, S. L.; Cai, Z. T.; Jiang, Y. S. *New J. Chem.* **2003**, *27*, 626-633.
(35) Sieval, A. B.; van den Hout, B.; Zuilhof, H.; Sudhölter, E. J. R. *Langmuir* **2000**, *16*, 2987-2990.
(36) Eves, B. J.; Sun, Q. Y.; Lopinski, G. P.; Zuilhof, H. *J. Am. Chem. Soc.* **2004**, *126*, 14318-14319.
(37) de Smet, L. C. P. M.; Pukin, A. V.; Sun, Q. Y.; Eves, B. J.; Lopinski, G. P.; Visser, G. M.; Zuilhof, H.; Sudhölter, E. J. R. *Appl. Surf. Sci.* **2005**, *252*, 24-30.
(38) Scheres, L.; Giesbers, M.; Zuilhof, H. *Langmuir* **2010**, ASAP, doi: la100858q
(39) Puniredd, S. R.; Assad, O.; Haick, H. *J. Am. Chem. Soc.* **2008**, *130*, 13727-13734.
(40) Scheres, L.; Rijksen, B.; Giesbers, M.; Zuilhof, H. **2010**, submitted to Langmuir.
(41) Takeuchi, N.; Kanai, Y.; Selloni, A. *J. Am. Chem. Soc.* **2004**, *126*, 15890-15896.

Chapter 5

Molecular Modeling of Alkyl and Alkenyl Monolayers on Hydrogen-Terminated Si(111)

Abstract. In Chapter 4 considerable structural differences between alkyl and alkenyl monolayers are described, including an increased thickness, improved packing and higher surface coverage for the alkenyl monolayers. The precise origin thereof is not experimentally clarified yet. Therefore octadecyl and octadecenyl monolayers on Si(111) were studied in detail by molecular modeling, via PCFF molecular mechanics calculations on periodically repeated slabs of modified surfaces. After energy minimization the packing energies, structural properties, close contacts, and deformations of the Si surfaces of monolayers structures with various substitution percentages and substitution patterns were analyzed. For the octadecyl monolayers all data pointed to the same substitution percentage, which is due the compactness of the CH_2 groups close to the Si surface close to 50-55%. This agrees with literature and the experimentally determined coverage of octadecyl monolayers. For the octadecenyl monolayers the minimum in packing energy is calculated to be higher, namely around 60% coverage, which is close to the experimentally observed value of 65%, and this packing energy is much less dependent on the substitution percentage than calculated for alkyl layers. At a structural level this becomes clear since even at coverages above 60% a relative low number of close contacts and negligible deformation of the Si substrate was observed. In order to evaluate the thermodynamic feasibility of the monolayer structures, the binding energies of 1-alkenes and 1-alkynes to the hydrogen-terminated Si surface were obtained by composite high-quality G3 calculations. It was shown that due to the significantly larger reaction exothermicity of the 1-alkynes, thermodynamically even a substitution percentage as high as 75% is possible for octadecenyl chains. However, because sterically (based on Van der Waals footprint) a coverage of 69% is the maximum for alkyl and alkenyl monolayers, the optimal substitution percentage of octadecenyl monolayers will be presumably close to this latter value.

This chapter is submitted for publication as:
'*Molecular Modeling of Alkyl and Alkenyl Monolayers on Hydrogen-Terminated Si(111)*' Scheres, L.; Rijksen, B.; Giesbers, M.; Zuilhof, H. *submitted to Langmuir.*

5.1 Introduction

Due to the ongoing miniaturization of semiconductor devices, there is a still growing interest in the surface modification of silicon.[1-5] In this perspective, organic monolayers directly bound to oxide-free silicon surfaces are interesting candidates as they can easily be implemented in the existing technology for fabrication of silicon-based micro- and nanostructured devices. On H–Si(111), thermal or light-induced reactions with 1-alkenes,[6-10] 1-alkynes,[6,7,9-11] alcohols[12,13] and aldehydes[12-14] yield alkyl (Si–C–C), alkenyl (Si–C=C) and alkoxyl (Si–O–C) monolayers, respectively. For all three types of monolayers the direct covalent linkage to the silicon surface creates a well-defined organic monolayer-silicon interface, in which especially Si–C–C and Si–C=C linked monolayers are both thermally and chemically very robust.[7,15,16] Moreover, because an intervening SiO_2 layer is essentially absent, direct electronic coupling between any organic functionality and the silicon substrate is possible, which provides an opportunity to enhance the device performance compared to SiO_2-covered devices.[17-21] As a result these monolayers have great potential in fields of biosensors and molecular electronic and photovoltaic devices.[2-5,20-23]

Nevertheless, for all these potential applications the long-term stability of the oxide-free monolayer-silicon interface is the most important property, because even trace amounts of oxide can act as interface states that degrade the electronic properties of the underlying Si. Therefore, both the chemical stability of the surface linkage and the quality (or packing density) of the monolayer, play an important role. For instance, despite a surface coverage as high as 67%,[14] an inferior chemical stability was reported for the alkoxyl monolayers with respect to alkyl monolayers with a surface coverage of only 50-55%.[16] Most probably caused by the Si–O–C linkage of the alkoxyl monolayers, which is more susceptible to hydrolysis than the Si–C linkage of the alkyl monolayers.[12,16]

When comparing alkyl and alkenyl monolayers on H–Si(111), the highest chemical stability is expected for alkenyl monolayers, because the Si–C=C linkage is known to suppress oxidation of the underlying Si substrate.[24] However, as monolayer formation with both 1-alkenes and 1-alkynes occurs via the same meandering radical chain reaction at the H–Si surface,[7,25] steric hindrance of already bound chains can prevent insertion of new chains. As a result, filling of the last pinholes to obtain a defect-free monolayer will be hard with both 1-alkenes and 1-alkynes. In addition, since only 50-55% of the reactive H-Si sites can be substituted by alkyl chains,[7,10,26-31] 45-50% of the H-Si sites remains unreacted after monolayer formation. As a consequence only minor defects in the monolayer are sufficient for water and oxygen to penetrate through the monolayer to the monolayer-silicon interface,

where they can react with the large number of unreacted H-Si sites. The resulting oxide patches create electrically active surface states that will change the electrical properties of the underlying silicon drastically.[19] Thus, although hard to achieve, defect-free and well-ordered monolayer structures with a chemically stable linkage are the most important prerequisites for successful implementation of organic monolayers on oxide-free silicon in molecular electronic and biosensor devices.

In Chapter 4 the structural differences between alkyl and alkenyl monolayers on Si(111) were investigated in detail by ellipsometry, attenuated total reflectance infrared spectroscopy (ATR-IR) and X-ray photoelectron spectroscopy (XPS).[6] The monolayer characteristics (thickness, tilt angle, packing and surface coverage) of the alkyl monolayers were in good agreement with literature, however, for the alkenyl monolayers higher thicknesses, an improved packing and a surface coverage as high as 65% were observed. This was an exciting but also surprising result, especially if one considers that the structural difference between both is rather small, i.e. a single carbon-carbon bond (C–C) is replaced by a double carbon-carbon bond (C=C) (see Figure 1).

So far only a few molecular modeling studies on organic monolayers on H–Si(111) are reported in literature. Most of them deal solely with alkyl monolayers and report an optimal coverage close to 50% on H-Si(111).[14,27,28,30,31] Apart from alkyl monolayers, Pei et al.[14] also examined alkoxyl monolayers by molecular modeling and found, due to the smaller Van der Waals radius of the Si–O–C linkage, an packing density of 67% for these monolayers. Up to now, only Yuan et al.[30] compared alkyl and alkenyl monolayers, however, they only focused on relative short chains (C_8; octyl and octenyl) in combination with the UFF force field that was previously shown to yield erroneous results.[28] In contrast to the considerable differences that were found experimentally for long alkyl and alkenyl monolayers (C_{12} to C_{18}),[6] only minor structural differences and roughly equal optimal substitution percentages (~50%) were observed for these short alkyl and alkenyl monolayers.[30]

All this stimulated us to compare long alkyl and alkenyl monolayers on Si(111) in detail by molecular modeling. As the experimentally observed structural differences were most pronounced for C_{18} monolayers, only octadecyl and octadecenyl monolayers were examined (see Figure 1). For both types of monolayers, simulation cells with 50, 60, 67 and 75% substitution and various substitution patterns were built, and after optimization the packing energies of the chains, the structural properties of the final monolayer, the interpenetration of Van der Waals radii and the deformation of the Si substrate were compared. Finally, in order to evaluate the thermodynamic feasibility of all monolayer

structures, we used the composite high-quality ab initio G3 method[32] to calculate the binding energies of 1-alkenes and 1-alkynes to H-Si, and subsequently determined the total energy gains of monolayer formation with 1-octadecene and 1-octadecyne on H-Si(111).

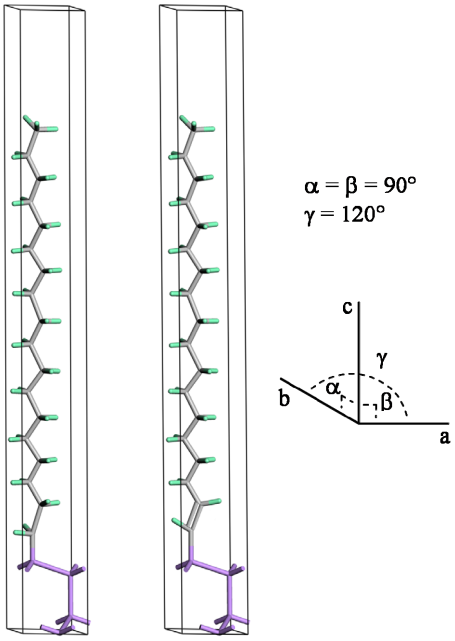

Figure 1. Structures of the initial octadecyl (left) and octadecenyl unit cells (right).

5.2 Experimental

In this study Materials Studio software (version 2.2) was used to construct and optimize the structure of octadecyl and octadecenyl monolayers on H-Si(111). All monolayer structures were built from two initial unit cells containing an octadecyl or octadecenyl chain attached to four Si atoms, which represent the first four layers of the Si surface (Figure 1). These initial unit cells were obtained by cleaving the Si crystal structure along the (111) plane and subsequent attachment of a pre-optimized, vertically aligned all-trans octadecyl or octadecenyl chain to the top Si atom. These new structures were placed in a box, with dimensions a = b = 3.840 Å (from the Si bulk unit cell) and c = 35 Å and angles $\alpha = \beta = 90°$ and $\gamma = 120°$. Then these boxes were copied in the a and b direction by as many times as necessary to generate the required larger unit cells. By replacing the proper octadecyl or octadecenyl chains by hydrogen atoms, unit cells with different substitution percentages

and substitution patterns were obtained. Finally, the unit cells were copied several times in the a and b direction to obtain the final big simulation cells (see Table 1).[14,27,28,30,31]

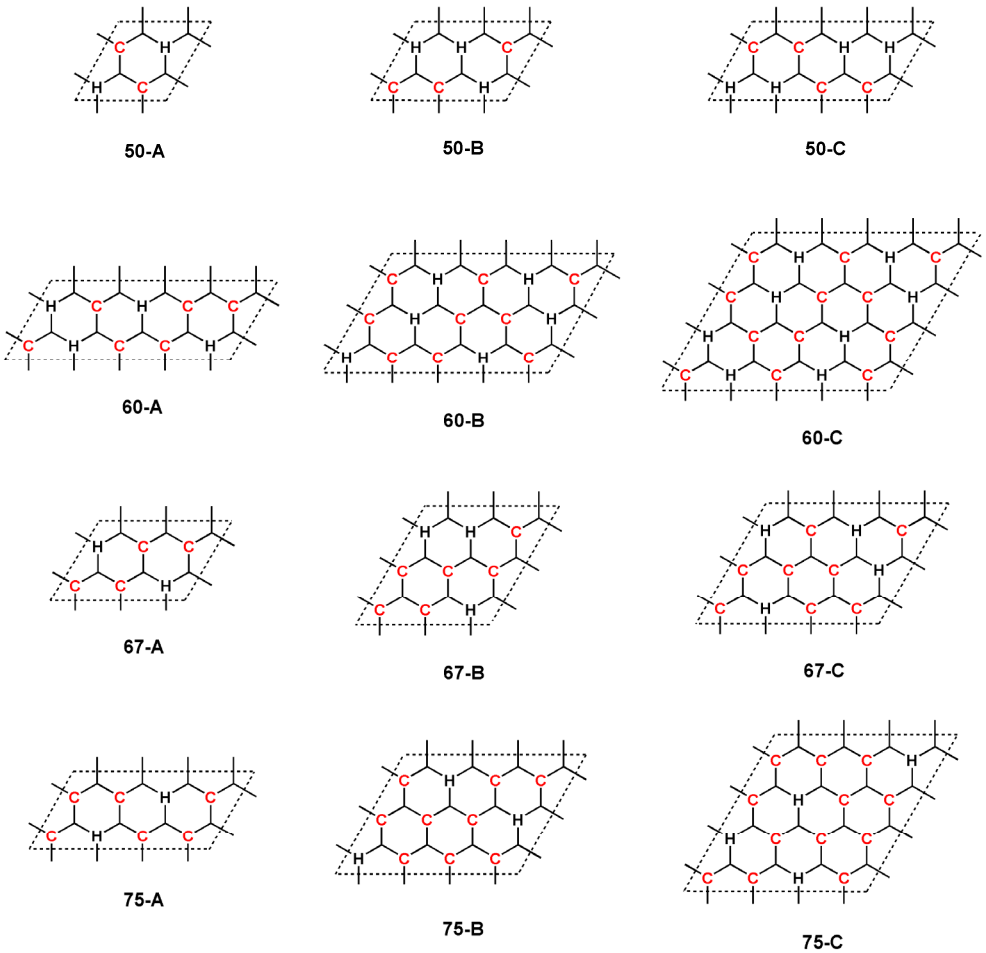

Figure 2. Overview of all unit cells used to create the simulation cells with 50, 60, 67 and 75% substitution. An **H** corresponds to an unreacted H-Si site and a **C** represents an octadecyl or octadecenyl chain.

All simulation cells were optimized using a polymer consistent force field (PCFF), as this has been shown to give a proper account of interchain interactions,[27,28] with the "Smart Minimizer" routine and "high-convergence" criteria.[33] By applying periodic boundary conditions, edge effects were eliminated (i.e. chains at on side of the simulation cell "feel" the presence of the chains at the opposite side of the cell) and as result an infinitely large

surface is represented by only one simulation cell. In addition, to mimic the rigidity of the bulk Si crystal, the positions of the two Si layers at the bottom of the box were fixed at their crystal positions and the two top Si layers, which are closest to the organic substituents, were allowed to be optimized.[14,27,28,30,31]

Binding energies were estimated by calculating the G3 energies for attachment of 1-butene and 1-butyne to a small silicon cluster, $HSi(SiH_3)_3$, (Figure 6). The binding energy was calculated as the difference of the G3 energy of the product and the G3 energy of the reactants. Calculations were performed using the Gaussian09 program package.[32,34] All geometries were fully optimized and shown to be minima on the potential energy surface.

5.3 Results and Discussion

To determine the optimal substitution percentage of the alkenyl monolayers on H-Si(111) and to investigate the structural differences between alkyl and alkenyl monolayers by molecular modeling, a series of unit cells with different substitution percentages and various substitution patterns were designed. Because experimental data and molecular modeling studies reveal an optimal substitution percentage close to 50-55% for long alkyl monolayers,[7,10,26-31] and because in Chapter 4 a surface coverage of approximately 65% was found for long alkenyl monolayers,[6] only substitution percentages of 50, 60, 67 and 75% were examined in this study. Nevertheless, for every substitution percentage three different unit cells (small, medium and big) were used to create the final simulation cells. The small unit cells result in relative simple patterns, whereas the big unit cells yield more complex and disordered monolayer structures. The whole series of unit cells is depicted in Figure 2.[35]

All minimizations were carried out with high-convergence criteria[33] and periodic boundary conditions to eliminate the edge effects and to mimic an infinitely large surface with only a finite simulation cell.[14,27,28,30,31,33] To obtain a reliable outcome of the calculation, i.e. an outcome independent of the number of the chains in the simulation cell, the simulation cells were made sufficiently large to give data that were invariant to further enlargement of the unit cell (see Table 1, 12 × 12 or 10 × 15 Si surface atoms).[27,28] As an example simulation cell 50A after optimization with octadecyl and octadecenyl chains is shown in Figure 3.

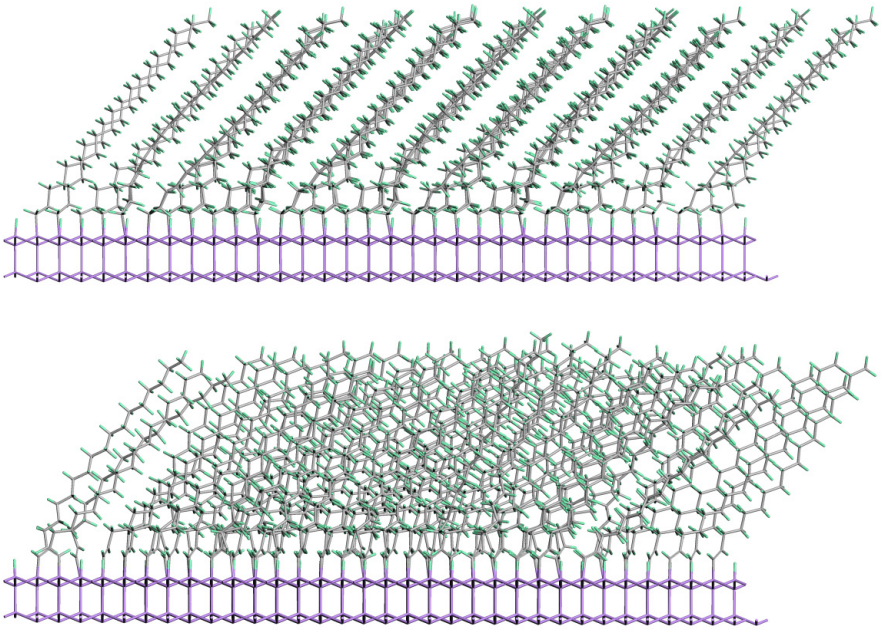

Figure 3. Side views of simulation cell 50A after optimization with octadecyl (top) and octadecenyl chains (bottom).

To solely investigate the interchain interactions we first cut the chains loose from the silicon substrate and then derived the average packing energy ($E_{packing}$) per octadecyl or octadecenyl chain with following equation:

$$E_{packing} = \frac{E_{chains}}{n} \qquad (1)$$

where E_{chains} is total potential energy of all chains in the simulation cell after optimization and substitution of the carbons that were linked to the Si with hydrogen atoms, and n is the total number of chains in the simulation cell. The resulting packing energies of the octadecyl or octadecenyl chains in all simulation cells are shown in Table 1.

For the octadecyl monolayer structures the lowest packing energies are obtained at 50% substitution and are on average close to -41 kcal/mol. As expected, the packing energy of the octadecyl chains gradually increases with the substitution percentage to more or less -15 kcal/mol at 75% substitution, most probably caused by crowdedness and steric constraints

of the CH_2 groups near the Si surface and the related unfavorable conformations that emerge at higher packing densities. An optimal coverage of 50% is in excellent agreement with experimental data and previous modeling studies of alkyl monolayers on Si(111).[6,7,26-28,30,31] Since for octadecenyl monolayers the experimental packing density is around 65% coverage,[6] the optimum packing energy was expected to be found at coverages significantly higher than 50%. The data in Table 1 indeed clearly show that ~60% displays the lowest packing energy per chain. In addition, we note that – compared to the octadecyl monolayers – the packing energies of the octadecenyl chains increase only slightly with the surface coverage over the range 60% – 75%. We attribute this to the smaller Van der Waals radius of the C=C bond, which leads to less interpenetration of the Van der Waals radii and therefore to less unfavorable conformations near the Si surface at higher substitution percentages.

Table 1. Packing energies per octadecyl and octadecenyl chain ($E_{packing}$) for various substitution patterns at 50, 60, 67 and 75% substitution.

Unit cell	Simulation cell size	Number of chains *n*	Packing Energy per chain, $E_{packing}$ (kcal/mol)	
			Octadecyl	Octadecenyl
50A	12×12	72	-38.3	-37.3
50B	10×15	75	-42.8	-38.6
50C	12×12	72	-40.9	-38.8
60A	10×15	90	-36.0	-43.0
60B	12×15	108	-39.3	-41.5
60C	12×15	108	-39.4	-37.8
67A	12×12	96	-30.5	-37.3
67B	12×12	96	-33.8	-36.3
67C	12×12	96	-33.7	-38.0
75A	10×15	120	-14.0	-33.2
75B	12×12	108	-13.7	-34.9
75C	12×12	108	-17.1	-24.5

Because the radical chain mechanism by which these monolayers are formed is a random process, it very likely that, instead of only one substitution pattern, a real monolayer exists of numerous random substitution patterns. Therefore, as shown in Figure 4, we averaged the packing energies of the three different unit cells for every substitution percentages.[35] These averaged packing energies per chain can, around the minimum packing energies, be fitted well with a parabolic function. These fits suggest that although the lowest packing energies are obtained at 50% substitution, the minimum packing energy for the octadecyl monolayer structures might even be at a few percent higher coverage, a result in line with earlier work of Sieval et al.[27,28] For octadecenyl chains the lowest packing energy remains close to 60% substitution, but as can be clearly seen, the minimum is rather broad, and will thus allow other factors to influence the overall degree of substitution (vide infra).

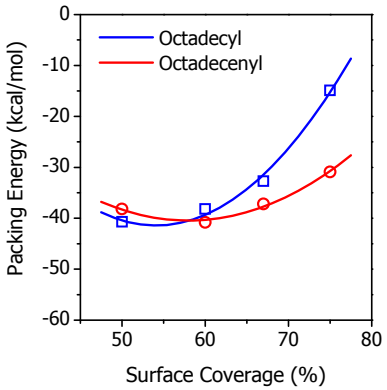

Figure 4. Averaged packing energies of octadecyl (□) and octadecenyl (○) monolayers on H-Si(111) (lines are fitted with a second order polynomial as a guide to the eye).

Besides information on the packing energies, molecular modeling also provides structural information of the optimized monolayers, like the chain tilt angles, monolayer thicknesses, bond lengths and bond angles. A comparison with available experimental data can give, in addition to the packing energies, a good impression whether a substitution percentage or substitution pattern is a good representation of the real monolayer structure or not. For instance, octadecyl monolayers on Si(111) are known to have a monolayer thickness of 18 - 19 Å, and a corresponding tilt angle in the range of 30 - 40°.[6,7,31] As shown in Table 2, after minimization only simulation cells with a substitution percentage of 50% match with the structural properties of the real octadecyl monolayer and thus verifies the optimal substitution percentage of 50 - 55% as derived from the packing energies.

Furthermore, in the ideal case the Si–C bonds in the octadecyl monolayers should be nearly perpendicular to the Si surface and the Si–C–C angles have to be close to 109° because of the sp^3-hybridization. However, at higher substitutions percentages, when the monolayer structures are too dense near the Si surface and CH_2 groups interpenetrate each other's Van der Waals radius, it is very likely that the Si–C bonds and the adjacent C–C bond deform to reduce these unfavorable interactions. This is clearly demonstrated by the increasing tilt of the Si–C bonds and the increasing Si–C–C angles of the octadecyl monolayers at coverages above 50% (Table 2).

Table 2. Structural properties of octadecyl and octadecenyl monolayers for various substitution patterns at 50, 60, 67 and 75% substitution.

Unit Cell	Octadecyl				Octadecenyl			
	tilt angle (θ)	thickness (d_{ML})	tilt Si-C (°)[a]	angle Si-C-C (°)	tilt angle (θ)	thickness (d_{ML})	tilt Si-C (°)[a]	angle Si-C=C (°)
50A	36	18.4	4-17	111-122	37	18.3	4-10	121-127
50B	37	18.2	3-14	113-118	41	17.8	3-8	120-125
50C	38	18.1	6-16	115-117	41	17.8	9	123-124
60A	31	21.0	4-23	115-126	26	21.2	7-10	121-130
60B	23	22.2	3-14	114-125	31	19.8	5-12	124-126
60C	23	22.3	0-15	116-124	29	20.6	0-6	124-126
67A	14	23.0	6-16	119-131	17	22.4	5-11	121-131
67B	14	23.0	3-27	116-128	18	22.3	3-13	122-130
67C	12	23.3	5-18	119-125	22	22.1	3-12	119-130
75A	4	23.4	2-21	119-130	3	23.2	4-14	121-134
75B	3	23.5	8-22	119-133	3	23.2	6-22	122-130
75C	5	23.5	4-25	115-130	3	23.0	5-11	121-133

[a] tilt of Si–C bond with the surface normal.

In Chapter 4 the octadecenyl monolayers were characterized in detail by ellipsometry, ATR-IR and XPS, and all three techniques revealed a monolayer thickness of 22 - 23 Å and a corresponding tilt angle of ~20°.[6] The structural properties of the simulated octadecenyl monolayers with a coverage of 67% display an excellent match with the thickness and tilt angle of real octadecenyl monolayers that were determined to have a packing density of 65%. Moreover, the effect of the less spacious C=C bond near the Si surface is clearly demonstrated by the Si–C bonds that stay almost perpendicular to the Si surface (i.e. tilts of

0 - 10° w.r.t. the surface normal), and by the Si–C=C angles that deviate only a few degrees from the ideal 120° for the sp^2-hybridized double bond, at 67% octadecenyl substitution.

To visualize the interpenetration of the Van der Waals radii of the CH_2 groups at high substitution percentages we used the "Close Contacts" option in the Materials Studio software. This option calculates the distances between all atoms in the simulation cells and only if the distance between two atoms is less than the sum of their Van der Waals radii it recognizes this distance as a close contact, i.e. only if interpenetration of the Van der Waals radii occurs. To investigate the degree of interpenetration of the Van der Waals radii in our monolayer structures, all distances less than 2.4 Å (twice the Van der Waals radius of a H-atom) are identified as a close contact. As a typical example simulation cell 67C with octadecyl and octadecenyl substitution is shown in Figure 5 (see Appendix 2 for enlarged images). It is obvious that there are less unfavorable close contacts between the octadecenyl chains, especially close to the monolayer-silicon interface where the more compact C=C bond is situated. Simply counting the number of close contacts in the simulations cells showed that all octadecyl structures contain roughly the double amount of close contacts compared to the corresponding octadecenyl structures. And although the total number of close contacts is increasing with the substitution percentage for both types of monolayers, their ratio is independent of the substitution percentage and remains roughly 2:1.

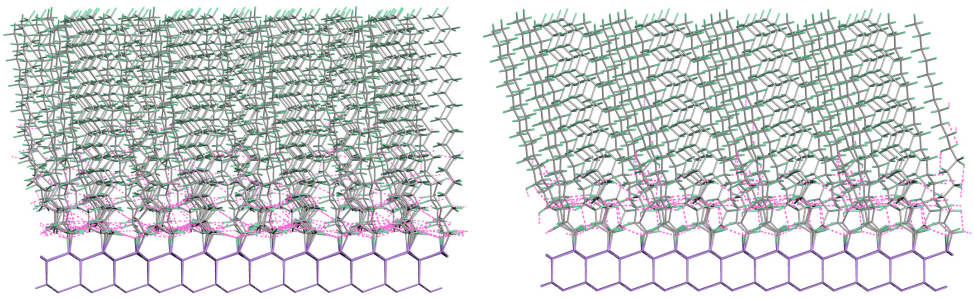

Figure 5. Side view of simulation cell 67C after optimization. The pink dashed lines represent the close contacts. On the left with octadecyl chains and on the right with octadecenyl chains.

As discussed above, at high substitution percentages, and in particular with the octadecyl monolayer structures, the chains are too densely packed near the Si surface and there is simply not enough space to accommodate all atoms. To diminish the unfavorable Van der Waals repulsions, the CH_2 groups tend to move away from each other as far as possible and this can lead to significant deformation of the Si–C and C–C bonds. However,

as the two top layers of the Si surface are free to move during minimization, also deformation of the Si substrate can contribute in releasing the strain and reducing the unfavorable interactions near the monolayer-silicon interface. Therefore, to study the extent of Si deformation induced by the octadecyl or octadecenyl chains attached, we calculated the total potential energy per Si unit (E_{Si}) after optimization with the following equation:

$$E_{Si} = \frac{E_{Total\ Si} \times \varphi}{n} \qquad (2)$$

where $E_{Total\ Si}$ = total potential energy of the complete Si substrate in a simulation cell after optimization and replacement of the octadecyl or octadecenyl chains by H atoms, φ = substitution percentage, and n = total number of chains in the simulation cell.

Table 3. Total potential energy per Si unit (E_{Si}) after optimization for various substitution patterns at 50, 60, 67 and 75% substitution.

Pattern	Total Potential Energy per Si unit E_{Si} (kcal/mol)	
	Octadecyl	Octadecenyl
50A	-15.3	-15.4
50B	-15.3	-15.4
50C	-15.2	-15.3
60A	-15.0	-15.4
60B	-15.2	-15.3
60C	-15.2	-15.3
67A	-15.0	-15.3
67B	-14.9	-15.3
67C	-15.0	-15.3
75A	-14.5	-15.2
75B	-14.9	-15.2
75C	-14.4	-15.0

As shown in Table 3, there are clear differences between the E_{Si} values after optimization with octadecyl and octadecenyl chains. For the octadecyl simulation cells the only substitution percentage with negligible deformation of the Si substrate is 50% (E_{Si} = -15.3 kcal/mol). Higher chain densities yield a gradual decrease of the potential energies of the Si

surface to -14.6 kcal/mol at 75% coverage. As expected for the smaller Van der Waals radius of the C=C bond, the potential energy of the Si substrate is stable at 50, 60 and 67% octadecenyl substitution (-15.3 or -15.4 kcal/mol), only at 75% coverage there is some deformation of the Si substrate as demonstrated by the average energy of -15.1 kcal/mol. In line with the structural properties and the close contact measurements, these data imply an optimal packing close to 50% for octadecyl monolayers and a coverage of ~67% for the octadecenyl monolayers.

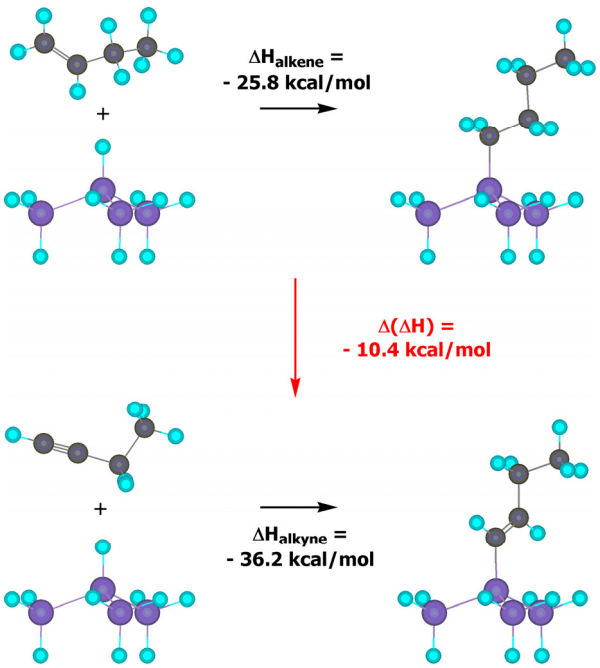

Figure 6. Models used for the G3 calculations to obtain the binding energy of 1-alkynes and 1-alkenes onto a hydrogen-terminated Si surface.

In contrast to the packing energy data, which suggest a optimal coverage of 60%, the structural properties, the relative low number of close contacts and the negligible deformation of the Si surface indicate an optimal substitution percentage close to 67% for octadecenyl monolayers. Thus it seems that solely calculating the packing energy is not always sufficient to verify whether a certain substitution percentage or substitution pattern is favorable or not. This is actually not really surprising because the energy associated with the chemisorption of a chain on the Si substrate (i.e. the binding energy) is not considered in the packing energy, while it is the main driving force for the monolayer formation. In

addition, one can easily imagine that a large exothermic binding energy can have a significant effect on the final monolayers structure, because a large binding energy can make higher substitution percentages thermodynamically possible, despite strain and unfavorable conformations close to the monolayer-silicon interface.[26] Consequently, we studied the reaction of 1-alkenes and 1-alkynes with a hydrogen-terminated silicon cluster (as depicted in Figure 6) by composite high-quality ab initio G3 calculations.[32] These computations yield a binding energy to hydrogen-terminated silicon of -25.8 kcal/mol for 1-alkenes and -36.2 kcal/mol for 1-alkynes. Therefore the enthalpy for the attachment of 1-alkynes is ~10 kcal/mol more negative than that for 1-alkenes.

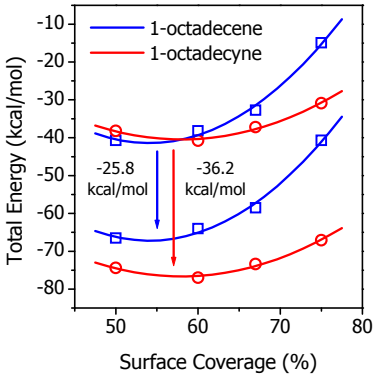

Figure 7. The packing and binding energy were summed to obtain the total energy gain of monolayer formation with 1-octadecene (□) and 1-octadecyne (○) onto H-Si(111).

The more negative reaction enthalpy will likely contribute to the higher packing density of 1-alkyne-derived monolayers, as the more negative enthalpy of the attachment reaction can compensate the growing steric hindrance upon increase of the packing density beyond the minimum steric energy per chain for a longer time than possible for 1-alkenes. A better picture to compare the reactivity of 1-alkenes and 1-alkynes is therefore depicted in Figure 7, in which the total energy (E_{Tot}) of monolayer formation per chain was estimated by adding up the binding energy and the average packing energy. Due to the larger exothermicity of the binding reaction of 1-alkynes to H–Si(111), monolayer assembly is for all substitution percentages thermodynamically more favorable with 1-octadecyne than with 1-octadecene. In addition, we note that for the 1-alkyne-derived surface even at 75% coverage – where also for this type of monolayer deformation of the Si substrate and the unfavorable conformations near the Si surface starts to play an important role – the total energy is more negative than for octadecyl chains at only 50% coverage. It can be

calculated from the cross section of a long alkyl (and alkenyl) chain (18.5 - 18.6 $Å^2$) and the surface area of a H–Si group on the H–Si(111) surface (12.8 $Å^2$),[28] that the maximum coverage would be 69% if only steric constraints would be relevant. The data in Figure 7 suggest that in fact, the maximally obtainable packing density may perhaps be slightly higher, as the enthalpy of attachment can still compensate the increasing steric repulsion. Most likely the coverage will not be significantly larger than 69%, because kinetically it will be hard to add extra chains to a well-ordered monolayer, and the best possible coverage will therefore be close to the remarkably high surface coverage that was found for long alkenyl monolayers on H-Si(111) (see Chapter 4).[6]

5.4 Conclusions

A combination of PCFF molecular mechanics studies and ab initio G3 calculations was used to investigate the structural differences between octadecyl and octadecenyl monolayers on hydrogen-terminated Si(111) surfaces. PCFF modeling shows that the minimum steric energy occurs for octadecenyl monolayers at significantly higher packing densities than for the fully saturated octadecyl monolayers. This more attractive packing for the unsaturated octadecenyl monolayer is shown to result from the compactness of the C=C moiety near the surface, which leads to strongly diminished steric repulsions and distortions of the Si–C linkage. While for octadecyl monolayer the minimum steric energy is found around 50 - 55%, for octadecenyl monolayers the minimum is found around 60%, while the dependence of the steric energy on the packing density is significantly smaller than for the saturated analog (even 75% coverage yields only 3 - 10 kcal/mol steric penalty/chain, depending on the substitution pattern). In addition, composite high-quality G3 ab initio computations reveal that the binding energy of 1-alkynes onto the Si surface is 10 kcal/mol more negative than of 1-alkenes. This makes the octadecenyl monolayers significantly more stable at any degree of coverage than octadecyl monolayers, explains the recently found experimental coverage of 65%,[6] suggests the possibility for even further improvement, and further substantiates the attractiveness of these unsaturated organic monolayers on silicon.

References

(1) Aswal, D. K.; Lenfant, S.; Guerin, D.; Yakhmi, J. V.; Vuillaume, D. *Anal. Chim. Acta* **2006**, *568*, 84-108.

(2) Buriak, J. M. *Chem. Rev.* **2002**, *102*, 1271-1308.

(3) Boukherroub, R. *Curr. Opin. Solid State Mater. Sci.* **2005**, *9*, 66-72.

(4) Vilan, A.; Yaffe, O.; Biller, A.; Salomon, A.; Kahn, A.; Cahen, D. *Adv. Mater.* **2009**, *22*, 140-159.

(5) Hamers, R. J. *Ann. Rev. Anal. Chem.* **2008**, *1*, 707-736.

(6) Scheres, L.; Giesbers, M.; Zuilhof, H. *Langmuir* **2010**, *26*, 4790-4795.

(7) Linford, M. R.; Fenter, P.; Eisenberger, P. M.; Chidsey, C. E. D. *J. Am. Chem. Soc.* **1995**, *117*, 3145-3155.

(8) Sieval, A. B.; Linke, R.; Zuilhof, H.; Sudhölter, E. J. R. *Adv. Mater.* **2000**, *12*, 1457-1460.

(9) Sun, Q. Y.; de Smet, L. C. P. M.; van Lagen, B.; Giesbers, M.; Thune, P. C.; van Engelenburg, J.; de Wolf, F. A.; Zuilhof, H.; Sudhölter, E. J. R. *J. Am. Chem. Soc.* **2005**, *127*, 2514-2523.

(10) Cicero, R. L.; Linford, M. R.; Chidsey, C. E. D. *Langmuir* **2000**, *16*, 5688-5695.

(11) Scheres, L.; Arafat, A.; Zuilhof, H. *Langmuir* **2007**, *23*, 8343-8346.

(12) Hacker, C. A.; Anderson, K. A.; Richter, L. J.; Richter, C. A. *Langmuir* **2005**, *21*, 882-889.

(13) Boukherroub, R.; Morin, S.; Sharpe, P.; Wayner, D. D. M.; Allongue, P. *Langmuir* **2000**, *16*, 7429-7434.

(14) Pei, Y.; Ma, J.; Jiang, Y. S. *Langmuir* **2003**, *19*, 7652-7661.

(15) Sung, M. M.; Kluth, G. J.; Yauw, O. W.; Maboudian, R. *Langmuir* **1997**, *13*, 6164-6168.

(16) Sano, H.; Maeda, H.; Ichii, T.; Murase, K.; Noda, K.; Matsushige, K.; Sugimura, H. *Langmuir* **2009**, *25*, 5516-5525.

(17) Salomon, A.; Böcking, T.; Chan, C. K.; Amy, F.; Girshevitz, O.; Cahen, D.; Kahn, A. *Phys. Rev. Lett.* **2005**, *95*.

(18) Salomon, A.; Böcking, T.; Seitz, O.; Markus, T.; Amy, F.; Chan, C.; Zhao, W.; Cahen, D.; Kahn, A. *Adv. Mater.* **2007**, *19*, 445-450.

(19) Seitz, O.; Böcking, T.; Salomon, A.; Gooding, J. J.; Cahen, D. *Langmuir* **2006**, *22*, 6915-6922.

(20) Har-Lavan, R.; Ron, I.; Thieblemont, F.; Cahen, D. *Appl. Phys. Lett.* **2009**, *94*.

(21) Yaffe, O.; Scheres, L.; Puniredd, S. R.; Stein, N.; Biller, A.; Lavan, R. H.; Shpaisman, H.; Zuilhof, H.; Haick, H.; Cahen, D.; Vilan, A. *Nano Lett.* **2009**, *9*, 2390-2394.

(22) Wayner, D. D. M.; Wolkow, R. A. *J. Chem. Soc., Perkin Trans. 2* **2002**, 23-34.

(23) Hamers, R. J. In *Bioelectronics: From Theory to Applications* Willner, I., Katz, E., Eds. 2005; Vol. Chapter 7, p 209-230.

(24) Puniredd, S. R.; Assad, O.; Haick, H. *J. Am. Chem. Soc.* **2008**, *130*, 13727-13734.

(25) Eves, B. J.; Sun, Q. Y.; Lopinski, G. P.; Zuilhof, H. *J. Am. Chem. Soc.* **2004**, *126*, 14318-14319.

(26) Nemanick, E. J.; Solares, S. D.; Goddard, W. A.; Lewis, N. S. *J. Phys. Chem. B* **2006**, *110*, 14842-14848.

(27) Sieval, A. B.; van den Hout, B.; Zuilhof, H.; Sudhölter, E. J. R. *Langmuir* **2000**, *16*, 2987-2990.

(28) Sieval, A. B.; van den Hout, B.; Zuilhof, H.; Sudhölter, E. J. R. *Langmuir* **2001**, *17*, 2172-2181.

(29) Wallart, X.; de Villeneuve, C. H.; Allongue, P. *J. Am. Chem. Soc.* **2005**, *127*, 7871-7878.

(30) Yuan, S. L.; Cai, Z. T.; Jiang, Y. S. *New J. Chem.* **2003**, *27*, 626-633.

(31) Zhang, L. Z.; Wesley, K.; Jiang, S. Y. *Langmuir* **2001**, *17*, 6275-6281.

(32) Curtiss, L. A.; Raghavachari, K.; Redfern, P. C.; Rassolov, V.; Pople, J. A. *J. Chem. Phys.* **1998**, *109*, 7764-7776.

(33) Convergence: 1.0 x 10^{-5} kcal/mol/Å; Line Search: 0.01; Algorithm: Polak-Ribière.

(34) Frisch, M. J.; et al. *Gaussian09* **2009**, revision A.02; Gaussian, Inc.: Wallingford, CT.

(35) For all substitution percentages at least six different substitution patterns were tested. The substitution patterns depicted in this work were selected as being representative structures.

Chapter 6

Microcontact Printing onto Oxide-Free Silicon via Highly Reactive Acid Fluoride-Functionalized Monolayers

Abstract. This chapter describes a new route for patterning organic monolayers on oxide-free silicon by microcontact printing (μCP) on a preformed, reactive acid fluoride-terminated monolayer. In contrast to direct printing on H-Si, where the contact time is relatively long and the monolayer quality is difficult to control, this indirect printing approach is fast, and easily preserves the oxide-free and well-defined monolayer-silicon interface, which is the most important property for potential applications in biosensing and molecular electronics. Water contact angle measurements, ellipsometry, attenuated total reflection infrared spectroscopy (ATR-IR) and X-ray photoelectron spectroscopy (XPS) demonstrate the formation of the initial acid fluoride-terminated monolayers without upside-down attachment. Subsequent printing for 20 seconds with an *n*-hexadecylamine-inked PDMS stamp results in well-defined 5 μm *N*-hexadecylamide dots as evidenced by atomic force microscopy (AFM) and scanning electron microscopy (SEM). Printing with a flat stamp allows investigation of the efficiency of amide formation by μCP and water contact angle measurements, ellipsometry and XPS, and reveals the quantitative conversion of the acid fluoride groups to the corresponding amide within 20 seconds. The absence of silicon oxide (SiO_2), even after immersion in water for 16 h, demonstrates that the oxide-free monolayer-silicon interface is easily preserved by this patterning route. Finally, it is shown by fluorescence microscopy that also complex biomolecules, like functionalized oligo-DNA, can be immobilization on the oxide-free silicon surface via μCP.

This chapter is published as:
'*Microcontact Printing onto Oxide-Free Silicon via Highly Reactive Acid Fluoride-Functionalized Monolayers*' Scheres, L.; ter Maat, J.; Giebers, M.; Zuilhof, H. *Small*, **2010**, *6*, 642-650.

6.1 Introduction

Organic monolayers on oxide-free silicon are directly bound to silicon via a chemically stable Si–C bond. The absence of an intermediate SiO_2 layer results in a well-defined monolayer-silicon interface that allows direct electronic coupling between the organic functionality and the silicon substrate.[1-7] As a consequence these monolayers possess great potential in the field of molecular electronics, biosensing and photovoltaics.[8-15] Over the years numerous methods to prepare this type of monolayers have been described. Nearly all reported methods require a certain type of activation for monolayer formation, such as heating,[16-18] UV light,[19-21] visible light,[22-24] catalysts,[25-29] Grignard and lithium reagents,[30-32] electrochemistry,[33,34] and chemomechanical scribing.[35-37] Recently, a route has been developed that even yields high-quality monolayers under ambient conditions.[38] Despite of this variety of methods available for functionalization, the chemistry of oxide-free silicon is underdeveloped with respect to that of e.g. gold and silicon oxide/glass surfaces due to the following three reasons:

(1) Preparation of ω-functionalized monolayers on hydrogen-terminated silicon (H-Si) is considerably more difficult than the preparation of simple alkyl monolayers since many functional groups (including -OH, -CHO, $-NH_2$, -Br, -SH) are reactive towards H-Si.[8,39-42] An exception is the carboxylic acid (-COOH) functionality, thermal and microwave assisted modification of porous Si[42-44] and photochemical modification of flat Si surfaces[40,45] have been reported with only small to negligible indications of upside-down attachment. Nevertheless, hydrogen bonding causes acid bilayer formation, which makes these monolayers hard to clean,[39,46] while for further functionalization still an additional activation step via carboxylic anhydrides or *N*-hydroxysuccinimide (NHS) chemistry is needed.[45,47,48] To circumvent these problems our group recently reported a mild photochemical route for direct attachment of NHS-functionalized 1-alkenes on silicon.[49]

(2) The quality of organic monolayers on oxide-free silicon, in particular ω-functionalized monolayers, can be hard to control.[8] For potential applications in biosensing and molecular electronics the stability of the organic monolayers on oxide-free Si in ambient conditions and in aqueous media is an important issue, as trace amounts of oxide result in degradation of the electronic properties of the underlying Si.[1-7] To prevent penetration of water and oxygen through the monolayer, the monolayer should be densely packed, and free of defects. In addition, monolayer formation with 1-alkenes or 1-alkynes only substitutes 50% of the H-Si sites,[50] thus the remaining unreacted H-Si sites will react easily with water and oxygen if the monolayer quality is low.

(3) Microcontact printing (μCP) - a fast and simple patterning technique[51,52] - is currently not feasible with 1-alkenes or 1-alkynes directly on H-Si due to the extended reaction times (8 h) needed for monolayer formation under printing conditions, i.e. at room temperature.[38] To shorten reaction times, Zhu and coworkers activated H-Si by chlorination and printed alcohols on the chloride-terminated silicon (Cl–Si) at 70 °C. Although the reaction time was reduced to 30 min, the resulting alkoxyl monolayers (C–O–Si) are not oxide-free anymore and therefore susceptible to hydrolysis.[53] Very recently Mizuno and Buriak developed an elegant soft lithography route making use of Pd nanoparticles on the PDMS surface that catalyzes monolayer formation of 1-alkynes on H-Si.[27] However, as indicated by the monolayer thickness (1.3 nm for 1-octadecyne) after 20 min of contact, monolayer formation is likely not fully complete. This may eventually result in oxidation and interfaces states that change the electronic properties of the underlying Si, and is thus worthy of further investigations.

These three reasons motivated us to develop a new, fast and efficient μCP route for patterning of organic monolayers on oxide-free silicon. As mentioned before, direct printing on H-Si is not feasible, and therefore indirect printing on a preformed reactive monolayer, also called "reactive μCP", has our preference. In addition, this has the advantage that the oxide-free monolayer-silicon interface can be easily preserved during patterning. To the best of our knowledge reactive μCP has never been applied to organic monolayers on oxide-free silicon, most probably because an highly reactive ω-functionalized monolayer can not be obtained as easily as on gold and silicon oxide/glass surfaces. [8,39-42] On these last mentioned substrates, reactive μCP is already an established concept and printing on many reactive monolayers, including anhydride,[54-56] amine,[57] aldehyde[58] and azide[59]-terminated monolayers, has been reported. However, still there is some room for improvements, because ideally reactive μCP has:

(1) Short printing contact times, preferably seconds instead of the minutes or hours that were needed for reactive printing on azide[59] and amine[57]-terminated monolayers. To this aim a highly reactive ω-functionalized monolayer is required.

(2) A homogenous and high density transfer of the pattern. As a consequence the reactive functional group has to be small and – in contrast to anhydride-terminated monolayers where only 50% of the original acid-terminated monolayer is converted[54-56] – the conversion has to be complete.

(3) A high chemical selectivity, and is therefore compatible with many functional groups and allows printing of complex (bio)molecules.

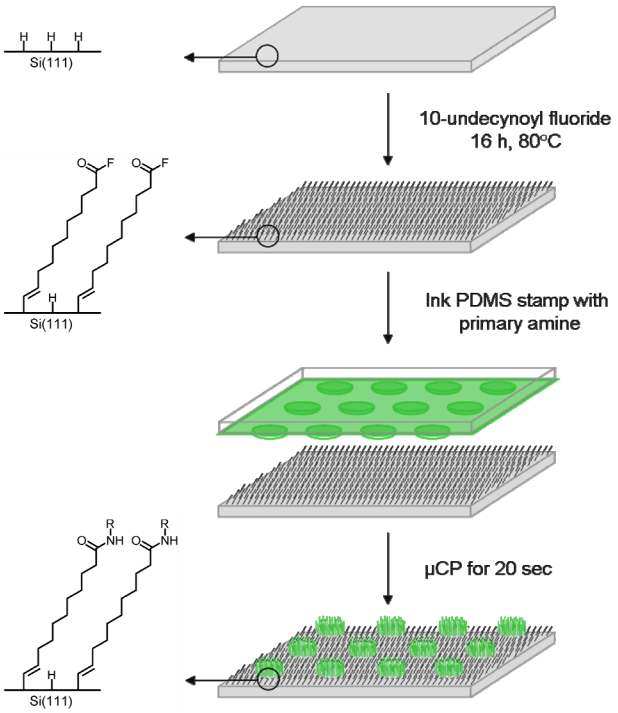

Figure 1. Schematic representation of the procedure used for µCP on oxide-free silicon via highly reactive acid fluoride-functionalized monolayers.

Trying to fulfill all these requirements, reactive ω-functionalized monolayers were prepared on oxide-free silicon with 10-undecynoyl fluoride. The terminal alkyne functionality on one end of 10-undecynoyl fluoride can react with H-Si under mild conditions,[38] and yields on Si(111) stable Si–C=C bonds[19,38] that are known to inhibit the oxidation of the underlying Si substrate.[60] The acid fluoride group on the other terminus was chosen because it can easily be synthesized from the corresponding carboxylic acid[61] and – due to the homolytically strong C–F bond – is expected not to react with H-Si surfaces. In contrast to the corresponding acid chloride, which does react with H-Si surfaces,[16] the acid fluoride functionality is stable under ambient conditions and reacts solely with strong nucleophiles, like anionic nucleophiles and amines, resulting in a high selectivity.[62,63] In addition, acid fluoride-terminated monolayers are easier to clean than carboxylic acid-terminated monolayers, because bilayer formation upon hydrogen bonding cannot occur.[39,46]

In this work we describe the formation of the initial reactive acid fluoride-terminated monolayer with 10-undecynoyl fluoride on H-Si(111) (Figure 1) and its characterization by contact angle measurements, ellipsometry, attenuated total reflection infrared spectroscopy (ATR-IR) and X-ray photoelectron spectroscopy (XPS). The acid fluoride-terminated monolayers were then used as a reactive platform for further functionalization and patterning by μCP with primary amines, and the resulting structures were analyzed by atomic force microscopy (AFM) and scanning electron microscopy (SEM). The efficiency of amide formation by μCP was studied by printing with a flat PDMS stamp and comparison with solution phase amine coupling, and the stability of the resulting *N*-hexadecylamide-terminated monolayers in water was investigated by XPS. Finally, we demonstrate that even complex (bio)molecules, like oligo-DNA labeled with fluorescent groups, can easily be immobilized on the oxide-free silicon surface by μCP on acid fluoride-terminated monolayers.

6.2 Experimental

6.2.1 Materials

PE40/60, EtOH and CH_2Cl_2 were distilled prior to use. For rinsing and contact angle measurements deionized water (18.3 MΩ cm resistivity) was used. 10-Undecynoic acid (ABCR, Germany, 97%), cyanuric fluoride (Aldrich, +97%), anhydrous pyridine (Aldrich, 99.8%), anhydrous CH_2Cl_2 (Aldrich, +99.8%), *n*-hexadecylamine (Aldrich, 98%), cysteamine (Aldrich, +98%), anhydrous 1-methyl-2-pyrrolidinone (Aldrich, 99.5%), gold nanoparticles (15 nm gold sol, Aurion, The Netherlands), 40% NH_4F solution (Honeywell, semiconductor grade), poly(dimethylsiloxane) (PDMS) (Sylgard 184, Dow Corning), Tris-EDTA buffer pH 8 (Fluka), 2-(2-aminoethoxy)ethanol (EG_2-NH_2, Aldrich, +98%), poly(propyleneimine) tetrahexacontaamine dendrimers, generation 5 (G5-PPI, Aldrich) and 20 × standard saline citrate (SSC) (20 × SSC = 3.0 M sodium chloride, 0.3 M sodium citrate in H_2O) buffer solution (Serva, VWR) were used as received. Both oligonucleotides were purchased from IBA (Germany). The strand we used for μCP, has sequence 5'-CCA CGG ACT ACT TCA AAA CTA-3' and was modified at the 5' terminus with an amino group via a six-carbon linker (NH_2-$(CH_2)_6$-) and at the 3' terminus with Cy3. The target strand has sequence 5'-TAG TTT TGA AGT AGT CCG TGG-3' with Cy5 modification at the 5' terminus. Silicon wafers were (111)-oriented single-side and double polished, 475-550 μm thick, n-type, P-doped samples, with a resistivity 1.0-5.0 Ω cm (Siltronix, France).

6.2.2 Synthesis of 10-Undecynoyl Fluoride

10-Undecynoic acid (36.5 g, 0.2 mol) was dissolved in 400 ml anhydrous CH_2Cl_2 under argon atmosphere, and anhydrous pyridine (11.7 g, 0.15 mol) and subsequently cyanuric fluoride (20.0 g, 0.15 mol) were added at 0 °C. A white precipitate was formed and the mixture was stirred for at least 2 h at room temperature. The progress of the reaction was followed by TLC and ^{1}H-NMR. Upon completion, ice was added, the precipitate was filter off and the organic layer was extracted three times with water. The combined organic layers were concentrated under reduced pressure. The crude product was purified by flash column chromatography (eluent CH_2Cl_2), followed by distillation under reduced pressure yielded 33.1 g (0.18 mol, 90%) of 10-undecynoyl fluoride: TLC R_f(CH_2Cl_2) = 0.91; ^{1}H NMR (400 MHz, $CDCl_3$, δ) 2.51 (dt, 2H, J = 1.1 Hz, J = 6.3 Hz), 2.19 (dt, 2H, J = 2.6 Hz, J = 7.0 Hz), 1.94 (t, 1H, J = 2.7 Hz), 1.67 (m, 2H, J = 7.4 Hz), 1.53 (m, 2H, J = 7.3 Hz), 1.33-1.44 (br s, 8H); ^{13}C NMR (400 MHz, $CDCl_3$, δ) 163.56 (J = ~361 Hz), 84.59, 68.12, 32.10 (J = ~40 Hz), 28.89, 28.76, 28.60, 28.55, 28.36, 23.89 (J = 1.5 Hz), 18.33; MS *m/z* 183.1191 (calculated for $C_{11}H_{16}OF$ ($M\text{-}H^+$), 183.1185).

6.2.3 Monolayer Preparation

Pieces of n-Si(111) single-side polished wafer were rinsed several times with acetone (semiconductor grade), sonicated in acetone for 10 min and treated with an oxygen plasma (set-up: Harrick PDC-002) for 3 min. Subsequently, the Si(111) substrates were etched in an argon-saturated 40% aqueous NH_4F solution for 15 min under an argon atmosphere. After being etched, the samples were thoroughly rinsed with deionized water and finally blown dry with a stream of dry nitrogen. A small three-necked flask equipped with a capillary as the argon inlet, a reflux condenser that was connected to a vacuum pump, and a stopper was charged with neat, freshly distilled 10-undecynoyl fluoride, followed by positioning of tip of the capillary in the reactive compound and turning on the argon flow through the capillary. The pressure in the flask was reduced to approximately 10 mbar, and the flask was immersed in an oil bath at 80 °C. The setup was deoxygenated with argon for at least 30 min. Subsequently, the pressure was raised by filling the setup with argon until atmospheric pressure was achieved. The freshly etched Si(111) substrate was transferred into the reaction flask while an argon flow was maintained. The setup was closed again, the pressure was reduced to ~10 mbar, and the capillary was moved away as far as possible from the surface of the liquid to prevent the disturbance of monolayer formation by the

argon flow. After 16 h at 80 °C, the reaction flask was backfilled with argon until atmospheric pressure was attained, and the sample was taken out. After rinsing excessively with CH_2Cl_2 and sonication in CH_2Cl_2 for 5 min to remove physisorbed molecules, the samples were blown dry with a stream of dry nitrogen.

6.2.4 Preparation of PDMS Stamps

PDMS stamps (flat and with pillar-like features of 5 μm or 10 μm) were prepared by casting a prepolymer of PDMS on a photolithographically patterned silicon master, cured for 20 h at 60 °C and released at 60 °C. Subsequently, the stamps were cleaned by extensive soxlet extraction and ultrasonicated with EtOH and dried in a stream of N_2.[64]

6.2.5 Coupling of Primary Amines

For microcontact printing the PDMS stamps were inked with in 2.5 mM solution of *n*-hexadecylamine in EtOH. Prior to printing, the stamps were blown dry in a stream of N_2. The stamps were brought in conformal contact with the acid fluoride-terminated monolayers for 20 sec. The stamp was released and the patterned monolayers were rinsed and ultrasonicated with CH_2Cl_2.

For the solution-phase reaction the acid fluoride-terminated monolayers were immersed in a 25 mM solution of *n*-hexadecylamine in 1-methyl-2-pyrrolidinone for 1 h. Afterwards they were rinsed and ultrasonicated with CH_2Cl_2. The *n*-hexadecylamine-printed monolayers were backfilled by immersion in a 25 mM solution of cysteamine in 1-methyl-2-pyrrolidinone for 1 h, rinsed and sonicated with CH_2Cl_2 and finally dipped in aqueous suspension of Au nanoparticles (~15 nm) for 15 min.

For printing of DNA we used “dendri-stamps” as described by Rozkiewicz et al.[58,65] Briefly, the PDMS were oxidized with an oxygen plasma (set-up: Harrick PDC-002) for 10 min. Subsequently the hydrophilic stamps were immersed in 1 μM ethanolic solution of G5-PPI dendrimers for 30 sec. and blown dry with a flow of nitrogen. A drop of the Cy3-labeled oligonucleotide solution (2.5 μM in Tris-EDTA buffer, pH 8) was incubated on the stamp for 20 min at room temperature. The stamp was dried with a flow of nitrogen and brought in conformal contact with the acid fluoride-terminated monolayer. After 20 sec. the stamp was lifted off and the substrate was thoroughly rinsed with ethanol containing a drop of triethylamine to remove the G5-PPI dendrimer layer and dried with a flow of nitrogen. To passivate the remaining acid fluoride-terminated areas and to prevent non-specific

adsorption during later hybridization steps, the DNA printed surfaces were immersed in a 25 mM solution of EG_2-NH_2 in EtOH for 1 h. Subsequently, the substrates were rinsed with EtOH and dried with a stream of nitrogen. For hybridization, the substrate was immersed in a target oligonucleotide (Cy5-labeled) solution (1 μM in 5 × SSC containing 0.2% SDS) at room temperature in dark for overnight. The nonhybridized and physically bound target oligonucleotides were removed by copious rinsing with 1 × SSC with 0.1% SDS and water and finally the substrate was dried with nitrogen.

6.2.5 Monolayer Characterization

Static water contact angles were measured with an automated Krüss DSA 100 goniometer. At least six small droplets of 2.0 μl deionized water were dispensed and the contact angles was determined using a Tangent 2 fitting model. The error in the contact angles is < 1°.

Attenuated total reflectance infrared (ATR-IR) spectra were collected with a Bruker spectrometer (model Tensor 27) equipped with a Harrick ATR accessory and an MCT detector. A Harrick grid polarizer was placed in front of the sample for measuring spectra with p-polarized (parallel) light. Double polished n-Si(111) wafers were cut into pieces of 5 × 1 cm and polished to obtain ATR crystals with 45º bevels (± 100 internal reflections). The spectra were taken at a resolution of 4 cm^{-1} by adding 2048 scans while flushing with dry N_2 and referenced to a clean native oxide-covered ATR crystal. A slight linear baseline correction was applied.

Ellipsometric measurements were performed with a Sentech Instruments (Type SE-400) ellipsometer, operating at 632.8 nm (He-Ne-laser) and an angle of incidence of 70°. The optical constants of the substrate were determined with a piece of freshly etched n-Si(111) (n = 3.819 and k = 0.057). The thicknesses of the monolayers were determined with a planar three-layer (ambient, monolayer, substrate) isotropic model with refractive index of 1.46 for the organic monolayer. The reported values are the average of eight measurements taken at different locations on the sample and the error is < 1 Å.

X-ray photoelectron spectroscopy (XPS) analysis were performed using a JPS-9200 photoelectron spectrometer (JEOL, Japan). High-resolution spectra were obtained under UHV conditions using monochromatic Al Kα X-ray radiation at 12 kV and 25 mA, using an analyzer pass energy of 10 eV. All high-resolution spectra were corrected with a linear background before fitting.

Electronic core level calculations were done with GAUSSIAN03 program.[66] The geometries of the different systems were optimized at the B3LYP/6-311G(d,p) level of theory. Natural bond orbital (NBO) analysis[67] was employed to obtain the core orbital energies.

Atomic force microscopy (AFM) topography images were made using a scanning probe microscope in non-contact mode (NC-AFM) under vacuum conditions (10^{-4} Pa) (JSPM-5400, JEOL, Japan) and in tapping mode (AC-AFM) in air (MFP3D, Asylum Research, Santa Barbara, CA). For both, a high frequency (320 kHz) silicon cantilever (NCHR-20, NanoWorld) was used.

SEM measurements were performed by using ultra-high vacuum scanning electron microscopy (UHV-SEM) with a Gemini electron gun (Omicron, Germany).

The fluorescence images were recorded on a Zeiss Axioplan II imaging photomicroscope, equipped with epifluorescence illumination and small band filter sets for the Cy3 and Cy5 fluorescent labels. Selected images were captured with a 63 ×, N.A. 1.0 Plan Apochromatic objective using a Photometrics Sensys 1305 × 1024 pixel CCD camera. Contrast optimization and pseudocoloring of the grey scale fluorescence images was done with Adobe Photoshop software.

6.3 Results and Discussion

6.3.1 Reactive Acid Fluoride-Terminated Monolayers

Pieces of freshly etched hydrogen-terminated Si(111) were immersed in deoxygenated neat 10-undecynoyl fluoride for 16 h at 80 °C to obtain acid fluoride-terminated monolayers on Si(111). The water contact angle of the 10-undecynoyl fluoride-treated Si(111) is 83° (Table 1). Since this is rather close to ~87° for a freshly etched H-Si(111) surface,[38] this value is no direct evidence for formation of an acid fluoride-terminated monolayer. However, the ellipsometric layer thickness of 12 Å – a value consistent with the length of the molecule and the expected tilt angle of 30 - 35º with respect to the surface normal[17] – does confirm monolayer formation.

In principle, monolayer formation can involve reactivity of the alkyne moiety, or of the acid fluoride moiety or of both. Therefore, a double-polished Si(111) crystal was modified with 10-undecynoyl fluoride and examined by ATR-IR (Figure 2). The presence of a sharp peak at 1843 cm^{-1}, attributed to the carbonyl stretching ($\nu_{C=O}$) of the acid fluoride moiety,[62,63,68] and the absence of an absorbance at 1719 cm^{-1}, characteristic of the carbonyl

stretching ($\nu_{C=O}$) of a carboxylic acid[62] provide evidence for the presence and intactness of the acid fluoride functionality. Due to the appearance of a small peak at 1603 cm^{-1}, assigned to the double bond stretching ($\nu_{C=C}$) of the Si–C=C moiety, and the lack of an absorbance around 3309 cm^{-1}, corresponding to the alkyne C–H stretching (ν_{C-H}),[69] upside-down attachment is excluded, i.e. the reaction of 10-undecynoyl fluoride with H-Si(111) occurs selectively at the alkyne terminus. In addition, from ATR-IR dichroism experiments[17,18] on the resulting monolayer a tilt angle of approximately 30-35º with respect to the surface normal can be derived, in good agreement with the tilt angle determined from the ellipsometric thickness.

Table 1. Static water contact angle (θ) and ellipsometric layer thickness (*d*) of acid fluoride monolayers on hydrogen-terminated Si(111) and after coupling with *n*-hexadecylamine by μCP and immersion with a flat stamp.

	θ (°)	*d* (Å)
C(=O)F Terminated	83 ± 1	12 ± 1
μCP with $C_{16}H_{33}NH_2$	104 ± 1	26 ± 1
Immersion with $C_{16}H_{33}NH_2$	104 ± 1	26 ± 1

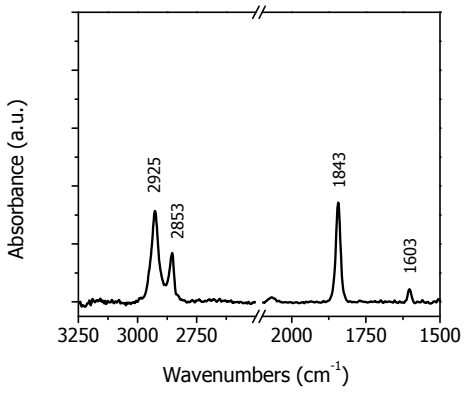

Figure 2. ATR spectrum (p-polarization) of an acid fluoride-terminated monolayer on hydrogen-terminated Si(111).

XPS analyses further support these findings. The XPS C_{1s} narrow scan and deconvolution of the acid fluoride-terminated monolayer are depicted in Figure 3. The assignment of the distinct carbon atoms is supported by density functional theory (DFT)

calculations (see Appendix 3 for details).[49,66,67] The contributions at (i) 283.8 (ii) 285.0 (iii) 286.2 and (iv) 291.0 eV are assigned to the carbon covalently bonded to the relatively electropositive silicon (E_{calc} = 284.2 eV), the aliphatic carbons (E_{calc} = 285.0 eV), two carbons adjacent to the acid fluoride group (E_{calc} = 286.1 eV) and the acid fluoride carbon (E_{calc} = 290.7 eV), respectively, all in excellent agreement with the theoretical energy values and ratios (Table 2). The F_{1s} narrow scan (see Appendix 3 for F_{1s}, O_{1s} and Si_{2p} narrow scans) is fit with two components: one peak at 688.0 eV, corresponding to the fluorine of the acid fluoride group, and one peak at 685.9 eV, assigned to adventitious fluorine contamination due to the NH_4F etching process. Including only the fluorine of the acid fluoride functionality gives a F/C ratio of 1/11, which equals the expected ratio for the acid fluoride monolayer under study. The O_{1s} narrow scan also consists of two contributions: the peak at 534.2 eV is characteristic for carbonylic oxygen of the acid fluoride group, while the peak at 532.3 eV is attributed to airborne contaminations. In addition, the Si_{2p} narrow scan shows the expected $Si_{2p3/2}$ and $Si_{2p1/2}$ peaks and no sign of oxidized silicon around 103 - 104 eV.

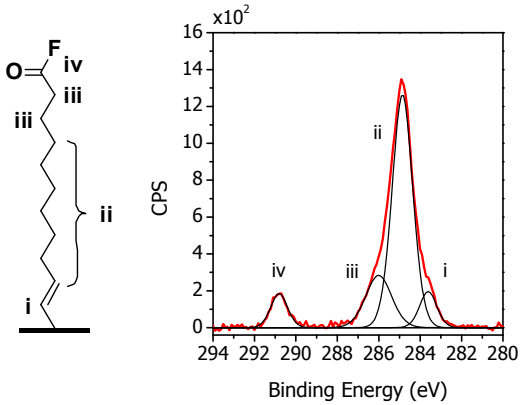

Figure 3. Different types of carbon atoms that can be distinguished by XPS in the acid fluoride-terminated monolayer (left) and the corresponding XPS C_{1s} narrow scan (right).

Table 2. XPS-derived atomic ratios of distinct carbons (see Figure 3 and 6) of acid fluoride monolayer before and after coupling with *n*-hexadecylamine by μCP with a flat stamp or by immersion.

	Ci / Cii / Ciii / Civ	
	Theory	Experimental
C(=O)F Terminated	1 / 7 / 2 / 1	0.9 / 7.2 / 2.0 / 0.9
μCP with $C_{16}H_{33}NH_2$	1 / 24 / 1 / 1	1.2 / 23.6 / 1.1 / 1.1
Immersion in $C_{16}H_{33}NH_2$	1 / 24 / 1 / 1	1.2 / 23.6 / 1.1 / 1.1

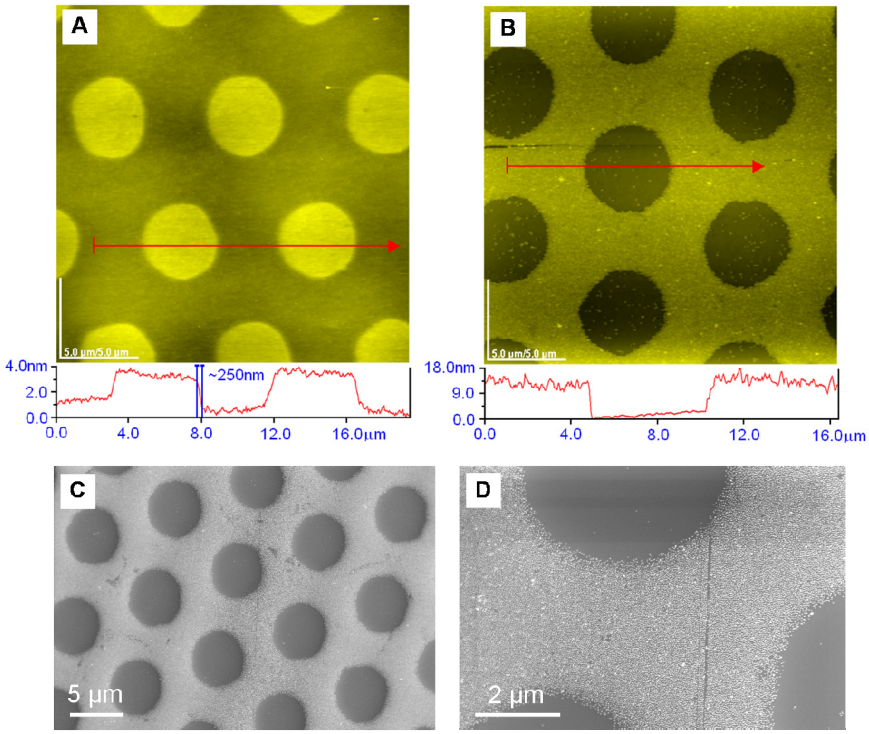

Figure 4. AFM topography images (22.5 × 22.5 μm) of an acid fluoride monolayer after μCP (5 μm dots) with *n*-hexadecylamine (A), and after backfilling with cysteamine and subsequent assembly of Au nanoparticles (~15 nm) (B), and the corresponding SEM images after Au nanoparticles deposition (C) and (D).

6.3.2 Reactive μCP with Primary Amines

The acid fluoride functionality is known to be highly reactive towards primary amines, and therefore the preformed acid fluoride-terminated monolayers can act as a platform for further functionalization and pattern construction by μCP. A PDMS stamp with pillar-like 5 μm-sized features was inked with *n*-hexadecylamine and brought in conformal contact for 20 sec with an acid fluoride-terminated monolayer. The resulting structure was characterized by non-contact AFM which revealed that the acid fluoride in the contacted areas reacted with *n*-hexadecylamine to produce well-defined 5 μm-sized *N*-hexadecylamide patterns with an approximate height of ~2 nm (Figure 4A). In addition, the high contrast (edge resolution < 250 nm) and uniformity suggest a very efficient amide formation by μCP. Subsequently the remaining acid fluoride groups in the uncontacted areas were converted into thiol-terminated areas by immersion in a cysteamine solution for 1 h. Dipping in an aqueous suspension of Au nanoparticles (~15 nm) resulted in an opposite AFM topography height profile in Figure 4B as compared to Figure 4A. As confirmed by SEM, the Au nanoparticles predominantly assembled at the thiol-terminated areas and do not bind at the printed *N*-hexadecylamide dots.

6.3.3 Reaction Efficiency

The reaction efficiency of μCP with *n*-hexadecylamine on acid fluoride-terminated monolayers was examined by a comparison of the monolayers derived from printing for 20 seconds with a flat stamp and from immersion in a solution with *n*-hexadecylamine for 1 h. As shown in Table 1, both procedures result in a significant increase in contact angle and layer thickness. The contact angle rises from 83° for the acid fluoride monolayer to 104° for the *N*-hexadecylamide monolayers in both cases, i.e. clearly indicative of a methyl-terminated monolayer.[17,38] The increase in layer thickness from 12 Å to 26 Å was also identical for both methods. This implies that via both routes *N*-hexadecylamide monolayers of similar quality were obtained. More detailed information about the coupling reaction was obtained with ATR-IR (Figure 5),[70] which shows an increased intensity of the methylene stretching vibrations ($\nu_{C\text{-}H,\ antisymm}$) and ($\nu_{C\text{-}H,\ symm}$), the complete disappearance of the acid fluoride absorption at 1843 cm^{-1}, the appearance of an amide N-H stretching ($\nu_{N\text{-}H}$) at 3313 cm^{-1} and of amide bonds I ($\nu_{C=O}$) and II ($\delta_{N\text{-}H}$) at 1641 and 1545 cm^{-1}, respectively. All these spectral data point to the quantitative conversion of the acid fluoride groups into the

corresponding amides. Surprisingly, coupling of *n*-hexadecylamine also induces a small but significant frequency shift for the antisymmetric and symmetric methylene stretching vibrations ($\nu_{C\text{-}H,\ antisymm}$) and ($\nu_{C\text{-}H,\ symm}$). The values of 2925 and 2853 cm^{-1}, respectively, that are observed for the acid fluoride monolayer are indicative of a disordered monolayer. The shift to 2922 cm^{-1} and 2852 cm^{-1}, respectively, for the *N*-hexadecylamide monolayer indicate an improved packing in the *N*-hexadecylamide monolayer, which is most probably caused by increased Van der Waals interactions and hydrogen bonding between neighboring amide groups.[71,72]

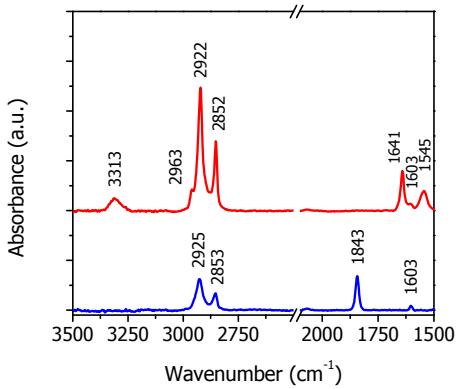

Figure 5. ATR spectra (p-polarization) of an acid fluoride monolayer before (lower blue curve) and after immersion in 25 mM *n*-hexadecylamine in 1-methyl-2-pyrrolidinone for 1 h (upper red curve).

Furthermore, XPS analysis of the obtained *N*-hexadecylamide monolayers also confirms a complete conversion of the acid fluoride to the corresponding amide. The C(=O)F peak at 291.0 eV in the C_{1s} narrow scan of the acid fluoride monolayer (Figure 3) disappears completely, independent of the procedure (stamping or immersion) used, and the resulting amide carbon is detected at 287.9 eV (E_{calc} = 288.1 eV) (Figure 6). Again the experimental and theoretical energy values and atomic ratios are in excellent agreement. (Table 2). As expected, the acid fluoride F_{1s} signal at 688.0 eV (see Appendix 3 for F_{1s}, O_{1s}, N_{1s} and Si_{2p} narrow scans) disappeared completely upon coupling of *n*-hexadecylamine by μCP or immersion, and an amide nitrogen peak showed up at 400.7 eV. In the O_{1s} narrow scan the peak at 534.2 eV assigned to the carbonylic oxygen of the acid fluoride shifts to 532.1 eV for the amide oxygen, while a trace of oxygen contaminations remained at higher binding energy (533.4 eV). A strongly reduced Si_{2p} signal, caused by the increased thickness of the organic layer upon *n*-hexadecylamine binding, is observed in the Si_{2p} narrow scan. Finally,

no traces of silicon oxide (at 103 - 104 eV) are detected, neither after 20 sec μCP nor after 1 h immersion in the *n*-hexadecylamine solution.

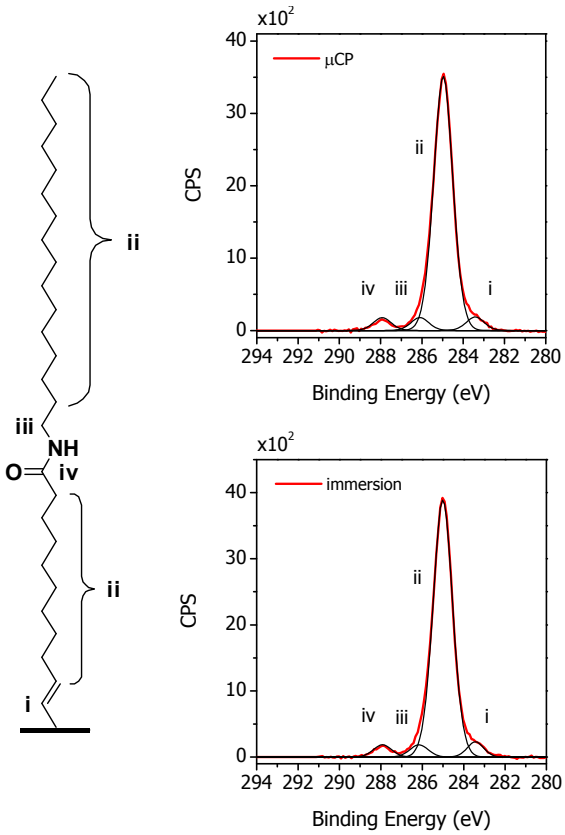

Figure 6. Different types of carbon atoms that can be distinguished by XPS in *N*-hexadecylamide-terminated monolayer (left) and the corresponding XPS C1s narrow scans of this monolayer prepared by the μCP (top right) and by immersion (bottom right).

6.3.4 Interface Stability

For applicability of this type of monolayer in biosensing and molecular electronic devices, the stability of the monolayer-silicon interface under ambient conditions and in aqueous media is an important issue. To investigate the oxidation-inhibiting properties of our *N*-hexadecylamide-terminated monolayers, XPS spectra were recorded before and after

immersion of Si wafers with this monolayer in water for 16 h. As shown in Figure 7, the Si_{2p} narrow scans before and after water immersion are identical, with no traces of silicon oxide and independent of the method used for coupling of *n*-hexadecylamine. As the *N*-hexadecylamide-terminated monolayers are only moderately ordered, as indicated by the positions of the antisymmetric and symmetric stretching vibrations ($\nu_{C\text{-}H,\ antisymm}$ and $\nu_{C\text{-}H,\ symm}$) in the ATR-IR spectrum in Figure 5 (2922 and 2852 cm^{-1}, respectively), the high stability in aqueous media might be ascribed to the combination of hydrogen bonding between the amide groups and the presence of a Si–C=C linkage to the surface, which is known to suppress oxidation.[60]

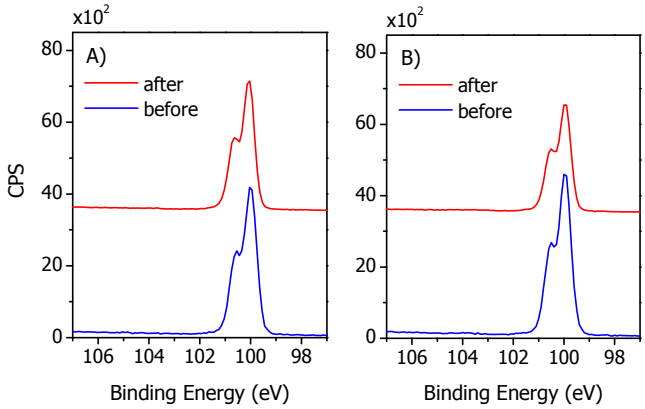

Figure 7. XPS Si_{2p} narrow scans of *N*-hexadecylamide-terminated monolayer before (lower blue curves) and after immersion in water for 16 h (upper red curves). Prepared by coupling with *n*-hexadecylamine by μCP (A) and by immersion (B).

6.3.5 Printing of DNA

In view of the great potential of this type of monolayers in the field of biosensing, immobilization and pattern construction of complex biomolecules on oxide-free silicon is of great interest. The reactivity combined with the high selectivity of the acid fluoride functionality towards primary amines makes these acid fluoride-terminated monolayers excellent substrates for reactive printing with complex biomolecules, like DNA. To this aim PDMS stamps were oxidized by oxygen plasma, and subsequently filled with fifth generation positively charged dendrimers of poly(propylene imine) (G5-PPI, to obtain so-called ”dendri-stamps”).[58,65] These were used to bind electrostatically a negatively charged

oligo-DNA with a primary amine functionality at the 5'-terminus and a Cy3 label at the 3'-terminus, which was subsequently printed on an acid fluoride-terminated monolayer. After 20 sec of conformal contact, the surface was rinsed and immediately immersed in an 2-(2-aminoethoxy)ethanol (EG_2-NH_2) solution for 1 h, to passivate the remaining unreacted acid fluoride-terminated areas. The 10 µm-sized Cy3-labeled DNA dots on the silicon surface were visualized by fluorescence microscopy (excitation at 488 nm) and tapping mode AFM (Figure 8). The homogeneity and well-defined distribution of the fluorescent DNA dots displays the efficiency of the coupling reaction and consequently the high density of Cy3-labeled DNA printed on the acid fluoride monolayer. To investigate whether the printed oligo-DNA is still available for hybridization, the substrate was immersed in a Cy5-labeled target DNA solution at room temperature in the dark for 16 h. After hybridization the fluorescent DNA dots were detected by exciting Cy5 at 633 nm instead of Cy3. The resulting fluorescent image (Figure 8B) corresponds to a high density of hybridized target DNA in the 10 µm dots and shows that the printed DNA is still available for hybridization with the target DNA. Furthermore, the fact that the Cy3-labeled DNA still hybridizes with the target DNA indicates that the printed DNA is mainly bound via the primary amine functionality at the 5'-terminus.

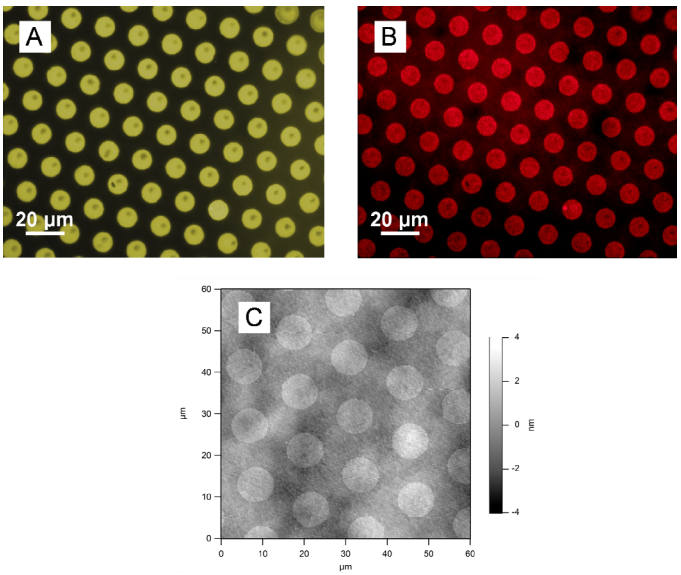

Figure 8. Fluorescent images of Cy3-labeled oligo-DNA patterns made by µCP with dendri-stamps (A) and after hybridization with Cy5-labeled target DNA (B), AC-AFM topography image of surface after printing Cy3-labeled DNA (C).

6.4 Conclusions

A new route was developed for patterning organic monolayers onto oxide-free silicon by microcontact printing amine-containing materials onto highly reactive acid fluoride-terminated monolayers. This acid fluoride-terminated monolayer can easily be prepared by reaction of ω-alkynoyl fluorides with hydrogen-terminated Si, and shows no signs of upside-down attachment or oxidation of the underlying silicon surface. The high reactivity towards amines makes acid fluoride-terminated monolayers excellent platforms for reactive μCP, while the high selectivity of the amide formation makes them excellent intermediates for introducing a broad range of functionalities on oxide-free silicon surfaces. It was shown that the amide formation on the acid fluoride monolayer is highly efficient and rapid (20 seconds for quantitative conversion) by μCP, fully preserves the oxide-free monolayer-silicon interface, and can even be used to immobilize complex biomolecules, such as fluorescent-labeled oligo-DNA on oxide-free silicon, which is still accessible for hybridization.

References

(1) Liu, Y. J.; Yu, H. Z. *ChemPhysChem* **2002**, *3*, 799-802.

(2) Liu, Y. J.; Yu, H. Z. *ChemPhysChem* **2003**, *4*, 335-342.

(3) Faber, E. J.; de Smet, L. C. P. M.; Olthuis, W.; Zuilhof, H.; Sudhölter, E. J. R.; Bergveld, P.; van den Berg, A. *ChemPhysChem* **2005**, *6*, 2153-2166.

(4) Faber, E. J.; Sparreboom, W.; Groeneveld, W.; de Smet, L. C. P. M.; Bomer, J.; Olthuis, W.; Zuilhof, H.; Sudhölter, E. J. R.; Bergveld, P.; van den Berg, A. *ChemPhysChem* **2007**, *8*, 101-112.

(5) Salomon, A.; Böcking, T.; Seitz, O.; Markus, T.; Amy, F.; Chan, C.; Zhao, W.; Cahen, D.; Kahn, A. *Adv. Mater.* **2007**, *19*, 445-450.

(6) Seitz, O.; Böcking, T.; Salomon, A.; Gooding, J. J.; Cahen, D. *Langmuir* **2006**, *22*, 6915-6922.

(7) Salomon, A.; Böcking, T.; Chan, C. K.; Amy, F.; Girshevitz, O.; Cahen, D.; Kahn, A. *Phys. Rev. Lett.* **2005**, *95*.

(8) Hamers, R. J. In *Bioelectronics: From Theory to Applications* Willner, I., Katz, E., Eds. 2005; Vol. Chapter 7, p 209-230.

(9) Boukherroub, R. *Curr. Opin. Solid State Mater. Sci.* **2005**, *9*, 66-72.

(10) Buriak, J. M. *Chem. Rev.* **2002**, *102*, 1271-1308.

(11) Sieval, A. B.; Linke, R.; Zuilhof, H.; Sudhölter, E. J. R. *Adv. Mater.* **2000**, *12*, 1457-1460.

(12) Wayner, D. D. M.; Wolkow, R. A. *J. Chem. Soc., Perkin Trans. 2* **2002**, 23-34.
(13) Yaffe, O.; Scheres, L.; Puniredd, S. R.; Stein, N.; Biller, A.; Lavan, R. H.; Shpaisman, H.; Zuilhof, H.; Haick, H.; Cahen, D.; Vilan, A. *Nano Lett.* **2009**, *9*, 2390-2394.
(14) Har-Lavan, R.; Ron, I.; Thieblemont, F.; Cahen, D. *Appl. Phys. Lett.* **2009**, *94*.
(15) Maldonado, S.; Knapp, D.; Lewis, N. S. *J. Am. Chem. Soc.* **2008**, *130*, 3300-3301.
(16) Linford, M. R.; Chidsey, C. E. D. *J. Am. Chem. Soc.* **1993**, *115*, 12631-12632.
(17) Linford, M. R.; Fenter, P.; Eisenberger, P. M.; Chidsey, C. E. D. *J. Am. Chem. Soc.* **1995**, *117*, 3145-3155.
(18) Sieval, A. B.; Demirel, A. L.; Nissink, J. W. M.; Linford, M. R.; van der Maas, J. H.; de Jeu, W. H.; Zuilhof, H.; Sudhölter, E. J. R. *Langmuir* **1998**, *14*, 1759-1768.
(19) Cicero, R. L.; Linford, M. R.; Chidsey, C. E. D. *Langmuir* **2000**, *16*, 5688-5695.
(20) Terry, J.; Linford, M. R.; Wigren, C.; Cao, R. Y.; Pianetta, P.; Chidsey, C. E. D. *Appl. Phys. Lett.* **1997**, *71*, 1056-1058.
(21) Effenberger, F.; Gotz, G.; Bidlingmaier, B.; Wezstein, M. *Angew. Chem., Int. Ed.* **1998**, *37*, 2462-2464.
(22) de Smet, L. C. P. M.; Stork, G. A.; Hurenkamp, G. H. F.; Sun, Q. Y.; Topal, H.; Vronen, P. J. E.; Sieval, A. B.; Wright, A.; Visser, G. M.; Zuilhof, H.; Sudhölter, E. J. R. *J. Am. Chem. Soc.* **2003**, *125*, 13916-13917.
(23) Sun, Q. Y.; de Smet, L. C. P. M.; van Lagen, B.; Giesbers, M.; Thune, P. C.; van Engelenburg, J.; de Wolf, F. A.; Zuilhof, H.; Sudhölter, E. J. R. *J. Am. Chem. Soc.* **2005**, *127*, 2514-2523.
(24) Sun, Q. Y.; de Smet, L. C. P. M.; van Lagen, B.; Wright, A.; Zuilhof, H.; Sudhölter, E. J. R. *Angew. Chem., Int. Ed.* **2004**, *43*, 1352-1355.
(25) Buriak, J. M.; Allen, M. J. *J. Lumin.* **1998**, *80*, 29-35.
(26) Buriak, J. M.; Allen, M. J. *J. Am. Chem. Soc.* **1998**, *120*, 1339-1340.
(27) Mizuno, H.; Buriak, J. M. *J. Am. Chem. Soc.* **2008**, *130*, 17656-17657.
(28) Buriak, J. M.; Stewart, M. P.; Geders, T. W.; Allen, M. J.; Choi, H. C.; Smith, J.; Raftery, D.; Canham, L. T. *J. Am. Chem. Soc.* **1999**, *121*, 11491-11502.
(29) Boukherroub, R.; Morin, S.; Bensebaa, F.; Wayner, D. D. M. *Langmuir* **1999**, *15*, 3831-3835.
(30) Hurley, P. T.; Nemanick, E. J.; Brunschwig, B. S.; Lewis, N. S. *J. Am. Chem. Soc.* **2006**, *128*, 9990-9991.
(31) Juang, A.; Scherman, O. A.; Grubbs, R. H.; Lewis, N. S. *Langmuir* **2001**, *17*, 1321-1323.
(32) Royea, W. J.; Juang, A.; Lewis, N. S. *Appl. Phys. Lett.* **2000**, *77*, 1988-1990.
(33) deVilleneuve, C. H.; Pinson, J.; Bernard, M. C.; Allongue, P. *J. Phys. Chem. B* **1997**, *101*, 2415-2420.
(34) Gurtner, C.; Wun, A. W.; Sailor, M. *Angew. Chem., Int. Ed.* **1999**, *38*, 1966-1968.
(35) Lua, Y. Y.; Fillmore, W. J. J.; Yang, L.; Lee, M. V.; Savage, P. B.; Asplund, M. C.; Linford, M. R. *Langmuir* **2005**, *21*, 2093-2097.

(36) Niederhauser, T. L.; Jiang, G. L.; Lua, Y. Y.; Dorff, M. J.; Woolley, A. T.; Asplund, M. C.; Berges, D. A.; Linford, M. R. *Langmuir* **2001**, *17*, 5889-5900.

(37) Niederhauser, T. L.; Lua, Y. Y.; Jiang, G. L.; Davis, S. D.; Matheson, R.; Hess, D. A.; Mowat, I. A.; Linford, M. R. *Angew. Chem., Int. Ed.* **2002**, *41*, 2353-2356.

(38) Scheres, L.; Arafat, A.; Zuilhof, H. *Langmuir* **2007**, *23*, 8343-8346.

(39) Faucheux, A.; Gouget-Laemmel, A. C.; de Villeneuve, C. H.; Boukherroub, R.; Ozanam, F.; Allongue, P.; Chazalviel, J. N. *Langmuir* **2006**, *22*, 153-162.

(40) Asanuma, H.; Lopinski, G. P.; Yu, H. Z. *Langmuir* **2005**, *21*, 5013-5018.

(41) Boukherroub, R.; Morin, S.; Sharpe, P.; Wayner, D. D. M.; Allongue, P. *Langmuir* **2000**, *16*, 7429-7434.

(42) Petit, A.; Delmotte, M.; Loupy, A.; Chazalviel, J. N.; Ozanam, F.; Boukherroub, R. *J. Phys. Chem. C* **2008**, *112*, 16622-16628.

(43) Boukherroub, R.; Petit, A.; Loupy, A.; Chazalviel, J. N.; Ozanam, F. *J. Phys. Chem. B* **2003**, *107*, 13459-13462.

(44) Boukherroub, R.; Wojtyk, J. T. C.; Wayner, D. D. M.; Lockwood, D. J. *J. Electrochem. Soc.* **2002**, *149*, H59-H63.

(45) Perring, M.; Dutta, S.; Arafat, S.; Mitchell, M.; Kenis, P. J. A.; Bowden, N. B. *Langmuir* **2005**, *21*, 10537-10544.

(46) Li, Y.; Tero, R.; Nagasawa, T.; Nagata, T.; Urisu, T. *Appl. Surf. Sci.* **2004**, *238*, 238-241.

(47) Böcking, T.; Wong, E. L. S.; James, M.; Watson, J. A.; Brown, C. L.; Chilcott, T. C.; Barrow, K. D.; Coster, H. G. L. *Thin Solid Films* **2006**, *515*, 1857-1863.

(48) Voicu, R.; Boukherroub, R.; Bartzoka, V.; Ward, T.; Wojtyk, J. T. C.; Wayner, D. D. M. *Langmuir* **2004**, *20*, 11713-11720.

(49) Yang, M.; Teeuwen, R. L. M.; Giesbers, M.; Baggerman, J.; Arafat, A.; de Wolf, F. A.; van Hest, J. C. M.; Zuilhof, H. *Langmuir* **2008**, *24*, 7931-7938.

(50) Sieval, A. B.; van den Hout, B.; Zuilhof, H.; Sudhölter, E. J. R. *Langmuir* **2001**, *17*, 2172-2181.

(51) Xia, Y. N.; Whitesides, G. M. *Angew. Chem., Int. Ed.* **1998**, *37*, 551-575.

(52) Love, J. C.; Estroff, L. A.; Kriebel, J. K.; Nuzzo, R. G.; Whitesides, G. M. *Chem. Rev.* **2005**, *105*, 1103-1169.

(53) Jun, Y.; Le, D.; Zhu, X. Y. *Langmuir* **2002**, *18*, 3415-3417.

(54) Yan, L.; Zhao, X. M.; Whitesides, G. M. *J. Am. Chem. Soc.* **1998**, *120*, 6179-6180.

(55) Yan, L.; Huck, W. T. S.; Zhao, X. M.; Whitesides, G. M. *Langmuir* **1999**, *15*, 1208-1214.

(56) Lahiri, J.; Ostuni, E.; Whitesides, G. M. *Langmuir* **1999**, *15*, 2055-2060.

(57) Sullivan, T. P.; van Poll, M. L.; Dankers, P. Y. W.; Huck, W. T. S. *Angew. Chem., Int. Ed.* **2004**, *43*, 4190-4193.

(58) Rozkiewicz, D. I.; Brugman, W.; Kerkhoven, R. M.; Ravoo, B. J.; Reinhoudt, D. N. *J. Am. Chem. Soc.* **2007**, *129*, 11593-11599.

(59) Rozkiewicz, D. I.; Janczewski, D.; Verboom, W.; Ravoo, B. J.; Reinhoudt, D. N. *Angew. Chem. Int. Ed.* **2006**, *45*, 5292-5296.

(60) Puniredd, S. R.; Assad, O.; Haick, H. *J. Am. Chem. Soc.* **2008**, *130*, 13727-13734.

(61) Gross, S.; Laabs, S.; Scherrmann, A.; Sudau, A.; Zhang, N.; Nubbemeyer, U. *J. Prakt. Chem.* **2000**, *342*, 711-714.

(62) Chi, Y. S.; Choi, I. S. *Langmuir* **2005**, *21*, 11765-11772.

(63) Niemz, A.; Jeoung, E.; Boal, A. K.; Deans, R.; Rotello, V. M. *Langmuir* **2000**, *16*, 1460-1462.

(64) Nijhuis, C. A.; ter Maat, J.; Bisri, S. Z.; Weusthof, M. H. H.; Salm, C.; Schmitz, J.; Ravoo, B. J.; Huskens, J.; Reinhoudt, D. N. *New J. Chem.* **2008**, *32*, 652-661.

(65) Rozkiewicz, D. I.; Gierlich, J.; Burley, G. A.; Gutsmiedl, K.; Carell, T.; Ravoo, B. J.; Reinhoudt, D. N. *ChemBioChem* **2007**, *8*, 1997-2002.

(66) Frisch, M. J.; et al. *Gaussian03* **2004**, revision D.01; Gaussian, Inc.: Wallingford, CT.

(67) Glendening, E. D.; Reed, A. E.; Carpenter, J. E.; Weinhold, F. *NBO*, version 3.1.

(68) Chi, Y. S.; Lee, K. B.; Kim, Y.; Choi, I. S. *Langmuir* **2007**, *23*, 1209-1214.

(69) Ciampi, S.; Böcking, T.; Kilian, K. A.; Harper, J. B.; Gooding, J. J. *Langmuir* **2008**, *24*, 5888-5892.

(70) Only the solution-phase reaction was studied as microcontact printing on an ATR cyrstal was impractical.

(71) Clegg, R. S.; Hutchison, J. E. *J. Am. Chem. Soc.* **1999**, *121*, 5319-5327.

(72) Tam-Chang, S. W.; Biebuyck, H. A.; Whitesides, G. M.; Jeon, N.; Nuzzo, R. G. *Langmuir* **1995**, *11*, 4371-4382.

Chapter 7

Micro- and Nanopatterning of Functional Organic Monolayers on Oxide-Free Silicon by Laser-Induced Photothermal Desorption

Abstract. This chapter describes photothermal laser patterning of functional organic monolayers, which had been prepared on oxide-free, hydrogen-terminated silicon, and subsequent backfilling of the laser-written lines with a second organic monolayer that differs in its terminal functionality. Since the thermal monolayer decomposition process is highly nonlinear in the applied laser power density, sub-wavelength patterning of the organic monolayers was feasible. After photothermal laser patterning of hexadecenyl monolayers the lines freed up by the laser were backfilled with functional acid fluoride monolayers. Coupling of cysteamine to the acid fluoride groups and subsequent attachment of Au nanoparticles allowed an easy characterization of the functional lines by atomic force microscopy (AFM) and scanning electron microscopy (SEM). Depending on the laser power and writing speed, functional lines with a width between 1.1 μm and 250 nm were created. In addition, also trifluoroethyl-terminated monolayers (TFE monolayer) were patterned. Subsequently the decomposed lines were backfilled with a nonfunctional hexadecenyl monolayer, the TFE stripes were converted into thiol stripes, and finally covered with Au nanoparticles. By reducing the lateral distance between the laser lines, Au nanoparticles stripes with a width close to 100 nm were obtained. Finally, in view of the great potential of this type of monolayers in the field of biosensing, the ease of fabricating biofunctional patterns was demonstrated by covalent binding of fluorescently labeled oligo-DNA to acid fluoride backfilled laser lines, which was – as shown by fluorescence microscopy – accessible for hybridization.

This chapter will be published as:
'*Micro- and Nanopatterning of Functional Organic Monolayers on Oxide-Free Silicon by Laser-Induced Photothermal Desorption*' Scheres, L.; Klingebiel, B.; ter Maat, J.; Giesbers, M.; de Jong, H.; Hartmann, N.; Zuilhof, H. *Small*, **2010**, in press.

7.1 Introduction

Due to the ongoing miniaturization of semiconductor devices, there is a significant interest in the surface modification of silicon. In this perspective, organic monolayers directly bound to oxide-free silicon are interesting candidates as they can easily be implemented in the existing technology for fabrication of silicon-based micro- and nanostructured devices. The direct covalent linkage (Si–C bond) to the silicon surface creates a well-defined organic monolayer-silicon interface and makes these monolayers thermally and chemically very robust.[1,2] Moreover, because an intervening SiO_2 layer is essentially absent, direct electronic coupling between any organic functionality and the silicon substrate is possible, which provides an opportunity to enhance the device performance compared to SiO_2-covered devices.[3-7] As a result these monolayers have great potential in fields of biosensors and molecular electronic and photovoltaic devices.[6-12]

In the last years also significant process has been reported in the preparation of densely-packed robust ω-functionalized monolayers. Due to reproducibility problems of such monolayers,[5] and the small number of compatible functional groups,[8,12,13] the oxide-free monolayer-silicon interface, generally, has a limited long-term stability.[5,14] Consequently, the development and fabrication of real functional hybrid organic monolayer-silicon devices is hampered. Recently, however, significant efforts were made to solve these problems. For instance, an improved monolayer coverage was reported for long alkenyl monolayers on Si(111) (Chapter 4 and 5)[15] and the central Si–C=C linkage was found to inhibit oxidation.[16] In addition, some interesting ω-functionalized monolayers were prepared, without any sign of upside-down attachment.[13,17-24]

Patterning of self-assembled organic monolayers, in general, can be carried out using a variety of techniques including photolithography, soft lithographic techniques, i. e. micro contact printing, electron beam lithography and scanning probe techniques such as dip pen nanolithography and scanning near-field optical lithography.[25-33] In view of this broad field, however, so far only comparatively few studies addressed patterning of organic monolayers on oxide-free silicon. In particular, mainly photolithographic procedures were applied.[17,34-38] In addition, also electron beam lithographic[39] and more recently also a number of elegant soft lithographic[20,40-45] and scanning probe[46-54] methods were described. In general, parallel techniques, such as soft lithography and photolithography are fast, simple and easy applicable to large areas, but they lack the flexibility necessary in applications where the required design of the patterns frequently change, i.e. for every distinct pattern a new stamp or mask is required. Sequential techniques, such as electron beam lithography and scanning

probe techniques, in turn, do allow the formation of arbitrary patterns with high lateral resolution, but are relative slow and restricted to small areas. In this respect, laser beam lithography, represents a useful alternative method for monolayer patterning. It combines high flexibility in pattern design with high throughput, and therefore nicely complements the more established techniques for patterning on flat substrates.[55] Moreover, as it is a noncontact patterning method, it also provides unique opportunities for patterning of buried interfaces in more complex device geometries, e. g. in microfluidic channels and micro- and nanostructured devices or porous media, such as silica aerogels.[56,57] Typically, of course, the lateral resolution of laser beam lithography is limited by optical diffraction, that is, minimum structure sizes are not much smaller than the wavelength of the laser system even when highly focusing optics are used.[58] Using nonlinear processing routines, though, patterning with subwavelength resolution has been demonstrated. In conjunction with all those general features of laser beam lithography, this clearly provides promising perspectives in maskless large-scale nanofabrication.[55]

For processing, laser beam lithography can use either photochemical or photothermal reactions or a combination thereof to achieve the desired patterning.[59] In photochemical laser patterning, direct or substrate-mediated electronic excitations are used for processing. Two recent examples are laser-induced cleavage of photosensitive groups,[60] and laser-written lines by photo-induced thiol-ene chemistry.[61] If multiphoton absorption processes are exploited photochemical routines also allow for subwavelength patterning.[62,63] Similarly to photochemical laser patterning, in the last years, also photothermal laser patterning has gained a lot of interest.[64-73] In photothermal laser patterning the substrate surface is locally heated by a focused laser beam that induces thermal decomposition of the organic monolayer. Since this process is highly nonlinear in the applied laser power density, the lateral resolution of the pattern is not restricted by the laser spot diameter or the optical diffraction limit, i.e. subwavelength patterning of the monolayer is feasible.[65-67,73] Generally, the achievable lateral resolution depends on the activation energy of the decomposition process and hence on the thermal and chemical stability of the coating.[58] Strongly bound coatings, such as alkylsiloxane monolayers on oxidized silicon, can be patterned at length scales down in the sub-100 nm range.[65-67] However, photothermal processing is not limited to silane-based monolayers, but can be applied to a broad range of organic coatings, including much more weakly bound supported phospholipid layers.[74,75] In addition, it can also be used for constructive patterning,[59,76-78] such as local bromination of organic monolayers.[59]

In a recent report we demonstrated photothermal laser pattering of organic monolayers on oxide-free silicon.[73] In line with the thermal and chemical stability of these monolayers,[1,2] well-defined local decomposition of the organic monolayer yielded narrow monolayer stripes with a lateral resolution significantly below the laser spot diameter. However, in this study only laser patterning of non-functionalized alkyl monolayers on oxide-free silicon was considered, whereas for biosensor and molecular electronic applications it would be of significant interest to create micro- and nanopatterns of functional monolayers. Therefore, we here describe two complementary photothermal laser patterning routes to obtain narrow functional monolayer stripes on oxide-free silicon.

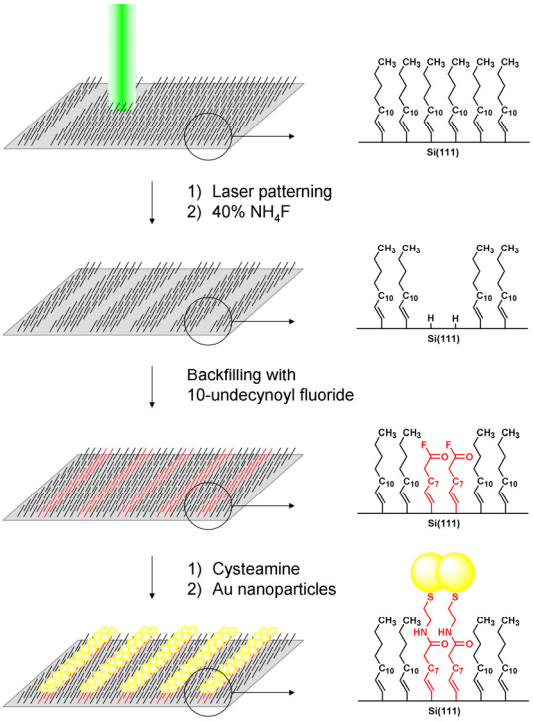

Figure 1. Schematic representation of the laser patterning procedure of non-functional monolayers, backfilling with an acid fluoride-terminated monolayer and final Au nanoparticles deposition.

In the first approach, we backfilled the laser-written lines in a nonfunctional hexadecenyl monolayer with a functional acid fluoride-terminated monolayer, to create narrow functional lines embedded in a nonfunctional monolayer. In order to test the functionality of the chemical pattern, the acid fluoride groups first were converted into thiol groups, and

subsequently Au nanoparticles were assembled onto the functional lines. The final Au nanoparticles patterns were analyzed by atomic force microscopy (AFM) and scanning electron microscopy (SEM). In the second approach, we applied photothermal laser patterning to a functional trifluoroethyl (TFE)-terminated monolayer and backfilled the decomposed lines with a nonfunctional hexadecenyl monolayer. Again, the functional areas were converted into thiol groups to bind Au nanoparticles and the final pattern was analyzed by SEM. Finally, to demonstrate the ease of biofunctionalization, we modified acid fluoride backfilled laser lines with Cy3-labeled oligo-DNA and hybridized with the Cy5-labeled target oligo-DNA.

7.2 Experimental

7.2.1 Materials

Light petroleum ether (PE 40/60), EtOH and CH_2Cl_2 were distilled prior to use. For rinsing and contact angle measurements, deionized water (18.3 MΩcm resistivity) was used. Acetone (Sigma/Honeywell, semiconductor grade), 40% ammonium fluoride solution (40% NH_4F, Sigma/Honeywell, semiconductor grade), anhydrous dichloromethane (CH_2Cl_2, Aldrich, +99.8%), anhydrous dimethyl sulfoxide (DMSO, Aldrich, +99.9%), 4-(dimethylamino)pyridine (DMAP, Aldrich, +99%), 2,2,2-trifluoroethanol (Aldrich, 99%) *N,N'*-dicyclohexyl carbodiimide (DCC, Aldrich, 99%), potassium *tert*-butoxide (BuOK, Aldrich, +97%), *N*-hydroxysuccinimide (NHS, Aldrich, 98%), *n*-(3-dimethylaminopropyl)-*N'*-ethylcarbodiimide hydrochloride (EDC · HCl, Aldrich), cysteamine (Aldrich, +98%), gold nanoparticles (d ~15 nm gold sol, Aurion, The Netherlands) and 20 × standard saline citrate (SSC) (20 × SSC = 3.0 M sodium chloride, 0.3 M sodium citrate in H_2O) buffer solution (Serva, VWR) were used as received. Oligonucleotides were purchased from IBA (Germany). The strand used for coupling to the acid fluoride laser lines, had sequence 5'-CCA CGG ACT ACT TCA AAA CTA-3' and was modified at the 5' terminus with an amino group via a six-carbon linker (NH_2-$(CH_2)_6$-) and at the 3' terminus with Cy3. The target strand had sequence 5'-TAG TTT TGA AGT AGT CCG TGG-3' with Cy5 modification at the 5' terminus. 1-Hexadecyne (ABCR, Germany, 90%) was first purified by column chromatography (eluent hexane) and subsequently distilled twice before use. 10-Undecynoyl fluoride was synthesized in one step from 10-undecynoic acid (ABCR, Germany, 97%), anhydrous pyridine (Sigma, 99.8%) and cyanuric fluoride (Aldrich, 97%) following a previously reported procedure.[20] Silicon wafers were (111)-oriented, single-side

polished, 475-550 μm thick, n-type, phosphorus-doped samples, with a resistivity of 1.0 - 5.0 Ω cm (Siltronix, France).

7.2.2 Synthesis of 2,2,2-Trifluoroethyl Undec-10-ynoate

2,2,2-Trifluoroethanol (10.0 ml, 137 mmol) was added to a solution of 4-(dimethylamino)pyridine (1.34 g, 11 mmol) and 10-undecynoic acid (10.0 g, 55 mmol) in anhydrous CH_2Cl_2 (150 ml). The solution was cooled to 0 ºC and a solution of *n,n'*-dicyclohexyl carbodiimide (13.8 g, 68 mmol) in anhydrous CH_2Cl_2 (50 ml) was added drop wise. The reaction mixture was stirred for 4 h, after which it was allowed to warm up to RT. The mixture was filtered over a glass filter and the filtrate was concentrated under reduced pressure. Purification by flash column chromatography (eluent: PE40/60 : CH_2Cl_2 = 2 : 1) yielded 10.5 g (40 mmol, 70%) of 2,2,2-trifluoroethyl undec-1-ynyl ester as a colorless oil. ^{1}H NMR (400 MHz, $CDCl_3$, δ): 4.49 (q, 2H, J = 8.5 Hz), 2.44 (t, 2H, J = 7.3 Hz), 2.21 (m, 2H, J = 7.3 Hz), 1.96 (t, 1H, J = 2.6 Hz), 1.68 (m, 2H, J = 7.2 Hz), 1.55 (m, 2H, 7.3 Hz), 1.35 (br, s, 8 H); ^{13}C NMR (400 MHz, $CDCl_3$, δ): 172.07, 122.99 (J = 1.10 × 10^3 Hz), 84.64, 68.07, 60.10 (J = 145 Hz), 33.59, 28.97, 28.85, 28.81, 28.58, 28.38, 24.62, 18.34; MS: *m/z* 264.134 (calculated for $C_{13}H_{19}F_3O_2$ ($M^{+\cdot}$): 264.134.

7.2.3 Monolayer Preparation

For preparation of the organic monolayers we followed a previously reported procedure.[15,79] Briefly, pieces of Si wafer were cleaned by sonication in acetone and oxidized by an oxygen plasma (Harrick PDC-002 setup) for 3 min. Subsequently, the Si(111) substrates were etched in an argon-saturated 40% NH_4F solution for 15 min. After etching the samples were rinsed with water, blown dry with nitrogen, and immersed in argon-saturated neat 1-hexadecyne or 2,2,2-trifluoroethyl undec-1-ynyl ester (both GC purity > 99.9%) at 80 °C and ~10 mbar. After 4 h (1-hexadecyne) or 16 h (2,2,2-trifluoroethyl undec-10-ynoate, TFE monolayer), the reaction was stopped and the monolayers were rinsed extensively with CH_2Cl_2 and sonicated for 5 min in CH_2Cl_2 to remove physisorbed molecules.

7.2.4 Photothermal Laser Patterning

Laser processing was carried out under ambient conditions. A detailed description of the optical setup can be found elsewhere.[80] Briefly, the beam of an Ar^+-laser operating at λ = 514 nm was focused onto the sample and scanned across its surface. The laser spot exhibited a Gaussian beam shape with a $1/e^2$ focal spot diameter of 2.6 ± 0.3 µm. An acousto-optical tunable filter (AOTF) was used to adjust the laser power. Processing with this set up can be carried out over an area of 25 × 25 cm^2 at writing speeds up to 25 mm/s. In general, patterning was carried out in continuous-mode operation, that is, in a line after line manner by moving the sample at a writing speed of up to 10 mm/s.

7.2.5 Backfilling of Laser Lines

After local photothermal removal of the organic monolayers oxidation of the silicon substrate sets in along the laser-written lines. Therefore, prior to backfilling, the laser lines were etched by immersion in an argon-saturated 40% NH_4F solution for 3 min. After etching the samples were rinsed with water, blown dry with nitrogen, and immersed in argon-saturated neat 10-undecynoyl fluoride (patterned hexadecenyl monolayer) or in 1-hexadecyne (patterned TFE monolayer) (both GC purity > 99.9%) at 80 °C and ~10 mbar. After 16 h (10-undecynoyl fluoride) or 4 h (1-hexadecyne) the reaction was stopped and the backfilled monolayers were rinsed extensively with CH_2Cl_2 and sonicated for 5 min in CH_2Cl_2 to remove physisorbed molecules.

7.2.6 Au Nanoparticles Deposition

To obtain thiol termination, the acid fluoride backfilled hexadecenyl monolayers were immersed in a 25 mM solution of cysteamine in CH_2Cl_2 for 30 min, while the hexadecenyl backfilled TFE monolayers were first deprotected with 250 mM *tert*-BuOK in DMSO for 90 s, rinsed with 1.0 M HCl, activated overnight in an aqueous solution of 100 mM NHS and 400 mM EDC, rinsed with EtOH and CH_2Cl_2 and sonicated for 5 min in CH_2Cl_2 to remove physisorbed NHS and EDC molecules, and then immersed in a 25 mM solution of cysteamine in CH_2Cl_2 for 30 min. Finally, the samples were dipped in an aqueous Au nanoparticles solution (d ~15 nm) for 30 min, after which the samples were rinsed extensively with EtOH and water to remove physisorbed Au nanoparticles.

7.2.7 Coupling of Oligo-DNA

An acid fluoride-backfilled hexadecenyl monolayer was submerged in a solution of an oligonucleotide with a primary amine functionality at the 5'-terminus and a Cy3 label at the 3'-terminus (20 μM in 5 × SSC) for 4 h. Subsequently, the surfaces were rinsed with 1 × SSC with 0.1 % SDS, water and EtOH and dried with a stream of nitrogen. For hybridization, the patterned substrate was immersed in a Cy5-labeled target oligonucleotide solution (10 μM in 5 × SSC) at room temperature in the dark overnight. The nonhybridized and physically bound target oligonucleotides were removed by thoroughly rinsing with 1 × SSC with 0.1 SDS and water, and finally the sample was dried with nitrogen.

7.2.8 Sample Characterization

Static water contact angles were measured with an automated Krüss DSA 100 goniometer. At least six small droplets of 2.0 μl deionized water were dispensed and the contact angles was determined using a Tangent 2 fitting model. The error in the contact angles is < 1°.

Ellipsometric measurements were performed with a Sentech Instruments (Type SE-400) ellipsometer, operating at 632.8 nm (He-Ne-laser) and an angle of incidence of 70°. The optical constants of the substrate were determined with a piece of freshly etched n-Si(111) (n = 3.819 and k = 0.057). The thicknesses of the monolayers were determined with a planar three-layer (ambient, monolayer, substrate) isotropic model with refractive index of 1.46 for the organic monolayer. The reported values are the average of eight measurements taken at different locations on the sample and the error is < 1 Å.

X-ray photoelectron spectroscopy (XPS) analysis were performed using a JPS-9200 photoelectron spectrometer (JEOL, Japan). High-resolution spectra were obtained under UHV conditions using monochromatic Al Kα X-ray radiation at 12 kV and 25 mA, using an analyzer pass energy of 10 eV. All high-resolution spectra were corrected with a linear background before fitting.

Atomic force microscopy (AFM) topography images were made using a scanning probe microscope (JSPM-5400, JEOL, Japan) in tapping mode (AC-AFM) with a standard silicon cantilever (320 kHz, NCHR-20, NanoWorld).

Scanning electron microscopy (SEM) measurements were performed by using an ESEM Quanta 400 (FEI Company).

The fluorescence images were recorded on a Zeiss Axioplan II imaging photomicroscope, equipped with epifluorescence illumination and small band filter sets for the Cy3 and Cy5 fluorescent labels. Selected images were captured with a 63 ×, N.A. 1.0 Plan apochromatic objective using a Photometrics Sensys 1305 × 1024 pixel CCD camera. Contrast optimization and pseudocoloring of the grey-scale fluorescence images was done with Adobe Photoshop software.

7.3 Results and Discussion

7.3.1. Laser Patterning of Non-Functional Monolayers

The initial hexadecenyl monolayers were prepared by immersing small pieces of freshly etched hydrogen-terminated Si(111) in neat argon-saturated 1-hexadecyne for 4 h at 80 °C. After monolayer formation all hexadecenyl monolayers were hydrophobic with static water contact angles of 110 - 111° and had ellipsometric thicknesses of 19 - 20 Å, both indicative of densely packed nonfunctionalized monolayers. Subsequently, as described previously,[73] photothermal laser patterning was carried out with a focused Ar^+-laser beam (λ = 514 nm, with a $1/e^2$ spot diameter of 2.6 µm), under ambient conditions in a line after line manner by moving the sample under the laser at a fixed writing speed and constant laser power. After photothermal removal of the protective organic monolayer oxidation of the silicon substrate set in along the laser-written lines. Therefore, prior to backfilling with a functional monolayer, the samples were treated with an argon-saturated 40% NH_4F solution (3 min) to obtain oxide-free and hydrogen-terminated Si(111) areas in the decomposed lines. For backfilling 10-undecynoyl fluoride was used, having an alkyne group for the reaction with H-Si surface on one end of the molecule and a reactive acid fluoride functionality on the other end. In Chapter 6 we studied the resulting acid fluoride-terminated monolayers in detail and demonstrated that, due to the high and selective reactivity towards amines, acid fluoride-terminated monolayers are excellent intermediates for introducing a broad range of (bio)functionalities on oxide-free silicon surfaces.[20] To facilitate easy examination of the final pattern by atomic force microscopy (AFM) and scanning electron microscopy (SEM), the acid fluoride-backfilled samples were immersed in a cysteamine solution to obtain thiol-termination and finally dipped in an aqueous Au nanoparticles solution (d ~15 nm).

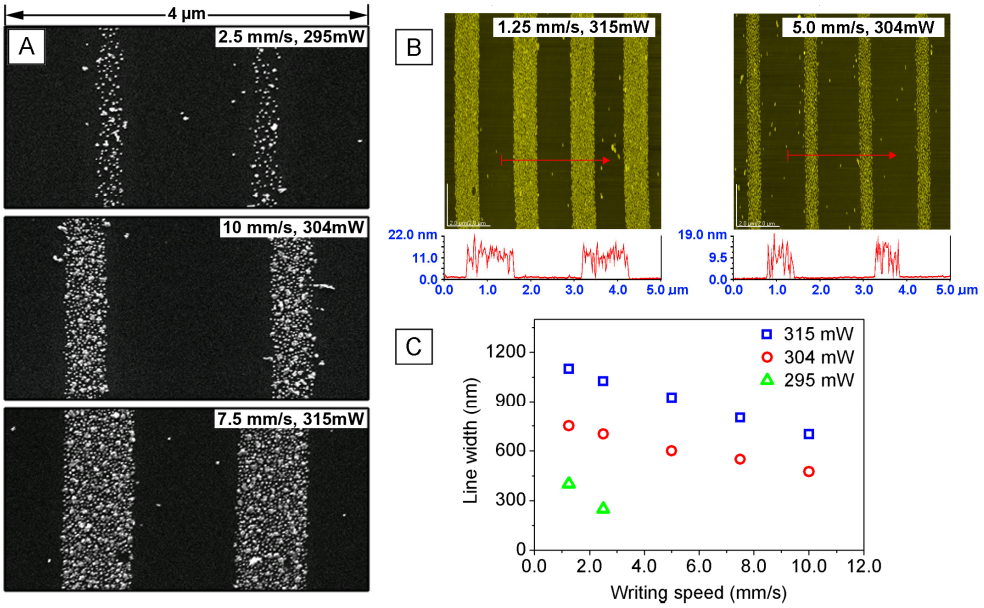

Figure 2. Some typical SEM (A) and AFM topography images (B) of a laser-patterned hexadecenyl monolayer after backfilling with 10-undecenoyl fluoride, cysteamine coupling and Au nanoparticles (d ~15 nm) deposition. (C) Diagram displaying of the widths of the functional lines obtained at distinct laser powers and writing speeds.

To investigate the effect of laser power and writing speed on the width of the functional lines in the hexadecenyl monolayer, laser patterning was carried out at distinct laser powers: 295 mW, 304 mW and 315 mW (for comparison: a laser power of 330 mW was required to initiate local melting of the Si substrate), and writing speeds between 1 and 10 mm/s. Some typical SEM and AFM images, displaying sharp and well-defined lines of densely packed Au nanoparticles, are depicted in Figure 2. As expected for thermally stable monolayers, a significant dependence of the functional line width on the laser power and the writing speed was observed.[63,65-67,73] For reference, a diagram displaying the widths of the functional lines (after labeling with Au nanoparticles) obtained at the distinct laser powers and writing speeds considered here is given in Figure 2C. The broadest functional lines with widths of 1.1 µm are produced at a laser power of 314 mW and a writing speed of 1.25 mm/s, whereas the narrowest lines with widths of 250 nm are obtained at a laser power of 295 mW and a writing speed of 2.5 mm/s. We note, that these narrow lines also exhibit a reduced nanoparticle density. Usually, the nanoparticle density is known to scale with the density of surface functional groups.[81] This suggests, that backfilling of narrow

lines yields structures with a lower degree of functionalization, presumably because of incomplete removal of the primary monolayer as reported in previous work.[73] In particular, we note, that at low laser powers the local temperature rise is only comparatively small.[65,73] Hence, under these conditions the overall process is too slow to induce complete decomposition of the monolayer throughout irradiation.[73] This is also in agreement with the fact, that no lines are observed at again lower laser powers and/or higher writing speeds.

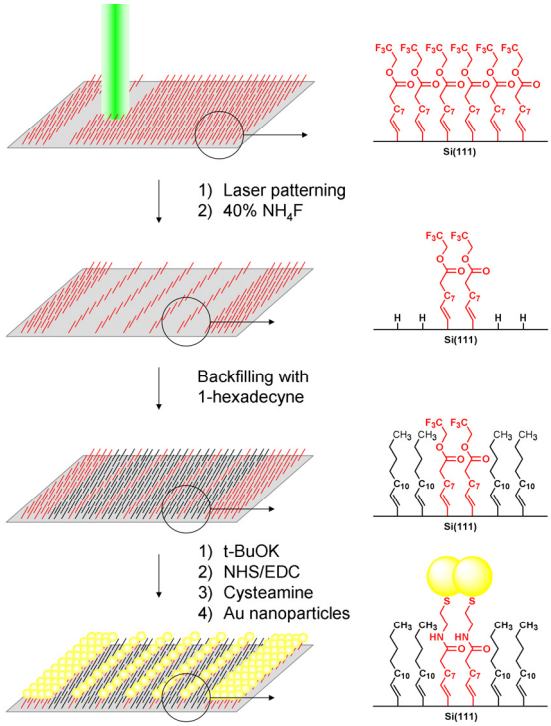

Figure 3. Schematic representation of the laser patterning procedure of functional monolayers, backfilling with an hexadecenyl monolayer and final Au nanoparticles deposition.

7.3.2. Laser Patterning of Functional Monolayers

Alternatively, by applying photothermal laser patterning to a functional monolayer and by reducing the lateral distance between the laser lines, it should be possible to produce even narrower functional stripes.[66,73] To this aim we started with patterning experiments on acid fluoride-terminated monolayers. Similar as for hexadecenyl monolayers, laser

patterning resulted in sub-micron lines in which the original acid fluoride monolayer was removed by photothermally induced decomposition. However, although backfilling of the laser lines with hexadecenyl monolayer occurred smoothly, it turned out that the NH_4F etching step was incompatible with the acid fluoride functionality, i.e. after cysteamine treatment no Au nanoparticles could be detected in the supposed thiol-terminated areas.[82] To overcome this problem during the etching step, 2,2,2-trifluoroethyl undec-10-ynoate (TFE), a trifluoroethyl ester protected derivative of 10-undecynoic acid, was synthesized and used for monolayer formation. The resulting TFE-terminated monolayers were hydrophobic with static contact angles of ~87° and had ellipsometric thicknesses of ~15 Å, both in good agreement with literature and indicative of densely packed TFE-terminated monolayers.[14] As shown in Figure 3, further surface reactions were used to convert the TFE functionality into a thiol group, which is favorable for Au nanoparticles assembly.

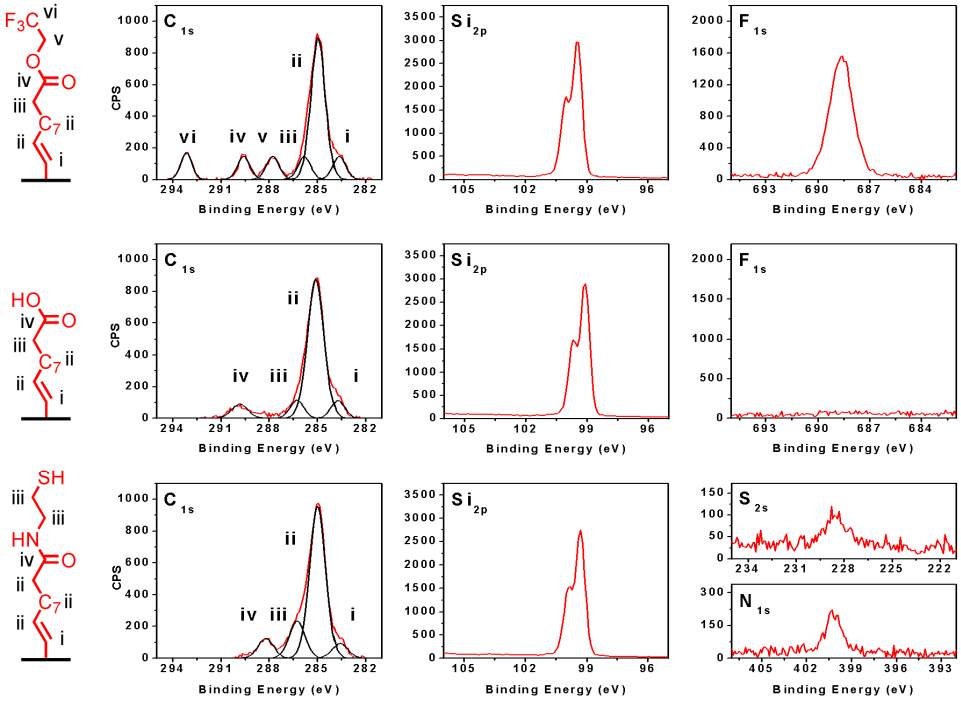

Figure 4. XPS C_{1s}, Si_{2p} and F_{1s} narrow scans of a TFE monolayer before (upper row) and after hydrolysis with *t*-BuOK (middle row), and XPS C_{1s}, Si_{2p}, S_{2s} and N_{1s} narrow scans of the final thiol-terminated monolayer after NHS/EDC activation and cysteamine coupling (lower row).

Before starting the laser patterning experiments we first studied the efficiency of these consecutive surface reactions and their effect on the overall monolayer quality, i.e. degree of oxidation of the Si substrate, by XPS analysis on an unpatterned TFE-terminated monolayer. As shown in Figure 4, the typical XPS C_{1s} narrow scan of a TFE monolayer consists of six distinct types of carbon atoms. The contributions at (i) 283.7 (ii) 285.0 (iii) 285.9 (iv) 287.8 (v) 289.6 (vi) 293.2 eV are assigned to the carbon covalently linked to the silicon substrate (E_{calc} = 284.0 eV), the aliphatic carbons (E_{calc} = 285.0 eV), the carbon adjacent to the TFE group (E_{calc} = 285.8 eV), the methylene carbon adjacent to the trifluoro group (E_{calc} = 288.1 eV), the carbonyl carbon (E_{calc} = 289.7 eV), and the trifluoro carbon (E_{calc} = 293.4 eV), respectively, all in excellent agreement with theoretical energy values and ratios (see Appendix 4).[83,84] Furthermore, the F_{1s} narrow scan reveals one large peak at 688.6 eV, corresponding to the three fluorides of the TFE group. The resulting F/C ratio is ~3/13 and equals the expected ratio for a TFE-terminated monolayer. Finally, the Si_{2p} narrow scan shows the typical $Si_{2p3/2}$ and $Si_{2p1/2}$ peaks and no sign of oxidized silicon around 103 - 104 eV. These XPS data clearly demonstrate that solely the terminal alkyne group is reacting with the H-Si surface and that the TFE functionality is intact after monolayer formation. After hydrolysis of the TFE group with potassium *tert*-butoxide in DMSO,[14,85] the C_{1s} emissions at 293.2 and 287.8 eV have disappeared and the carbonyl carbon shifted slightly to (iv) 289.8 eV (E_{calc} = 289.5 eV), characteristic for a carboxylic acid carbon. In the F_{1s} spectrum the large fluorine peak at 688.6 eV is completely gone, indicating that the deprotection is practically quantitative. Subsequent NHS/EDC activation and cysteamine coupling yields the terminal thiol group. The amide bond formation shifts the carbonyl carbon a little to (iv) 288.2 eV (E_{calc} = 288.1 eV), and the carbon next to the thiol group and its neighbor, which is adjacent to the amide bond, are both detected at (iii) 286.2 eV (E_{calc} = 286.6 eV). In addition, due to their lower photoemission cross-section, the S_{2s} and N_{1s} narrow scans display relative small peaks attributed to the thiol and amide functionality, respectively.[86] In contrast to earlier work of Strother et al.[14] we did not observe any silicon oxide, after the potassium *tert*-butoxide treatment as after NHS/EDC activation (16 h in water) as well as after cysteamine coupling. We attribute this enhanced stability to the higher packing densities that can be obtained with 1-alkynes on Si(111)[15,79] and the oxidation-inhibiting nature of the Si–C=C linkage.[16]

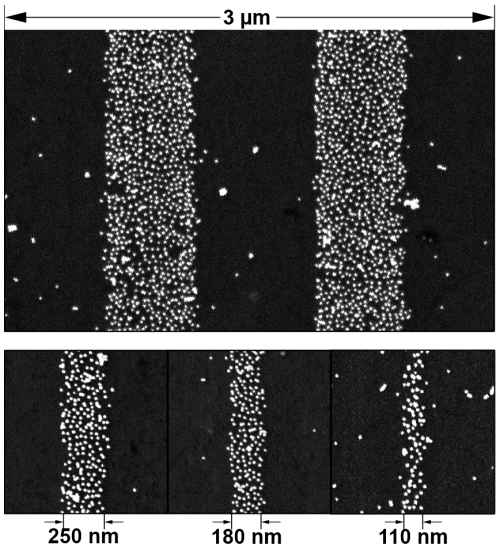

Figure 5. SEM images of laser-patterned TFE monolayer after backfilling with 1-hexadecyne, deprotection, NHS activation, cysteamine coupling and immersion in an Au nanoparticles solution (d ~15 nm). Laser patterning was carried out at a laser power of 323 mW and 297 mW (top and bottom image, respectively) and a writing speed of 2 mm/s.

For a laser-patterned TFE monolayer that was backfilled with a hexadecenyl monolayer, exactly the same deprotection/activation route was used to obtain the thiol functionality in the narrow monolayer stripes of the primary monolayer. After a final dip in an aqueous Au nanoparticles solution (d ~15 nm) the surface was characterized by SEM. In Figure 5 some typical SEM images are depicted and it is obvious that the Au nanoparticles solely assemble in the narrow thiol-terminated stripes. By reducing the lateral distance between the laser-written lines, Au nanoparticles stripes with widths as small as 110 nm were obtained. A remarkable result, i.e. if one considers that the used laser beam had a $1/e^2$ spot diameter of about 2.6 µm.[73]

7.3.3. Biofunctional Laser Patterns

In view of the great potential of this type of monolayers in the field of biosensing, the immobilization and pattern construction of complex biomolecules on oxide-free silicon is of great interest. To demonstrate the ease and flexibility of our approach we patterned a hexadecenyl monolayer, backfilled the laser lines with an acid fluoride-terminated

monolayer and submersed the sample in a solution of an oligo-DNA with a primary amine functionality at the 5'-terminus and a Cy3 label at the 3'-terminus. As evidenced by fluorescence microscopy (excitation of Cy3 at 488 nm), the Cy3-labeled DNA solely binds to the acid fluoride modified laser lines and not to the original hexadecenyl monolayer areas. It is expected, that, due to the high and selective reactivity of the acid fluoride groups towards primary amines, the Cy3-labeled oligo-DNA strands are mainly coupled to the acid fluoride laser lines via the primary amine group at the 5'-terminus. Consequently, the Cy3-labeled oligo-DNA should still be available for hybridization with target DNA. To investigate this, the sample was immersed in a Cy5-labeled target DNA solution at room temperature in the dark for 16 h. After hybridization the fluorescent DNA lines were detected by exciting Cy5 at 633 nm. The clear red fluorescent laser lines indicate that the Cy3-labeled DNA is still available for hybridization with the target DNA, and thus is mainly bound via the primary amine functionality at the 5'-terminus. This two-step photothermal approach thus leads to a facile biofunctionalization that is highly advantageous in the development of Si-based biosensors.

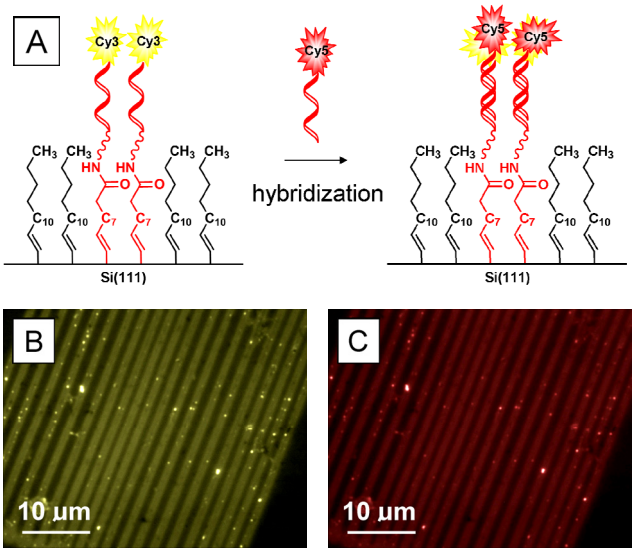

Figure 6. Fluorescent images of laser-patterned surface area with Cy3-labeled oligo-DNA lines (left) and the same surface area after hybridization with Cy5-labeled target DNA (right).

7.4 Conclusions

Photothermal laser patterning was demonstrated for nonfunctional and functional organic monolayers on oxide-free silicon, and was followed by backfilling of the laser-written lines with a second organic monolayer that differs in its terminal functionality. Because the thermal monolayer decomposition process is highly nonlinear in the applied laser power density, patterns with lateral dimensions far below the optical diffraction limit were fabricated (close to 100 nm width with a laser spot of 2.6 μm). Two complementary approaches were shown: a) pattering of homogeneous alkyl monolayers followed by back-filling with reactive acid fluoride monolayers, and subsequent functionalization thereof; b) patterning of homogeneous active ester monolayers followed by back-filling with unreactive alkyl monolayers, and subsequent functionalization of the active ester moieties. Coupling of cysteamine to the acid fluoride or active ester groups and subsequent assembly of Au nanoparticles allowed an easy characterization of the functional lines by atomic force microscopy (AFM) and scanning electron microscopy (SEM). Finally, in view of the great potential of this type of monolayers in the field of biosensing, acid fluoride backfilled laser lines were modified with fluorescently labeled NH_2-terminated oligo-DNA, which was shown to hybridize readily. In combination with the flexibility in pattern design, the high writing speeds, and the feasibility for patterning in more complex device geometries, e.g. in microfluidic channels and microstructured devices, these results show that photothermal laser patterning of organic monolayers on oxide-free silicon, provides promising perspectives in the fabrication of new small-scale biosensor and molecular electronic devices.

References

(1) Linford, M. R.; Fenter, P.; Eisenberger, P. M.; Chidsey, C. E. D. *J. Am. Chem. Soc.* **1995**, *117*, 3145-3155.

(2) Sung, M. M.; Kluth, G. J.; Yauw, O. W.; Maboudian, R. *Langmuir* **1997**, *13*, 6164-6168.

(3) Salomon, A.; Böcking, T.; Chan, C. K.; Amy, F.; Girshevitz, O.; Cahen, D.; Kahn, A. *Phys. Rev. Lett.* **2005**, *95*.

(4) Salomon, A.; Böcking, T.; Seitz, O.; Markus, T.; Amy, F.; Chan, C.; Zhao, W.; Cahen, D.; Kahn, A. *Adv. Mater.* **2007**, *19*, 445-450.

(5) Seitz, O.; Böcking, T.; Salomon, A.; Gooding, J. J.; Cahen, D. *Langmuir* **2006**, *22*, 6915-6922.

(6) Har-Lavan, R.; Ron, I.; Thieblemont, F.; Cahen, D. *Appl. Phys. Lett.* **2009**, *94*.
(7) Yaffe, O.; Scheres, L.; Puniredd, S. R.; Stein, N.; Biller, A.; Lavan, R. H.; Shpaisman, H.; Zuilhof, H.; Haick, H.; Cahen, D.; Vilan, A. *Nano Lett.* **2009**, *9*, 2390-2394.
(8) Boukherroub, R. *Curr. Opin. Solid State Mater. Sci.* **2005**, *9*, 66-72.
(9) Buriak, J. M. *Chem. Rev.* **2002**, *102*, 1271-1308.
(10) Hamers, R. J. *Ann. Rev. Anal. Chem.* **2008**, *1*, 707-736.
(11) Wayner, D. D. M.; Wolkow, R. A. *J. Chem. Soc., Perkin Trans. 2* **2002**, 23-34.
(12) Hamers, R. J. In *Bioelectronics: From Theory to Applications* Willner, I., Katz, E., Eds. 2005; Vol. Chapter 7, p 209-230.
(13) Faucheux, A.; Gouget-Laemmel, A. C.; de Villeneuve, C. H.; Boukherroub, R.; Ozanam, F.; Allongue, P.; Chazalviel, J. N. *Langmuir* **2006**, *22*, 153-162.
(14) Strother, T.; Cai, W.; Zhao, X. S.; Hamers, R. J.; Smith, L. M. *J. Am. Chem. Soc.* **2000**, *122*, 1205-1209.
(15) Scheres, L.; Giesbers, M.; Zuilhof, H. *Langmuir* **2010**, *26*, 4790-4795.
(16) Puniredd, S. R.; Assad, O.; Haick, H. *J. Am. Chem. Soc.* **2008**, *130*, 13727-13734.
(17) Voicu, R.; Boukherroub, R.; Bartzoka, V.; Ward, T.; Wojtyk, J. T. C.; Wayner, D. D. M. *Langmuir* **2004**, *20*, 11713-11720.
(18) Ng, A.; Ciampi, S.; James, M.; Harper, J. B.; Gooding, J. J. *Langmuir* **2009**, *25*, 13934-13941.
(19) Yang, M.; Teeuwen, R. L. M.; Giesbers, M.; Baggerman, J.; Arafat, A.; de Wolf, F. A.; van Hest, J. C. M.; Zuilhof, H. *Langmuir* **2008**, *24*, 7931-7938.
(20) Scheres, L.; ter Maat, J.; Giesbers, M.; Zuilhof, H. *Small* **2010**, *6*, 642-650.
(21) Ciampi, S.; Böcking, T.; Kilian, K. A.; James, M.; Harper, J. B.; Gooding, J. J. *Langmuir* **2007**, *23*, 9320-9329.
(22) Asanuma, H.; Lopinski, G. P.; Yu, H. Z. *Langmuir* **2005**, *21*, 5013-5018.
(23) Li, Y.; Wang, D.; Buriak, J. M. *Langmuir* **2009**, *26*, 1232-1238.
(24) Böcking, T.; Killan, K. A.; Gaus, K.; Gooding, J. J. *Langmuir* **2006**, *22*, 3494-3496.
(25) Onclin, S.; Ravoo, B. J.; Reinhoudt, D. N. *Angew. Chem. Int. Ed.* **2005**, *44*, 6282-6304.
(26) Garcia, R.; Martinez, R. V.; Martinez, J. *Chem. Soc. Rev.* **2006**, *35*, 29-38.
(27) Smith, R. K.; Lewis, P. A.; Weiss, P. S. *Prog. Surf. Sci.* **2004**, *75*, 1-68.
(28) Woodson, M.; Liu, J. *Phys. Chem. Chem. Phys.* **2007**, *9*, 207-225.
(29) Ginger, D. S.; Zhang, H.; Mirkin, C. A. *Angew. Chem. Int. Ed.* **2004**, *43*, 30-45.
(30) Xia, Y. N.; Whitesides, G. M. *Angew. Chem., Int. Ed.* **1998**, *37*, 551-575.
(31) Zharnikov, M.; Grunze, M. *J. Vac. Sci. Technol. B* **2002**, *20*, 1793-1807.
(32) Leggett, G. J. *Chem. Soc. Rev.* **2006**, *35*, 1150-1161.
(33) Love, J. C.; Estroff, L. A.; Kriebel, J. K.; Nuzzo, R. G.; Whitesides, G. M. *Chem. Rev.* **2005**, *105*, 1103-1169.
(34) Effenberger, F.; Gotz, G.; Bidlingmaier, B.; Wezstein, M. *Angew. Chem., Int. Ed.* **1998**, *37*, 2462-2464.

(35) Stewart, M. P.; Buriak, J. M. *Angew. Chem. Int. Ed.* **1998**, *37*, 3257-3260.
(36) Wojtyk, J. T. C.; Tomietto, M.; Boukherroub, R.; Wayner, D. D. M. *J. Am. Chem. Soc.* **2001**, *123*, 1535-1536.
(37) Fabre, B.; Hauquier, F.; Herrier, C.; Pastorin, G.; Wu, W.; Bianco, A.; Prato, M.; Hapiot, P.; Zigah, D.; Prasciolu, M.; Vaccari, L. *Langmuir* **2008**, *24*, 6595-6602.
(38) Yin, H. B.; Brown, T.; Wilkinson, J. S.; Eason, R. W.; Melvin, T. *Nucl. Acids Res.* **2004**, *32*, e118.
(39) Küller, A.; Eck, W.; Stadler, V.; Geyer, W.; Gölzhäuser, A. *Appl. Phys. Lett.* **2003**, *82*, 3776-3778.
(40) Perring, M.; Dutta, S.; Arafat, S.; Mitchell, M.; Kenis, P. J. A.; Bowden, N. B. *Langmuir* **2005**, *21*, 10537-10544.
(41) Jun, Y.; Le, D.; Zhu, X. Y. *Langmuir* **2002**, *18*, 3415-3417.
(42) Mizuno, H.; Buriak, J. M. *J. Am. Chem. Soc.* **2008**, *130*, 17656-17657.
(43) Rosso, M.; Giesbers, M.; Schroën, K.; Zuilhof, H. *Langmuir* **2009**, *26*, 866-872.
(44) Perring, M.; Mitchell, M.; Kenis, P. J. A.; Bowden, N. B. *Chem. Mater.* **2007**, *19*, 2903-2909.
(45) Mizuno, H.; Buriak, J. M. *ACS Appl. Mater. & Interfaces* **2009**, *1*, 2711-2720.
(46) Yang, M. L.; Zheng, Z. K.; Liu, Y. Q.; Zhang, B. L. *Nanotechnology* **2006**, *17*, 330-337.
(47) Yang, M. L.; Zheng, Z. K.; Liu, Y. Q.; Zhang, B. L. *J. Phys. Chem. B* **2006**, *110*, 10365-10373.
(48) Yang, M.; Wouters, D.; Giesbers, M.; Schubert, U. S.; Zuilhof, H. *ACS Nano* **2009**, *3*, 2887-2900.
(49) Yang, L.; Lua, Y. Y.; Lee, M. V.; Linford, M. R. *Acc. Chem. Res.* **2005**, *38*, 933-942.
(50) Niederhauser, T. L.; Lua, Y. Y.; Jiang, G. L.; Davis, S. D.; Matheson, R.; Hess, D. A.; Mowat, I. A.; Linford, M. R. *Angew. Chem., Int. Ed.* **2002**, *41*, 2353-2356.
(51) Niederhauser, T. L.; Jiang, G. L.; Lua, Y. Y.; Dorff, M. J.; Woolley, A. T.; Asplund, M. C.; Berges, D. A.; Linford, M. R. *Langmuir* **2001**, *17*, 5889-5900.
(52) Lua, Y. Y.; Fillmore, W. J. J.; Yang, L.; Lee, M. V.; Savage, P. B.; Asplund, M. C.; Linford, M. R. *Langmuir* **2005**, *21*, 2093-2097.
(53) Hurley, P. T.; Ribbe, A. E.; Buriak, J. M. *J. Am. Chem. Soc.* **2003**, *125*, 11334-11339.
(54) Khatri, O. P.; Han, J.; Ichii, T.; Murase, K.; Sugimura, H. *J. Phys. Chem. C* **2008**, *112*, 16182-16185.
(55) Roy, S. *J. Phys. D: Appl. Phys.* **2007**, *40*, R413-R426.
(56) Vong, T.; ter Maat, J.; van Beek, T. A.; van Lagen, B.; Giesbers, M.; van Hest, J. C. M.; Zuilhof, H. *Langmuir* **2009**, *25*, 13952-13958.
(57) Ghosal, S.; Baumann, T. F.; King, J. S.; Kucheyev, S. O.; Wang, Y. M.; Worsley, M. A.; Biener, J.; Bent, S. F.; Hamza, A. V. *Chem. Mater.* **2009**, *21*, 1989-1992.
(58) Bäuerle, D. *Laser Processing and Chemistry*; 3rd ed.; Springer-Verlag: Berlin, 2000.

(59) Klingebiel, B.; Schröter, A.; Franzka, S.; Hartmann, N. *ChemPhysChem* **2009**, *10*, 2000-2003.

(60) Alvarez, M.; Best, A.; Pradhan-Kadam, S.; Koynov, K.; Jonas, U.; Kreiter, M. *Adv. Mater.* **2008**, *20*, 4563-4567.

(61) Jonkheijm, P.; Weinrich, D.; Köhn, M.; Engelkamp, H.; Christianen, P. C. M.; Kuhlmann, J.; Maan, J. C.; Nüsse, D.; Schroeder, H.; Wacker, R.; Breinbauer, R.; Niemeyer, C. M.; Waldmann, H. *Angew. Chem. Int. Ed.* **2008**, *47*, 4421-4424.

(62) Franzka, S.; Koch, J.; Chichkov, B. N.; Hartmann, N. *J. Vac. Sci. Technol. A* **2010**, in press.

(63) Hartmann, N.; Franzka, S.; Koch, J.; Ostendorf, A.; Chichkov, B. N. *Appl. Phys. Lett.* **2008**, *92*, 223111.

(64) Mathieu, M.; Friebe, A.; Franzka, S.; Ulbricht, M.; Hartmann, N. *Langmuir* **2009**, *25*, 12393-12398.

(65) Balgar, T.; Franzka, S.; Hartmann, N. *Appl. Phys. A* **2006**, *82*, 689-695.

(66) Dahlhaus, D.; Franzka, S.; Hasselbrink, E.; Hartmann, N. *Nano Lett.* **2006**, *6*, 2358-2361.

(67) Hartmann, N.; Balgar, T.; Bautista, R.; Franzka, S. *Surf. Sci.* **2006**, *600*, 4034-4038.

(68) Iversen, L.; Younes-Metzler, O.; Martinez, K. L.; Stamou, D. *Langmuir* **2009**, *25*, 12819-12824.

(69) Rhinow, D.; Hampp, N. A. *Adv. Mater.* **2007**, *19*, 1967-1972.

(70) Shadnam, M. R.; Kirkwood, S. E.; Fedosejevs, R.; Amirfazli, A. *Langmuir* **2004**, *20*, 2667-2676.

(71) Geldhauser, T.; Leiderer, P.; Boneberg, J.; Walheim, S.; Schimmel, T. *Langmuir* **2008**, *24*, 13155-13160.

(72) Zhang, F.; Gates, R. J.; Smentkowski, V. S.; Natarajan, S.; Gale, B. K.; Watt, R. K.; Asplund, M. C.; Linford, M. R. *J. Am. Chem. Soc.* **2007**, *129*, 9252-9253.

(73) Klingebiel, B.; Scheres, L.; Franzka, S.; Zuilhof, H.; Hartmann, N. *Langmuir* **2010**, *26*, 6826-6831.

(74) Mathieu, M.; Schunk, D.; Franzka, S.; Mayer, C.; Hasselbrink, E.; Hartmann, N. *Small* **2009**, *5*, 2099-2105.

(75) Mathieu, M.; Schunk, D.; Franzka, S.; Mayer, C.; Hasselbrink, E.; Hartmann, N. *J. Vac. Sci. Technol. A* **2010**, in press.

(76) Balgar, T.; Franzka, S.; Hartmann, N.; Hasselbrink, E. *Langmuir* **2004**, *20*, 3525-3527.

(77) Balgar, T.; Franzka, S.; Hasselbrink, E.; Hartmann, N. *Appl. Phys. A* **2006**, *82*, 15-18.

(78) Hartmann, N.; Klingebiel, B.; Balgar, T.; Franzka, S.; Hasselbrink, E. *Appl. Phys. A* **2009**, *94*, 95-103.

(79) Scheres, L.; Arafat, A.; Zuilhof, H. *Langmuir* **2007**, *23*, 8343-8346.

(80) Urch, H.; Franzka, S.; Dahlhaus, D.; Hartmann, N.; Hasselbrink, E.; Epple, M. *J. Mater. Chem.* **2006**, *16*, 1798-1802.

(81) Bhat, R. R.; Fischer, D. A.; Genzer, J. *Langmuir* **2002**, *18*, 5640-5643.

(82) Most probably NH_4^+ and NH_3 in the NH_4F etching solution react with the acid fluoride groups.

(83) Frisch, M. J.; et al. *Gaussian03* **2004**, revision D.01; Gaussian, Inc.: Wallingford, CT.

(84) Glendening, E. D.; Reed, A. E.; Carpenter, J. E.; Weinhold, F. *NBO*, version 3.1.

(85) Rosso, M.; Giesbers, M.; Arafat, A.; Schroën, K.; Zuilhof, H. *Langmuir* **2009**, *25*, 2172-2180.

(86) Because of overlap of the S_{2p} emission with the large Si_{2s} signal we measured the S_{1s} emission. .

Chapter 8

Hg/Molecular Monolayer-Si Junctions: Electrical Interplay between Monolayer Properties and Semiconductor Doping Density

Abstract. Metal - Organic Monolayer - Semiconductor junctions are controlled not only by the molecular properties, as in Metal - Organic Molecule - Metal junctions, but also by effects of the molecular dipole, the dipolar molecule-semiconductor link, molecule-semiconductor charge transfer, and by the effects of all these on the semiconductor depletion layer, (i.e., on the internal semiconductor barrier to charge transport). Here, we report on and compare the electrical properties (current-voltage, capacitance-voltage and work function) of large area Hg/organic monolayer-Si junctions with alkyl and alkenyl monolayers on moderately and highly doped n-Si, and combine the experimental data with simulations of charge transport and electronic structure calculations. We show that for moderately doped Si the internal semiconductor barrier completely controls transport and that the attached molecules influence the transport of such junctions only in that they drive the Si into inversion. The resulting minority carrier-controlled junction is not sensitive to molecular changes in the organic monolayer at reverse and low forward bias, and is controlled by series resistance at higher forward bias. However, in the case of highly doped Si, the internal barrier is smaller, and as a result the charge transport properties of the junction are affected by changing from an alkyl to an alkenyl monolayer. We propose that the double bond near the surface primarily increases the coupling between the organic monolayer and the Si, which increases the current density at a given bias by increasing the contact conductance.

This chapter is published as:
'*Hg/Molecular Monolayer-Si Junctions: Electrical Interplay between Monolayer Properties and Semiconductor Doping Density'* Yaffe, O.* / Scheres, L.*; Segev, L.; Biller, A.; Ron, I.; Salomon, E.; Giesbers, M.; Kahn, A.; Kronik, L.; Zuilhof, H.; Vilan, A; Cahen D. *J. Phys. Chem. C* **2010**, ASAP, doi: jp101656t (* contributed equally)

8.1 Introduction

Incorporating molecular elements into electronic devices poses a fascinating scientific challenge.[1] By varying the molecular chemistry, we hope to tailor the device's electrical properties, possibly leading to flexible and scalable fabrication schemes. Much of the work in this direction focuses on single molecules or monolayer ensembles on metal electrodes.[2-4] Using a semiconductor instead of a metal provides significant physical and technological advantages,[5-9] among which are possibly tunable interactions between the semiconductor bands and the molecular energy levels that may lead to novel electrical behavior.[5] Semiconductor (SC) surfaces, as well as metal ones, can be functionalized with organic molecules to yield stable and high-quality monolayers.[10-13] However, unlike metals, the bulk electronic properties of semiconductors can be tailored through doping and the (near-) surface properties can be modified via electrical dipoles and (monopole) charges, thereby considerably expanding the possibilities for tuning the device performance.[14,15]

Adsorbing molecules on the SC surface generally changes the surface potential and, thus, the SC work function (and electron affinity).[16] This potential change at the SC surface can extend from roughly a few nm to a few microns into the semiconductor, forming a space charge region (SCR), which constitutes an internal barrier for charge transport. Therefore, if a metal contact is made to the SC, the presence of molecules at the interface can change the internal charge transport barrier across the resulting junction.[9,17] This internal SC barrier changes the current-voltage (J-V) characteristics of the junction, in addition to the specific charge transport barrier imposed by the molecules. Hence, the "molecular effect" of hybrid Metal/Organic Molecule/Semiconductor (MOMS) junctions can be divided into:

(1) The overall dipole of the molecules on the surface, plus any molecule-substrate charge transfer that affects the effective SC electron affinity;
(2) The electronic transport barrier, presented by the molecules, especially if they form a continuous monolayer.

In addition, the introduction of surface/interface states can also have a large effect on the electrical properties of the junction. However, it was shown in the past that the interface state density of well-prepared Si-organic monolayer interfaces is very low.[18,19]

The doping density of the SC affects the relative importance of effects (1) and (2), because an increase in doping density can:

(1) Induce image charge lowering of the barrier,
(2) Decrease the SC depletion layer width[20,21] and, thereby, increase the probability of tunneling through the SCR barrier (field emission),
(3) Affect the magnitude of the surface dipole, induced by the monolayer.[22]

Therefore, the molecular properties (e.g., degree of conjugation, presence of redox active centers, molecular length) will have different overall effects for different doping levels of otherwise identical semiconductors.

To study and comprehend this interplay between the molecular and Si properties, we compare here the electrical characteristics of Hg/monolayer-Si junctions with alkyl and alkenyl monolayers on n-Si(111) (see Figure 1), where saturated alkene-derived monolayers are referred to as "alkyl" and unsaturated alkyne-derived ones as "alkenyl". Both types of monolayer were formed on moderately and on highly doped n-Si(111), with $N_d \sim 10^{15}$ cm^{-3} (labeled MD) and 10^{19} cm^{-3} (labeled HD), respectively. This choice for a test system is convenient, because Hg has proven to be an efficient "soft", non-destructive top contact for molecular electronics,[23-25] and both alkyl and alkenyl monolayers were shown to be densely packed and with good chemical passivation properties.[26,27] This behavior then allows us to examine the extent to which a minor difference such as one double bond in a long alkyl chain can change the overall electrical transport properties of such junctions.

We find clear differences between J-V characteristics of MOMS on MD and HD n-Si(111). Furthermore, while the J-V characteristics of alkyl and alkenyl-based MOMS are almost identical for MOMS on MD Si, they differ for those on HD Si.

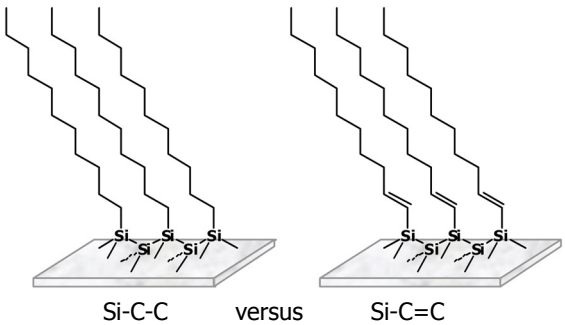

Figure 1. Idealized representation of the alkyl (left) and alkenyl (right) monolayers on n-Si(111).

8.2 Experimental

8.2.1 Monolayer Preparation

Single side polished n-type Si(111) wafers with a nominal resistivity of 1-10 Ω-cm (MD Si, N_d~10^{15} cm^{-3}) and 0.006 Ω-cm (HD Si, N_d~10^{19} cm^{-3}) were purchased from Siltronix (France). Sample preparation and characterization followed literature descriptions.[12,24] Briefly, pieces of Si wafer were cleaned by sonication in acetone and oxidized by an oxygen plasma (Harrick PDC-002 setup) for 3 min. Subsequently, the Si(111) substrates were etched in an argon-saturated 40% NH_4F solution for 15 min. After etching the samples were rinsed with water, blown dry with nitrogen, and immersed in argon-saturated neat 1-alkyne or 1-alkene (GC purity > 99.9%) at 120 °C and ~10 mbar. After 16 h, the reaction was stopped and the monolayers were rinsed extensively with PE40/60,[28] EtOH and CH_2Cl_2 and sonicated for 5 min in CH_2Cl_2 to remove physisorbed molecules. For MD Si, the examined monolayers were made with molecules with chain lengths of 12, 16 and 18 carbons, while for HD Si the molecules had chain lengths of 14, 16 and 18 carbons. This mismatch is due to the varying quality of the precursor molecules that were available at given times.

8.2.2 Monolayer Characterization

Static water contact angles were measured with an automated Krüss DSA 100 goniometer. At least six small droplets of 2.0 μl deionized water were dispensed and the contact angles was determined using a Tangent 2 fitting model. The error in the contact angles is < 1°.

Ellipsometric measurements were performed with a Sentech Instruments (Type SE-400) ellipsometer, operating at 632.8 nm (He-Ne-laser) and an angle of incidence of 70°. The optical constants of the substrate were determined with a piece of freshly etched n-Si(111) (n = 3.819 and k = 0.057). The thicknesses of the monolayers were determined with a planar three-layer (ambient, monolayer, substrate) isotropic model with refractive index of 1.46 for the organic monolayer. The reported values are the average of eight measurements taken at different locations on the sample and the error is < 1 Å.

X-ray photoelectron spectroscopy (XPS) analyses were performed using a JPS-9200 Photoelectron Spectrometer (JEOL, Japan). High-resolution spectra were obtained under UHV conditions using monochromatic Al Kα X-ray radiation at 12 kV and 25 mA, using

an analyzer pass energy of 10 eV. All high-resolution spectra were corrected with a linear background before fitting.

Infrared reflection-absorption (IRRA) spectra were collected with a Bruker spectrometer (model Tensor 27), equipped with a liquid N_2-cooled MCT detector and a variable-angle reflection accessory (AutoSeagull). A Harrick grid polarizer was placed in front of the sample for measuring spectra with p-polarized (parallel) light. In order to get the optimal signal to noise ratio on HD n-Si, the variable-angle reflection accessory was set to 50°, i.e., the incoming light makes an angle of 50° with respect to the surface normal.[29] The spectra were taken by adding 2048 scans at a resolution of 2 cm^{-1} and referenced to a clean native oxide-covered Si sample without further data manipulation.

The ultra-violet photoemission spectroscopy (UPS) experiments involved detailed measurements of the valence states of the monolayer-covered Si, including the photoemission cut-off, from which the vacuum level position and the work function are determined. HeI (21.22 eV) and HeII (40.8 eV) radiation lines were used for these experiments. The methodology followed for these measurements has been described elsewhere.[14] Band bending in the Si substrate, prior to the formation of a metal contact, was extracted from XPS scans of the Si_{2p} core level and from previous knowledge of the energy difference between the core level and the top of the Si valence band.

Atomic force microscopy (AFM) was performed in the tapping mode (AC), using a Nanoscope V Multimode AFM (Veeco, USA) and standard Si probes (OMCL-AC240TS-W2, Olympus, Japan). Typical peak forces were around 5 nN; typical scan rates were 1-2 Hz.

8.2.3 Electronic Characterization

J-V measurements were performed on n-Si/monolayer/Hg junctions, formed by placing a Hg (99.9999% purity) drop on the monolayer, using a controlled growth hanging mercury drop (HMD) electrode (Polish Academy of Sciences, Poland). The samples were contacted on the back by applying In-Ga eutectic, after scratching the surface with a diamond knife. Measurements were carried out in a controlled environment glove box with 10% relative humidity. The contact area between the Hg drop and the monolayer (typically 0.6 mm in diameter) was determined using an optical microscope.

Current-Voltage (J-V) measurements were done with a Keithley 6430 sub-fA current/voltage source-measure unit. Several scans from -1 to 2 V (applied to Hg) were measured for each junction with a scan rate of 20 mV/s. At least 7 junctions were made on

each sample, and the results represent the average of all the measurements. None of the measurements was rejected.

Impedance measurements were performed with an HP4284A precision LCR meter. The ac amplitude was 10 mV, and the measurement frequency was 500 kHz. This frequency was sufficiently high to prevent quasi-static behavior and to prevent possible interface states from following the ac signal. The impedance model used for the C-V measurements was a parallel circuit of a resistor and capacitor, commonly used to characterize such monolayers.[17,18]

Contact potential difference (CPD) measurements were performed with a custom-made Kelvin Probe set-up, based on a commercial Besocke Delta Phi Kelvin probe + controller which are placed in a glove box with controlled 10% relative humidity. The surface potential of the monolayers was measured, relative to that of a vibrating Au grid that was calibrated prior to the measurements against freshly peeled highly ordered pyrolytic graphite (HOPG).

Electronic structure calculations were performed for octyl and octenyl chains bound to Si(111), as shown in Figure 1. A (2×1) surface structure, with alkyl chains attached to one of the two surface Si atoms, was used. Dangling surface Si bonds were passivated by H atoms. The double bond was placed between the carbon atoms closest and second closest to the Si surface. All calculations were performed within a three-dimensional periodic super cell, using a symmetric slab configuration. This guarantees that the structure is devoid of a net dipole perpendicular to the Si-molecule interface, which would be inconsistent with the periodic boundary condition.[31,32] All calculations were performed with twelve atomic layers of silicon and a vacuum region equivalent to ten atomic layers of silicon. These values were found to be sufficient for a well-converged calculation that mimics a surface-terminated material. The electronic structure was determined by solving the Kohn-Sham equations of density functional theory, using the plane wave approach as implemented in the Vienna ab initio simulation package (VASP).[33] The local density approximation (LDA)[34] that was previously shown to be sufficient for describing the electronic structure of alkyl chains on Si,[35-37] was employed for the exchange-correlation functional. Surface dipole changes were computed by calculating the average electrostatic potential from the electronic charge density and nuclear coordinates along the direction perpendicular to the surface.[32] Specifically, we compared the potential difference between the vacuum region and a local maximum point found in the middle of the slab of the reference system, for an alkyl and alkenyl monolayer structure.[35]

For interpretation of the XPS data, additional computations of the charge distribution within the organic chain were preformed using B3LYP/6-311G(d,p) calculations with the Gaussian 09 (Rev A2) suite of programs. For technical reasons, a $(SiH_3)_3Si$ cluster (rather than a Si slab) was used in the simulation, to which either an alkyl or an alkenyl chain was attached (several lengths - C_4 was shortest). To properly compare the charges on the sp^2-hybridized C (underline marks the carbon that charge density was computed for) in Si–C=C and the sp^3-hybridized C in Si–C–C, light-in-heavy charges were used, in which the charge of the attached H atoms was added to that of the C atom.[38]

Device numerical simulations were based on the approach of Tarr et al.[30] for ultra-thin insulator MIS devices. In essence, the algorithm solves self-consistently both the total potential drop over the device and the total current density supported by it. The framework is that of a p^+-n junction, with charge carrier transport across it suppressed by tunneling. Following reference number 26, tunneling can be approximated by a WKB-based integral, attributing a band structure to the monolayer. This simplified approach can produce hole currents within 20% of the experimental data, which is sufficiently accurate for our purposes. Semiconductor and metal parameters used in the simulations are given in the table in the Appendix 5. The monolayer was modeled as a wide band gap insulator (E_g = 7.3 eV as experimentally measured for alkenes)[14] with a dielectric constant of 2.

8.3 Results and discussion

8.3.1 Monolayer characterization

The structural quality of a monolayer is a very important issue when studying the electrical properties of organic monolayers linked to Si.[18,26,39] Therefore, prior to the electrical measurements, the quality of all organic monolayers was studied in detail. Since one characterization method is not sufficient to determine that the monolayers are densely packed and of high quality a combination of static water contact angle measurements, ellipsometry, infrared spectroscopy (ATR-IR or IRRAS) and X-ray photoelectron spectroscopy (XPS) was used in this study. The preparation of high quality (in terms of carbon density, homogeneity and chemical passivation of the Si surface) alkyl and alkenyl monolayers on MD n-Si(111) has been reported,[12,26,27] and we refer to refs. for details of the characterization that we performed on the monolayers that we used. Because only lower quality monolayers have been reported on HD n-Si(111),[15,40] we report here on their

characterization. Table 1 summarizes the static contact angles (θ) and the ellipsometric thicknesses (d) of all alkyl and alkenyl monolayers on HD n-Si(111).

Table 1. Ellipsometric thicknesses (d) and static water contact angle (θ) of alkyl and alkenyl monolayers on HD n-Si(111).

Number of carbons	Ellipsometric thickness *d* (Å ± 1 Å)		Static water contact angle θ (° ± 1°)	
	Alkyl	Alkenyl	Alkyl	Alkenyl
14	16	15	107	107
16	19	20	110	111
18	20	21	108	109

The range of measured contact angles is well above the 102°-104° reported before on Si with identical doping level,[15] and close to the 110°-111° that has been reported for monolayers on MD n-Si.[14,18,27] This indicates that these alkyl and alkenyl monolayers on HD n-Si(111) are of a quality comparable to those on MD n-Si(111). Furthermore, the thickness of these alkyl and alkenyl monolayers on HD n-Si(111) agrees well with the values reported for these monolayers on MD n-Si(111).[26,27] Although the thickness increase from C_{16} to C_{18} is smaller than expected, the differences compared to the C_{16} and C_{18} monolayers on MD n-Si(111) are still within experimental error (±1 Å).

In addition, IRRAS was used to analyze the alkyl and alkenyl monolayers on HD n-Si(111). Spectra of the octadecyl and octadecenyl monolayers on HD n-Si(111) are shown in Figure 2. We note that, because on HD n-Si(111) we measured the external reflection of the p-polarized light at an incidence angle of 50° with respect to the surface normal, the resulting IRRA spectra exhibit positive peaks for the anti-symmetric and symmetric methylene stretching vibrations ($\nu_a(CH_2)$ and $\nu_s(CH_2)$), respectively, and a negative peak for the anti-symmetric methyl stretching vibration ($\nu_a(CH_3)$).[15,29] The position of $\nu_a(CH_2)$ is commonly used as an indicator of the intermolecular environment of the organic chains. Values of 2919-2920 cm^{-1} are typical for crystalline, solid alkanes and 2926-2928 cm^{-1} values characterize liquid, isotropic alkanes. For the octadecyl and octadecenyl monolayers on HD n-Si(111) the $\nu_a(CH_2)$ and $\nu_s(CH_2)$ peaks were detected at 2919 and 2851 cm^{-1} and at 2918 and 2850 cm^{-1}, respectively, indicating that both monolayers on HD n-Si(111) are densely packed.[41,42] In Chapter 4 it was also shown that in the case of alkenyl monolayers on MD Si, there is a peak at 1602.8 cm^{-1}, which is assigned to the C=C vibration mode.[27]

This peak was not observed for the same monolayer on HD Si, probably due to the fact that only IRRA can be used for HD Si, while in the case of MD the ATR-IR technique that was (and could be) used is significantly more sensitive than the former technique.

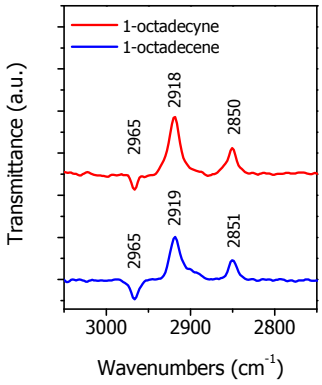

Figure 2. IRRA spectra (p-polarization) of octadecyl (bottom, red) and octadecenyl (top, blue) monolayers on HD n-Si(111).

As shown in Figure 3, the XPS C_{1s} narrow scans clearly show the different linkage of the two monolayers to the HD n-Si(111). For the 1-octadecyl monolayer the energy of the C_{1s} electrons from the silicon-bound carbon (Si–C) is very close to that of the aliphatic carbons, and, therefore, the narrow scan consists of only one main peak at ~285.0 eV. In contrast, the C_{1s} peak of the octadecenyl monolayer can easily be deconvoluted into two contributions, as the carbon, bound to the relatively electropositive Si shifts to ~283.5 eV. The higher electron density on the Si–C=C carbon present in the alkenyl chain shifts the emission peak in comparison to the Si–C–C carbon present in the alkyl chain. Furthermore, the ratio of peak areas between the small 283.5 eV peak ant the large 285.0 eV peak is 0.73/17. Taking into account the attenuation of the 283.5 eV peak due to the buried nature of the Si-C=C atom, the theoretically expected ratio would have been 0.75/17.[27,43] As a result, the ratio of the Si-C=C/other C atoms is 1/17, which agrees with the ratio of the one C bound to the Si and the number of C atoms remaining in the total C_{18} chain. This is also borne out by the natural population charge calculations on $(SiH_3)_3Si$-organic chain clusters, in which the organic chain was at least four carbon atoms long (butyl or butenyl). The results with chains longer than 4 carbons were essentially the same as those for the 4 carbon chains. For the Si–C=C carbon the light-in-heavy charge was calculated to be -0.42, while for the Si–C–C carbon this was -0.37. Such a difference is consistent with the positions of

the minor peak in the XPS-measured C_{1s} binding energies. This shift might also indicate differences in the interaction between the attached organic chain and the Si substrate, as discussed in section 3.3 below. We note that the XPS Si_{2p} narrow scans of both monolayers did not show any traces of oxidized Si around 103-104 eV,[12,26,27] an important criterion when studying electrical properties of organic monolayer - Si systems.

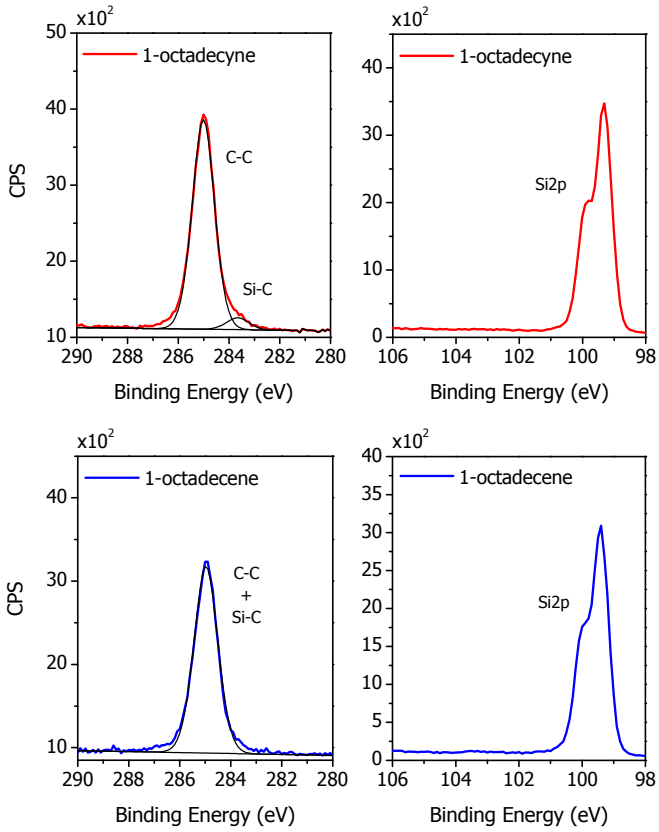

Figure 3. High-resolution XPS C_{1s} and Si_{2p} narrow scans of 1-octadecyl (bottom, blue) and 1-octadecenyl (top, red) monolayers on HD n-Si(111).

Finally, AFM (Figure 4) shows that the topography of the octadecene-derived monolayer reproduces the typical features of the underlying H-Si(111) surface,[44,45] indicating that these monolayers on HD-n-Si are smooth and dense, which was not the case for earlier reported ones on HD n-Si(111).[15] All the above data clearly demonstrate that high-quality alkyl and alkenyl monolayers were prepared on HD n-S(111), with contact angles, widths and densities comparable to those of alkyl and alkenyl monolayers on MD n-Si(111) (see

Chapter 4).[27] However, as shown earlier,[26] the most sensitive indication of monolayer quality is the current-voltage behavior of the MOMS, which is the primary subject of this report.

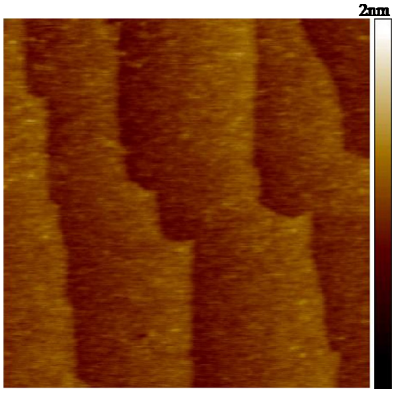

Figure 4. AFM topography (400 × 400 nm) of an octadecyl monolayer on HD n-Si(111). Note that the monolayer topography reproduces the typical topography of the H-terminated Si(111) surface, after etching in NH_4F.[40,41]

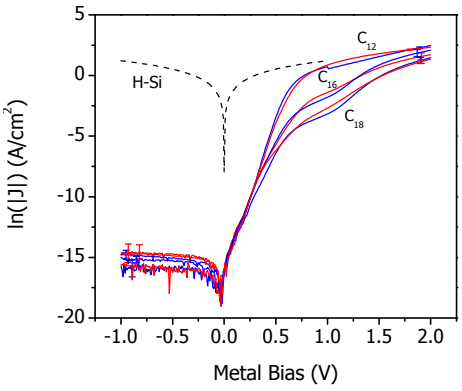

Figure 5. ln(|J|)-V curves of MD n-Si/organic molecular monolayer/Hg of 12, 16 and 18 carbon chain alkyl (blue) and alkenyl (red) monolayers, together with the ln(J)-V curve of a freshly etched H-Si(111) MOMS (black dashed). Bias is applied to the Hg and the Si is grounded. Scan rate: 20 mV/s. Results are logarithmic averages of at least 7 different junctions. The error bars represent the standard deviations, which are typically less than 5% of the measured current.

8.3.2 Electrical Properties of MOMS Junctions on MD Si

Figure 5 shows the ln(|J|)-V curves of MD n-Si/monolayer/Hg junctions with both alkyl (blue) and alkenyl (red) monolayers of three different chain lengths (12, 16 and 18 carbon chains). For reference, the black dashed line shows the current-voltage behavior of a Hg/H-Si(111) junction, which is ohmic and symmetric, i.e., currents are linear with bias. For the MOMS structures it is clear that there are two distinct bias ranges, as predicted by numerical simulations[46] and shown experimentally.[8]

In agreement with earlier studies,[8,9] the reverse and low forward bias characteristics of the different MOMS structures on MD n-Si are indistinguishable, within experimental error (but clearly different from the H-Si one). This range is denoted as the 'semiconductor-limited' regime.[46] At higher forward bias both the chain length and the type of monolayer (i.e., alkyl or alkenyl) affect the magnitude and shape of the current density curve. We now discuss these two regimes and the effect of series resistance on the latter.

8.3.2.1 Reverse and Low Forward Bias Range

The SC internal barrier of an ideal junction between a non-interacting metal and semiconductor can be calculated from:

$$\varphi_b = \Phi_m - \chi_{eff} \qquad (1)$$

which represents the Schottky limit.[21] Here any change in the effective electron affinity (χ_{eff})[47] of the SC directly affects the barrier to transport in the SC (ϕ_b) for a given metal work function (Φ_m).[48]

However, metal-Si Schottky diodes usually exhibit Fermi level pinning, yielding a barrier height that is lower or higher than predicted.[49] The presence of an ultra-thin insulating layer (such as our dense organic monolayers) can prevent metal–Si chemical interactions and, if the Si surface is well-passivated, make the junction behave as an ideal one.[9,48] Furthermore, it is known that no Fermi level pinning occurs in the case of a Si-H/Hg junction.[50] Therefore, that junction should follow the Schottky equation (equation 1) and the effective electron affinity of a given surface can be used in equation 1 to estimate ϕ_b. From UPS measurements a H-Si work function of 4.39 eV is derived, corresponding to an effective electron affinity of 4.15 eV, which agrees with the values of 4.17-4.23 eV reported earlier.[51] By using equation 1 and Φ_{Hg} = 4.49 eV, the ϕ_b for ideal Hg/H-Si(n)

contacts is estimated to be 0.34 eV. Such a low internal barrier is usually negligible if measurements are performed at room temperature,[17] and is consistent with the experimentally observed ohmic behavior of the Si:H/Hg junction (Figure 5).

The effective electron affinity of Si-monolayer samples was extracted from UPS and CPD measurements. Both methods gave similar results. The work function of all examined samples on MD n-Si(111) was 3.9 ± 0.1 eV, irrespective of chain length or monolayer type. This ~0.5 eV reduction in work function compared to that for Si-H (with a work function of 4.39 eV) is ascribed to the interfacial dipole of the adsorbed molecules, as discussed elsewhere.[16,35,52-54] From the position of the XPS Si_{2p} peak, a band bending of 0.06 eV was deduced. Because (E_V-E_F) is about 0.8 eV, the effective electron affinity is 3.6 ± 0.1 eV.[47,55] The independence of the measured electron affinity on the chain length is not surprising. It was shown in the past that the overall change in surface dipole of a given surface, due to the adsorption of an organic monolayer, is a sum of the surface-molecule bond dipole and dipole of the molecule before adsorption.[35,52] Hence, an additional CH_2 group in the middle of the chain should not have any effect on the interface dipole, because it does not change the molecular dipole. However, what is surprising is that we do not find a difference between alkyl and alkenyl monolayers, because there are differences in the average tilt angle in the monolayer, the molecular dipole of the isolated molecules and in the overall coverage of the atop Si atoms (~50% for alkyl and ~65% for alkenyl).[27] Furthermore, the presence of the double bond adjacent to the Si surface (in case of alkenyl) should induce charge transfer between the molecules and the Si slab, because of overlap between the π-orbitals of the double bond and the Si surface orbitals, as is discussed further in section 3.3. We can speculate that the reason for the lack of variation in experimental effective electron affinities is that the combination of all of the above-mentioned factors, leads to accidental cancellation of effects, resulting in work function values that are the same within the ±0.1 eV experimental error. This issue is currently being studied further. In the following we will use the experimental effective electron affinity in analyzing the charge transport.

Based on the effective electron affinity, extracted with the aid of equation 1, ϕ_b is predicted to be 0.9 ± 0.1 eV at the Hg/organic molecular monolayer/n-Si junction. This large value explains why the presence of the monolayer at the interface transforms the electrical behavior of the Si-H/Hg junction from ohmic to rectifying. All these results are summarized in the band diagram of MD n-Si surface, modified with an organic monolayer, before (left) and after (right) contact with Hg (Figure 6).

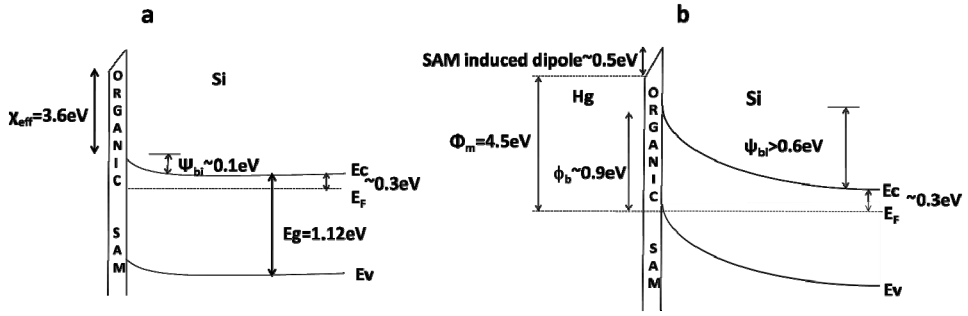

Figure 6. Band diagrams of organic monolayer/MD n-Si structure before (left) and after (right) contact with Hg, where χ_{eff} is the effective electron affinity (measured), ψ_{bi} is the built-in potential, measured as band bending, ϕ_b is the barrier for transport (calculated), E_g is the Si band gap and Φ_m is the Hg work function.[56]

Based on reverse bias C-V and temperature-dependent J-V measurements on MD n-Si/alkyl monolayer/Hg junctions, it was reported that in contact with a Hg drop, the molecularly modified Si is strongly inverted and that transport across these junctions is minority carrier-controlled.[9,48]

Our J-V and UPS results on alkenyl monolayers indicate that also with alkenyl monolayers the MD n-Si in such MOMS junctions is inverted. The reverse bias C-V measurements on MD n-Si/alkenyl monolayer/Hg junctions yielded results, identical to those for n-Si/alkyl monolayer/Hg ones (see Appendix 5). In addition, we found for the alkenyl monolayers a built-in potential (ψ_{bi}), doping density (N_d) and barrier height of 0.62 ± 0.03 eV, (8 ± 1)·10^{14} cm^{-3} and 0.89 ± 0.03 eV, respectively.[57] For the MD n-Si used here (doping density of N_d ~10^{15} cm^{-3}), the strong inversion potential (ψ_{inv}) is calculated to be 0.58 eV,[20] i.e., all the junctions on MD n-Si, studied here are strongly inverted, minority carrier-controlled junctions, with behavior similar to that of an abrupt, one-sided p^+-n one[30,46] rather than the previously assumed majority carrier thermionic emission controlled one.[8,18,58] J-V characteristics of a p^+-n junction are governed by diffusion of minority carriers in the neutral range of the semiconductor and/or generation-recombination in the SCR.[59] Because both minority carrier diffusion and recombination in the SCR are intrinsic semiconductor-related phenomena, to a first approximation the J-V behavior in this range will not be affected by the type or length of the molecules, beyond their effect to drive the Si into inversion.

As explained elsewhere, from C-V measurements only a lower limit of the built-in potential can be extracted,[9,60] and the 'real' value will generally be higher. That 'real' value

of ψ_{bi} is important from a technological point of view. An increase in ψ_{bi} will not change the magnitude of the current density in the minority carrier-controlled range (at a given voltage), but will widen that voltage range (relevant for a photovoltaic effect). Camporese and Pulfrey showed numerically that for metals with different work functions on the same SC-insulator combination (i.e., junctions with different ϕ_b), the onset of tunneling-limited behavior occurs at different current densities.[61] This implies that under strong inversion, the monolayer's dipole moment controls the electrical properties of the junction only by varying the voltage range over which the current is semiconductor-limited.

8.3.2.2 High Forward Bias Range

The results in Figure 5 show that the current density, at voltages where length/type dependence initiates, increases as the thickness of the monolayer decreases. To understand the nature of the transition between low and high forward bias, we start with the simplified MIS tunnel diode model of Tarr et al.,[30] and use as the insulator dielectric constant that of the organic monolayer rather than that of SiO_2, as was done in the original calculations (see Table 1 in the Appendix 5).

The results of these simulations are presented in Figure 7. The solid lines are ln(J) -V curves of the four junctions, with 1.5, 1.7, 1.9 or 2.1 nm insulator thickness, i.e., covering the experimental thickness range of the C_{12}-C_{18} monolayers.

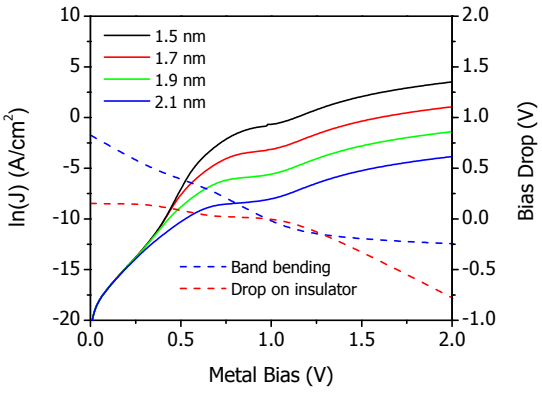

Figure 7. Calculated dependences of J-V curves (solid lines) on monolayer thickness (1.5, 1.7, 1.9 and 2.1 nm), as well as the calculated dependences of the semiconductor band bending (top-dashed, blue) and voltage drop on the insulator (bottom-dashed, red) on the applied bias, for a 2.1 nm thick monolayer. Calculations are based on the model of Tarr et al.[30]

The dashed lines present the semiconductor band bending (top, blue) and the voltage drop over the insulator (bottom, red) as a function of applied voltage. For clarity we show the computation only for a 2.1 nm thick monolayer. The results for the thinner monolayers (1.5, 1.7 and 1.9 nm) are almost identical to those for the 2.1 nm one with only slight differences in the 0.6-1.2 V transition range. Below 0.6 V, the voltage drop over the insulator is close to constant and negligible, while most of the applied bias falls across the SC, reducing the band bending. Over this range the current is completely semiconductor-limited and independent of the insulator thickness. In the intermediate 0.6 - 1.2 V bias range, the applied bias falls both across the SC and the insulator. Over this range the current starts to level off with increasing bias. Above 1.2 V the bias that falls over the semiconductor saturates and any additional bias falls across the insulator. In this regime there is no significant band-bending left in the semiconductor (semiconductor surface is in accumulation) and transport is dominated by tunneling across the insulator.

Over the intermediate voltage range the current is extremely sensitive to the molecular properties of the monolayer, i.e. the monolayer width and the surface state density.[46] In this range, the C_{18} and C_{16} J-V curves of alkyl and alkenyl monolayers are different and the current densities of the alkenyl junctions are higher than those of the alkyl junctions (see Figure 5).

8.3.2.3 The Effect of Series Resistance

Interpretation of the experimental data at high forward bias is complicated by series resistance effects. As the molecules grow shorter, the current increases and so does the effect of the series resistance.

Qualitatively, our experimentally measured ln(J) - V curves (Figure 5) are in good qualitative agreement with the simulation (Figure 7), with a first transition bias at ~ 0.6 V and a second at ~ 1.1 V. Figure 8 compares the theoretical and experimental conductance (dJ/dV = G) - voltage characteristics (semi-log plots) of the Hg/alkyl/MD n-Si junctions (similar curves are obtained with alkenyl monolayers). It is clear that theory and experiment agree at low forward bias, i.e., over the semiconductor-limited bias range. However, they deviate significantly over the transition and high bias ranges.

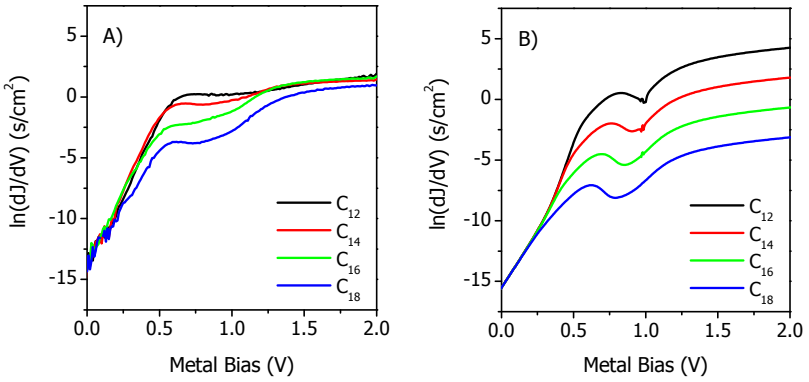

Figure 8. Comparison between the dependence of experimental (A) and simulated (B) conductance (G=dJ/dV) as function of applied bias on Hg/alkyl/MD n-Si junctions. The widths used in the simulations (1.5, 1.7, 1.9, and 2.1 nm) correspond to the experimentally measured thicknesses of the alkyl monolayers (C_{12}, C_{14}, C_{16} and C_{18}).

Theoretically, the transition range is characterized by a local maximum in the conductance, which correlates with the onset of the non-exponential J-V behavior, followed by a local minimum that correlates with the bias for which the semiconductor goes into accumulation. The experimental G-V curve of the n-Si/C_{18}/Hg system shows the theoretically predicted local maximum and minimum; however, these features become less pronounced as the molecules become shorter and vanish for the C_{12} junction. Furthermore, the conductance of the C_{12}-C_{16} systems at 2 V is nearly independent of the molecular length. This implies that the current density at high applied voltage ($V_{app} > 0.6V$) is limited by series, rather than by the tunneling, resistance.

We estimated experimentally, using Ohm's law, the series resistance, R_S, for the Si-H/Hg junction in our measurement set-up to be ~ 30 Ohm over the 1.5 – 2 V bias range. The measured current at 0.6 V, the onset of the transition range, was 9 μA for the C_{18} and 150 μA for the C_{12} system. Hence, the resistive voltage losses (= I × R_S) are 0.26 mV and 4.6 mV, respectively. Although the voltage drop over R_S is ~15 times larger in the case of the C_{12} than for the C_{18} system, it is remarkable that a ~5 mV voltage drop can have such an effect on the charge transport characteristics, while the applied bias is 130 times larger (600 mV). The reason is that up to the transition between semiconductor and tunneling limited region, the bias drop is mainly on the depletion layer of the SC (dashed blue line, Figure 7), while the bias drop on the insulator is negligible (dashed red line, Figure 7). Therefore, a 5

mV bias drop on series resistance is small compared to the total applied bias. but is significant compared to the actual bias drop on the insulator.

So far we presented an example for two different monolayers on Si that exhibit identical electrical properties over most of the examined bias range. This identical behavior originates from the inverted Si surface, which is induced by the molecular dipole (at reverse and low forward bias) and series resistance (at high forward bias). Sensitivity to molecular transport properties (e.g., length) was expressed only over a small part of the bias range, and over the transition range, where neither the semiconductor, nor the molecular contributions can be neglected. Therefore, although a length-dependent current is observed for MD-junctions, quantitative analysis of molecularly controlled transport[8,14,58,62,63] (e.g., extracting the current decay parameter, β) is ill-defined at this stage and might lead to misleading conclusions. This problem can be overcome by using HD Si as is described in the next section.

8.3.3 Electrical Properties of MOMS Junctions on HD n-Si

Figure 9 shows the averaged ln(|J|)-V curves of junctions with either alkyl (blue) or alkenyl monolayers (red) on HD n-Si(111), as well as the J-V curve of such a junction with freshly etched H-Si(111) (black dashed).

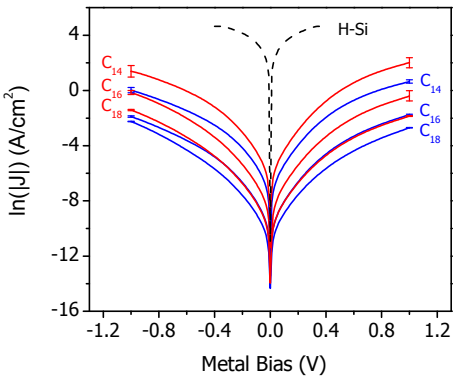

Figure 9. Ln(|J|)-V curves of HD n-Si/monolayer/Hg of both alkenes (blue) and alkynes (red) of several lengths (14, 16 and 18 carbon chains), and of freshly etched Hg/H-Si(111) (black dashed). Bias is applied to the Hg. Si is grounded. Results are logarithmic average of at least 7 different junctions with a scan rate of 20 mV/s. The error bars represent standard deviations, typically less than 5% of the measured current.

Compared to MOMS junctions on MD n-Si (Figure 5), we note three important features:

(1) The reverse bias (negative on the metal) current density is comparable to the forward bias current density. Furthermore, ln(J)-V characteristic in the forward bias (positive bias on the metal) is not exponential as expected for diode-like transport (i.e., it is not linear in Figure 9).
(2) The current density is length-dependent over all of the measured bias range.
(3) The current density of an alkenyl monolayer junction is higher than that of the analog alkyl monolayer over the whole measured bias range.

8.3.3.1 Rectifying vs. Non-Rectifying Behavior

The characterizations of our monolayers (vide supra) on Si with different doping levels show no or maximally a marginal effect of the doping level on the monolayer structure. Therefore we ascribe the transition from rectifying (MD n-Si, Figure 5) to non-rectifying behavior (HD n-Si, Figure 9) mainly to the electronic effects of the doping density of the Si.

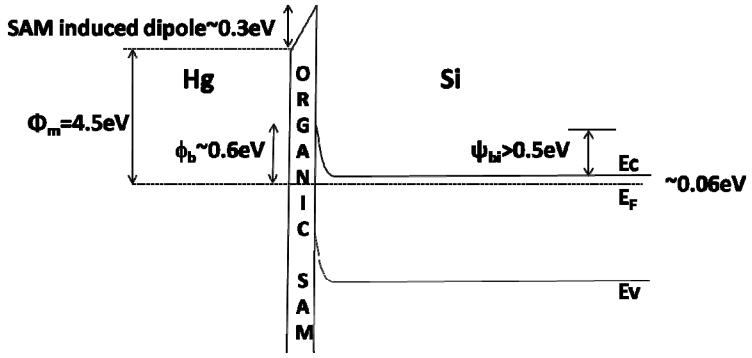

Figure 10. Band diagram of organic monolayer/HD n-Si structure after contact with Hg, where ψ_{bi} is the built-in potential, measured as band bending, ϕ_b is the barrier for transport (calculated) and Φ_m is the Hg work function.

First, while the strong inversion potential for MD n-Si is 0.58 eV, it is > 1 eV[20] for HD n-Si at room temperature. CPD measurements indicated that the work function of the HD samples is ~4.0 ± 0.1 eV, which can be compared to 4.25 ± 0.1 eV for freshly etched n-Si-H.[22] Based on the nominal doping density (N_d~10^{19} cm^{-3}), $|E_V - E_F|_{Bulk}$ is about 1 eV. Hence, the effective electron affinity is expected to be ~4 eV and according to the Schottky

limit (equation 1) under a Hg contact, the barrier height for charge transport and the surface potential of the HD n-Si are expected to be 0.6 eV and 0.5 eV, respectively. All these results are summarized in the band diagram for the HD n-Si junction (Figure 10).

This means that, in contrast to the surface of MD n-Si under Hg, the surface of HD n-Si is not inverted and charge transport is majority carrier-controlled.[46] Nevertheless, a potential barrier of 0.6 eV is expected to induce a stronger asymmetry in the J-V curves than that observed in Figure 9. There are three different mechanisms that can lead to non-rectifying J-V curves on the HD n-Si substrate:

(1) Interfacial layer-induced barrier lowering, i.e., the potential drop across the insulating layer makes the equilibrium barrier height lower than it would be without the layer;[21,64]
(2) Tunneling through the barrier, i.e., with increasing doping density thermionic field emission becomes more significant, due to the narrower depletion layer width;
(3) Field dependence of the barrier height, which can arise from the effect of the image force, which in turn depends strongly on doping density, or from the effect of trapped charges in interface states and/or in an interfacial layer (which can increase with doping density).[21]

The non-rectifying J-V curves indicate that, in contrast to what is the case for MD n-Si, the internal barrier in the HD n-Si is quite small and the J-V characteristics are dominated mainly by the presence of the monolayer. Indeed, both the length dependence within a single type of monolayer (C_{14}-C_{18}) and the differences in current density between monolayer types (alkyl vs. alkenyl) with identical number of carbons indicate that this is the case (Figure 9).

8.3.3.2 J-V Length Dependence

It is clear from Figure 9 that for alkyl monolayers the decrease in current between C_{14} and C_{16} is much larger than that between C_{16} and C_{18}. This result is very reproducible, correlates with the ellipsometry measurements (Table 1) and agrees with previously reported results on a similar system.[65] The same phenomenon is also seen, but less pronounced, for the alkenyl monolayers. A possible reason might be a difference in structure between longer (C_{16} and C_{18}) and shorter monolayers, consistent with the ellipsometric thicknesses of the monolayers. Such difference will cause an error in the

extraction of length-dependent parameters. Still, even with such errors, the approximate values that we can get from calculating these parameters can give an idea of the main differences between alkyl and alkenyl monolayers. For this purpose, we briefly summarize the expected length effect on electronic transport.

Transport of electrons through a saturated molecular system is commonly considered as an elastic scattering problem of free electrons (described by the Landauer relation),[52,66,67] where the tunneling probability through the barrier, introduced by the molecule, decays exponentially with the length. In this model, the conductance of a single channel (G) is described as:[4,68,69]

$$G = G_C \exp(-\beta l) \quad (2)$$

where 'l' is the length of the molecule, β is the length-decay parameter and G_C is the contact conductance. The averaged reported β value for transport across saturated alkyl chains is 0.9 ± 0.2/CH_2.[4] Here, we extracted β values of 0.9/CH_2 for the alkyls and 0.95/CH_2 for the alkenyls at an applied bias of 0.2 V with a fitting error of 0.2 (see Appendix 5), similar to the reported average values. The relative similarity between alkyl and alkenyl monolayers is expected as only one bond out of 14 (or more) in these chains is changed. However, because the double bond is close to the substrate, its effect is more likely to be felt in the coupling to the contact than in the transmission through the molecules. This result is consistent with the results presented by Engelkes et al., where variations in the metal work function for MIM junctions of alkyl thiols or dithiols had a pronounced effect on the net current, but not on the length-decay (β).[70] Also Nesher et al., considering transport through alkyls on GaAs,[63] and Thieblemont et al., considering Si–O vs. Si–C bound alkyls on Si,[58] concluded that the charge-transport properties of saturated alkyl chain MOMS with different anchoring groups, differ mainly in the molecule - substrate coupling.[65,66] In the case of the work by Nesher et al, we can also derive β and G_C values (see next section) from their data (0.65/CH_2 and 2.5 10^{-6} G_0, respectively).

8.3.3.3 Alkyl vs. Alkenyl - The Effect of Electrode-Monolayer Electrical Coupling

While β is similar for the two types of monolayers, the values for G_C, which is determined by the molecule-electrode coupling strength, is different. Assuming that every molecule presents a single conductance channel and that the footprint of a single molecule is ~ 0.2 nm^2/molecule,[61,67,71] we find that the contact conductances are (4.7 ± 1.3) · $10^{-7}G_0$

(with $G_0 \equiv \frac{2q^2}{h} = 77.4\mu S$) for alkyl and $(13 \pm 8)\cdot 10^{-7} G_0$ for alkenyl monolayers. As noted earlier for alkyl chain (and other molecular) junctions, the experimental G_C values are much lower than G_0[48] and are sensitive to interface chemistry.[69,70,72,73] One possible factor that reduces G_C is the limited density of states available for transport in a semiconductor (cf. also for GaAs[65] as mentioned above), compared to a metal. However, also in metal /molecule/metal junctions G_C is much smaller than G_0. Akkerman and De Boer[4] compiled the conductance for a large number of metal/alkyl/metal junctions, and correlated it with the molecular length. The intercept of their fit reveals a $G_C = 2.4\cdot 10^{-4} G_0$ for one (bottom electrode) and $1.6\cdot 10^{-2} G_0$, for two chemical contacts (bottom & top), respectively, in qualitative agreement with earlier reports by Selzer et al.[74] and Salomon et al.[67] The higher contact conductance for the two chemi-contact junction can be ascribed to enhanced coupling (orbital overlap) between the electrode and molecules, if there is a covalent bond between them. Furthermore, the contact conductance is sensitive to the metal of the electrode and was found to vary by up to 4 orders of magnitude, depending on whether Ag, Au or Pt served as the electrode,[70] with an exponential dependence on the metal's work function. This suggests that the coupling term depends on the energy difference between the electrode's Fermi level and the relevant molecular levels.[70,75] Such dependence is readily understood if we consider that the molecule-electrode coupling leads to new levels. The original LUMO and HOMO of the molecules should, at the interface, be replaced by the LUSO and HOSO (Lowest Unoccupied and Highest Occupied System Orbitals), which will be closer to the semiconductor band edges than the HOMO and LUMO of the isolated molecules or free monolayer.[37] These orbitals will influence tunneling, as well as hopping transport. In addition, tunneling will depend strongly on states that result from the interactions between the conduction band and valence band levels and the molecular levels, the so-called "Induced Density of Interface States", IDIS,[76] which will be the energy levels closest to the SC band edges.

To further examine the Si - organic chain coupling, we performed a DFT calculation of the alkyl and alkenyl systems. The local densities of states of the two systems are shown as a function of position (in the direction perpendicular to the surface) and energy in Figure 11. Clearly, Si-related states are found to extend further into the molecular region in the alkenyl case (up to the third carbon) than in the alkyl case (up to the second carbon). In the latter case, the dominant states contributing to the extension of the Si states are of the IDIS type.[37] In the alkenyl case they are a combination of IDIS and π-orbitals. These π-orbitals originate from the double bond between the first carbon, found closest to the surface, and

the second carbon. This is due to the overlap between the unbound allowed Si surface levels and the C=C π-bonding levels of the isolated alkenyl molecule, i.e., the HOMO-LUMO gap of the double bond in the isolated molecule is similar to the Si band gap. The extended nature of Si-related states is consistent with enhanced coupling between the Si substrate and the alkenyl SAM, relative to that of the alkyl SAM. Hence, due to molecule-semiconductor coupling even just one double bond in a long alkyl chain can affect the electrical characteristics of a MOMS device, as long as the effect of the internal barrier of the SC does not dominate transport (as is the case with MD Si).

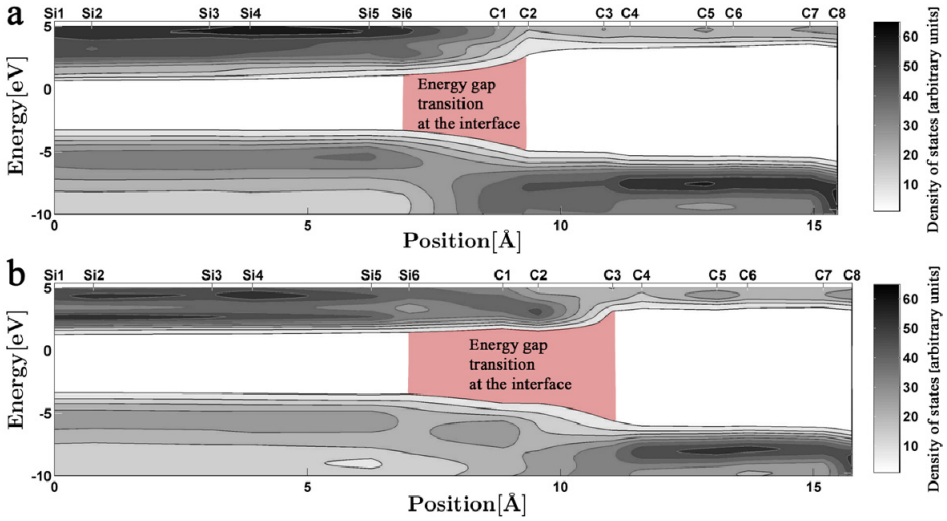

Figure 11. Contour maps of the local density of states for (a) alkyl and (b) alkenyl monolayers on Si(111).[77] The interfacial transition region is emphasized in red.

8.4 Conclusions

By comparing alkyl and alkenyl self-assembled monolayers that differ only by a double bond adjacent to the surface (Figure 1), on two different n-Si substrates (moderately and heavily doped) we find that with moderately doped Si the combination of the relatively wide space charge region of the Si, together with the large surface dipole layer, induced by the molecular monolayer, creates a minority carrier-controlled junction. Transport across such a junction is indifferent to the charge-transport properties of the attached monolayer at

reverse and low forward bias and, in our case, is affected by series resistance at high forward bias. For highly doped Si, the internal SC barrier decreases so as to become less significant, compared to the barrier posed by the molecular monolayer. As a result we can no observe effects of the double bond near the surface and find that the main influence is to enhance Si-molecule coupling, which increases the contact conductance and by that increases the current density at a given applied bias. Taking a more general view, our results show that molecular features, i.e., the surface dipole, induced by the molecules and the molecular effect on the charge transport barrier, are expressed differently for different doping levels of otherwise identical semiconductor substrates. While the electrical properties of MOMS junctions on a moderately doped semiconductor are strongly dependent on the surface dipole that is induced by the molecules, the electrical properties of a similar junction on a heavily doped semiconductor are very sensitive to the charge transport barrier that is strongly influenced by the molecule. Thus, the electrical properties of MOMS junctions on HD and MD semiconductor substrates are complementary and present a micro-laboratory to study a given molecular system.

References

(1) Heath, J.; Ratner, M. A. *Physics today*. May 2003, p. 43.

(2) Aviram, A.; Ratner, M. A. *Molecular Electronics: Science and Technology*; The Annals of the New York Academy of Sciences; New York Academy of Sciences: New York, 1998; Vol. 852.

(3) Ulman, A. *An introduction to ultrathin organic films: from Langmuir-Blodgett to self assembly*; Boston, MA, 1991.

(4) Akkerman, H. B.; de Boer, B. *J. Phys.: Condens. Matter* **2008**, *20*, 013001.

(5) Guisinger, N. P.; Greene, M. E.; Basu, R.; Baluch, A. S.; Hersam, M. C. *Nano Lett.* **2004**, *4*, 55-59.

(6) Wang, W.; Scott, A.; Gergel-Hackett, N.; Hacker, C. A.; Janes, D. B.; Richter, C. A. *Nano Lett.* **2008**, *8*, 478-484.

(7) Adina, S.; David, B. J.; Chad, R.; Mark, A. R. *App. Phys. Lett.* **2007**, *91*, 033508.

(8) Salomon, A.; Böcking, T.; Seitz, O.; Markus, T.; F., A.; Chan, C.; Zhao, W.; Cahen, D.; Kahn, A. *Phys. Rev. Lett.* **2005**, *95*, 266807.

(9) Yaffe, O.; Scheres, L.; Puniredd, S. R.; Stein, N.; Biller, A.; Lavan, R. H.; Shpaisman, H.; Zuilhof, H.; Haick, H.; Cahen, D.; Vilan, A. *Nano Lett.* **2009**, *9*, 2390-2394.

(10) Buriak, J. M. *Chem. Rev.* **2002**, *102*, 1271-1308.

(11) Ciampi, S.; Böcking, T.; Kilian, K. A.; James, M.; Harper, J. B.; Gooding, J. J. *Langmuir*

2007, *23*, 9320-9329.
(12) Scheres, L.; Arafat, A.; Zuilhof, H. *Langmuir* **2007**, *23*, 8343-8346.
(13) Puniredd, S. R.; Assad, O.; Haick, H. *J. Am. Chem. Soc.* **2008**, *130*, 13727-13734.
(14) Salomon, A.; Böcking, T.; Seitz, O.; Markus, T.; Amy, F.; Chan, C.; Zhao, W.; Cahen, D.; Kahn, A. *Adv. Mater.* **2007**, *19*, 445-450.
(15) Miramond, C.; Vuillaume, D. *J. Appl. Phys.* **2004**, *96*, 1529-1536.
(16) Ralf, H.; Rainer, F.; Bengt, J.; Wolfram, J.; Lauren, J. W.; Lewis, N. *Phys. Rev. B* **2005**, *72*, 045317.
(17) Maldonado, S.; Plass, K. E.; Knapp, D.; Lewis, N. S. *J. Phys. Chem. C* **2007**, *111*, 17690-17699.
(18) Faber, E. J.; de Smet, L.; Olthuis, W.; Zuilhof, H.; Sudhölter, E. J.; Bergveld, P.; Van den Berg, A. *ChemPhysChem* **2005**, *6*, 2153-2166.
(19) Kar, S. *Appl. Surf. Sci.* **2006**, *252*, 3961.
(20) Sze, S. M.; Ng, K. K. *Physics of Semiconductor Devices*; third.; New York: John Wiley & Sons, Inc., 2007.
(21) Rhoderick, E.; Williams, R. *Monographs in Electrical and Electronic Engineering. Metal-Semiconductor Contacts*; second.; Clarendon press: Oxford, 1988.
(22) It seems that the dipole effect of the adsorbed molecular monolayer on heavily doped Si is smaller than on moderately doped Si. A quantitative study of this issue is currently in progress.
(23) Rampi, M. A.; Whitesides, G. M. *Chem. Phys.* **2002**, *281*, 373.
(24) Mann, B. *J. Appl. Phys.* **1971**, *42*, 4398.
(25) Liu, Y.; Yu, H. *ChemPhysChem* **2002**, *3*, 799-802.
(26) Seitz, O.; Böcking, T.; Salomon, A.; Gooding, J. J.; Cahen, D. *Langmuir* **2006**, *22*, 6915-6922.
(27) Scheres, L.; Giesbers,, M.; Zuilhof, H. *Langmuir* **2010**, *26*, 4790-4795.
(28) Petroleum Ether with a boiling point between 40 and 60 °C.
(29) Brunner; Mayer, U.; Hoffman *Appl. Spectrosc 51*, 209-217.
(30) Tarr, N. G.; Pulfrey, D. L.; Camporese, D. S. *Electron Devices, IEEE Transactions on* **1983**, *30*, 1760.
(31) Makov, G.; Payne, M. C. *Phys. Rev. B* **1995**, *51*, 4014.
(32) Natan, A.; Kronik, L.; Shapira, Y. *App. Surf. Sci.* **2006**, *252*, 7608-7613.
(33) Kresse, G.; Furthmüller, J. *Phys. Rev. B* **1996**, *54*, 11169.
(34) Gross, E. K. U.; Dreizler, R. M. *Density functional theory*; Springer, 1995.
(35) Magid, I.; Burstein, L.; Seitz, O.; Segev, L.; Kronik, L.; Rosenwaks, Y. *J. Phys. Chem. C* **2008**, *112*, 7145-7150.
(36) Amy, F.; Chan, C. K.; Zhao, W.; Hyung, J.; Ono, M.; Sueyoshi, T.; Kera, S.; Nesher, G.; Salomon, A.; Segev, L.; Seitz, O.; Shpaisman, H.; Scholl, A.; Haeming, M.; Böcking, T.; Cahen, D.; Kronik, L.; Ueno, N.; Umbach, E.; Kahn, A. *J. Phys. Chem. B* **2006**, *110*,

21826-21832.

(37) Segev, L.; Salomon, A.; Natan, A.; Cahen, D.; Kronik, L.; Amy, F.; Chan, C. K.; Kahn, A. *Phys. Rev. B* **2006**, *74*, 165323-6.

(38) van Alem, K.; Lodder, G.; Zuilhof, H. *J. Phys. Chem. A* **2002**, *106*, 10681-10690.

(39) Faber, E. J.; Sparreboom, W.; Groeneveld, W.; Smet, L. C. P. M. D.; Bomer, J.; Olthuis, W.; Zuilhof, H.; Sudhölter, E. J. R.; Bergveld, P.; Berg, A. V. D. *ChemPhysChem* **2007**, *8*, 101-112.

(40) Sun, Q.; de Smet, L. C. P. M.; van Lagen, B.; Giesbers, M.; Thune, P. C.; van Engelenburg, J.; de Wolf, F. A.; Zuilhof, H.; Sudhölter, E. J. R. *J.Am.Chem.Soc.* **2005**, *127*, 2514-2523.

(41) Porter, M. D.; Bright, T. B.; Allara, D. L.; Chidsey, C. E. D. *J.Am.Chem.Soc.* **1987**, *109*, 3559-3568.

(42) Snyder, R. G.; Strauss, H. L.; Elliger, C. A. *J. Phys.Chem.* **1982**, *86*, 5145-5150.

(43) Wallart, X.; Henry de Villeneuve, C.; Allongue, P. *JACS* **2005**, *127*, 7871-7878.

(44) Allongue, P.; Henry de Villeneuve, C.; Morin, S.; Boukherroub, R.; Wayner, D. D. M. *Electrochimica Acta* **2000**, *45*, 4591-4598.

(45) Ramonda, M.; Dumas, P.; Salvan, F. *Surf. Sci.* **1998**, *411*, L839-L843.

(46) Green, M. A.; King, F. D.; Shewchun, J. *Solid-State Electron.* **1974**, *17*, 551.

(47) The effective electron affinity is given by $\chi eff = \Phi_{SC}$ - (Eg-|Ev-Ef|s), where Φ_{SC} is the work function of the Si + molecules substrate, Eg is the Si band gap, and |Ev-Ef|s is the difference between the energy level of the valence band (Ev) and the Fermi level (Ef) at the surface. Both Φ_{SC} and |Ev-Ef|s can by directly measured either by UPS or combined CPD/SPV (Surface Photo Voltage) measurement. See ref 51 fig.4 p.18.

(48) Vilan, A.; Yaffe, O.; Biller, A.; Salomon, A.; Kahn, A.; Cahen, D. *Adv. Mater.* **2010**, *22*, 140-159.

(49) Brillson, L. *Surf. Sci. R.* **1982**, *2*, 123-326.

(50) Wittmer, M.; Freeouf, J. L. *Phys. Rev. Lett.* **1992**, *69*, 2701.

(51) Hunger, R.; Fritsche, R.; Jaeckel, B.; Jaegermann, W.; Webb, L. J.; Lewis, N. S. *Phys. Rev. B* **2005**, *72*, 045317.

(52) Heimel, G.; Romaner, L.; Zojer, E.; Bredas, J. *Accounts Chem. Res.* **2008**, *41*, 721-729.

(53) Jaeckel, B.; Hunger, R.; Webb, L. J.; Jaegermann, W.; Lewis, N. S. *J.Phys.Chem.C* **2007**, *111*, 18204-18213.

(54) Natan, A.; Kronik, L.; Haick, H.; Tung, R. *Adv. Mater.* **2007**, *19*, 4103-4117.

(55) Kronik, L.; Shapira, Y. *Surf. Sci. R.* **1999**, *37*, 1-206.

(56) Walker, P.; Tarn, W. H. *CRC handbook of metal etchants*; CRC Press, 1990.

(57) The error represents the standard deviation between the samples.

(58) Thieblemont, F.; Oliver, O.; Vilan, A.; Cohen, H.; Salomon, E.; Kahn, A.; Cahen, D. *Adv. Mater.* **2008**, *20*, 3931-3936.

(59) Sah, C. T.; Noyce, R. N.; Shockley, W. *Proc. IRE* **1957**, *45*, 1228.

(60) Shewchun, J.; Green, M. A.; King, F. D. *Solid-State Electron.* **1974**, *17*, 563.

(61) Camporese, D. S.; Pulfrey, D. L. *J. Appl. Phys.* **1985**, *57*, 373-376.
(62) Salomon, A.; Böcking, T.; Gooding, J. J.; Cahen, D. *Nano Lett.* **2006**, *6*, 2873-2876.
(63) Nesher, G.; Shpaisman, H.; Cahen, D. *J.Am.Chem.Soc.* **2007**, *129*, 734-735.
(64) provided that there is no charge contained in the layer.
(65) Furuhashi, M.; Omura, A.; Yamashita, Y.; Mukai, K.; Yoshinobu, J.; Akagi, K.; Tsuneyuki, S. *Jpn. J. Appl. Phys.* **2009**, *48*, 055003.
(66) Adams, D. M.; Brus, L.; Chidsey, C. E. D.; Creager, S.; Creutz, C.; Kagan, C. R.; Kamat, P. V.; Lieberman, M.; Lindsay, S.; Marcus, R. A.; Metzger, R. M.; Michel-Beyerle, M. E.; Miller, J. R.; Newton, M. D.; Rolison, D. R.; Sankey, O.; Schanze, K. S.; Yardley, J.; Zhu, X. *J. Phys. Chem. B* **2003**, *107*, 6668-6697.
(67) Salomon, A.; Cahen, D.; Lindsay, S.; Tomfohr, J.; Engelkes, V. B.; Frisbie, C. D. *Adv.Mater.* **2003**, *15*, 1881-1890.
(68) Magoga, M.; Joachim, C. *Phys. Rev. B* **1997**, *56*, 4722.
(69) Chen, F.; Li, X.; Hihath, J.; Huang, Z.; Tao, N. *J.Am.Chem.Soc.* **2006**, *128*, 15874-15881.
(70) Engelkes, V. B.; Beebe, J. M.; Frisbie, C. D. *J.Am. Chem. Soc.* **2004**, *126*, 14287-14296.
(71) York, R. L.; Nacionales, D.; Slowinski, K. *Chem.Phys.* **2005**, *319*, 235.
(72) Monnell, J. D.; Stapleton, J. J.; Dirk, S. M.; Reinerth, W. A.; Tour, J. M.; Allara, D. L.; Weiss, P. S. *J. Phys. Chem. B* **2005**, *109*, 20343-20349.
(73) Yoo, H.; Choi, J.; Wang, G.; Kim, T.; Noh, J.; Lee, T. *J.Nanosci.Nanotech.* **2009**, *9*, 7012-7015.
(74) Selzer, Y.; Salomon, A.; Cahen, D. *J.Phys.Chem.B* **2002**, *106*, 10432-10439.
(75) Quinn, J. R.; Foss, F. W.; Venkataraman, L.; Breslow, R. *J.Am.Chem.Soc.* **2007**, *129*, 12376-12377.
(76) Vazquez, H.; Dappe, Y. J.; Ortega, J.; Flores, F. *J.Chem.Phys.* **2007**, *126*, 144703.
(77) The unoccupied levels have been rigidly shifted so as to yield the correct alkyl chain gap (as inferred from a combination of UPS and IPES). As a consequence, the silicon gap is larger than the experimental one.

Chapter 9

Covalent Attachment of Bent-Core Mesogens to Silicon Surfaces

Abstract. Two vinyl-terminated bent core-shaped liquid crystalline molecules that exhibit thermotropic antiferroelectric $SmCP_A$ phases, have been covalently attached onto a hydrogen-terminated Si(111) surface. The surface attachment was achieved via a mild procedure from a mesitylene solution, using visible light at room temperature. Atomic force microscopy (AFM) measurements indicate that a smooth monolayer has been formed. The thickness of the monolayer was evaluated with ellipsometry and X-ray reflectivity. Although the molecules differ in length by four carbon atoms, the thickness of the resulting monolayers was the same. The measured thicknesses correspond quite well with the smectic layer thickness in the bulk liquid crystalline material, suggesting a similar self-organization within the monolayer. From attenuated total reflection infrared spectroscopy (ATR-IR), which clearly shows the C–H and C=O vibrations, a tilt angle of the mesogens is deduced that also corresponds well with the tilt angle in the liquid crystalline state. X-ray photoelectron spectroscopy (XPS) measurements confirm the high quality of the monolayers, with only marginal silicon oxide formation. The elemental composition and amounts of different O and C atoms deduced from the high-resolution XPS correspond very well with the calculated compositions.

This chapter is published as:
'*Covalent Attachment of Bent-Core Mesogens to Silicon*' Scheres, L.; Achten, R.; Giesbers, M.; de Smet, L.; Arafat, A.; Sudhölter, E.; Marcelis, T.; Zuilhof, H. *Langmuir* **2009**, *25*, 1529-1533

9.1 Introduction

The covalent attachment of organic monolayers to solid surfaces is a research area that is recently attracting a huge interest, because the resulting monolayers are thermally robust and chemically stable. [1-6] Furthermore, they offer the possibility to perform subsequent chemical reactions on the modified surface. The modified surfaces are obtained by reacting a H-terminated Si surface with molecules containing terminal alkene or alkyne groups. Several methods have been developed and improved for this attachment reaction, ranging from rather harsh thermal methods[7-10] to much milder methods at room temperature under thermal activation or using irradiation with visible light.[11-14] The presence of additional synthetic handles allows one to obtain (bio)functional surfaces containing groups like sugars,[15] proteins,[16] DNA,[17] fullerenes,[18] etc. Recently, self-assembled carboxylate group-containing monolayers on Si were reported, that showed switching behavior in an electrical field[19,20] and stilbene monolayers on Si that showed photoswitching.[21]

However, to obtain a densely packed monolayer that also protects the underlying Si surface, usually simple long-tailed alkenes or alkynes are used, sometimes mixed with alkenes or alkynes that contain the desired functional groups. To make thicker protective monolayers using alkenes with very long tails or polymeric groups is usually not an option, due to both the prohibitive costs and the preferential coiled conformations of such long tails, which leads to a significant reduction in the density and thickness of the resulting monolayer.[22]

Molecules that tend to form self-assembling well-packed layers in which the molecules have stretched conformations are smectic liquid crystals. Recently, we and others studied bent-core (or banana-shaped) liquid crystals that contain a terminal alkene group.[23,24] These molecules are rather long and have some very interesting ordering and switching properties. These achiral bent-core compounds can form tilted polar smectic layers with ferroelectric or antiferroelectric switching properties. The dipoles of the molecules in one layer all point along a common director, and the molecules are tilted with respect to the layer normal. This gives rise to chiral layer symmetry, and – if the layer chirality is the same in adjacent layers – macroscopically chiral structures can exist. The most widely observed and studied bent-core-phase is the SmCP phase, which can exist in an antiferroelectric (P_A) or a ferroelectric ground state (P_F), with either synclinic (C_s) or anticlinic (C_a) layer organization.[25-29]

The properties of bent-core mesogens have almost always been studied in bulk or in at least micrometer thick films. Langmuir films,[30-34] vacuum-deposited films,[35,36] two-dimensional assemblies[37] and free-standing films[38] of bent-core (sub)monolayers, are, to the

best of our knowledge, the only examples where these compounds have been characterized in (sub)monolayers. On highly ordered pyrolytic graphite (HOPG) the bent-core molecules form a monolayer as they lie flat on the surface and form rows with an antiferroelectric relation between the rows.[37] On water the orientation of the molecules depends on the hydrophobicity of the tails.[30-34]

Alkene-terminated bent-core molecules[23,24] can, in principle, also be used to obtain covalently bound monolayers on silicon surfaces by a hydrosilylation reaction.[7-14] The covalent attachment of liquid crystals, and especially bent-core liquid crystals, might be applied to overcome surface alignment problems often observed for smectic liquid crystals, and could make these materials suitable for applications like switchable alignment layers.[39-42]

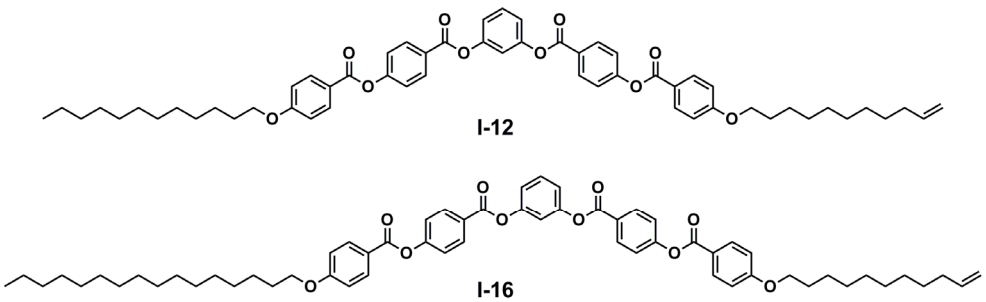

Scheme 1. Structures of the bent-core mesogens.

Here we present the first monolayers of covalently attached bent-core liquid crystals to a silicon surface. Two bent-core mesogens (Scheme 1) were attached to H-terminated Si(111) via a very mild procedure,[11-14] using visible light (447 nm) at room temperature. The presence, quality and orientation of these monolayers were investigated using a wide variety of techniques, including ellipsometry, attenuated total reflectance infrared (ATR-IR) spectroscopy, X-ray reflectivity and X-ray photoelectron spectroscopy (XPS).

9.2 Experimental

9.2.1 Materials

PE40/60, EtOH and CH_2Cl_2 were distilled prior to use. For rinsing and contact angle measurements, deionized water (18.3 MΩ cm resistivity) was used. Acetone (Sigma/Honeywell, semiconductor grade) and 40% ammonium fluoride solution (40% NH_4F) (Sigma/Honeywell, semiconductor grade) were used as received. Silicon wafers were (111)-oriented single-side and double polished, 475 - 550 μm thick, n-type, phosphorus-doped samples, with a resistivity of 1.0-5.0 Ω cm (Siltronix, France). The synthesis and characterization of bent-core-shaped compounds **I-12** and **I-16** was published elsewhere.[23,24]

9.2.2 Monolayer Preparation

Before the hydrosilylation reaction, double polished n-Si(111) wafers (phosphorus doped, 475-550 μm thick, resistivity 1-5 Ωcm; Siltronix, France) were cut into pieces of 5 x 1 cm and polished to obtain crystals with 45º bevels. After wiping the crystals with a tissue that was saturated with acetone (semiconductor grade), the samples were sonicated for at least 10 min. in acetone or rinsed excessively with acetone and dried in a stream of nitrogen. Subsequently, the crystals were placed in a plasma cleaner (Harrick PDC-32G) with an oxygen plasma for at least 3 min. Then, the samples were etched in an argon-saturated 40% aqueous NH_4F solution for 15 min, washed thoroughly with demineralized water and dried in a stream of nitrogen.

The monolayers were prepared according to the following procedure: a 0.1 M solution of the vinyl-terminated bent-core molecules in dry mesitylene was flushed with argon for at least 30 min. Then the freshly etched hydrogen-terminated Si wafers were added, and the solution was flushed with argon for another 30 min. Then the light was switched on (Jelight Co. Inc., Irvine CA: 84-247-2 (447 ± 32 nm), at a distance of 0.5 cm from the reaction vessel. After illumination for the desired time (~64 h), the wafer was removed from the solution, and the surface was rinsed with subsequently petroleum ether 40-60, ethanol, and dichloromethane, and finally dried in a stream of nitrogen.

9.2.3 Monolayer Characterization

Static water contact angles were measured with an automated Krüss DSA 100 goniometer. At least six small droplets of 2.0 µl deionized water were dispensed and the contact angles were determined using a Tangent 2 fitting model. The error in the contact angles is less than 1°.

The ellipsometric thicknesses were measured with a Sentech Instruments (Type SE-400) ellipsometer, operating at 632.8 nm (He-Ne-laser) and an angle of incidence of 70°. First the optical constants of the substrate were determined with a piece of freshly etched H-Si(111) (n = 3.822 and k = 0.055). The thicknesses of the monolayers were determined with a planar three-layer (ambient, organic monolayer, substrate) isotropic model with assumed refractive indices of 1.00 and 1.46 for ambient and the organic monolayer, respectively. The reported values are the average of at least eight measurements taken at different locations on several samples and the error is less than 1 Å.

Attenuated total reflectance infrared spectroscopy (ATR-IR) spectra were collected with a Bruker spectrometer (model Tensor 27) equipped with a Harrick ATR accessory and MCT detector. A Harrick grid polarizer was placed in front of the sample for measuring spectra with p-and s-polarized light. The homemade ATR crystals of 5 × 1 cm with 45° bevels (± 100 internal reflections) were placed in the spectrometer and the spectra were taken at a resolution of 4 cm^{-1} from 2048 scans while flushing with dry N_2, using a clean native oxide-covered ATR crystal as reference.

The surface topography was imaged using a JSPM 5400 atomic force microscope (Jeol Ltd, Tokyo) operating in AC mode with silicon cantilevers, model NSC35/AlBS (MikroMasch) with a spring constant of ~ 4.5 N/m.

X-ray photoelectron spectroscopy (XPS) analyses were performed using a JPS-9200 photoelectron spectrometer (JEOL Ltd, Japan). The high-resolution spectra were obtained under UHV conditions using monochromatic Al Kα X-ray radiation at 12 kV and 25 mA, using an analyzer pass energy of 10 eV. All high-resolution spectra were corrected with a linear background before fitting.

X-ray reflectivity measurements were performed on a Panalytical X'pert Pro diffractometer. The monolayer thickness is calculated from the interference fringes.

9.3 Results and discussion

A frequently used method for preparing covalently bound organic monolayers on silicon surfaces, i.e. refluxing an alkene solution in mesitylene in the presence of a hydrogen terminated silicon wafer, [7-10] has proven to be too harsh for these bent-core molecules, despite the relative stability of most bent-core molecules. In a control experiment it was found that after refluxing **I-12** in mesitylene for 2 h, some impurities were detected by TLC. Therefore, a recently reported, much milder attachment method,[11-14] using visible light at room temperature, was used to prepare the covalently attached monolayers. Due to the high molecular weights of the mesogens – **I-12**: M_r = 911.13; **I-16**: M_r = 967.232 – a relatively long reaction time (64 h) was employed. Shorter reaction times yielded less complete monolayers; longer reaction times did not result in better monolayers.

The presence and quality of the monolayers of the bent-core mesogens on a Si(111) surface were investigated using measurement of static water contact angles, attenuated total reflection infrared spectroscopy (ATR-IR), atomic force microscopy (AFM), X-ray reflectivity, and X-ray photoelectron spectroscopy (XPS). The static water contact angle of the modified Si surfaces was 100 ± 1° for both bent-core molecules. The observed contact angle is slightly lower than the ~110-112° normally observed for densely packed pure alkyl monolayers,[11-14] but much higher than the ~87° observed for hydrogen-terminated Si(111). Given the presence of polar ester groups in the organic monolayer,[12] this suggest monolayer formation under these mild conditions.

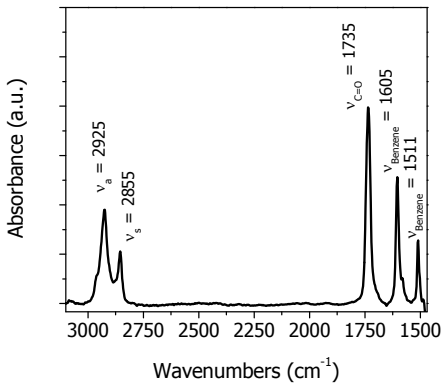

Figure 1. ATR-IR spectrum (p-polarized) of a **I-12** monolayer on Si(111).

The density and ordering of the monolayers were investigated with ATR-IR, which provided peaks for C–H and C=O stretching vibrations (see Figure 1). The antisymmetric and symmetric C–H stretching vibrations are for both monolayers found at 2924 ± 1 and 2855 ± 1 cm^{-1}, indicative of disordered organic monolayers. Such disorder is frequently observed for organic monolayers with large functional groups.[15] A C=O stretching vibration was observed at 1735 cm^{-1}, which confirms the presence of ester groups in the bent-core monolayers. Furthermore, the vibrations at 1605 and 1511 cm^{-1} are indicative for aromatic groups.

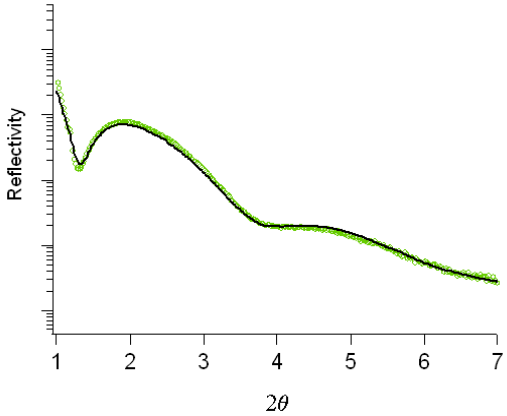

Figure 2. X-ray reflectivity curve of a **I-16** monolayer on Si (green data points) and the fit (black line).

From the differences between the p- and s-polarized ATR-IR spectra an average tilt angle of the alkyl tails with respect to the layer normal can be obtained.[7,8] These values are 50 ± 5° for **I-12** and 54 ± 5° for **I-16.** Although the spacers and tails of the mesogens probably have a different orientation in the monolayer due to the bent core, the long axes of the molecules will still correspond roughly with the average of the tilt angle direction. With molecular modeling the length of the molecules can be estimated, and combined with the tilt angle this gives a thickness of about 35 Å for the monolayers of both compounds (see Table 1). Other methods to obtain the layer thickness are ellipsometry and X-ray reflectivity. Ellipsometry yields a layer thickness of 40 ± 1° for both monolayers. However, these values are strongly dependent on the refractive indices, which are not accurately known. For the organic layer a refractive index of 1.46 was assumed. A more direct method to obtain the layer thickness is X-ray reflectivity. The X-ray reflectivity curve of **I-16** is given in Figure 2. From the fringes and the simulated fitting curve a layer thickness of 33 ±

1 Å is obtained. Within the experimental error the same thickness is obtained for the monolayer of **I-12**. Ellipsometry also suggests the same layer thickness for both monolayers. This is attributed to the difference in tilt angle that balances the difference in the length of the terminal alkyl chain by 4 carbon atoms.

Finally, the monolayer thickness can be compared with the bulk smectic layer thickness in the liquid crystalline phase. In bulk both compounds show the antiferroelectric $SmCP_A$ phase over a reasonably wide temperature range around 100 °C. At this temperature, the smectic *d*-spacings are 35.4 Å for **I-12** and 38.1 Å for **I-16**.[23,24] Although a larger smectic layer thickness is found for the longer compound **I-16,** all these values are clearly in the same range as the values obtained from X-ray reflectivity, ellipsometry and those deduced from IR. The values of the layer thickness obtained by different techniques and under different conditions are given in Table 1. The main difference between the ordering in the bulk and in the monolayer is that in the covalently attached monolayer all molecules will have a parallel orientation with the C_{11} spacer attached to the surface and the tail pointing towards the air. In the bulk liquid crystalline phase the orientation will be random, i.e. largely antiparallel. As a result, the difference between the ordering in the monolayer and in the bulk will be larger for the more asymmetric **I-16** than for the more symmetric **I-12** compound. Nevertheless, the similarity between the monolayer thickness and bulk smectic layer thickness is remarkable, and strongly suggest that the ordering in the monolayer is very similar to the ordering in the bulk $SmCP_A$ phase.

Table 1 Comparison of the layer thickness (Å) of the bent-core molecules obtained from X-ray reflectivity, ellipsometry, calculated from ATR-IR data and the estimated length of the molecules and the bulk smectic layer thickness.

Compound	X-ray reflectivity	Ellipsometry	ATR-IR	in bulk LC phase[23,24]
I-12	33 ± 1	40 ± 1	35	35.4
I-16	33 ± 1	40 ± 1	34	38.1

It also suggests that the bent-core mesogens in the monolayer are tilted. However, we cannot be sure that the direction of the tilt is cooperative and that domains with the same tilt angle direction are present. From the relatively high tilt angle it can be derived that the occupation of the silicon sites at the surface is lower than in the dense alkyl monolayers found for simple 1-alkenes. Whether the high tilt angle is caused by the preferred ordering

of the mesogens similar as in the liquid crystalline phase or by the lower occupation of attachment sites on the surface dictated by the shape and cross sectional area of the mesogens is an interesting question for future research.

The uniformity of the monolayers was evaluated using AFM. On a bare H-terminated Si surface, the domain boundaries due to the terraces on the surface are clearly visible (Figure 3). After modification the terrace structure of the underlying Si-surface is not seen anymore, while the roughness hardly increases. So the modified surface is rather smooth and uniform without the presence of clear defects, This is in line with the presence of a thick, disordered, but homogeneous monolayer on the modified surface.

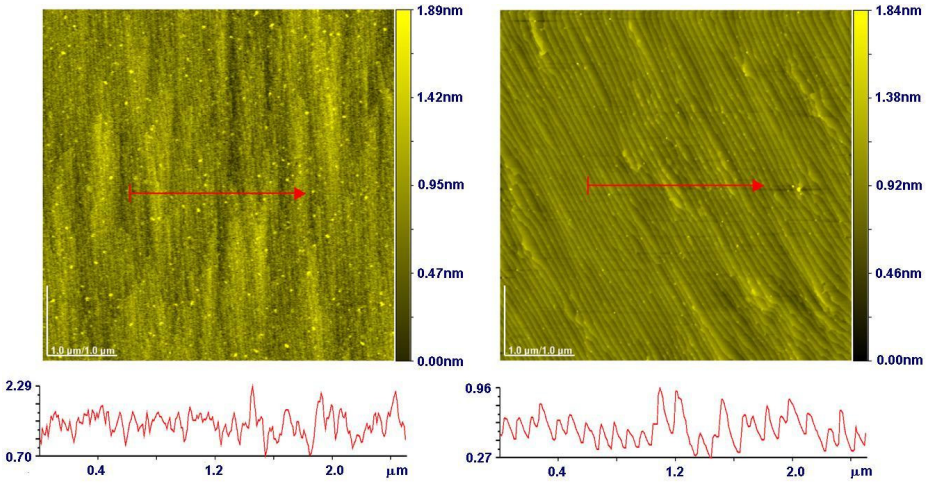

Figure 3. AC mode AFM images of a 5 x 5 µm area of a monolayer of **I-12** on Si(111) surface (left) and of a bare H-terminated Si(111) surface (right), and section analyses along a line across the surface.

X-ray photoelectron spectroscopy (XPS) of these monolayers provides quantitative information about the elemental composition of the surface.[12,17,43] The XPS spectrum of a monolayer of **I-16** clearly shows peaks due to silicon, carbon and oxygen. No fluorine peaks were detected. In Figure 4 the expanded regions of the Si_{2p}, C_{1s} and O_{1s} peaks are shown. The almost complete absence of a peak at 103.0 eV in the Si_{2p} region shows that hardly any Si-bound oxygen is present and thus confirms the high passivating properties of the monolayer. The present monolayer effectively prevents the unmodified Si-sites from reaction with water or oxygen from the air. Although no rigorous solvent and oxygen exposure experiments were done,[44] upon exposure to air for 3 months no changes were found in the contact angle and layer thickness by ellipsometry.

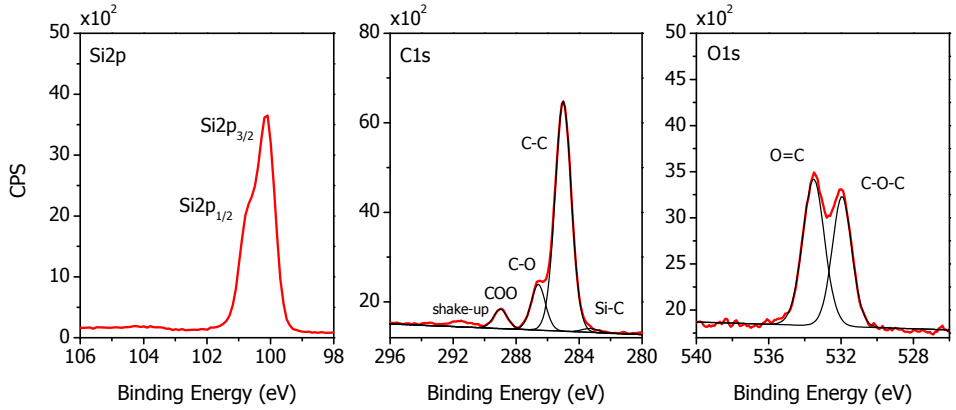

Figure 4. Expanded Si_{2p}, C_{1s} and O_{1s} regions of the XPS-spectrum of a monolayer of **I-16** on Si(111).

The expanded C_{1s}-region shows several peaks that can be attributed to C bound to two O atoms at 289.0 eV, C bound to one O atom at 286.5 eV, C bound to C at 285.0 eV and C bound to Si at 283.5 eV. Fitting and integration of these peaks leads to a composition that agrees very well with the composition calculated from the molecular structures of the molecules that are attached to the silicon surface (see Table 2). In the O_{1s}-region, two peaks can be distinguished, one from O=C and one from C–O–C groups. Integration of these peaks also leads to a composition which corresponds very well with the calculated composition. In Table 2 the data for the monolayers of both compounds **I-12** and **I-16** are given. As can be seen, the experimentally determined compositions correspond well with the calculated compositions. The derived atomic percentages were determined from the fits of the XPS data. Their accuracy depends on several factors, like peak separation and peak intensity. This implies, for example, that the accuracy of the integration for the C–C peak is most accurate. The C–Si peak integration is least accurate, due to the fact that this is the smallest peak while it also partially overlaps with the C–C peak. Nevertheless, the XPS results clearly show that the monolayers of the bent-core mesogens are attached to the surface with the expected composition.

Table 2. Ratio analysis of the peaks in the XPS spectra of monolayers of **I-16** and **I-12** in the C_{1s} region and O_{1s}-region[a]

I-16	*n*	% found	% calc.	**I-12**	*n*	% found	% calc.
C-region							
C–O	8	14.0	13.0	C–O	8	15.9	14.0
C(=O)–O	4	5.7	6.5	C(=O)–O	4	5.1	7.0
C–C	48	79.0	79.0	C–C	44	76.3	77.2
C–Si	1	1.3	1.6	C–Si	1	2.6	1.7
O-region							
O=C	4	42	40	O=C	4	39	40
C–O–C	6	58	60	C–O–C	6	61	60

[a]: *n* = number of specific atoms in the attached molecules

9.4 Conclusions

We have demonstrated for the first time that it is possible to make well-ordered and good quality organic monolayers of long and semi-rigid molecules, like bent-core mesogens, on hydrogen-terminated Si. The layer thickness, determined from XRD and ellipsometry, and the tilt angle, calculated from the layer thickness and from ATR-IR data of the monolayers of the attached mesogens correspond very well with the layer thickness and tilt angle of these mesogenic compounds in the liquid crystalline bulk phase. This suggests that the tilt angle is not solely determined by the density of the surface attachment sites, but also by the self-organization of the attached mesogens, i.e. via the "normal" smectic ordering properties of these liquid crystals. This liquid crystal-like organization could make these monolayers good and thin alignment layers for smectic (inluding bent-core) liquid crystalline materials. Furthermore, the obtained monolayers could contain domains with lateral polarity like the SmCP layers in bulk, and could therefore be useful for certain LC applications. Due to the similarity of the ordering in the monolayer and the ordering in bulk, these monolayers could, theoretically, show switching behavior in the presence of electrical fields. This would require a rotation of the molecules around a tilt cone, or around the long molecular axis, reversing the polar direction parallel to the surface.[45]

References

(1) Sieval, A. B.; Linke, R.; Zuilhof, H.; Sudhölter, E. J. R. *Adv. Mater.* **2000**, *12*, 1457-1460.

(2) Wayner, D. D. M.; Wolkow, R. A. *J. Chem. Soc., Perkin Trans. 2* **2002**, 23-34.

(3) Buriak, J. M. *Chem. Rev.* **2002**, *102*, 1271-1308.

(4) Boukherroub, R. *Curr. Opin. Solid State Mater. Sci.* **2005**, *9*, 66-72.

(5) Shirahata, N.; Hozumi, A.; Yonezawa, T. *Chem. Rec.* **2005**, *5*, 145-159.

(6) Bent, S. F. In *Chemical Bonding at Surfaces and Interfaces*; Nilsson, A., Petterson, L. G. M., Norskov, J. K., Eds.; Elsevier: Amsterdam, 2008, p 323-396.

(7) Linford, M. R.; Fenter, P.; Eisenberger, P. M.; Chidsey, C. E. D. *J. Am. Chem. Soc.* **1995**, *117*, 3145-3155.

(8) Sieval, A. B.; Demirel, A. L.; Nissink, J. W. M.; Linford, M. R.; van der Maas, J. H.; de Jeu, W. H.; Zuilhof, H.; Sudhölter, E. J. R. *Langmuir* **1998**, *14*, 1759-1768.

(9) de Smet, L. C. P. M.; Zuilhof, H.; Sudhölter, E. J. R.; Wittstock, G.; Duerdin, M. S.; Lie, L. H.; Houlton, A.; Horrocks, B. R. *Electrochim. Acta* **2002**, *47*, 2653-2663.

(10) Sieval, A. B.; Huisman, C. L.; Schonecker, A.; Schuurmans, F. M.; van der Heide, A. S. H.; Goossens, A.; Sinke, W. C.; Zuilhof, H.; Sudhölter, E. J. R. *J. Phys. Chem. B* **2003**, *107*, 6846-6852.

(11) Sun, Q. Y.; de Smet, L. C. P. M.; van Lagen, B.; Giesbers, M.; Thune, P. C.; van Engelenburg, J.; de Wolf, F. A.; Zuilhof, H.; Sudhölter, E. J. R. *J. Am. Chem. Soc.* **2005**, *127*, 2514-2523.

(12) Sun, Q. Y.; de Smet, L. C. P. M.; van Lagen, B.; Wright, A.; Zuilhof, H.; Sudhölter, E. J. R. *Angew. Chem., Int. Ed.* **2004**, *43*, 1352-1355.

(13) de Smet, L. C. P. M.; Pukin, A. V.; Sun, Q. Y.; Eves, B. J.; Lopinski, G. P.; Visser, G. M.; Zuilhof, H.; Sudhölter, E. J. R. *Appl. Surf. Sci.* **2005**, *252*, 24-30.

(14) Scheres, L.; Arafat, A.; Zuilhof, H. *Langmuir* **2007**, *23*, 8343-8346.

(15) de Smet, L. C. P. M.; Stork, G. A.; Hurenkamp, G. H. F.; Sun, Q. Y.; Topal, H.; Vronen, P. J. E.; Sieval, A. B.; Wright, A.; Visser, G. M.; Zuilhof, H.; Sudhölter, E. J. R. *J. Am. Chem. Soc.* **2003**, *125*, 13916-13917.

(16) Dancil, K. P. S.; Greiner, D. P.; Sailor, M. J. *J. Am. Chem. Soc.* **1999**, *121*, 7925-7930.

(17) Lin, Z.; Strother, T.; Cai, W.; Cao, X. P.; Smith, L. M.; Hamers, R. J. *Langmuir* **2002**, *18*, 788-796.

(18) Feng, W. J.; Miller, B. *Langmuir* **1999**, *15*, 3152-3156.

(19) Pei, Y.; Ma, J. *J. Am. Chem. Soc.* **2005**, *127*, 6802-6813.

(20) Okano, T.; Inari, H.; Ishizaki, T.; Saito, N.; Sakamoto, W.; Takai, O. *Chem. Lett.* **2005**, *34*, 600-601.

(21) Gulino, A.; Lupo, F.; Condorelli, G. G.; Fragala, M. E.; Amato, M. E.; Scarlata, G. *J. Mater. Chem.* **2008**, *18*, 5011-5018.

(22) Maas, J. H.; Stuart, M. A. C.; Sieval, A. B.; Zuilhof, H.; Sudhölter, E. J. R. *Thin Solid Films* **2003**, *426*, 135-139.
(23) Achten, R.; Koudijs, A.; Giesbers, M.; Marcelis, A. T. M.; Sudhölter, E. J. R. *Liquid Cryst.* **2005**, *32*, 277-285.
(24) Achten, R.; Smits, E. A. W.; Reddy, R. A.; Giesbers, M.; Marcelis, A. T. M.; Sudhölter, E. J. R. *Liquid Cryst.* **2006**, *33*, 57-65.
(25) Tschierske, C.; Dantlgraber, G. *Pramana* **2003**, *61*, 455-481.
(26) Pelzl, G.; Diele, S.; Weissflog, W. *Adv. Mater.* **1999**, *11*, 707-724.
(27) Shen, D.; Pegenau, A.; Diele, S.; Wirth, I.; Tschierske, C. *J. Am. Chem. Soc.* **2000**, *122*, 1593-1601.
(28) Weissflog, W.; Nadasi, H.; Dunemann, U.; Pelzl, G.; Diele, S.; Eremin, A.; Kresse, H. *J. Mater. Chem.* **2001**, *11*, 2748-2758.
(29) Weissflog, W.; Murthy, H. N. S.; Diele, S.; Pelzl, G. *Phil. Trans. R. Soc. A* **2006**, *364*, 2657-2679.
(30) Zou, L.; Wang, J.; Beleva, V. J.; Kooijman, E. E.; Primak, S. V.; Risse, J.; Weissflog, W.; Jakli, A.; Mann, E. K. *Langmuir* **2004**, *20*, 2772-2780.
(31) Wang, J.; Zou, L.; Jakli, A.; Weissflog, W.; Mann, E. K. *Langmuir* **2006**, *22*, 3198-3206.
(32) Kinoshita, Y.; Park, B.; Takezoe, H.; Niori, T.; Watanabe, J. *Langmuir* **1998**, *14*, 6256-6260.
(33) Ashwell, G. J.; Amiri, M. A. *J. Mater. Chem.* **2002**, *12*, 2181-2183.
(34) Baldwin, J. W.; Amaresh, R. R.; Peterson, I. R.; Shumate, W. J.; Cava, M. P.; Amiri, M. A.; Hamilton, R.; Ashwell, G. J.; Metzger, R. M. *J. Phys. Chem. B* **2002**, *106*, 12158-12164.
(35) Tang, Y. H.; Wang, Y.; Wang, X. D.; Xun, S. D.; Mei, C. Y.; Wang, L. X.; Yan, D. H. *J. Phys. Chem. B* **2005**, *109*, 8813-8819.
(36) Tang, Y. H.; Wang, Y.; Wang, G.; Wang, H. B.; Wang, L. X.; Yan, D. H. *J. Phys. Chem. B* **2004**, *108*, 12921-12926.
(37) Gong, J. R.; Wan, L. J. *J. Phys. Chem. B* **2005**, *109*, 18733-18740.
(38) Olson, D. A.; Cady, A.; Weissflog, W.; Nguyen, H. T.; Huang, C. C. *Phys. Rev. E* **2001**, *64*, 6.
(39) Jakli, A.; Chien, L. C.; Kruerke, D.; Sawade, H.; Heppke, G. *Liquid Cryst.* **2002**, *29*, 377-381.
(40) Jakli, A.; Kruerke, D.; Nair, G. G. *Phys. Rev. E* **2003**, *67*, 6.
(41) Park, C. S.; Furtak, T. E.; Clark, N. A.; Liberko, C. A.; Walba, D. M. *Phys. Rev. E* **2003**, *67*, 5.
(42) Komitov, L.; Helgee, B.; Felix, J.; Matharu, A. *Appl. Phys. Lett.* **2005**, *86*, 3.
(43) Linford, M. R.; Chidsey, C. E. D. *Langmuir* **2002**, *18*, 6217-6221.
(44) Puniredd, S. R.; Assad, O.; Haick, H. *J. Am. Chem. Soc.* **2008**, *130*, 13727-13734.
(45) Reddy, R. A.; Schröder, M. W.; Bodyagin, M.; Kresse, H.; Diele, S.; Pelzl, G.; Weissflog, W. *Angew. Chem. Int. Ed.* **2005**, *44*, 774-778.

Chapter 10

General Discussion

Abstract. This chapter gives a brief overview of the most striking achievements presented in this thesis, and several of the remaining questions, additional ideas, and recommendations for further research.

In the previous chapters all results, new insights and newly developed methods that have been obtained in this project were described in detail. The wealth of new results has, as always hoped for, also generated new, as yet unanswered questions and novel ideas. In this chapter some remaining questions, additional ideas and recommendations for further research are discussed that place this work into context.

In Chapter 2 the self-assembly of 1-alkynes on H-Si(111) at room temperature was reported, and in Chapter 3 this process was ascribed to the enhanced reactivity of 1-alkynes. In practice the high reactivity of 1-alkynes will speed up the monolayer formation process that is relatively slow with 1-alkenes. Since during the reaction there is always a competition between monolayer formation and oxide formation, the higher reactivity of 1-alkynes will lead to easier and more reproducible preparation of oxide-free monolayers on silicon. In addition, it will extend the range of functional groups that can be attached directly onto Si, as side reactions and upside-down attachment will be suppressed under the mild reaction conditions that now can be used.

After comparing the reactivity of 1-alkenes and 1-alkynes, the higher reactivity of 1-alkynes was attributed to a higher nucleophilicity, a better stabilization of the β-radical, and a lower energy barrier for H-abstraction. However, it is still unknown to what extent each of these steps is contributing to the self-assembly of 1-alkynes. To answer this question, additional scanning tunneling microscopy (STM) experiments could offer an outcome.[1] By carefully analyzing the early stages of monolayer formation, the radical chains in the reaction of 1-alkenes and 1-alkynes can be compared directly at the molecular level. Since easier initiation will lead to a larger number of islands, while easier propagation will result in bigger islands, the relative efficiency of these steps in the chain reaction can be visualized. Moreover, considering the role of nucleophilicity and stabilization of the β-radical on the efficiency of monolayer formation, it might be worthwhile to investigate monolayer formation with, for instance, long 3-en-1-ynes (Figure 1). Due to the conjugated terminus it is expected that 3-en-1-ynes are even more reactive than 1-alkynes.[2] With the reactivity also the rate of monolayer assembly will increase, perhaps making direct microcontact printing on H-Si surfaces feasible.

Besides the type of molecule used, also the doping type and doping level of the Si substrate will affect the progress of the radical chain reaction.[3-5] In this respect, the reactivity difference of 1-alkenes and 1-alkynes could be used as a tool to investigate the role of the Si substrate on the monolayer formation process. Because a Si dangling bond is an amphoteric defect, it is neutral on moderately doped Si, anionic on high-doped n-Si, and cationic on high-doped p-Si.[4,6] As a result, it is expected that on highly doped n-Si the

propagation is more facile for 1-alkenes than for 1-alkynes, while on highly doped p-Si the propagation might be easier for 1-alkynes than for 1-alkenes.[7] In addition, we note that Takeuchi et al.[2] by means of density functional theory (DFT) calculations – like for 1-alkenes and 1-alkynes – also predicted a reactivity difference for styrene and phenylacetylene, with phenylacetylene being more reactive than styrene. And, very recently Walsh et al.,[8] who studied the one-dimensional line growth of both compounds on highly doped n-Si(100) by STM, observed considerably longer lines for styrene as for phenylacetylene, which is fully in line with our expectations for 1-alkenes and 1-alkynes on highly doped n-Si substrates.

In Chapter 4 and 5 it was demonstrated that only a minor structural difference in the linkage to the silicon surface (Si–C–C versus Si–C=C) can have a substantial effect on the final monolayer structure. The smaller Van der Waals radius of the Si–C=C linkage and the larger exothermicity of 1-alkyne attachment to the H-Si surface, make surface coverages above 50% sterically and thermodynamically feasible for long alkenyl monolayers (from 55% for C_{12} to 65% for C_{18}). In view of the future applications, a long-term stability of the oxide-free monolayer-silicon interface is essential, however, due to the strong covalent Si–C bond diffusion of the absorbed chains to improve the ordering, as observed for alkylthiol monolayers on gold, cannot occur. As a result organic monolayers on oxide-free silicon are in general less ordered and almost never completely defect free. In this respect, the enhanced monolayer quality and increased surface coverage of the alkenyl monolayers, in combination with the oxidation-inhibiting nature of the Si–C=C linkage, is definitely an important improvement. The excellent stability of the functional monolayers described in Chapter 6 and 7 is an nice example thereof.

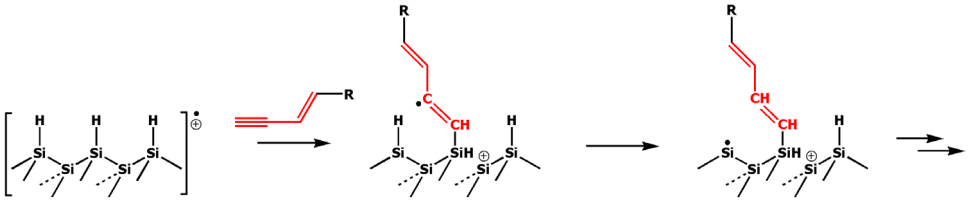

Figure 1. Representation of the proposed radical chain mechanism of 3-en-1-ynes on H-Si(111).

Nevertheless, the exact cause of the chain length dependence for the alkenyl monolayers is still unclear and requires further research. Additional molecular modeling experiments and DFT calculations could be useful to unravel the origin of this remarkable phenomenon. Obviously, it would also be interesting to prepare monolayers from 1-icosyne (C_{20}) and 1-

docosyne (C_{22}), to see whether with these longer molecules, or analogs based on e.g. 3-en-1-ynes, even higher surfaces coverages can be obtained and perhaps even the theoretical maximum coverage of 69% that is governed by the Van der Waals radius of an alkyl chain can be exceeded. It is in this context crucial to realize that it is not the remaining fraction of H-Si sites that is important, but the number of remaining monolayer defects and the ease by which it can be penetrated by other chemical agents. Steric interactions grow rather steeply with an increase beyond "optimal packing", yet it remains to be seen whether 70+ percentages can be obtained by longer chains combined with stronger linkages. While the state of theory is in fact pretty high, they should be put to the best possible tests by challenging experiments, and here is in my opinion a nice point in case.

In Chapter 6 the advantages of 1-alkynes were put into practice and well-defined acid fluoride-terminated monolayers, without any sign of upside-down attachment, were prepared on oxide-free Si. The high and selective reactivity of the acid fluoride functionality towards primary amines allowed us to use these monolayers as a platform for reactive μCP. In contrast to the direct μCP procedures on oxide-free silicon reported in literature, which are relative slow (contact time > 30 min), our μCP method is efficient and fast (contact time 20 sec), and because it is an indirect μCP approach, easily preserves the oxide-free monolayer-silicon interface. However, in view of the potential of this indirect printing approach, a milder synthesis route for 10-undecynoyl fluoride is desirable. Furthermore, so far only stamps with pillar-like features with a diameter of 5 and 10 μm were used, while for such efficient printing process it is expected that features with dimensions below 100 nm can be obtained.[9] In this respect, exploring the maximum achievable resolution is recommended. Besides for biofunctionalization, this technique can also be used to fabricate new hybrid molecular electronic devices on oxide-free silicon. For instance, by nanotransfer printing (nTP)[10] or flip-chip lamination[11] metal electrodes could be printed on top of the organic monolayer and by printing of polymerizable diacetylenes or oligo-thiophenes SAMFETs might be prepared on oxide-free silicon.[12]

In Chapter 7 a new and alternative patterning technique, namely photothermal laser patterning, is presented. By backfilling the laser-written lines with a second organic monolayer that differs in its terminal functionality, chemically patterned monolayers on oxide-free silicon were obtained. Due to the sub-wavelength resolution that can be achieved in this manner, the flexibility in pattern design, the high writing speeds, and the feasibility for patterning inside complex device geometries – like in microfluidic channels and microstructured devices – photothermal laser patterning is a promising technique for the fabrication of new small-scale biosensor and molecular electronic devices. Yet there is

some room for improvements. For instance, a functional group that is stable during the etching step but stays reactive for direct functionalization, would be a major advantage, because then the extra deprotection and subsequent activation steps, as required for the trifluoroethyl ester (TFE) functionality, are no longer needed. In addition, instead of decomposing the monolayer, it would be interesting to use the laser-induced photothermal process to locally initiate monolayer formation on H-Si. Of course, the freshly etched Si substrate needs to be covered with or immersed in a liquid cell with 1-alkene or 1-alkyne, and the laser power has to be adjusted to prevent decomposition of the molecules.[13] But, if carried out with due efforts, the use of a flow of 1-alkenes or 1-alkynes bearing different functional groups over the silicon surface, should allow laser-written multifunctional patterns on oxide-free silicon surfaces to be obtained relatively easy (Figure 2).

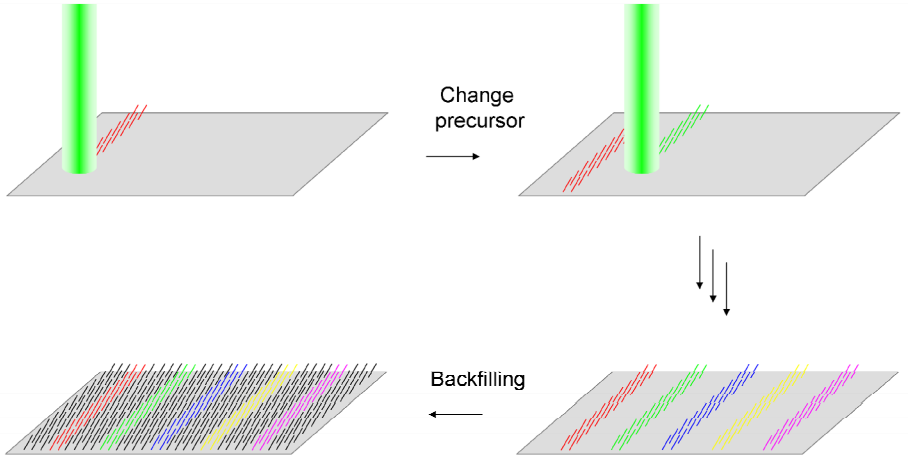

Figure 2. Laser-initiated monolayer formation for multifunctional pattern construction.

In Chapter 8 the electronic transport properties of alkyl and alkenyl monolayer on moderately doped and highly doped n-Si were studied in detailed by means of Hg/organic monolayer/Si junctions. It was shown that on moderately doped n-Si the charge transport is minority-carrier controlled and the type of monolayer hardly affects the electronic characteristics of the junctions, whereas on highly doped n-Si, due to the smaller barrier in the Si, charge transport is majority-carrier controlled and thus sensitive to type of monolayer. This work is, of course, essential for a better fundamental understanding of the charge transport mechanisms through these junctions, which in turn is critical for the design and development of biosensors and molecular electronic devices from these hybrid

structures. So far only n-type Si substrates were studied, but we note that the electronic characterization of alkyl and alkenyl monolayers on moderately and highly doped p-type Si is currently ongoing,[5] just like the experiments to clarify the remarkable metal-like temperature behavior observed for these molecular junctions, i.e. increasing conductivity with decreasing temperature.[6,14,15] Furthermore, considering the possibility to tune the electronic properties of these junctions by molecular dipoles, a logical next step would be the electronic characterization of junctions with functionalized monolayers.

In Chapter 9 the preparation and subsequent characterization of two bent-core liquid crystalline monolayers on H-Si is described. As it seems that the covalently bound mesogens retain their smectic liquid crystalline properties, these monolayers could be used as thin alignment layers for smectic liquid crystalline materials and, in theory, should be switchable under influence of an electrical field. Both properties would be interesting for further exploration. However, instead of an alkene, it is, of course, recommended to use an terminal alkyne for coupling with the H-Si surface, as this will enhance the quality of the liquid crystalline monolayer, and the stability of the oxide-free monolayer-silicon interface.

To summarize, many steps forward have been made within the research project described in this thesis, and fortunately these have generated not just answers but also opened up venues that allow the phrasing of new questions. These together may provide an even firmer basis for a promising future for organic monolayers on oxide-free silicon in the fields of biosensing, molecular electronics and photovoltaics. Such a future is needed to obtain a more sustainable balance between the increasing demand for functionality in and energy by silicon-based devices, and the possibilities to obtain that energy. This is by no means a trivial task, but by all means a very worthwhile one!

References

(1) Eves, B. J.; Sun, Q. Y.; Lopinski, G. P.; Zuilhof, H. *J. Am. Chem. Soc.* **2004**, *126*, 14318-14319.

(2) Takeuchi, N.; Kanai, Y.; Selloni, A. *J. Am. Chem. Soc.* **2004**, *126*, 15890-15896.

(3) Yaffe, O.; Scheres, L.; Segev, L.; Biller, A.; Ron, I.; Salomon, E.; Giesbers, M.; Kahn, A.; Kronik, L.; Zuilhof, H.; Vilan, A.; Cahen, D. *J. Phys. Chem. C* **2010**, ASAP, doi: jp101656t.

(4) Miramond, C.; Vuillaume, D. *J. Appl. Phys.* **2004**, *96*, 1529-1536.

(5) Yaffe, O.; Scheres, L.; Vilan, A.; Zuilhof, H.; Cahen, D. *manuscript in preparation*.

(6) Vilan, A.; Yaffe, O.; Biller, A.; Salomon, A.; Kahn, A.; Cahen, D. *Adv. Mater.* **2009**, *22*, 140-159.

(7) With the assumption that a better nucleophile is a worse electrophile.

(8) Walsh, M. A.; Walter, S. R.; Bevan, K. H.; Geiger, F. M.; Hersam, M. C. *J. Am. Chem. Soc.* **2010**, *132*, 3013-3019.

(9) Perl, A.; Reinhoudt, D. N.; Huskens, J. *Adv. Mater.* **2009**, *21*, 2257-2268.

(10) Loo, Y. L.; Willett, R. L.; Baldwin, K. W.; Rogers, J. A. *J. Am. Chem. Soc.* **2002**, *124*, 7654-7655.

(11) Coll, M.; Miller, L. H.; Richter, L. J.; Hines, D. R.; Jurchescu, O. D.; Gergel-Hackett, N.; Richter, C. A.; Hacker, C. A. *J. Am. Chem. Soc.* **2009**, *131*, 12451-12457.

(12) Smits, E. C. P.; Mathijssen, S. G. J.; van Hal, P. A.; Setayesh, S.; Geuns, T. C. T.; Mutsaers, K.; Cantatore, E.; Wondergem, H. J.; Werzer, O.; Resel, R.; Kemerink, M.; Kirchmeyer, S.; Muzafarov, A. M.; Ponomarenko, S. A.; de Boer, B.; Blom, P. W. M.; de Leeuw, D. M. *Nature* **2008**, *455*, 956-959.

(13) Zhang, F.; Pei, L.; Bennion, E.; Jiang, G. L.; Connley, D.; Yang, L.; Lee, M. V.; Davis, R. C.; Smentkowski, V. S.; Strossman, G.; Linford, M. R.; Asplund, M. C. *Langmuir* **2006**, *22*, 10859-10863.

(14) Shpaisman, H.; Seitz, O.; Scheres, L.; Yaffe, O.; Vilan, A.; Zuilhof, H.; Chabal, Y.; Cahen, D. *manuscript in preparation*.

(15) Salomon, A.; Shpaisman, H.; Seitz, O.; Böcking, T.; Cahen, D. *J. Phys. Chem. C* **2008**, *112*, 3969-3974.

Appendix 1

Calculation of Theoretical Monolayer Thickness.

As shown in the Figure A1:

- two CH_2 groups contribute 2.54 Å to the total length of the chain, whereas the CH=CH-CH_2 group of the alkenyl chain contributes 2.50 Å to the total length;
- as determined by DFT calculations, the Si-C bond length is 1.90 Å for the alkyl chains and 1.88 Å for the alkenyl chains.

Both differences are rather small and their contribution to the final monolayer thickness falls easily within the experimental error. Therefore we decided to use the same equation for alkyl and alkenyl monolayers:

$$d_{TH}(\text{Å}) = 1.89 + \left(\frac{n}{2} - 1\right) \times 2.54 \times \cos(\theta) + 1.56 \times \sin(35.5° + \theta)$$

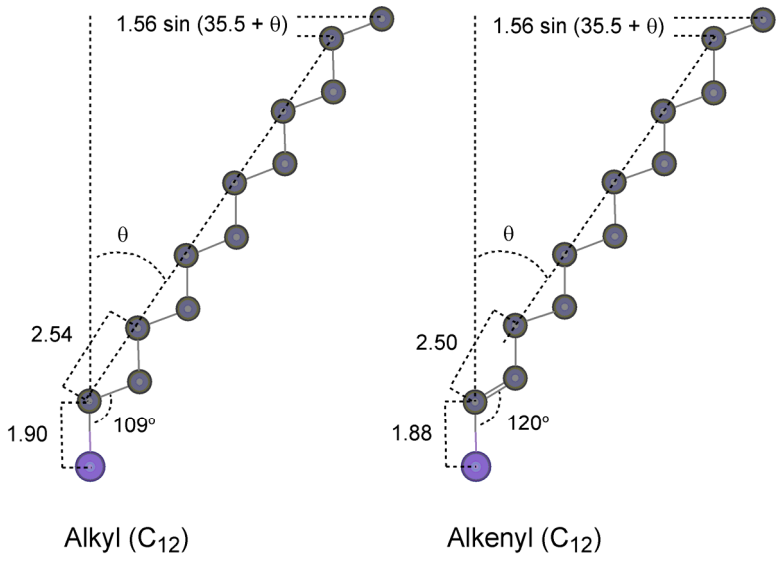

Figure A1: Schematic representations of an alkyl and alkenyl chain attached to a Si atom. The model was used to formulate equation 4 (see Chapter 4).

DFT Calculations of the Chemical Shifts of the Carbon Atoms.

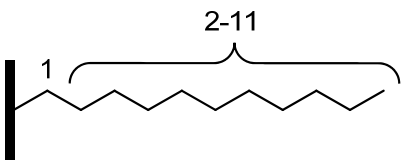

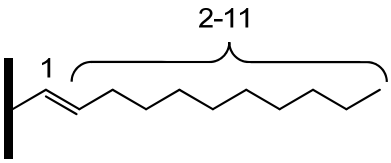

Table A1. Calculated chemical shifts of the carbon atoms.

Alkene		
Carbon	eV	Carbon type
1	284.9	Si-C
2-11	285.0	C-C

Alkyne		
Carbon	eV	Carbon type
1	284.2	Si-C
2-11	285.0	C-C

The assignment of the C_{1s} XPS spectra is supported by density functional theory B3LYP/6-311G(d,p) calculations of the core orbital energy levels by "initial state approximation". The absolute values of calculated binding energies cannot be compared directly with the experimental data because of the difference in reference energies in theory and experiment. As a point of reference the CH_2 moiety in the center of the aliphatic hydrocarbon chain was positioned at a binding energy of 285.0 eV. Electronic Core Level Calculations: all calculations were done using the GAUSSIAN03 program. The geometries of the different systems were optimized at the B3LYP/6-311G(d,p) level of theory. Natural bond orbital (NBO) analysis was employed to obtain the core orbital energies.

Full Reference for Gaussian 03.

Frisch, M. J.; Trucks, G. W.; Schlegel, H. B.; Scuseria, G. E.; Robb, M. A.; Cheeseman, J. R.; Montgomery, J. A.; Vreven, T.; Kudin, K. N.; Burant, J. C.; Millam, J. M.; Iyengar, S. S.; Tomasi, J.; Barone, V.; Mennucci, B.; Cossi, M.; Scalmani, G.; Rega, N.; Petersson, G. A.; Nakatsuji, H.; Hada, M.; Ehara, M.; Toyota, K.; Fukuda, R.; Hasegawa, J.; Ishida, M.; Nakajima, T.; Honda, Y.; Kitao, O.; Nakai, H.; Klene, M.; Li, X.; Knox, J. E.; Hratchian, H. P.; Cross, J. B.; Bakken, V.; Adamo, C.; Jaramillo, J.; Gomperts, R.; Stratmann, R. E.; Yazyev, O.; Austin, A. J.; Cammi, R.; Pomelli, C.; Ochterski, J. W.; Ayala, P. Y.; Morokuma, K.; Voth, G. A.; Salvador, P.; Dannenberg, J. J.; Zakrzewski, V.

G.; Dapprich, S.; Daniels, A. D.; Strain, M. C.; Farkas, O.; Malick, D. K.; Rabuck, A. D.; Raghavachari, K.; Foresman, J. B.; Ortiz, J. V.; Cui, Q.; Baboul, A. G.; Clifford, S.; Cioslowski, J.; Stefanov, B. B.; Liu, G.; Liashenko, A.; Piskorz, P.; Komaromi, I.; Martin, R. L.; Fox, D. J.; Keith, T.; Al-Laham, M. A.; Peng, C. Y.; Nanayakkara, A.; Challacombe, M.; Gill, P. M. W.; Johnson, B.; Chen, W.; Wong, M. W.; Gonzalez, C.; Pople, J. A. *Gaussian03*, revision D.01; Gaussian, Inc.: Wallingford, CT, 2004.

Appendix 2

Enlarged Close Contact Images of Simulation Cell 67C

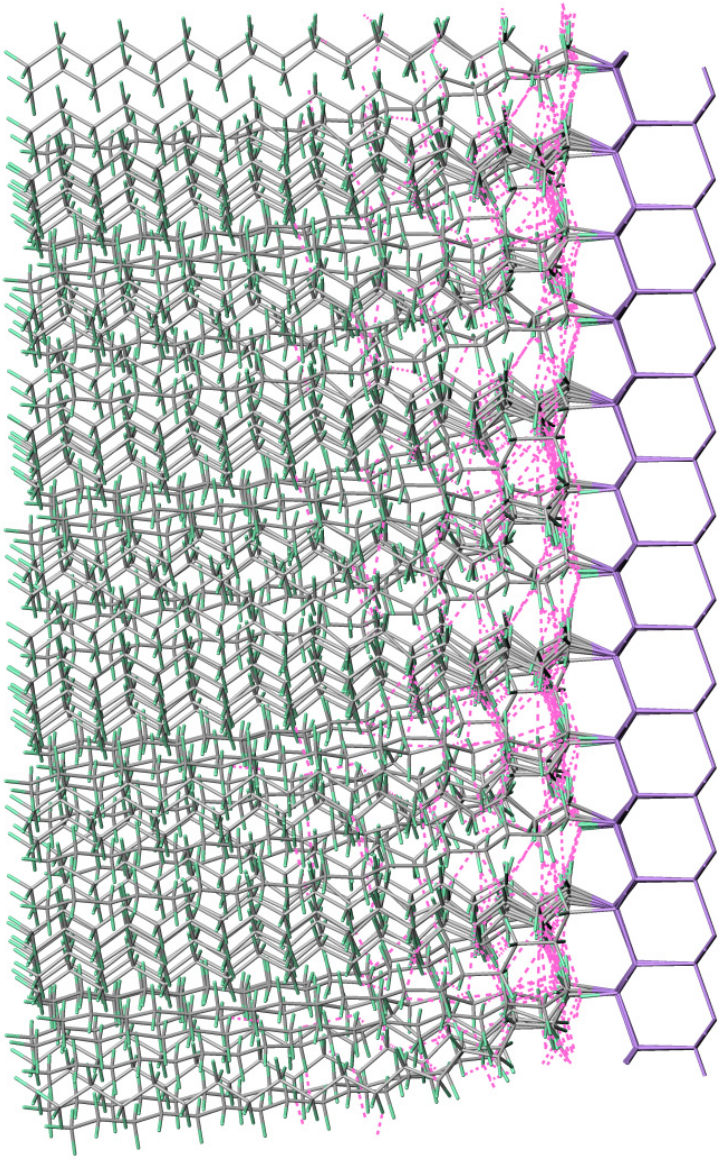

Figure A1. Large image of the side view of simulation cell 67C with octadecyl chains after optimization. The pink dashed lines represent the close contacts.

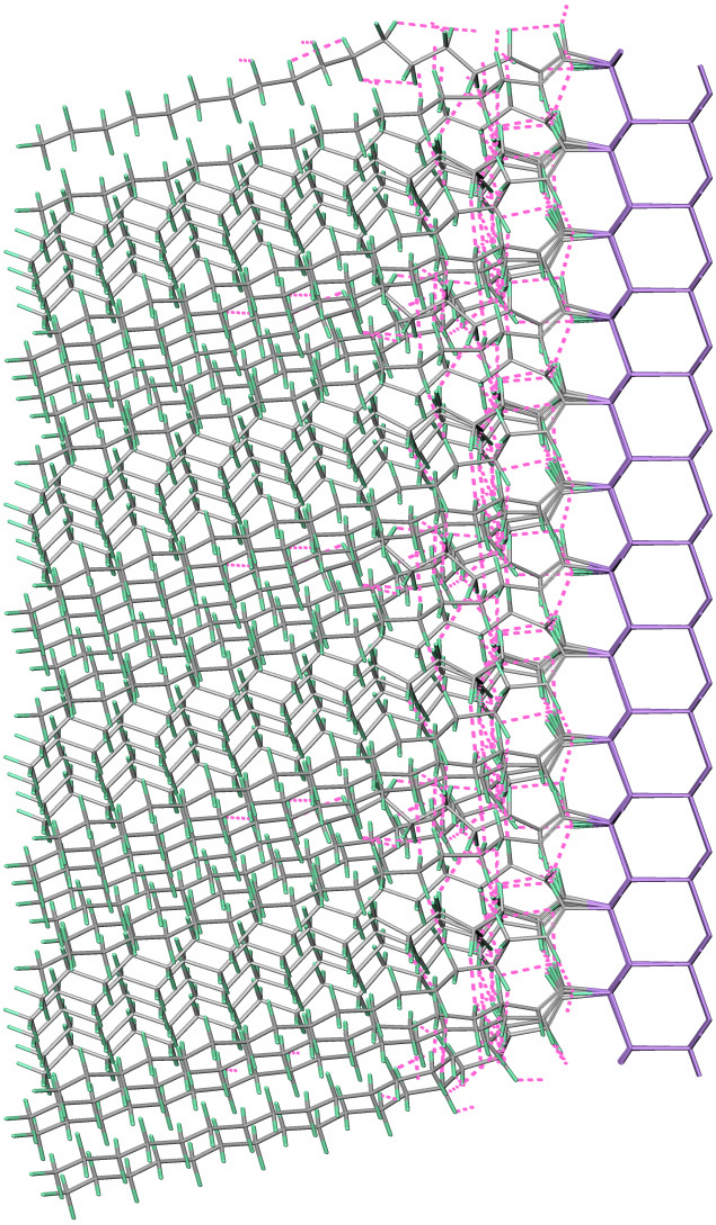

Figure A2. Large image of the side view of simulation cell 67C with octadecenyl chains after optimization. The pink dashed lines represent the close contacts.

Appendix 3

XPS Narrow Scans.

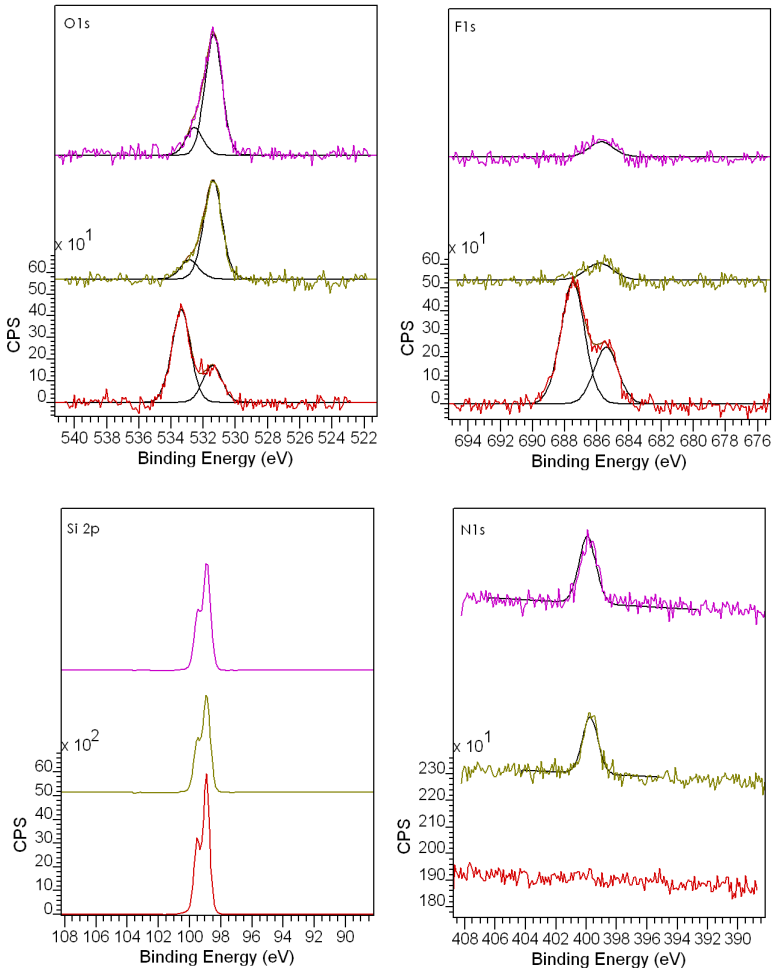

Figure A1. O_{1s}, F_{1s}, Si_{2p} and N_{1s} narrow scans of an acid fluoride monolayer on H-Si(111) (lower curves in red) and after coupling with *n*-hexadecylamine by μCP (middle curves in green) and by immersion in solution (upper curves in purple).

Simulated XPS C_{1s} Narrow Scans

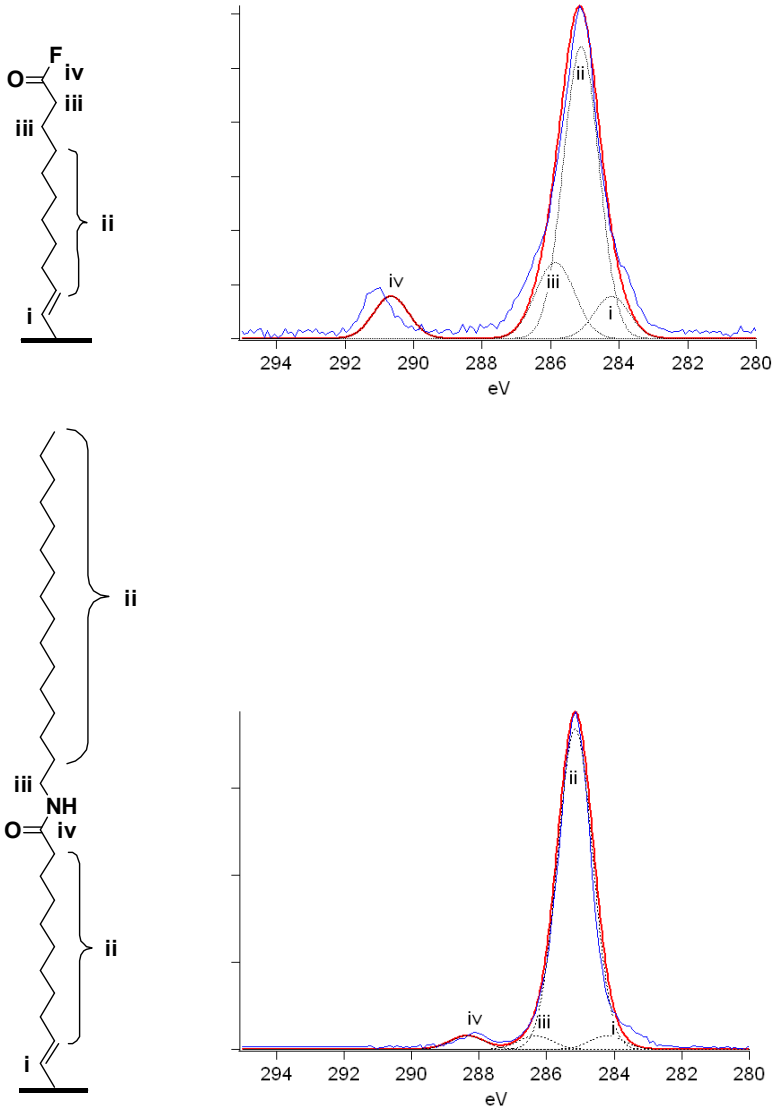

Figure A2. Experimental (blue line) and calculated (red line) core level C_{1s} XPS spectra of acid fluoride monolayer on H-Si(111) before (top) and after coupling with *n*-hexadecylamine. The dotted black lines are the calculated envelopes of the carbons used in fitting the data.

The assignment of the C_{1s} XPS spectra is supported by density functional theory B3LYP/6-311G(d,p) calculations of the core orbital energy levels by "initial state approximation". The absolute values of calculated binding energies cannot be compared directly with the experimental data because of the difference in reference energies in theory and experiment. As a point of reference the CH_2 moiety in the center of the aliphatic hydrocarbon chain was positioned at a binding energy of 285 eV. For every carbon atom, a gaussian centered at the corresponding binding energy was used with a fwhm of 1.2 eV. The sum of all Gaussians gave the simulated XPS spectra.

Electronic Core Level Calculations: All calculations were done using the GAUSSIAN03 program. The geometries of the different systems were optimized at the B3LYP/6-311G(d,p) level of theory. Natural bond orbital (NBO) analysis was employed to obtain the core orbital energies.

Full Reference for Gaussian 03.

Frisch, M. J.; Trucks, G. W.; Schlegel, H. B.; Scuseria, G. E.; Robb, M. A.; Cheeseman, J. R.; Montgomery, J. A.; Vreven, T.; Kudin, K. N.; Burant, J. C.; Millam, J. M.; Iyengar, S. S.; Tomasi, J.; Barone, V.; Mennucci, B.; Cossi, M.; Scalmani, G.; Rega, N.; Petersson, G. A.; Nakatsuji, H.; Hada, M.; Ehara, M.; Toyota, K.; Fukuda, R.; Hasegawa, J.; Ishida, M.; Nakajima, T.; Honda, Y.; Kitao, O.; Nakai, H.; Klene, M.; Li, X.; Knox, J. E.; Hratchian, H. P.; Cross, J. B.; Bakken, V.; Adamo, C.; Jaramillo, J.; Gomperts, R.; Stratmann, R. E.; Yazyev, O.; Austin, A. J.; Cammi, R.; Pomelli, C.; Ochterski, J. W.; Ayala, P. Y.; Morokuma, K.; Voth, G. A.; Salvador, P.; Dannenberg, J. J.; Zakrzewski, V. G.; Dapprich, S.; Daniels, A. D.; Strain, M. C.; Farkas, O.; Malick, D. K.; Rabuck, A. D.; Raghavachari, K.; Foresman, J. B.; Ortiz, J. V.; Cui, Q.; Baboul, A. G.; Clifford, S.; Cioslowski, J.; Stefanov, B. B.; Liu, G.; Liashenko, A.; Piskorz, P.; Komaromi, I.; Martin, R. L.; Fox, D. J.; Keith, T.; Al-Laham, M. A.; Peng, C. Y.; Nanayakkara, A.; Challacombe, M.; Gill, P. M. W.; Johnson, B.; Chen, W.; Wong, M. W.; Gonzalez, C.; Pople, J. A. *Gaussian03*, revision D.01; Gaussian, Inc.: Wallingford, CT, 2004.

Appendix 4

XPS Atomic Ratios of TFE Monolayer, Acid Monolayer and Thiol Monolayer.

Table A1. XPS atomic ratios of TFE monolayer, acid monolayer and thiol monolayer

	C_i / C_{ii} / C_{iii} / C_{iv} / C_v /C_{vi}	
	Theory	Experimental
-COO-CH_2-CF_3	1 / 8 / 1 / 1 / 1 / 1	1.0 / 7.1 / 1.0 / 1.1 / 1.0 / 1.1
-COOH	1 / 8 / 1 / 1	1.0 / 8.7 / 1.0 / 0.9
-CONH-$(CH_2)_2$-SH	1 / 9 / 2 / 1	0.9 / 8.8 / 2.1 / 1.2

Full Reference for Gaussian 03.

Frisch, M. J.; Trucks, G. W.; Schlegel, H. B.; Scuseria, G. E.; Robb, M. A.; Cheeseman, J. R.; Montgomery, J. A.; Vreven, T.; Kudin, K. N.; Burant, J. C.; Millam, J. M.; Iyengar, S. S.; Tomasi, J.; Barone, V.; Mennucci, B.; Cossi, M.; Scalmani, G.; Rega, N.; Petersson, G. A.; Nakatsuji, H.; Hada, M.; Ehara, M.; Toyota, K.; Fukuda, R.; Hasegawa, J.; Ishida, M.; Nakajima, T.; Honda, Y.; Kitao, O.; Nakai, H.; Klene, M.; Li, X.; Knox, J. E.; Hratchian, H. P.; Cross, J. B.; Bakken, V.; Adamo, C.; Jaramillo, J.; Gomperts, R.; Stratmann, R. E.; Yazyev, O.; Austin, A. J.; Cammi, R.; Pomelli, C.; Ochterski, J. W.; Ayala, P. Y.; Morokuma, K.; Voth, G. A.; Salvador, P.; Dannenberg, J. J.; Zakrzewski, V. G.; Dapprich, S.; Daniels, A. D.; Strain, M. C.; Farkas, O.; Malick, D. K.; Rabuck, A. D.; Raghavachari, K.; Foresman, J. B.; Ortiz, J. V.; Cui, Q.; Baboul, A. G.; Clifford, S.; Cioslowski, J.; Stefanov, B. B.; Liu, G.; Liashenko, A.; Piskorz, P.; Komaromi, I.; Martin, R. L.; Fox, D. J.; Keith, T.; Al-Laham, M. A.; Peng, C. Y.; Nanayakkara, A.; Challacombe, M.; Gill, P. M. W.; Johnson, B.; Chen, W.; Wong, M. W.; Gonzalez, C.; Pople, J. A. *Gaussian03*, revision D.01; Gaussian, Inc.: Wallingford, CT, 2004.

DFT Calculation of XPS Chemical Shifts of Carbon Atoms.

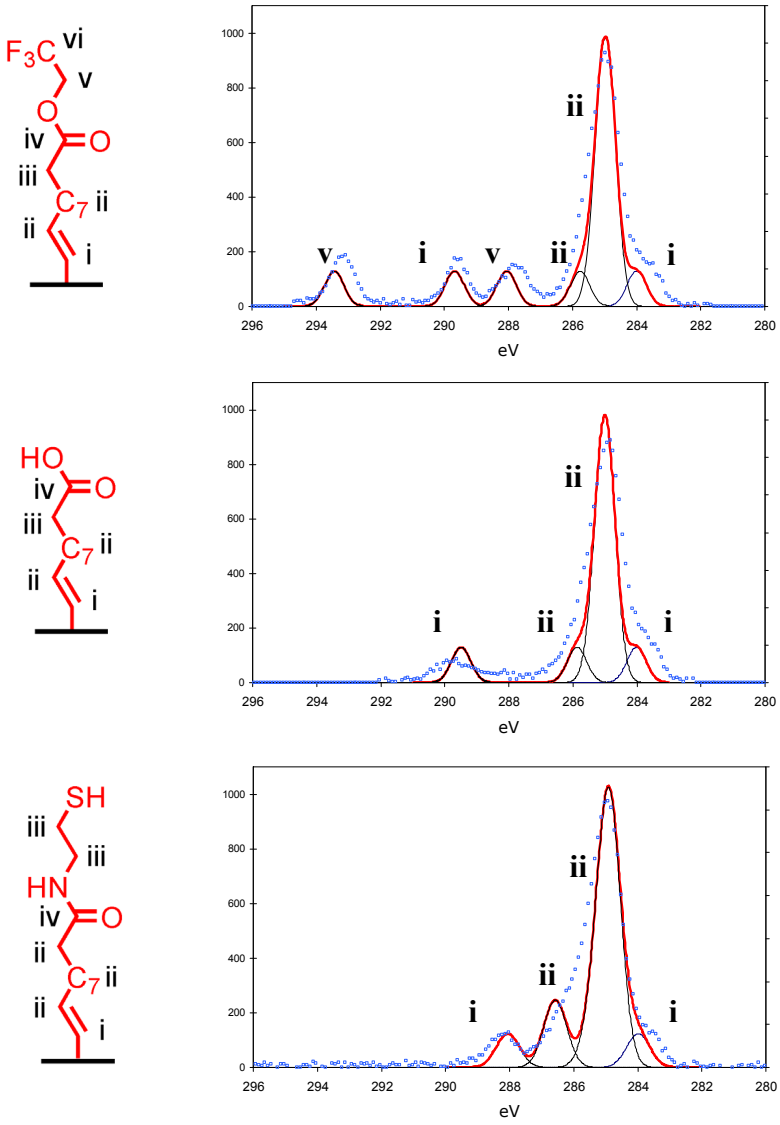

Figure A1. Experimental (blue dots) and calculated (red line) core level C_{1s} XPS spectra of TFE-terminated monolayer (top), carboxylic acid-terminated monolayer (middle) and thiol-terminated monolayer (bottom) on H-Si(111). The black lines are the calculated envelopes of the carbons used in fitting the data.

The assignment of the C_{1s} XPS spectra is supported by density functional theory (DFT) calculations of the core orbital energy levels. The absolute values of calculated binding energies cannot be compared directly with the experimental data because of the difference in reference energies in theory and experiment. As a point of reference the CH_2 moiety in the center of the aliphatic hydrocarbon chain was positioned at a binding energy of 285 eV. For every carbon atom, a Gaussian centered at the corresponding binding energy was used with a FWHM of 1.2 eV. The sum of all Gaussians gave the simulated XPS spectra.

Electronic Core Level Calculations: All calculations were done using the GAUSSIAN03 program. The geometries of the different systems were optimized at the B3LYP/6-311G(d,p) level of theory. Natural bond orbital (NBO) analysis was employed to obtain the core orbital energies.

Appendix 5

Electrical Transport Simulation Parameters.

Table 1. Electronic Transport Simulation Parameters.

Parameters Used to Describe Si-C_nH_{2n+1}-M junction			
ϕ_M	metal work function	5.2	eV
χ_{SC}	silicon electron affinity	4.05	eV
E_{GI}	monolayer bandgap	9	eV
m_I^*	carrier effective mass in monolayer	0.65	m_e
m_e^*	(transverse) electron effective mass in Si	0.37	m_e
m_h^*	(transverse) hole effective mass in Si	0.65	m_e
ε_{SI}	permittivity of Si	11.9	ε_0
ε_I	permittivity of monolayer	2	ε_0
μ_e	Si electron mobility	1450	$cm^2V^{-1}s^{-1}$
μ_h	Si hole mobility	500	$cm^2V^{-1}s^{-1}$
τ_e	electron lifetime (in depletion region)	10	μs
τ_h	hole lifetime (in depletion region)	10	μs
N_C	effective density of states in conduction band	2.8	$x10^{19}cm^{-3}$
N_V	effective density of states in conduction band	2.65	$x10^{19}cm^{-3}$
n_i	intrinsic carrier concentration	9.65	$x10^{9}cm^{-3}$
N_D	Donor (doping) concentration	5	$x10^{15}cm^{-3}$

Additional Electronic Characterization Alkyl and Alkenyl Junctions.

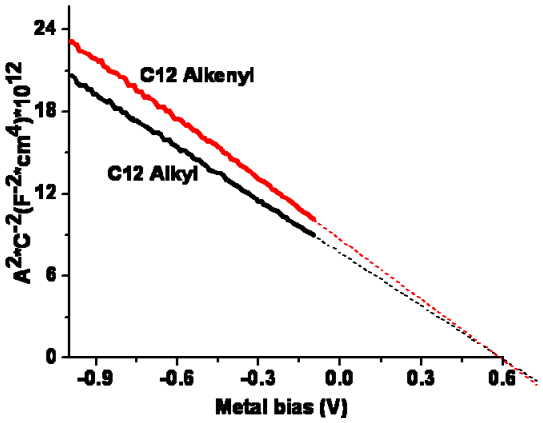

Figure A1. Mott-Schottky plots of C_{12} alkyl and alkenyl junctions on MD Si. Dashed lines are extrapolated to $(1/C^2) = 0$, where ψ_{bi} is extracted, according to the Mott-Schottky relation (see Chapter 8). The slope is not identical, because of small variations in doping density between the commercial wafers.

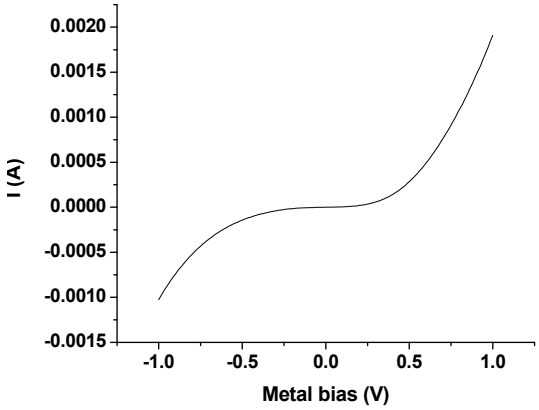

Figure A2. Linear representation of the J-V curve of C_{14} (alkyl) that demonstrates the non-ohmic behavior of the HD n-Si-Organic Monolayer/Hg Junctions.

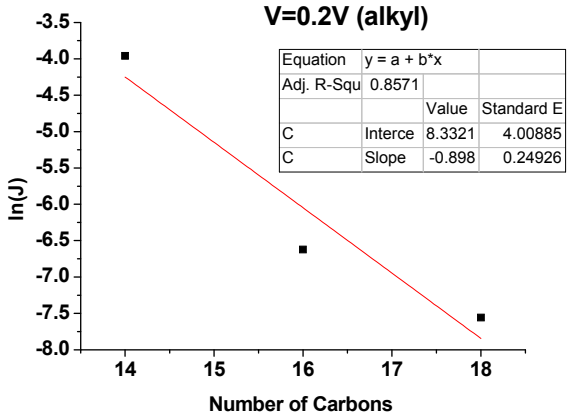

Figure A3. Beta analysis of alkyl monolayers on HD Si at applied bias of 0.2V.

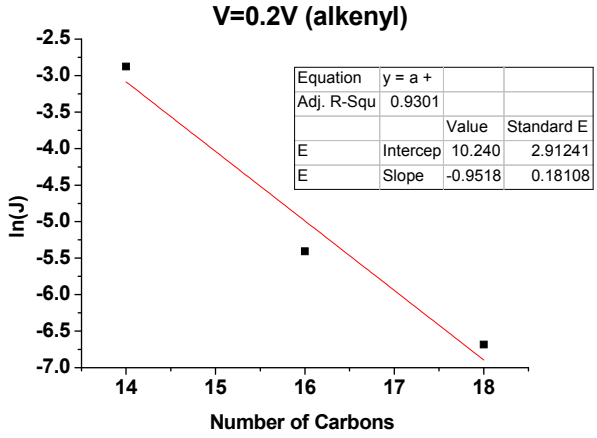

Figure A4. Beta analysis of alkenyl monolayers on HD Si at applied bias of 0.2V.

Summary

Due to the ongoing miniaturization of semiconductor devices, there is a significant interest in the surface modification of silicon. In this perspective, organic monolayers directly bound to oxide-free silicon are interesting candidates as they can easily be implemented in the existing technology for fabrication of silicon-based micro- and nanostructured devices. The direct covalent linkage (Si–C bond) to the silicon surface creates a well-defined organic monolayer-silicon interface and makes these monolayers thermally and chemically very robust. Moreover, because an intervening SiO_2 layer is essentially absent, direct electronic coupling between any organic functionality and the silicon substrate is possible, which provides an opportunity to enhance the device performance compared to SiO_2-covered devices. As a result these monolayers have great potential in the field of biosensing and optoelectronic devices.

At the start of this work we delineated the factors that still limited this potential, with the aim to push the barriers forward. First of all, the oxide-free monolayer-silicon interface typically has a limited long-term stability. Furthermore, because many functional groups are reactive towards a H-Si surface, only a few robust functional monolayers had been described in literature. In addition, only a limited number of patterning routes for this type of monolayers had been reported. Since these three issues hamper the development and fabrication of functional hybrid organic monolayer-silicon devices, the fundamental work presented in this thesis focused on solving the abovementioned problems.

After a general introduction in Chapter 1, a new and very mild method to produce covalently bound organic monolayers on hydrogen-terminated Si from 1-alkynes is described in Chapter 2. Because monolayer formation even occurs at room temperature in the dark, i.e. without any external activation, this is the mildest method reported thus far. Since at the same time this method yields the highest quality yet reported for organic monolayers on Si, as indicated by water contact angles, infrared reflection absorption spectroscopy (IRRAS) and X-ray photoelectron spectroscopy (XPS), this has become the new standard for making such monolayers.

To pinpoint the precise origin of this self-assembly process, we compared the reactivity of 1-alkenes and 1-alkynes towards H-Si(111) in Chapter 3. As follows from the development of the static water contact angle during reaction, 1-alkynes are considerably more reactive towards H-Si(111) than 1-alkenes, which is attributed to the higher nucleophilicity of 1-alkynes, a better stabilization of the β-radical, and a lower energy barrier for H-abstraction (Figure 1). In practice the higher reactivity of 1-alkynes will

further extend the range of functional groups that can be attached directly onto H-Si, and will lead to an easier and more reproducible preparation of oxide-free monolayers on Si.

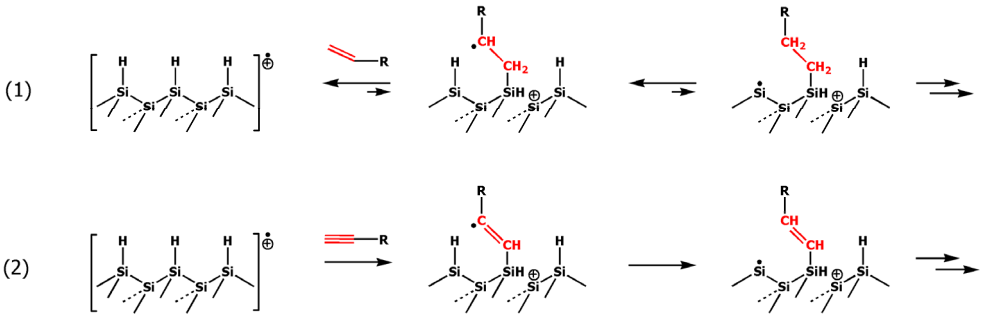

Figure 1. Representation of the proposed radical chain mechanism and the corresponding reactivity difference of (1) 1-alkenes and (2) 1-alkynes.

In Chapter 4 we studied the influence of the different linkages to the Si surface (Si–C–C versus Si–C=C) on the final monolayer structure. For this purpose organic monolayers were prepared from 1-alkenes and 1-alkynes with chain lengths from C_{12} to C_{18}. Although the static contact angles were similar for all monolayers, ellipsometry, ATR-IR and quantitative XPS revealed a higher packing density, higher ordering and smaller tilt angles with respect to the surface normal for the alkenyl monolayers. As expected, the surfaces coverages for alkyl monolayers was determined to be 50-55%, but for the alkenyl monolayers it increased with the chain length from 55% for C_{12} to as high as 65% for C_{18}, and thus starts to approach the theoretical maximum of 69% for long alkyl (and alkenyl) monolayers on H-Si(111).

Following Chapter 4, in Chapter 5 molecular modeling experiments and composite high-quality G3 calculations were combined to clarify the observed structural differences of alkyl and alkenyl monolayers on Si(111). It was found that due to the smaller Van der Waals radius of the Si–C=C linkage and the larger exothermicity of the reaction substitution percentages > 50% become feasible. In combination with the oxidation-inhibiting nature of the Si–C=C linkage, this significantly increases the chance of successful implementation of organic monolayers on oxide-free silicon into molecular electronic and biosensor devices.

In Chapter 6 the benefits of 1-alkynes were put into practice and well-defined acid fluoride-terminated monolayers, without any sign of upside-down attachment, were prepared on Si(111). These acid fluoride monolayers were used as a platform for reactive

microcontact printing (μCP) with an *n*-hexadecylamine-inked PDMS stamp, and yield within a minute well-defined 5 μm *N*-hexadecylamide dots on the surface (Figure 2). The high and selective reactivity of the acid fluorides towards primary amines even allowed printing of functionalized oligo-DNA, which was still accessible for hybridization. Since this indirect printing approach also preserves the oxide-free and well-defined monolayer silicon interface, it is a highly promising technique for the production of new hybrid biosensor and molecular electronic devices.

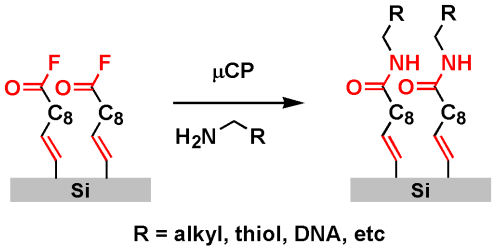

Figure 2. Reactive microcontact printing with primary amines on acid fluoride-terminated monolayers on oxide-free Si(111).

In Chapter 7, photothermal laser patterning of nonfunctional and functional organic monolayers on oxide-free silicon is described with feature sizes down to 100 nm. With a focused laser beam the silicon substrate surface is locally heated, initiating the thermal decomposition of the organic monolayer. Because this process is highly nonlinear in the applied laser power density, sub-wavelength patterning of the organic monolayers was feasible. A variety of multifunctional patterns can be obtained, depending on the starting monolayer, and the possibility of back-filling of the laser-written lines with a new functionality. The flexibility in pattern design, the high writing speeds, and the feasibility for patterning inside complex device geometries, like in microfluidic channels, make photothermal laser patterning a promising technique in the fabrication of new small-scale biosensor and molecular electronic devices.

Because a thorough understanding of the charge transport mechanisms through organic monolayers on oxide-free silicon is essential for their implementation in new electronic devices, Chapter 8 describes the electronic characterization of alkyl and alkenyl monolayers on moderately and highly doped n-Si(111) substrates. For the first time it is shown that the electric behavior of monolayers is dependent on the doping of the silicon: on moderately doped n-Si charge transport through the junction is a minority-carrier process at reverse and low forward bias, and is controlled by series resistance at higher forward bias, and thus the

alkyl and alkenyl monolayers exhibited nearly identical electrical properties. However, when using highly doped n-Si as substrate, the internal barrier is smaller and thus charge transport though the junction is majority-carrier controlled and sensitive for the type of monolayer in the junctions. It is proposed that the double bond in the alkenyl monolayers increases the coupling between the organic monolayer and the Si substrate, enhancing the contact conductance, which in turn increases the current density at a given bias.

Chapter 9 describes the preparation of two bent-core liquid crystalline monolayers on H-Si and the characterization thereof. The monolayer thickness, as determined with X-ray reflectivity, ellipsometry and ATR-IR, corresponded well with the layer spacing of these molecules in the liquid crystalline smectic phase, suggesting that even when covalently bound to a surface the mesogens retain their liquid crystalline ordering properties. Due to the similarity of ordering in the monolayer and ordering in the liquid crystalline bulk, these monolayers can be used as thin alignment layers for switchable smectic liquid crystalline materials.

Finally, Chapter 10 discusses several outstanding mechanistic and application-oriented issues and provides recommendations for further research.

Samenvatting

Door de aanhoudende miniaturisatie van elektronische systemen is er grote interesse ontstaan in de oppervlakte modificatie van silicium. In dit perspectief zijn organische monolagen die direct gebonden zijn aan oxidevrij silicium een interessante kandidaat omdat deze monolagen gemakkelijk geïmplementeerd kunnen worden in de bestaande technologie voor de productie van micro- en nano-gestructureerde silicium elektronica. De directe covalente koppeling (Si–C binding) aan het silicium oppervlak zorgt voor een goed gedefinieerd grensvlak tussen de organische monolaag en het silicium en maakt deze monolagen thermisch en chemisch zeer robuust. Bovendien, omdat er geen tussenliggende SiO_2 laag is, is directe elektronische koppeling tussen de organische functionaliteit en het silicium substraat mogelijk, wat dus de gelegenheid biedt om de elektronische prestaties te verbeteren ten opzichte van SiO_2-chips. Hierdoor zijn deze monolagen aantrekkelijk voor de ontwikkeling van nieuwe van biosensoren en opto-elektronische systemen.

Aan het begin van dit werk hebben we de tekortkomingen en problemen van deze monolagen bepaald en ons als doel gesteld om deze belemmeringen te verhelpen. Zo heeft bijvoorbeeld op lange termijn het oxidevrije grensvlak van de monolaag en het silicium oppervlak een beperkte stabiliteit, zijn veel functionele groepen reactief met het H-Si oppervlak waardoor er slechts enkele robuuste functionele monolagen staan beschreven in de literatuur en zijn er slechts een beperkt aantal methodes bekend voor het patterneren van deze monolagen. Aangezien deze drie kwesties de ontwikkeling en fabricage van hybride organische monolaag - silicium structuren belemmeren, is het fundamentele werk gepresenteerd in dit proefschrift gericht op het oplossen van de bovengenoemde problemen.

Na een algemene inleiding in Hoofdstuk 1 wordt in Hoofdstuk 2 een nieuwe en zeer milde methode beschreven om covalent gebonden organische monolagen op H-Si te bereiden met 1-alkynen. Monolaag formatie vindt zelfs plaats bij kamertemperatuur in het donker (dus zonder enige externe activering) en dit maakt deze methode de mildste tot nu toe beschreven in de literatuur. Omdat deze milde methode ook resulteert in de hoogste kwaliteit monolagen, zoals aangetoond met water contacthoek metingen, infrarood reflectie absorptie spectroscopie (IRRAS) en X-ray foto-elektron spectroscopie (XPS), is dit de nieuwe standaard geworden voor het maken van deze monolagen.

Om de precieze oorzaak van dit zelf-assemblage proces te kunnen bepalen, hebben we in Hoofdstuk 3 de reactiviteit van 1-alkenen en 1-alkynen met H-Si(111) vergeleken. Zoals blijkt uit de statische water contacthoek metingen tijdens de reacties, zijn 1-alkynen aanzienlijk reactiever met het H-Si(111) oppervlak dan 1-alkenen. Deze hogere reactiviteit

wordt toegeschreven aan de hogere nucleofiliciteit van 1-alkynen, een betere stabilisatie van het β-radicaal en de lagere energiebarrière voor H-abstractie (Figuur 1). In de praktijk zal de hogere reactiviteit van 1-alkynen er voor zorgen dat meer functionele groepen rechtstreeks aan het H-Si oppervlak gekoppeld kunnen worden en zal de bereiding van oxidevrije monolagen op Si eenvoudiger en beter reproduceerbaar zijn.

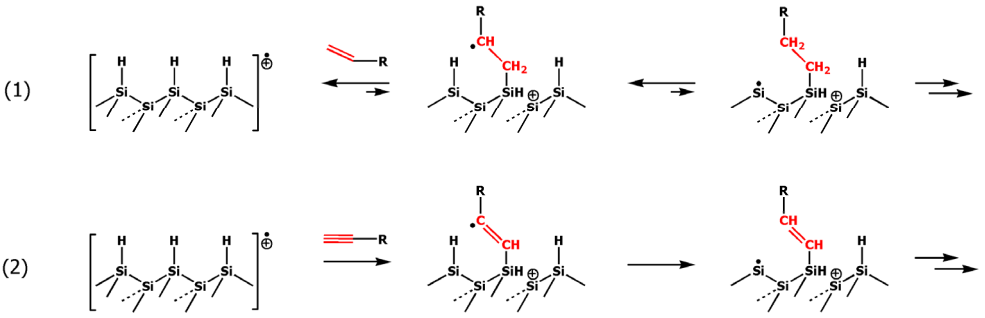

Figuur 1. Representatie van het voorgestelde radicaal mechanisme en het bijbehorende reactiviteitverschil van (1) 1-alkenen en (2) 1-alkynen.

In Hoofdstuk 4 hebben we de invloed van de verschillende koppelingen aan het Si oppervlak (Si–C–C versus Si–C=C) op de uiteindelijke structuur van de monolaag onderzocht. Hiervoor werden organische monolagen van 1-alkenen en 1-alkynen met een ketenlengte van C_{12} tot C_{18} bereid. Hoewel de statische water contacthoeken vergelijkbaar waren voor alle monolagen werden er met ellipsometrie, ATR-IR en kwantitatieve XPS metingen hogere pakkingsdichtheden, beter ordening en een meer rechtopstaande oriëntatie van ketens gemeten voor de alkenyl monolagen. Zoals verwacht was de bezettingsgraad voor de alkyl monolagen rond de 50-55%, maar voor de alkenyl monolagen neemt deze toe met de ketenlengte van ongeveer 55% voor C_{12} tot ongeveer 65% voor C_{18}. Een waarde dichtbij de theoretische maximale bezettingsgraad van 69% voor lange alkyl (en alkenyl) monolagen op H-Si(111).

In navolging van Hoofdstuk 4 zijn in Hoofdstuk 5 moleculaire modellering experimenten en hoogwaardige G3 berekeningen gecombineerd om de waargenomen structurele verschillen tussen alkyl en alkenyl monolagen op Si(111) te verklaren. Het werd duidelijk dat door de kleinere Van der Waals radius van de Si–C=C groep en de grotere exothermiciteit van de koppelingsreactie van 1-alkynen aan het H-Si oppervlak een bezettingsgraad boven de 50% haalbaar is. In combinatie met de oxidatie remmende

karakter van de Si–C=C koppeling verhoogt dit de kans op een succesvolle implementatie van organische monolagen op oxidevrij silicium in moleculaire elektronica en biosensoren.

In Hoofdstuk 6 zijn de voordelen van 1-alkynen in praktijk gebracht en goed gedefinieerde zuur fluoride getermineerde monolagen werden bereid zonder enig teken van moleculen die ondersteboven gebonden zijn aan het Si oppervlak. Deze zuur fluoride monolagen zijn vervolgens gebruikt als een platform voor reactief microcontact printen (μCP) met een *n*-hexadecylamine geïnkte PDMS stempel. Dit resulteerde binnen een minuut in goed gedefinieerde 5 μm grootte *N*-hexadecylamide stippen op het oppervlak (Figuur 2). De selectiviteit en hoge reactiviteit van de zuur fluoride groep met primaire amines maakt het zelfs mogelijk om gefunctionaliseerd oligo-DNA te printen wat daarna nog steeds toegankelijk is voor hybridisatie. Aangezien deze indirecte benadering van μCP gemakkelijk het oxidevrije en goed gedefinieerde grensvlak van de organische monolaag en het silicium behoudt, is het een veelbelovende techniek voor de productie van nieuwe hybride biosensoren en moleculaire elektronica.

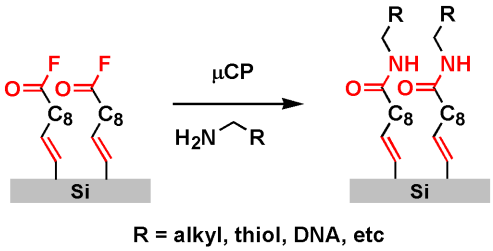

Figuur 2. Reactief microcontact printen met primaire amines op zuur fluoride getermineerde monolagen op ozidevrij Si(111).

In Hoofdstuk 7 wordt het fotothermisch laser schrijven van niet-functionele en functionele monolagen op oxidevrij Si beschreven. Met een gefocuste laserstraal wordt het silicium substraat lokaal verwarmd waardoor de thermische decompositie van de monolaag wordt geïnitieerd. Omdat dit proces non-lineair is in het gebruikte laser vermogen kunnen patronen met een resolutie beneden de golflengte van het laserlicht gecreëerd worden (lijntjes met een breedte van ongeveer 100 nm). Afhankelijk van de initiële monolaag en de mogelijkheid tot het opvullen van de laser geschreven lijntjes met een nieuwe functionele monolaag zorgt ervoor dat een grote verscheidenheid aan multifunctionele patronen geproduceerd kunnen worden. De flexibiliteit in patroon design, de hoge schrijfsnelheden, en de mogelijkheid om patronen de schrijven binnenin complexe structuren (zoals bijvoorbeeld in microfluidische kanaaltjes) maakt fotothermisch laser schrijven een

veelbelovende techniek voor de vervaardiging van nieuwe kleinschalige biosensoren en moleculaire elektronica.

Omdat een goed inzicht in de ladingstransport mechanismen van en door organische monolagen op oxidevrij silicium van essentieel belang is voor de implementatie van deze monolagen in nieuwe elektronische systemen, wordt in Hoofdstuk 8 de elektronische karakterisatie van alkyl en alkenyl monolagen op matig en hoog 'gedoped' n-Si(111). Voor het eerst wordt aangetoond dat de elektrische eigenschappen van deze monolagen afhankelijk is van de doping van het silicium substraat. Op matig 'gedoped' n-Si is ladingstransport door het systeem een 'minority-carrier' proces bij negatief en licht positief voltage en wordt gecontroleerd door serieweerstand bij hogere positieve voltages. Hierdoor hebben de alkyl en alkenyl monolagen nagenoeg identieke elektrische eigenschappen. Echter, op hoog 'gedoped' n-Si is de barrière in het silicium substraat veel kleiner waardoor ladingstransport in dit geval een 'majority-carrier' proces is en daardoor gevoelig is voor het type monolaag in het systeem. Het verschil tussen de alkyl en alkenyl monolagen wordt toegeschreven aan de dubbele binding in de alkenyl monolagen die de elektronische koppeling tussen de organische monolaag en het Si substraat verbeterd en zorgt voor een verhoogde contact geleiding wat vervolgens resulteert in een hogere stroomdichtheid.

Hoofdstuk 9 beschrijft de bereiding en karakterisatie van twee monolagen gemaakt van vloeibaar kristallijne moleculen met gebogen kern. De dikte van de monolagen, zoals bepaald met X-ray reflectie, ellipsometrie en ATR-IR, komt goed overeen met de laagdikte van deze moleculen in een vloeibaar kristallijne smectische fase en suggereert dat zelfs wanneer deze moleculen covalent gebonden zijn aan een oppervlak de vloeibaar kristallijne eigenschappen behouden blijven. Vanwege de vergelijkbare ordening in de monolaag en in de vloeibaar kristallijne bulk zouden deze monolagen gebruikt kunnen worden als dunne uitlijningslagen voor schakelbare vloeibaar kristallijne smectische materialen.

Tot slot worden in Hoofdstuk 10 een aantal onbeantwoorde mechanistische en toepassingsgerichte vragen besproken en worden aanbevelingen voor verder onderzoek gedaan.

Curriculum Vitae

Luc Scheres werd geboren op 18 oktober 1979 te Meijel. Na het behalen van zijn VWO-diploma aan het Bouwens van der Boye College te Panningen begon hij in 1998 aan de studie Chemie aan Fontys Hogeschool te Eindhoven. Na stages bij TNO Industrie te Eindhoven en Rockwool Lapinus Fibres te Roermond startte hij in 2002 aan de master Chemistry and Physics aan de Universiteit van Utrecht. Zijn afstudeeropdracht deed hij in de vakgroep Fysisch Organische Chemie onder leiding van Prof. dr. L. W. Jenneskens. Vervolgens begon hij in 2005 zijn promotie aan de Universiteit van Wageningen in de vakgroep Organische Chemie onder leiding van Prof. dr. H. Zuilhof. De belangrijkste resultaten van dit promotieonderzoek staan beschreven in dit proefschrift. Sinds november 2009 is hij werkzaam als postdoc in de groep van dr. Albert Schenning aan Technische Universiteit Eindhoven.

Luc Scheres was born on October 18th 1979 in Meijel. After finishing VWO at Bouwens van der Boye College in Panningen, he studied Chemistry at Fontys Hogeschool in Eindhoven. After internships at TNO Industrie in Eindhoven and Rockwool Lapinus Fibres in Roermond he graduated in 2002. Subsequently he started the master program Chemistry and Physics at the University of Utrecht and finished his master thesis in the Physical Organic Chemistry group of Prof. dr. L. W. Jenneskens. In 2005 he became a PhD student at Wageningen University in the Organic Chemistry group under supervision of Prof. dr. H. Zuilhof. The most important results of this research are described in this thesis. Since November 2009 he is working as a postdoc in the group of dr. Albert Schenning at the Technical University of Eindhoven.

List of Publications

'Self-Assembly of High-Quality Covalently Bound Organic Monolayers onto Silicon' L. Scheres, A. Arafat, H. Zuilhof, *Langmuir,* **2007**, *23*, 8343-8346.

'Covalent Attachment of Bent-Core Mesogens to Silicon Surfaces' L. Scheres, R. Achten, M. Giesbers, L. C. P. M. de Smet, A. Arafat, E. J. R. Sudhölter, T. Marcelis, H. Zuilhof, *Langmuir*, **2009**, *25*, 1529-1533.

'Molecular electronics at Metal / Semiconductor Junctions: Si inversion by Sub-nm Molecular Films' O. Yaffe, L. Scheres, S. R. Puniredd, N. Stein, A. Biller, R. Har-Lavan, H. Shpaisman, H. Zuilhof, H. Haick, D. Cahen, A. Vilan, *Nano Lett.*, **2009**, *9*, 2390-2394.

'Organic Monolayers onto Oxide-Free Silicon with Improved Surface Coverage: Alkynes versus Alkenes' L. Scheres, M. Giesbers, H. Zuilhof, *Langmuir,* **2010**, *26*, 4790-4795.

'Photothermal Micro- and Nanopatterning of Organic/Silicon-Interfaces' B. Klingebiel, L. Scheres, S. Franzka, H. Zuilhof, N. Hartmann, *Langmuir,* **2010**, *26*, 6826-6831.

'Microcontact Printing onto Oxide-Free Silicon via Highly Reactive Acid Fluoride-Functionalized Monolayers' L. Scheres, J. ter Maat, M. Giesbers, H. Zuilhof, *Small,* **2010**, *6*, 642-650.

'Tuning the Electronic Communication between Redox Centers Bound to Insulating Surfaces' D. Zigah, C. Herrier, L. Scheres, M. Giesbers, B. Fabre, P. Hapiot, H. Zuilhof, *Angew. Chem. Int. Ed,* **2010**, *49*, 3157-3160.

'Micro- and Nanopatterning of Functional Organic Monolayers on Oxide-Free Silicon by Laser-Induced Photothermal Desorption' L. Scheres, B. Klingebiel, J. ter Maat, M. Giesbers, H. de Jong, N. Hartmann, H. Zuilhof, *Small,* **2010**, in press.

'Hg/Molecular Monolayer-Si junctions: Electrical Interplay between Monolayer Properties and Semiconductor Doping Density' O. Yaffe / L. Scheres, L. Segev, A. Biller, I. Ron, E. Salomon, M. Giesbers, A. Kahn, L. Kronik, H. Zuilhof, A. Vilan, D. Cahen, *J. Phys. Chem.C,* **2010**, ASAP, doi: jp101656t.

'Self-Assembly of Organic Monolayers onto Hydrogen-Terminated Silicon: 1-Alkynes are Better than 1-Alkenes' L. Scheres, M. Giesbers, H. Zuilhof, *Langmuir,* **2010**, ASAP, doi: la100858q.

'Molecular Modeling of Alkyl and Alkenyl Monolayers on Hydrogen-Terminated Si(111)' L. Scheres, B. Rijksen, M. Giesbers, H. Zuilhof, **2010**, *submitted to Langmuir.*

'Light-Enhanced Microcontact Printing on Oxide-Free Silicon' J. ter Maat, M. Yang, L. Scheres, H. Zuilhof, *manuscript in preparation.*

'The Effect of Doping Type (p/n) on the Electrical Properties of Metal/Organic Monolayer/Heavy Doped Si Junctions' O. Yaffe, L. Scheres, A. Vilan, H. Zuilhof, D. Cahen, *manuscript in preparation*.

'Temperature-Dependent Electronic Transport through Alkyl Chain Monolayers' H. Shpaisman, O. Seitz, L. Scheres, O. Yaffe, A. Vilan, H. Zuilhof, Y. Chabal, D. Cahen, , *manuscript in preparation.*

'Transport Properties of Mercury-Molecular Monolayer-Silicon Junctions Incorporating Redox-active Functionalities' A. B. Fdjie-Djomkam, S. Ababou-Girard, B. Fabre, N. Tournerie, S. Cordier, Y. Molard, L. Scheres, J. Paulusse, H. Zuilhof, D. Bassani, H. Sabbah, F. Solal, C. Godet, *manuscript in preparation.*

Overview of Completed Training Activities

Discipline Specific Activities	**ECTS credits**
Courses	
Fundamentals of Nanotechnology, MESA+, University of Twente, 2006	1.4
Advanced Course Bio-Nanotechnology, VLAG, Wageningen University, 2006	1.0
Chemical Surface Analysis of Materials, EPFL, Lausanne, Switzerland, 2006	1.3
Photophysics, Photochemistry and Photobiology, HRSMC, VU Amsterdam, 2007	3.0
Meetings	
Dutch-Israel meeting on Molecular Materials, Rehovot, Israel, 2007	1.9
Semiconductor Surface Passivation Workshop, Zakopane, Poland, 2007	2.7
Wageningen Symposium on Organic Chemistry, KNCV, 2006/2008	2.2
Annual Structure and Reactivity session, NWO, Lunteren, 2005-2008	4.8
Annual MicroNano Conference, 2005-2009	4.6
General courses	
PhD Scientific Writing, Centa, Wageningen, 2009	1.8
Optionals	
Preparation PhD Research Proposal, 2005	4.0
Group Meetings, Laboratory of Organic Chemistry, 2005-2009	3.0
Colloquia, Laboratory of Organic Chemistry, 2005-2009	3.0
PhD Study Trip, Organized by Laboratory of Organic Chemistry, Sweden, 2007	2.5
PhD Study Trip, Organized by Laboratory of Organic Chemistry, China, 2009	2.5
Total	**39.7**

Dankwoord

Eindelijk is het zover, mijn proefschrift is klaar! Graag wil ik deze laatste pagina's gebruiken om een aantal mensen te bedanken voor hun steun en hulp tijdens mijn promotieonderzoek.

Allereerst natuurlijk mijn promotor prof. dr. Han Zuilhof. Han, bedankt voor al je adviezen, enthousiasme en kritische blik; ik heb er veel van geleerd. Tevens ben ik je zeer dankbaar voor de vrijheid bij de invulling van dit project en het creëren van de perfecte omstandigheden voor zeer efficiënt oppervlak gerelateerd onderzoek. Ook je medeleven, steun en begrip op de momenten dat er donkere onweerswolken boven ons privéleven hingen heb ik zeer gewaardeerd.

Ook prof. dr. Ernst Sudhölter wil ik graag bedanken. Ernst, ook al was het maar van korte duur, je optimisme en enthousiasme heb ik altijd als zeer prettig ervaren.

I would like to thank prof. dr. David Cahen (Weizmann Institute, Rehovot, Israel) for the hospitality during my stay in Israel and for the resulting collaboration with his group. In this respect, I'm very grateful to prof. dr. Leeor Kronik, Lior Segev, dr. Ayelet Vilan, Hagay Shpaisman and dr. Yaron Cohen, but most of all to Omer Yaffe. Omer, thanks a lot for the pleasant and very fruitful collaboration. Despite the large distance (approx. 3300 km), it really felt like teamwork due to the close email contact.

The nice collaboration on the photothermal laser patterning of organic monolayers with dr. Nils Hartmann and Benjamin Klingebiel (University Duisburg-Essen, Germany) is also highly appreciated. Although the efficiency of the functionalization experiments was sometimes a bit 'disappointing', the extra efforts at the end were luckily useful to finish a second shared paper. I really enjoyed our meetings and the trips to Essen, therefore thanks a lot!

I would like prof. dr. Bruno Fabre to thank for coming to Wageningen to participate in my committee, and, of course, also for the pleasant joint work on the ferrocene monolayers which resulted in a very nice Angewandte-paper.

Dr. Ton Marcelis wil ik graag bedanken voor de prettige samenwerking en zijn 'kartrekkersrol' wat betreft de 'bananen-paper'. Aangezien al veel mensen aan dit onderwerp hadden gewerkt en er toch nog steeds geen publiceerbare set data beschikbaar was, heeft jou volharding hier de doorslag gegeven. Met als resultaat een mooie paper!

Mijn kamergenoot Jurjen ter Maat wil ik graag bedanken voor vier mooie jaren en de vriendschap die hieruit ontstaan is. Ik heb er echt van genoten en zou het zo weer over willen doen. Ik denk nog vaak met veel plezier terug aan onze 'brainstorm-sessies' met een

kopje koffie, de Nederlandse les (gelukkig zit ik er nu minder vaak *langs*), de Gryère-kaas in mijn bureaulade, de tafelvoetbal spelletjes, de blauwe koe, de China reis, het prachtige feest in Oostenrijk, etc… Ik wens je veel geluk in de toekomst en doe alsjeblieft de groeten aan je vrouw!

I also would like to thank Milena and Michel for their friendship and being such nice colleagues. I really enjoyed all dinners, parties and 'bunny hunting'-games. Milena, thanks for the Serbian-lessons and the fact that you only threatened to use the whip and never really used it when I was whistling in the lab.

For all the exciting table football games and all the fun during the integration course for German speaking Indian postdocs I would like to thank Ruud Cuypers and Murali Sukumaran. Thanks guys!

For all the help during the first year of my PhD I would like to thank prof. dr. Ahmed Arafat. Ahmed, you taught me how to make good monolayers and were indirect responsible for the flying start of my PhD. Unfortunately, you left suddenly but luckily you fully recovered from cancer. And of course, congratulation with your professorship!

Graag wil ik Marcel Giesbers bedanken voor de ontelbare keren dat we, onder het genot van kopje koffie, experimenten maar ook alledaagse dingen hebben besproken. Mijn proefschrift staat nu vol met prachtige XPS spectra die we samen hebben gedraaid. Je bijdrage heb ik zeer gewaardeerd, wat natuurlijk ook al blijkt uit het groot aantal publicaties dat we samen hebben.

Of course, I would also like to thank the best actor of China and its surrounding areas. Menglong, I have enjoyed your inspiring questions and ideas and it seems to me that you really have the ability to make a smile on everyone's face, which made it wonderful to have you around. Thanks a lot for the arrangements, hospitality and guidance during our China-trip and I wish you and your family all the best!

Voor het wegwijs maken in het lab wil ik Louis de Smet bedanken. Voor een startende AIO is het altijd nuttig om af en toe met een ervaren rot in het vak te kunnen overleggen. En ook al was je toen nogal druk met het afronden van je eigen proefschrift, je wist toch altijd wel wat tijd te maken voor het beantwoorden van mijn vragen. Bedankt daarvoor!

Verder wil ik graag Elly en Aleida ook even noemen, want graag wil ik jullie bedanken voor alle hulp tijdens de afgelopen jaren, maar meer nog voor de flexibiliteit, interesse en begrip wat betreft Janneke's gezondheid.

Tijdens mijn onderzoek heb ik het genoegen gehad om twee Master studenten te mogen begeleiden; Bart Rijksen en Niels ten Brummelhuis. Bart en Niels bedankt voor jullie

bijdrage en inzet. Bart, tevens bedankt de berekeningen die Hoofdstuk 5 compleet maken en de gezellige biertjes op carnavalszaterdag in Venlo!

Graag wil ik ook dr. Hans de Jong van Genetica bedanken voor zijn hulp bij het schieten van de fluorescentie plaatjes die in Hoofdstuk 6 en 7 staan.

Ondanks dat de STM experimenten niet de gewenste resultaten opleverden, wil ik toch Prof. dr. Harold Zandvliet en Daan Kockmann bedanken voor de gastvrijheid en bereidheid om met STM op zoek te gaan naar de 'eilandjes' op het silicium oppervlak.

Iemand die ik echt niet mag vergeten is Ed Snoek van Jeol. Graag wil ik je bedanken voor al die keren dat je 'echte' en 'niet echte' (zoals die zogenaamde 1 µm scanner!) problemen met veel geduld en precisie heb opgelost. Ik heb al met Marcel overleg gehad en de jury is unaniem… de 'Houd je hoofd koel'-award 2006-2010 heb je dik verdiend!

Verder wil ik alle collega's van Organische Chemie bedanken voor de leuke werksfeer en ondersteuning, maar ook voor de gezelligheid tijdens de labuitjes, barbecues en AIO-reizen. In het bijzonder, Barend van Lagen voor de hulp met de IRRAS en ATR metingen, Remco Regeling voor het schoonhouden van het lab, draaien van Thunderdome 1 t/m 373 en de blijvende gehoorsbeschadiging die ik hieraan over heb gehouden, Maarten Posthumus voor de exacte massa bepalingen, Elbert van der Klift en Frank Claassen voor de hulp met de GC-MS metingen, en Ronald de Bruin voor de ontelbare keren dat je toch weer op zeer snelle wijze een oplossing had voor al mijn glaswerk of chemicaliën gerelateerde problemen.

Uiteraard wil ik ook graag mijn (schoon)ouders, familie en vrienden bedanken voor de steun, vertrouwen en interesse in mijn onderzoek, maar ook voor het luisterend oor, de helpende hand en het begrip en medeleven na Janneke's hartstilstand. Met name wil ik bedanken onze 'kuisvrouwen' die vaak bijsprongen in de huishouding, de taxichauffeur voor de retourtjes AZM, de gastvrouw van de beste all-inclusive carnavalsarrangementen, de fanatieke drukker van dit proefschrift en de aardappelschiller van de frietjes op vrijdagavond.

Uiteindelijk is er nu nog maar een persoon over die ik graag wil bedanken voor haar steun de afgelopen jaren en dat is mijn lieve Janneke. Janneke, jou altijd stralende lach en ongekend positieve instelling, ondanks de donkerste onweerswolken die af en toe boven je hoofd hangen, maken van elke regenachtige dag een stralende zonnige dag. En die dagen wil ik nog heel veel met jou beleven!

Luc

The research described in this thesis was financially supported by NanoNed, funded by the Dutch Ministry of Economic Affairs (project WSC.6972).

Design and Layout: Luc Scheres
Printed by: De Budelse BV, Budel, The Netherlands